University of Southampton

INVESTIGATION OF THE HECK REACTION AND THE ASSOCIATED CATALYTIC SYSTEMS USING XAFS AND PHOSPHORUS NMR TECHNIQUES

GRAHAM RAYNER

A thesis submitted for the Degree of Doctor of Philosophy

Department of Chemistry

December 2002

UNIVERSITY OF SOUTHAMPTON

ABSTRACT

FACULTY OF SCIENCE

CHEMISTRY

Doctor of Philosophy

INVESTIGATION OF THE HECK REACTION AND THE ASSOCIATED CATALYTIC SYSTEMS USING XAFS AND PHOSPHORUS NMR TECHNIQUES

by Graham Rayner

Palladium K-edge XAFS (Extended X-ray Absorption Fine Structure (EXAFS), Quick EXAFS (QEXAFS) and Energy Dispersive EXAFS (EDE)) techniques have been used in conjunction with phosphorus NMR to characterise the palladium species present in a variety of reactions.

The body of work was commenced by investigating the formation of a variety of 'catalytic' systems, formed by palladium acetate with a mixture of alkyl and aryl monodentate phosphine ligands (chosen due to the variety of their steric, electronic and catalytic properties). The first reaction to be studied was between palladium acetate and tri-*o*-tolylphosphine to form palladacycle (**1**). A time resolved X-ray Absorption Near Edge Structure (XANES) plot and ^{31}P NMR both showed the formation of an intermediate, which was attributed to coordination of the phosphine, but before formation of the Pd-C ring was observed. XAFS techniques were used to elucidate the structure of **1** in solution and the results were in close agreement with the quoted crystal structure interatomic distances. It was also shown that multiple scattering effects were negligible. The palladium phosphine investigation was extended to include analysis of palladium acetate reacting with tricyclohexylphosphine, tri(*t*-butyl)phosphine and triphenylphosphine.

The main body of work was conducted on the Heck reaction between 2-methylprop-2-en-1-ol and PhX (X = Cl, Br and I) to form 1-phenyl-2-methyl-propanal catalysed by the systems already examined in this thesis (the systems were also extended to include other phosphine ligands (tri(1-napthyl)phosphine and tris(*o*-methoxyphenyl)phosphine) and **3b** as catalyst). The results showed a variety of catalytic properties, from tricyclohexylphosphine which prevents any catalysis, to tri(*t*-butyl)phosphine which promotes catalysis in all reactions. Reactions catalysed by palladium acetate and tri-*o*-tolylphosphine, showed that the main phosphorus species present in solution were different, compared with using **1** as catalyst. As the reactions which were catalysed proceeded, the extent of halogenation to the palladium increased. Halogenated species present for reactions catalysed by palladacycles were of the form: (P-C)PdX(solv), $[(P\text{-}C)PdX_2]^-$ and $[(P\text{-}C)P(\mu\text{-}X)]$ (where (P-C) is the palladated ring) and $Pd(PR_3)_2(Ph)X$, $[Pd(Ph)(PR_3)(\mu\text{-}X)]_2$ and $[PdX(PR_3)(\mu\text{-}X)]_2$ for reactions catalysed by palladium acetate and phosphine ligand. It was noted for uncatalysed reactions that there was negligible or no coordination of halogen to the metal, which suggests that this is an important early step in the catalytic cycle. Enforced, since heating the catalytic species (**1**) with PhI led to a stable mixture of species, whilst heating with alcohol led to decomposition of the metal precatalytic complex and liberation of free phosphine. Also, $Pd(P^tBu_3)_2$ was isolated from the PhBr reaction catalysed by $Pd(OAc)_2$ / P^tBu_3 and characterised by X-ray crystallography.

Contents

Abstract i

Contents ii

Abbreviations viii

Key to compounds ix

Acknowledgements x

Chapter 1 – Introduction 1

1.1 Catalysis 2

1.1.1 Heterogeneous and Homogeneous Catalysts 2

1.1.2 Palladium and phosphine use in homogeneous catalysis 3

1.1.3 Palladacycles 4

1.2 The Heck reaction 7

1.2.1 The palladium (II) - palladium (0) catalytic cycle 7

1.2.2 The palladium (II) - palladium (0) catalytic cycle stabilised by phosphine ligands 9

1.2.3 The palladium (II) - palladium (IV) catalytic cycle 10

1.3 The Heck reaction studied 13

1.3.1 Choice of catalyst 14

1.4 Aim of research 16

1.5 References 18

Chapter 2 –Experimental 21

2.1 Introduction 22

2.2 X-ray Absorption Fine Structure (XAFS) 22

2.2.1 Synchrotron radiation 22

2.2.2 X-ray spectroscopy 23

2.2.3 Theory of XAFS 24

2.2.4 X-Ray Absorption Near Edge Structure (XANES) 26

2.2.5 Multiple scattering 26

2.2.6 EXAFS / Quick EXAFS (QEXAFS) experimental arrangement 27

2.2.7 Energy Dispersive EXAFS (EDE) 29

2.2.7.1 Advantages and disadvantages of EDE 30
2.2.7.2 Acquisition times 30
2.2.8 Sampling arrangement 32
2.2.9 Procedural differences 33
2.2.10 Data analysis 34
2.2.10.1 I_o and I_t 34
2.2.10.2 Background subtraction 35
2.2.10.3 Model fitting 37
2.3 Matrix Assisted Laser Desorption/Ionisation (MALDI) 43
2.4 Experimental 44
2.4.1 NMR analysis 44
2.4.2 MALDI 45
2.4.3 XAFS analysis 45
2.5 References 46

Chapter 3 - Reactions of palladium acetate with trialkyl and triarylphosphines 48

3.1 Introduction 49
3.2 Preparation and characterisation of species **1** 50
3.2.1 XAFS analysis of species **1** in solution 50
3.2.1.1 Background subtraction 51
3.2.1.2 Curve fitting 52
3.2.2 XAFS analysis of species **1** in the solid state 57
3.2.3 Conclusions 61
3.3 Comparison of the different XAFS techniques for species **1** 62
3.4 Heating species **1** 64
3.5 Formation reaction of species **1** 66
3.5.1 *In situ* NMR 66
3.5.2 EDE study of the formation of species **1** 67
3.5.3 EDE study of the formation of species **1** with a reduced phosphine concentration 71
3.6 Reactions between $Pd(OAc)_2$ and other tertiary phosphine ligands 72
3.6.1 Reaction between $Pd(OAc)_2$ and PCy_3 72
3.6.2 Reaction between $Pd(OAc)_2$ and P^tBu_3 76

3.6.3 Reaction between $Pd(OAc)_2$ and PPh_3 80
3.7 Conclusions 82
3.8 Experimental 84
3.9 References 85

Chapter 4 - The Heck reaction using preformed palladacycles 86
4.1 Introduction 87
4.2 XAFS standards 88
4.2.1 Synthesis and EXAFS analysis of species **3b** (*trans*-di(*μ*-bromo)-bis [*o*-(di-*o*-tolylphosphino) benzyl] dipalladium (II)) 89
4.2.2 QEXAFS analysis of species **4b** 91
4.2.3 Comparison of the XAFS for species **3b** and **4b** 93
4.2.4 QEXAFS analysis of species **4a** 94
4.2.5 QEXAFS analysis of species **4c** 96
4.2.6 Summary 98
4.3 Investigation of the Heck reaction between halobenzenes and 2-methylprop-2-en-1-ol, catalysed by species **1** 99
4.3.1 Investigation of the Heck reaction between methallyl alcohol and iodobenzene, catalysed by species **1** 99
4.3.1.1 NMR analysis 99
4.3.1.2 Palladium K-edge QEXAFS analysis 103
4.3.1.3 Iodine K-edge QEXAFS analysis 111
4.3.1.3a Reaction start 111
4.3.1.3b Reaction end 112
4.3.1.3c *In situ* QEXAFS experiments on the PhI system 114
4.3.1.4 The Heck reaction excluding methallyl alcohol or iodobenzene 119
4.3.1.4a NMR studies 119
4.3.1.4b XAFS analysis of the Heck reaction excluding PhI 120
4.3.1.4c Using this information to facilitate analysis of the Heck reaction 122
4.3.1.5 Conclusions 124
4.3.2 Investigation of the Heck reaction between methallyl alcohol and bromobenzene, catalysed by species **1** 126
4.3.2.1 NMR analysis 126

4.3.2.2 QEXAFS analysis 130
4.3.2.3 Summary 133
4.3.3 Investigation of the Heck reaction between methallyl alcohol and chlorobenzene, catalysed by species **1** 134
4.3.3.1 NMR results 134
4.3.3.2 XAFS analysis 137
4.3.4 Conclusions 139
4.4 Analysis of the Heck reaction with the bromine bridged palladacycle (**3b**) as catalyst 140
4.4.1 Analysis of the reaction between iodobenzene and methallyl alcohol, with species **3b** as catalyst 140
4.4.1.1 NMR 140
4.4.1.2 QEXAFS analysis - Start of reaction 142
4.4.1.3 QEXAFS analysis - End of reaction 144
4.4.2 Analysis of the reaction between bromobenzene and methallyl alcohol, with species **3b** as catalyst 146
4.4.2.1 NMR results 146
4.4.2.2 QEXAFS analysis 147
4.4.3 Analysis of the reaction between methallyl alcohol and chlorobenzene, with species **3b** as catalyst 150
4.4.3.1 NMR results 150
4.4.3.2 XAFS analysis 151
4.4.4 Summary from the Heck reactions using species **3b** as catalyst 153
4.5 Conclusions 154
4.6 Experimental 156
4.6.1 Preparation and characterisation of *trans*-di(μ-bromo)-bis[*o*-(di-*o*-tolylphosphino) benzyl] dipalladium (II) (**3b**) 156
4.7 References 157

Chapter 5 - The Heck reaction catalysed by palladium acetate and triaryl and trialkylphosphines 158
5.1 Introduction 159
5.2 Investigation of the Heck reaction with palladium acetate as catalyst 160
5.2.1 NMR analysis of the Heck reactions 160

5.2.2 X-Ray crystallography analysis of the iodobenzene reaction 160
5.2.3 XAFS analysis of the iodobenzene reaction 161
5.2.4 QEXAFS analysis of the PhCl and PhBr reactions 163
5.2.5 Conclusions on palladium acetate as catalyst 166
5.3 Investigation of the Heck reaction catalysed by palladium acetate and triphenylphosphine 167
5.3.1 Previous work on the iodobenzene reaction 167
5.3.2 Phosphorus NMR analysis of the iodobenzene reaction 168
5.3.3 QEXAFS analysis of the PhI experiment 170
5.3.4 QEXAFS analysis of the bromobenzene reaction 173
5.3.5 Conclusions on palladium acetate and triphenylphosphine as catalyst 175
5.4 Investigation of the Heck reaction with tri-*o*-tolylphosphine and palladium acetate as catalyst 176
5.4.1 NMR analysis of the Heck reactions 176
5.4.1.1 Phosphorus NMR analysis of the iodobenzene reaction 176
5.4.1.2 Phosphorus NMR analysis of the bromobenzene reaction 177
5.4.1.3 Phosphorus NMR analysis of the chlorobenzene reaction 178
5.4.2 Conclusions 179
5.5 Investigation of the Heck reaction with tri-*t*-butylphosphine and palladium acetate as catalyst 180
5.5.1 Phosphorus NMR analysis on the Heck reactions 180
5.5.2 X-ray crystallography analysis of crystals obtained from the bromobenzene reaction 182
5.5.3 QEXAFS analysis of the PhI reaction 183
5.5.4 QEXAFS analysis on the iodobenzene Heck reaction (excluding methallyl alcohol) 187
5.5.5 QEXAFS analysis of the bromobenzene reaction 188
5.5.6 QEXAFS analysis of the chlorobenzene reaction 191
5.5.7 Conclusions 192
5.6 An attempt to catalyse the Heck reaction with palladium acetate and tricyclohexylphosphine 194
5.6.1 NMR analysis of the Heck reactions 194
5.6.2 QEXAFS analysis of the iodobenzene reaction 196
5.6.3 QEXAFS analysis for the bromobenzene and chlorobenzene reactions 198

5.6.4 Conclusions 201
5.7 Investigation of the Heck reaction with tri(1-naphthyl)phosphine and palladium acetate as catalyst 202
5.7.1 Phosphorus NMR analysis of the iodobenzene Heck reaction 202
5.7.2 Matrix Assisted Laser Desorption Ionisation (MALDI) mass spectroscopy 203
5.7.3 QEXAFS analysis of the iodobenzene reaction 204
5.7.4 Conclusions 207
5.8 Investigation of the Heck reaction with tri(*o*-methoxyphenyl)phosphine and palladium acetate as catalyst 208
5.8.1 Phosphorus NMR analysis 208
5.8.2 MALDI analysis of the iodobenzene reaction 209
5.8.3 QEXAFS analysis of the iodobenzene reaction 210
5.8.4 Conclusions 212
5.9 Conclusions 213
5.10 References 215

Chapter 6 – Conclusions 216

Appendix 219
A.1. X-ray crystallography data for $Pd(P^tBu_3)_2$ (section 5.5.2) 220

Abbreviations

EDE	Energy Dispersive EXAFS
EXAFS	Extended X-ray Absorption Fine Structure
MALDI	Matrix Assisted Laser Desorption/Ionisation
QEXAFS	Quick EXAFS
RTP	Room Temperature and Pressure
w.r.t	with respect to
XANES	X-ray Absorption Near Edge Structure

AcO	CH_3CO_2
^{t}Bu	Tertiary butyl
Cp	η-C_5H_5
Cy	*c*-C_6H_{11}
dba	Dibenzylidene acetone
DMA	N,N-Dimethylacetamide
DMF	Dimethylformamide
Methallyl alcohol	2-methylprop-2-en-1-ol
NMP	1-Methyl-2-pyrrolidinone
Np	1-naphthyl
PhCl	Chlorobenzene
PhBr	Bromobenzene
PhI	Iodobenzene
$Pd(OAc)_2$	Palladium acetate
μ	Bridging

Key to compounds

1

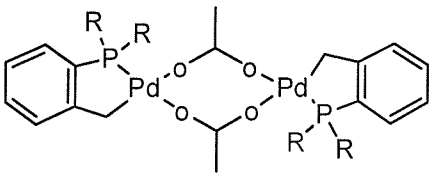

2

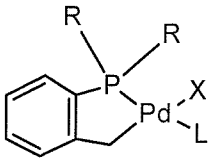

3

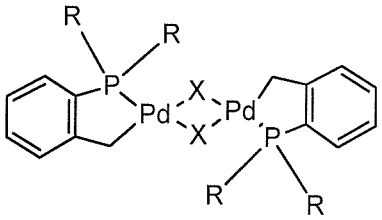

4

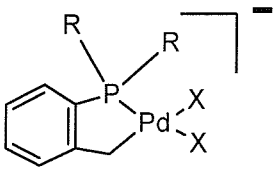

L = solvent molecule

R=*o*-tolyl

a (X = I), **b** (X = Br) and **c** (X = Cl)

Acknowledgements

I would firstly like to thank my supervisor Professor John Evans for all his support, advice and guidance during my time in Southampton. Without him this body of work would not have come to fruition.

I thank the EPSRC for a studentship during my time in Southampton and to Daresbury Laboratories and the ESRF for the use of their facilities for XAFS work.

Special thanks must go to my group over the years. Pete must get the first mention, just for being Pete. His enthusiasm and knowledge of computers has eventually made my life easier and produced many moments of amusement. Thanks to Sandra for her help, vitality and assistance over the years (not necessarily with chemistry) and to Steve for his help with chemistry and drinking. Also special thanks to Mark, Bhav, Bashya, Daryl, Ship, Tom, Sergi and the others for helping me over the years in one way or another (be it alcoholic or more functional). The final group member to thank is Brenda, for obtaining my results.

Other special thanks must go to people past from the 2nd and 3rd floor, especially Nick (Holmes) and Fiona for many philosophical nights over a few glasses of wine. Also people present, especially Colin, Matt and Vince for their help and creativity towards my viva celebrations (+ a couple of drinking sessions) and Rob, John Joy and the Weller group, for keeping me occupied in the Staff Club.

Other thanks go to the members of Stanley, for many a fun hour spent in the freezing cold at Wide Lane. My housemates for making my home life very interesting, in many respects. My family, for being my family. Sarah for her many words of wisdom and humour. Finally, a few other people, whom will remain anonymous.

A very big thanks to the people at ID24 whom made my few months at the ESRF very enjoyable. Especially the Mediterranean connection, whom kept me on my toes and gave me a good insight into their way of life. I must add a special thanks to Sakura and Sofia, whom are definitely the most attractive supervisors, I've had the pleasure to work with (sorry John).

Finally, if you have to read this, you must have been very bad in your last life!

Chapter 1

Introduction

1.1 Catalysis

A catalyst accelerates the rate of a reaction towards equilibrium, without itself being used during the reaction. The cycle of reactions that consume reactants, form products and regenerate the catalytic species is called catalysis. The catalyst will change form during the steps in the cycle, and in any side reactions. If any of the side reactions are not completely reversible then the catalyst will decompose. Catalysts lower the activation energy by opening a lower activation pathway. Usually the change in the activation entropy becomes more negative, because the transition metal assembles the reagents stepwise. If alternative routes exist, a catalyst can enhance product selectivity by enhancing just one of the competing reaction sequences.

The requirements for a successful catalytic process:[1]

- The reaction being catalysed must be thermodynamically favourable.
- The reaction being catalysed must run at a reasonable rate.
- The catalyst must have an appropriate selectivity toward the desired product.
- The catalyst must have a lifetime long enough to be economical.

The transition metal in the catalyst brings the reactants into close proximity to promote the reaction. It can do this by one of the reactants co-ordinating to the transition metal. The active catalytic system must contain a vacant co-ordination site or be able to generate one in the first dissociation step.[2]

Catalysts are widely used in nature, in industry and in the laboratory. It is estimated that they contribute to one-sixth of the value of all manufactured goods in industrialised countries. Catalysts are used in industry to increase yields and to reduce reaction time and conditions (e.g. temperature and pressure). This saves the industrial companies time and money.

1.1.1 Heterogeneous and Homogeneous Catalysts

A heterogeneous catalyst is in a different phase to the reactants while a homogeneous catalyst is in the same phase. In a heterogeneous catalysed system the vacant co-ordination

site is located at the phase boundary and only the surface atoms are catalytically active. Heterogeneous catalysis strongly dominates the industry at around 85% of all known catalytic processes.[3]

The impact of homogeneous catalysis on industrial process technology is growing constantly. This is because more is being discovered about organometallic compounds and new knowledge about structure and reactivity has created new catalytic processes in industry, or has re-established old catalytic features under improved conditions.

Homogeneous catalysts have several advantages over heterogeneous catalysts. Ligand variation can make the homogeneous catalyst tailor-made so high specificity is achieved and the reaction can often be carried out at low temperatures.[2] The mechanism of homogeneous catalysis is more accessible than that of heterogeneous catalysis because the interpretation of the rate data is frequently easier and species in solution are simpler to characterise than those on a surface. It is also possible to influence the steric and electronic properties of these molecularly defined catalysts and to optimise the homogeneous catalyst step-by-step for a particular problem.

The major disadvantage of homogeneous catalysis compared to heterogeneous catalysis is the difficulty of separation and recycling. This is necessary as the transition metals used are usually expensive. There are ways of overcoming this problem, higher reaction temperatures or polymer supported catalysts could be used. Research is aiming to try and develop methods for recycling the catalyst without the need of recovery each time.

1.1.2 Palladium and phosphine use in homogeneous catalysis

Palladium and phosphorus complexes are used extensively as homogeneous catalysts. This is because the phosphine ligands can stabilize low and high oxidation states of palladium, because they are σ donors and π acceptor ligands. A few of the many precursors and reactions it has catalysed are:

- Bis(tri-*t*-butylphosphine)palladium (0) to catalyse the Negishi cross-coupling of aryl and vinyl chlorides (e.g. R-ZnCl + R'-Cl ⟶ R-R' + $ZnCl_2$)[4]
- Tetrakis(triphenylphosphine)palladium (0) for various cross coupling reactions (e.g. R^1-X + R^2-SnR_3⟶ R^1-R^2 + X-SnR_3)[5]
- Palladium (II) acetate for various cross coupling reactions (e.g. RX + R^1BX_2⟶R-R^1 + BX_3)[6]
- *Trans*-dichlorobis(triphenylphosphine) palladium (II) for the double allylation of activated olefins[7]
- *Trans*-di(u-acetato)-bis[*o*-(di-*o*-tolylphosphino)benzyl] dipalladium (II) (species **1**) for various cross coupling reactions[8]

The majority of these catalysts have also been used to catalyse the Heck reaction (see section 1.2).

1.1.3 Palladacycles

Palladacycles can be used as catalysts for various reactions. The chemistry of palladacycles is very rich, launched by Cope[9] in 1965. The assumed mechanism of cyclopalladation for an amination reaction is shown in figure 1.1. After initial coordination of the amine ligand[10,11] via its donor atom to the metal, there is electrophilic attack by the palladium on the methyl group and reductive elimination of HOAc (figure 1.1).

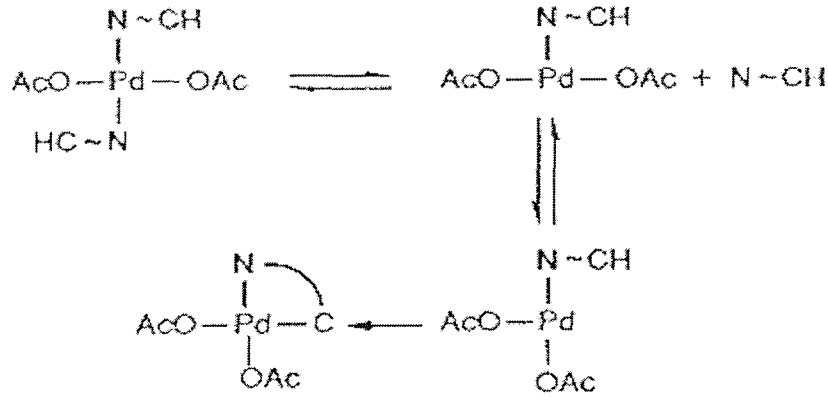

Figure 1.1 Mechanism of cyclopalladation for an amination reaction

Shaw *et al*[12] prepared the first cyclopalladated complex with phosphorus in 1972 $[Pd_2Cl_2(CH_2C_6H_4PBu^t_2)_2]$ was formed by the reaction of di-*t*-butyl-*o*-tolylphosphine and sodium tetrachloropalladite (II). In general orthopalladation occurs when a five membered ring can be formed. The precise nature of the reaction is not clear, since experiments with chiral phosphines lead to different results, depending on the reaction conditions.[13] Steric factors seem very important in the palladation of bulky phosphines; as one of the groups is forced sufficiently close to the palladium for metallation to be favoured

More recently Hermann reported the crystal structure of a phosphorus palladacycle **1**[14] formed by the reaction of palladium acetate ($Pd(OAc)_2$) and tri-*o*-tolylphosphine (P(*o*-tolyl)$_3$), shown in figure 1.2.

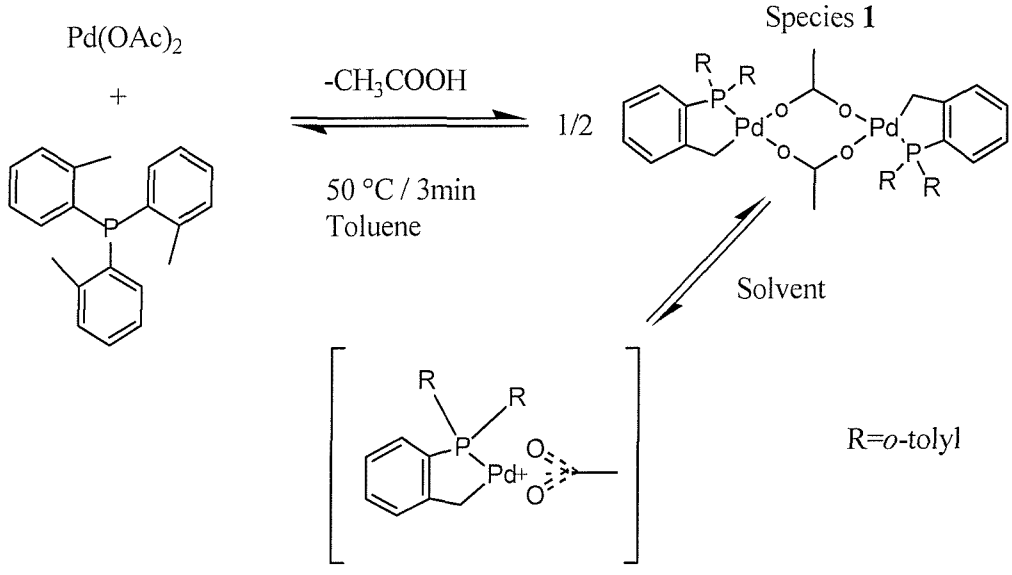

Figure 1.2 Formation of species 1 and structure in solution

Species **1** and acetic acid (by product) are formed by heating the reactants in toluene at 50 °C for three minutes. In solution it is hypothesised that there is a monomer / dimer equilibrium present since the phosphorus (^{31}P) NMR spectrum gives a broad peak at 35.4 ppm. This species is very easily converted into the halogen bridged palladacycles by stirring **1** with the appropriate tetrabutylammonium halide (iodine derivative **3a**, bromine derivative **3b** and chlorine derivative **3c**), or the monomer by reaction with excess tetrabutylammonium halide (iodine derivative **4a**, bromine derivative **4b** and chlorine derivative **4c**), shown in figure 1.3. Species **2a**, **2b** and **2c** are formed by the coordination of solvent molecules to the palladium.

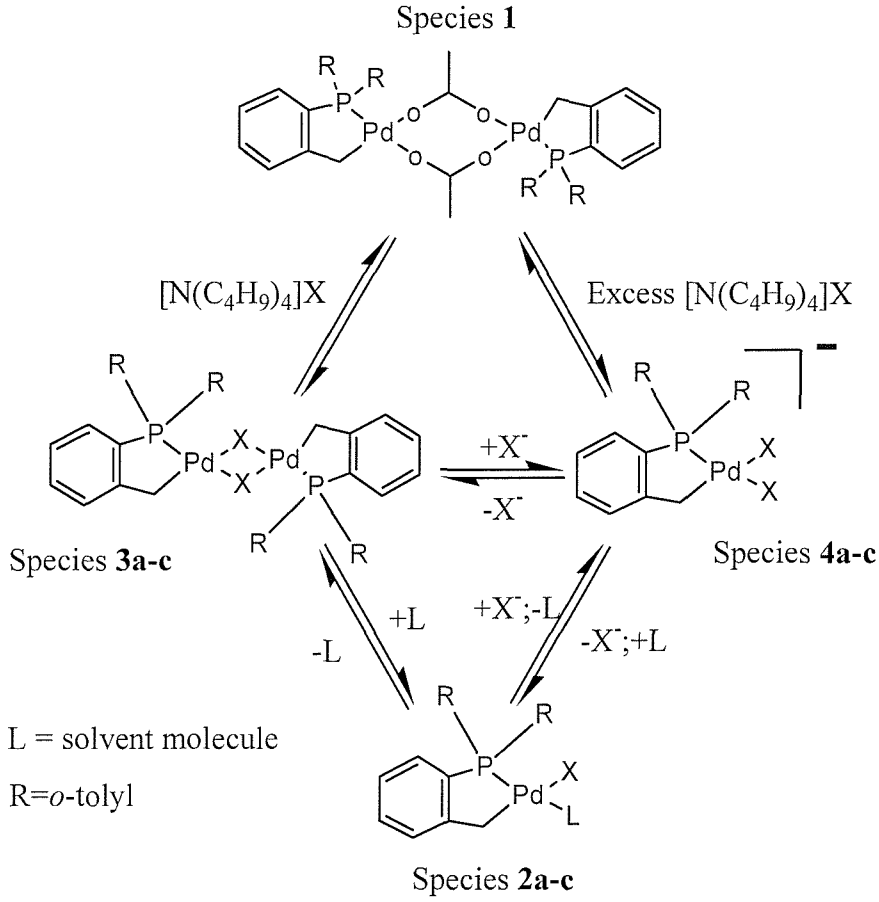

Figure 1.3 The reaction of species 1 with tetrabutylammonium halide

Species **1** is a very good catalyst for the Heck reaction (section 1.2) as regards stability, lifetime and turnover numbers, as well as enabling the activation of chloroarenes. Previous work has been undertaken using this catalyst in the Heck reaction[15,16] and it has been reported to have far superior turn over numbers compared with most conventional catalysts. Many cyclopalladated[17] or bidentate[18] species seem to have very high turn over numbers compared with more conventional catalysts

Kinetic studies[19] have shown that standard '*in situ*' catalysts are rapidly deactivated at temperatures above 120°C (normal Heck reaction temperatures). This is due to P-C bond cleavage during the formation of the arylpalladium (II) halide (section 1.2). This also causes Pd deposits, as the cleavage causes depletion of the catalyst stabilising phosphine. The accelerating effect of the *o*-tolyl groups in the Heck coupling, were initially explained by the steric effect of the *ortho* substitution stopping quaternization of the phosphorus atom, and excluding palladacycles as active species, which has now been refuted.[14]

1.2 The Heck reaction

The formation of carbon-carbon and carbon-nitrogen bonds plays an important role in the synthesis of organic chemicals. Palladium complexes catalyse a number of transformations leading to the formation of carbon-carbon bonds;[20] one of them is the Heck reaction. The Heck reaction, the palladium catalysed arylation or alkenylation of alkenes is shown in figure 1.4 (discovered by R.F. Heck in the sixties).[21]

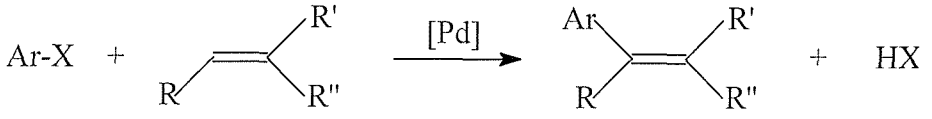

Figure 1.4 The Heck reaction of aryl or alkenyl halides with alkenes.

1.2.1 The palladium (II) - palladium (0) catalytic cycle

The broad scope of the Heck and related reactions such as Stille, Suzuki, Kumada, Negishi, and amination reactions has been partly responsible for the huge amount of interest in the area.[22,23] Although there has been a great deal of research, the full scope and mechanisms of these reactions still have many unknowns. The general accepted catalytic cycle for a reaction catalysed by palladium acetate is shown in figure 1.5.

Heck proposed the basic mechanism which started with the palladium (II) acetate being reduced to a palladium (0) species. The R'-X species oxidatively adds to this to create a new palladium (II) species. The olefin inserts into the Pd-R' bond (with the palladium coordinating to the least substituted carbon of the double bond). The required olefin is then eliminated from the palladium complex and reductive elimination of HX returns the palladium to its original Pd (0) species.

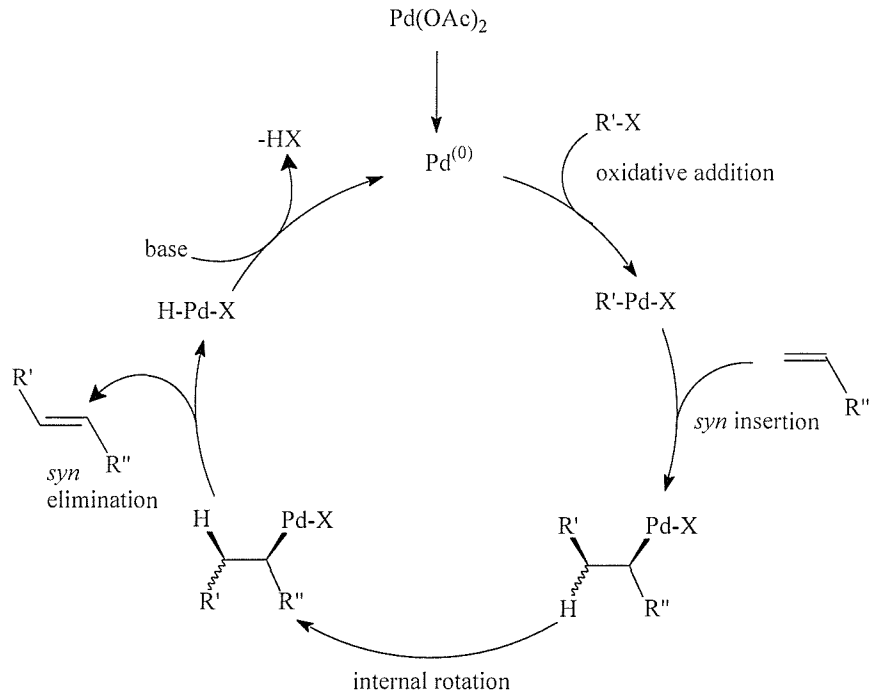

Figure 1.5 The Heck reaction catalysed by palladium acetate

This mechanism is still generally accepted by most, as a suitable general mechanism, but it does not explain the wide variety of different complexes that can act as effective pre-catalysts. Questions that still need to be answered are:

- Is the reaction taking place in solution (homogeneous) or on the surface of solid particles (heterogeneous) or can it run under both regimes under different conditions?
- What is the active catalyst?
- What is the operating mechanism?

Due to the diverse catalytic permeations available from all the precatalytic species used in literature these questions will not have the same answers and the solutions almost definitely are not simple. Other metals are also known to facilitate the same transformations.[24]

1.2.2 The palladium (II) - palladium (0) catalytic cycle stabilised by phosphine ligands

Phosphine ligands are used extensively in the Heck reaction to improve catalysis and some conclusions have been drawn on the mechanism.[21,22] It is thought that this is achieved by stabilising the Pd (0) species and preventing decomposition to palladium black. Therefore the active Pd(0) species at the start of catalysis is thought to be the 14 electron species PdL_2 (where L is usually a monodentate or bidentate phosphine).[25] These phosphine ligands are coordinated through the whole of the catalysis mechanism, which ensure the palladium is four coordinate through the majority of the cycle. Otherwise the cycle is the same as the cycle hypothesised for the Pd(0) Pd (II) scheme. The choice of the phosphine is very important to the activity of the catalytic system. Some phosphines promote activity presumably by stabilising the palladium (0) species, but also some hinder catalysis.

But, the start of the Heck reaction between $Pd(OAc)_2$ and PPh_3 has been investigated and the mechanism for the first step is shown in figure 1.6.[26] This does not agree with the afore mentioned hypothesised cycle, which again shows that the catalytic cycle is not facile.

$$Pd^{II}(OAc)_2 + 2PPh_3 \longrightarrow Pd^{II}(OAc)_2(PPh_3)_2 \qquad \text{fast (1)}$$

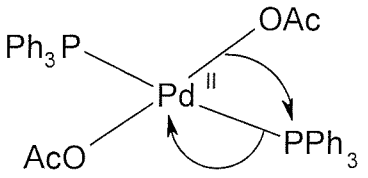

$$\longrightarrow \text{“}Pd^{0}(PPh_3)(OAc)^{-}\text{”} + AcO\text{-}PPh_3^{+} \qquad \text{slow (2)}$$

$$2\text{“}Pd^{0}(PPh_3)(OAc)^{-}\text{”} \longrightarrow [Pd^{0}(PPh_3)(OAc)]_2^{2-} \qquad \text{fast (3)}$$

Figure 1.6 Mechanism for the first step of the Heck reaction catalysed by palladium acetate and triphenylphosphine

The slow reaction (2) is the rate-determining step. The “$Pd^{0}(PPh_3)(OAc)^{-}$” then reacts with $2PPh_3$ to form $Pd^{0}(PPh_3)_3(OAc)^{-}$. This consequently undergoes oxidative addition with an aryl halide (ArX). However this does not yield the expected $ArPdX(PPh_3)_2$ complex but instead the product is $ArPd(OAc)(PPh_3)_2$.[27] The rate of this oxidative addition is higher when the triarylphosphine is substituted by an electron donating group and when the phosphine is more basic.[28]

If there is water in the reaction it converts the intermediate phosphonium salt into the phosphine oxide as in the Mitsunobu reaction.[29] This can happen as shown in figure 1.7:

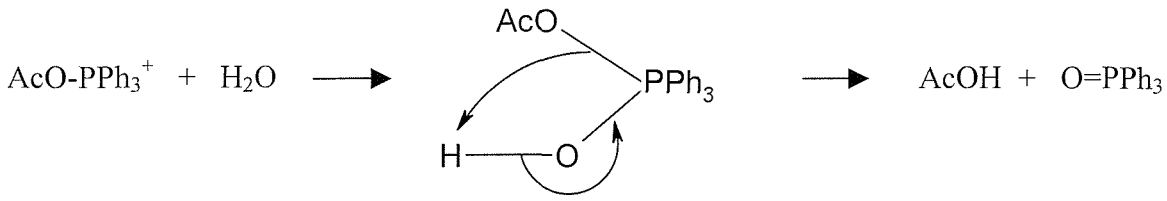

Figure 1.7 Phosphine Oxide Reaction

The slow intramolecular step (2), mentioned above is a reversible reaction that could be shifted to the formation of the palladium(0) complex by the reaction of water with the phosphonium salt.[30]

This shows there is a great complexity in the palladium acetate and triphenylphosphine reaction. This situation is further complicated by the wide range of ligands that act as homogeneous catalysts as well as the number of heterogeneous systems being able to perform effectively.[31,32] Ligands on palladium that have been used in the Heck and similar reactions include a range of pincer tridentate ligands,[33,34,35] cyclopalladated phosphines,[36,37,38] cyclopalladated phosphites,[39] cyclopalladated imines,[40] bidentate bis carbenes,[41] mixed donor bidentate carbenes,[42] monodentate carbenes,[43,44] monodentate phosphines[45,46,47,48] and bidentate phosphines.[18]

1.2.3 The palladium (II) - palladium (IV) catalytic cycle

It has also recently been suggested that the catalyst does not go via a palladium (0) intermediate, but the palladium (II) precursor is initially oxidise to a palladium (IV) species. The catalytic cycle or a palladacycle is shown in figure 1.8.[36]

This cycle involves (i) the attack of the coordinated olefin by a nucleophile, (ii) the oxidative addition of ArX, (iii) the elimination of the nucleophile, (iv) the insertion of Ar into the olefin, and (v) β-hydride elimination followed by (vi) the dissociation of the product followed by the removal of the hydride by the base.

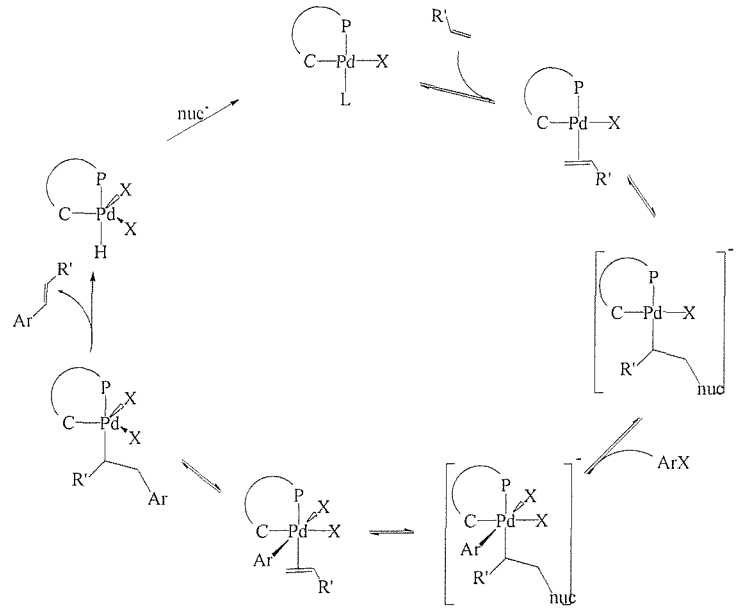

Figure 1.8 The catalytic cycle proposed by Shaw *et al.*[36] following a palladium (II)-palladium (IV) cycle with a bidentate palladacycle (nuc = nucleophile (Br^-, OH^-)).

There has been much debate over this newly suggested mechanism. The proposal is also supported since it is known that Pd(IV) complexes are known to be stable under certain reaction conditions.[49]

Hermann has reported on work he has carried out on an aryl bromide system.[37] He has reported that oxidative addition of the aryl bromides was only observed upon alkene addition, implying that the rate determining step is the coordination of the alkene. The only species detected *in situ* using phosphorus NMR spectroscopy was **1**, **2b** and **3b**. No formation of Pd(0) or Pd(IV) complexes oxidised by products of any kind were detected.

Recently Hermann reported that for his experiments that palladium (IV) intermediates can be ruled out for the activation of aryl bromides.[50] He proposed the formation of a highly active, anionic palladium (0) species (see figure 1.9)

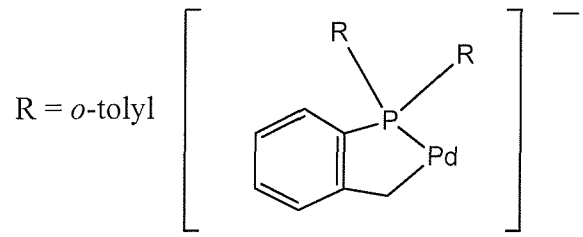

Figure 1.9 Proposed catalytic species for Heck reaction catalysed by species 1

1.3 The Heck reaction studied

The Heck reaction chosen for study involved the coupling of halobenzenes (iodobenzene (PhI), bromobenzene (PhBr) and chlorobenzene (PhCl)) with methallyl alcohol (2-methylprop-2-en-1-ol) to give an aldehyde product (1-phenyl-2-methyl-propanal), see figure 1.10. Chalk and Magennis started research on the PhI and PhBr systems with different isomers of methallyl alcohol catalysed by palladium chloride in the presence of sodium bicarbonate.[51,52] The work showed that the metal catalysed both reactions. This body of work was extended by Meopolder and Heck[53] with palladium acetate ($Pd(OAc)_2$) as catalyst. In the PhI reaction 1-phenyl-2-methyl-propanal was produced with a 96% yield. The other product formed in the reaction is due to addition of the benzene ring to the other end of the double bond in the alcohol to give $CH_3C(CH_3)(Ph)COH$, with a 4% yield. The palladium catalyst did not catalyse the PhBr reaction.

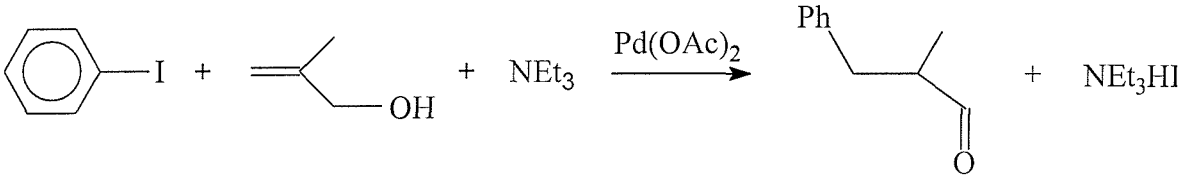

Figure 1.10 Reaction of methallyl alcohol and iodobenzene

This reaction was chosen due to its suitability for XAFS experiments:

- The reaction time is only a few hours with catalyst concentrations of 50 mM (appropriate concentrations for Extended X-Ray Absorption Fine Structure (EXAFS) techniques detection).
- The chemicals (used and synthesised) are suitable for use in the EXAFS hutch, with no requirement for a fumehood.
- N-methyl-pyrrolidinone was the solvent of choice because it had a high boiling point (necessary since the reaction was undertaken at 115 °C), had good solubility for the metal species and is a poor X-Ray absorber (compared with solvents with larger atoms than oxygen and carbon (e.g. dimethyl sulfoxide)), which is important for EXAFS analysis.

1.3.1 Choice of catalyst

Traditionally, for Heck reactions, the palladium catalytic system (originally the catalyst was palladium acetate, or more recently a mixture of palladium acetate and a phosphine) was added to the reaction vessel with reactants and base and heated to give the required product.[54,55] In this study the Heck reaction shown in figure 1.8 and the bromobenzene and chlorobenzene equivalents have been investigated,for palladium acetate as catalyst and palladium acetate 'stabilised' by triphenylphosphine, tri(*o*-tolylphosphine), tri(*tert*-butylphosphine), tricyclohexylphosphine, tri(1-naphthyl)phosphine and tri(*o*-methoxyphenyl)phosphine (the last two phosphines were only used to catalyse the iodobenzene reaction). These ligands were chosen since they encompass a variety of cone angles, include aryl and alkylphosphine ligands and cover a wide range of catalytic activity. Work has been undertaken on the catalytic properties of these phosphine to directly compare the yields for two different Heck reactions.

Phosphine ligand	Reaction 1*	Reaction 2**
Triphenylphosphine	12	13
Tri(*o*-tolylphosphine)	99	71
Tri(tert-butylphosphine)	95	83
Tricyclohexylphosphine	0	0
Tri(1-naphthyl)phosphine	96	-
Tri(*o*-methoxyphenyl)phosphine	20	24

*Heck reaction between methyl 4-bromobenzoate, butyl acrylate and sodium acetate, in DMF, catalysed by $Pd(dba)_2$ and the phosphine ligand.[56]

**Heck reaction between [3-(4-Bromophenyl)-propyl]-(2-methyl-4-*o*-tolylazo-phenyl)-*N*-(*tert*-butoxycarbonyl)-amine and dimethyl-(5-{[methyl-(4-vinyl-phenyl)-amino]-methyl}-napthalen-1-yl)-amine in DMF, catalysed by CpPd(allyl) and ligand.[57,58]

Table 1.1 The GC percentage yields of product for the two different Heck reactions, with the phosphine ligand as shown.

Both reactions (table 1.1) shown similar trends. The two alkyl phosphine ligands show the best (tri(*tert*-butylphosphine)) and the worst (tricyclohexylphosphine) activity. Independent studies[59] have corroborated that the tri(*tert*-butylphosphine) palladium complexes are unusually active catalysts for Heck coupling of aryl chlorides. The high activity of the *tert*-butyl substituted bis phosphines has been ascribed to their strongly electron donating character, which accelerates oxidative addition.[60] The steric demand of the phosphine ligands could also stabilise three coordinate complexes, which could increase their concentration and increase the olefin insertion process.

For the triphenylphosphine, tri(*o*-tolylphosphine) and tri(1-naphthyl)phosphine ligands, catalysis yields increase as the steric bulk in the ortho position increases, again this could be due to the larger ligands stabilising the two and three coordinated palladium complexes. The tri(*o*-methoxyphenyl)phosphine ligand agrees nicely with this trend, but there could also be strong electronic effects which need to be taken into consideration, since the methoxy ligand is an electronic withdrawing group.

The Heck reactions studied in this report were also catalysed by preformed palladacycles (species **1** and species **3b** (the bromine bridged derivative)). The use of species **1** as a catalyst meant that a direct comparison could be made with the species formed in reactions with this catalyst and with the same reactions catalysed by palladium acetate and tri(*o*-tolylphosphine).

1.4 Aim of research

The main aim of this research is to investigate the catalysis of the Heck reactions (figure 1.8) with iodobenzene, bromobenzene or chlorobenzene. The reactions were catalysed by a variety of palladium and phosphine mixtures. Carbon NMR was used to determine which reactions were catalysed and phosphorus NMR analysis was undertaken on the same samples to determine qualitatively and quantitatively the nature of the phosphine species present in the reaction solution. The information yielded was used to aid analysis of the XAFS results, but the XAFS analysis also helped to confirm or show if the phosphorus assignments were incorrect. *In situ* phosphorus NMR results were compared with *ex situ* results to establish whether the results were the same and if the *ex situ* technique was viable and that the same phosphine species were stable at lower than reaction temperatures.

Chapter 3 is concerned primarily with the formation of the palladacycle **1** from palladium acetate and tri(*o*-tolylphosphine) and its structure in solution. XAFS analysis was used to follow the reaction and also various EXAFS models were applied to the palladacycle in solution and solid state for structure determination. The remainder of the chapter entailed the investigation of the reactions between palladium acetate and various phosphine ligands, which were to be used as catalytic systems in chapter 5.

In chapter 4, analysis of the Heck reactions catalysed by preformed palladacycles (**1** and **3b**) was investigated. A QEXAFS study was taken of samples, taken from the reaction mixture during the iodobenzene reaction catalysed by **1**. Due to the XAFS beam time needed for this study, the other reactions were studied by XAFS for the reaction mixture taken from the start and the end of the reaction.

In the final results chapter (chapter 5), the same Heck reactions were again studied, but this time catalysed by palladium acetate and a variety of phosphine ligands. The first set of reactions to be investigated was using palladium acetate as a catalyst without any stabilising phosphine ligands. This was extended to the addition of triphenylphosphine (traditionally one of the main phosphine ligands of choice for the Heck reaction) to the solution. Work had already been started on the iodobenzene system catalysed by palladium acetate[61] and

palladium acetate stabilised by triphenylphosphine.[62] These investigations were expanded to include the bromobenzene and chlorobenzene reactions.

Tri(*o*-tolylphosphine) was the next ligand of choice. This was chosen to directly compare the results obtained for this ligand with the results from **1** (chapter 4). The work was completed by investigating the effect of tricyclohexylphosphine, tri(*tert*-butyl)phosphine, tri(1-naphthyl)phosphine and tri(*o*-methoxyphenyl)phosphine on the reactions. As stated earlier these were chosen due to their differing steric properties, electronic structure and catalytic activity.

1.5 References

1 D. Shriver, P. Atkins, C. Langford, *Inorganic Chemistry*, OUP, **1992**, 541.

2 C. Elschenbroich, A. Salzer, *Organometallics, 2nd Edition*, VCH Publishers Inc., New York, N.Y., **1992**.

3 W.A. Herrmann, B. Cornils, *Angew. Chem. Int. Ed. Eng.*, **1997**, *36*, 1048.

4 C. Dai, G.C. Fu, *J. Am. Chem. Soc.*, **2001**, *123*, 2719.

5 J.K. Stille, *Angew. Chem. Int. Ed.*, **1986**, *25*, 508.

6 T.I. Wallow, B.M. Novak, *J.Org. Chem.*, **1994**, *59*, 5034.

7 H. Nakamura, Jae-Goo Shim, Y. Yamamoto, *J. Am. Chem. Soc.*, **1997**, *119*, 8113.

8 L.F. Tietze, H. Schirok, *J. Am. Chem. Soc.*, **1999**, *121*, 10264.

9 A.C. Cope, R.W. Siekman, *J. Am. Chem. Soc.*, **1965**, *87*, 3272.

10 A.D. Ryabov, I.K. Sakodinskaya, A.K. Yatsimirsky, *J.Chem.Soc.Dalton.Trans.*, **1985**, 2629.

11 A.D. Ryabov, *Chem. Rev.*, **1990**, *90*, 403.

12 A.J. Cheny, B.L. Shaw, *J.Chem.Soc.,Dalton Trans.*, **1972**, 860.

13 W.A. Herrmann, M. Beller, T. Riermeier, S. Haber, H. Kleiner, *Chem. Ber.*, **1996**, *129*, 1259.

14 W.A. Herrman, C. Brossmer, C. Reisinger, T. Riermeier, K. Ofele, M. Beller, H.Fischer, *Angew. Chem. Int. Ed. Engl.*, **1995**, *34*, 1844.

15 W.A. Herrman, C. Brossmer, C. Reisinger, T. Riermeier, K. Ofele, M. Beller, *Chem. Eur. J.*, **1997**, *3*, 1357.

16 W.A. Herrmann, V.P.W. Bohm, *J.Organomet. Chem.*, **1999**, *572*, 141.

17 M. Ohff, A. Ohff, D. Milstein, *Chem. Comm.*, **1998**, 357.

18 B.L. Shaw, S.D. Perera, *Chem. Comm.*, **1998**, 1863.

19 W.A. Herrmann, C. Brossmer, K. Ofele, M. Beller, H. Fischer, *J.Organomet. Chem.* **1995**, 491, C1.

20 B. Cornils, W.A. Herrmann, *Applied Homogemeous Catalysis with Organometallic Compounds*, VCH, Weinheim, **1996**.

21 R.F. Heck, *Org. React.*, **1982**, *72*, 345.

22 A. de Meijere, F.E. Meyer, *Angew. Chem. Int. Ed. Engl.*, **1994**, *33*, 2379.

23 I.P. Beletskaya, A.V. Cheprakov, *Chem. Rev.*, **2000**, *100*, 3009.

24 S. Iyer, V.V. Thakur, *J. Mol. Cat.*, **2000**, *157*, 275.

25 W. Cabri, I. Candiani, *Acc. Chem. Res.*, **1995**, *28*, 2.

[26] C. Amatore, A. Jutand, M.A. M'Barki, *Organometallics*, **1992**, *11*, 3009.

[27] C. Amatore, E. Carré, A. Jutand, M.A. M'Barki, *Organometallics*, **1995**, *14*, 5605.

[28] R. Heck, *Acc. Chem. Res.*, **1979**, *12*, 146.

[29] A. Pautard-Cooper, A.E. Slayton, *J. Org. Chem.*, **1989**, *54*, 2485.

[30] C. Amatore, E. Carré, A. Jutand, M.A. M'Barki, *Organometallics*, 1995, **14**, 1818.

[31] A. Biffis, M. Zecca, M. Basato, *J. Mol. Cat.*, **2001**, *173*, 24.

[32] C.P. Mehnert, J.Y. Ying, *Chem. Commun.*, **1997**, 2215.

[33] M. Ohff, A. Ohff, M.E. van der Boom, D. Milstein, *J. Am. Chem. Soc.*, **1997**, *119*, 11687.

[34] E. Peris, J. A. Loch, J. Mata, R. H. Crabtree, *Chem. Commun.*, **2001**, 201.

[35] D. Morales-Morales, R. Redón, C. Yung, C.M. Jensen, *Chem. Commun.*, **2000**, 1619.

[36] B.L. Shaw, S.D. Perera, E.A. Staley, *Chem. Commun.*, **1998**, 1361.

[37] W.A. Herrmann, V.P.W. Böhn, C-P. Reisinger, *J. Organomet. Chem.*, **1999**, *576*, 23.

[38] T. Rosner, J. Le Bars, A. Pfaltz, D.G. Blackmond, *J. Am. Chem. Soc.*, **2001**, *123*, 1848.

[39] D.A. Albisson, R.B. Bedford, S.E. Lawrence, P.N. Scully, *Chem. Commun.*, **1998**, 2095.

[40] M. Nowotny, U. Hanefeld, H. van Koningsveld, T. Maschmeyer, *Chem. Commun.*, **2000**, 1877.

[41] W.A. Herrmann, M. Elison, J. Fischer, C. Köcher, G.R.J. Artus, *Angew. Chem. Int. Ed. Engl.*, **1995**, *34*, 2371.

[42] D.S. McGuinness, K.J. Cavell, *Organometallics*, **2000**, *19*, 741.

[43] D.S. McGuinness, M.J. Green, K.J. Cavell, B.W. Skelton, A.H. White, *J. Organomet. Chem.*, **1998**, *565*, 165.

[44] J. Huang, S.P. Nolan, *J. Am. Chem. Soc.*, **1999**, *121*, 9889.

[45] R. Stürmer, *Angew. Chem. Int. Ed. Engl.*, **1999**, *38*, 3307.

[46] M.G. Andreu, A. Zapf, M. Beller, *Chem. Commun.*, **2000**, 2475.

[47] A.F. Littke, C. Dai, G.C. Fu, *J. Am. Chem. Soc.*, **2000**, *122*, 4020.

[48] J.P. Wolfe, R.A. Singer, B.H.Yang, S.L. Buchwald, *J. Am. Chem. Soc.*, **1999**, *121*, 9550.

[49] A.J. Canty, *Acc. Chem. Res.*, **1992**, *25*, 83.

[50] W.A. Herrmann, V.P.W. Böhn, *Chem. Eur. J.*, **2001**, *7*, 4191.

[51] A.J. Chalk, S.A. Magennis, *J. Org. Chem.*, **1976**, *41*, 265.

[52] A.J. Chalk, S.A. Magennis, *J. Org. Chem.*, **1976**, *41*, 1206.

[53] J.B. Melpolder, R.F. Heck, *J. Org. Chem.*, **1976**, *41*, 2.

[54] H.A. Dieck, R.F. Heck, *J. Am. Chem. Soc.*, **1974**, *96*, 1133.

[55] C.B. Ziegler, R.F. Heck, *J. Org. Chem.*, **1978**, *43*, 15.

[56] K.H. Shaughnessy, P. Kim, J. F. Hartwig, *J. Am. Chem. Soc.*, **1999**, *121*, 2123.

[57] J.P. Stambuli, S.R. Stauffer, K.H. Shaughnessy, J.F. Hartwig, *J. Am. Chem. Soc.*, **2001**, *123*, 2677.

[58] J.P. Stambuli, S.R. Stauffer, K.H. Shaughnessy, J.F. Hartwig, *Supporting information*, Department of Chemistry, Yale University, P.O. Box 208107, New Haven, CT 06520-8107.

[59] A.F. Littke, G.C. Fu, *J. Org. Chem.*, **1999**, *64*, 10.

[60] B.C. Hamann, J.F. Hartwig, *J. Am. Chem. Soc.*, **1998**, *120*, 7369.

[61] V.L. Kambhampati, PhD Thesis, University of Southampton, **1998**.

[62] J. Evans, L. O'Neill, V.L. Kambhampati, G. Rayner, S. Turin, A. Genge, A.J. Dent, T. Neisus, *J. Chem. Soc., Dalton Trans.*, **2002**, 2207.

Chapter 2

Experimental

2.1 Introduction

Two classes of reactions were investigated in this thesis (chapter 1). The main class was the Heck reaction, whilst a smaller study was made on the reaction of palladium acetate with different phosphine ligands. The three main physical techniques used to elucidate information on the species present during the reactions were: X-ray Absorption Fine Structure Spectroscopy (XAFS), Nuclear Magnetic Resonance (NMR) and Matrix Assisted Laser Desorption / Ionisation mass spectroscopy (MALDI).

2.2 X-ray Absorption Fine Structure (XAFS)

XAFS has been described in much detail in the literature, in the forms of a monograph,[1] thesis[2] and review.[3] The two websites of the scientific institutions used to study the XAFS; the European Synchrotron Radiation Facility (ESRF) in Grenoble, France[4] and the Synchrotron Radiation Source at the Daresbury Laboratories (SRS), Warrington, England,[5] are also extremely good sources of information (about the capabilities of each site and also a wealth of information about the technique and its uses), so only the basics of the technique will be covered in this section.

XAFS is used to study the local structure up to 5 Å from the absorbing atom. It is element specific and gives a picture of the local coordination. It provides information on the number and the type of neighbouring atoms and their distances from the absorbing atom. The materials studied can be presented to the X-ray in any form, as crystalline solids, amorphous solids, solutions or gases. However, as XAFS gives equal weighting to all absorbing atoms in a sample, the local structure information derived is an average over all the environments experienced by the excited atom.

2.2.1 Synchrotron radiation

The main disadvantage of the XAFS technique is that it is a weak phenomenon, so requires high X-ray flux to obtain a reasonable signal to noise ratio. This flux is not normally

provided by the beamstability of laboratory X-ray sources, but is available at special scientific institutions (ESRF and SRS). Synchrotron radiation is produced when charged particles (e.g. electrons) are accelerated in a magnetic field, close to the speed of light. The light produced by a synchrotron source can cover a very broad range of the electromagnetic section from IR to gamma rays. The electrons are accelerated in a three stage process, electrons are fired from a linear accelerator into a booster synchrotron, where they are accelerated close to the speed of light, they are then injected into the storage ring. Electromagnets are used to bend the path of the electrons into a circular shape, as they pass these magnets, the path of the electrons is deflected and they emit synchrotron radiation tangentially to the electron beam.

The light produced is dependent on the energy of the electron beam and the magnetic fields used to direct the beam. The wavelength of light produced is shortened, if the beam energy is increased ($E = hc/\lambda$ where E = energy, h = Planck's constant, c = the velocity of light and λ = wavelength) or if the magnetic field is increased (i.e. the beam bends more sharply, hence greater acceleration and shorter wavelength).

Radio frequency waves are fed into the electron beam to replace energy "lost" to the emitting synchrotron radiation. This enables the same electron beam to emit synchrotron radiation for many hours. Finally mirrors and monochromators are then used to select the required energies for research. The X-ray beams produced (ESRF) are about a factor of 10^{12} times brighter than those of conventional X-ray sources used in laboratories and hospitals.

2.2.2 X-ray spectroscopy

In X-ray spectroscopy the absorption of an X-ray photon excites a core electron, which is emitted resulting in the ionisation of the absorbing atoms and the production of a core-hole. The energy needed to produce the ionisation is equal to the energy difference between the initial and final states. At the ionisation energy there is a rapid increase in the absorption of the sample, which is called an absorption edge.[6] The edges are given labels from the old shell terminology of the atom: K (1s electron), L(I) (2s electron) and L(II) and L(III) (2p electron).[7] In this thesis only the palladium K edge (24.351 keV) and the iodine K edge (33.158 keV) are studied.

If the area around an absorption edge is examined, small oscillations[8] after the edge are observable, (but not for monoatomic samples),[9] which is called the XAFS region. These oscillations can be divided into two overlapping regions called the X-ray Absorption Near Structure (XANES) and Extended X-ray Absorption Fine Structure (EXAFS) regions (sinusoidal oscillations found immediately after the edge from approximately 30 eV to 1000 eV). The XAFS for a palladium foil is shown in figure 2.1, with the XANES and EXAFS regions clearly marked.

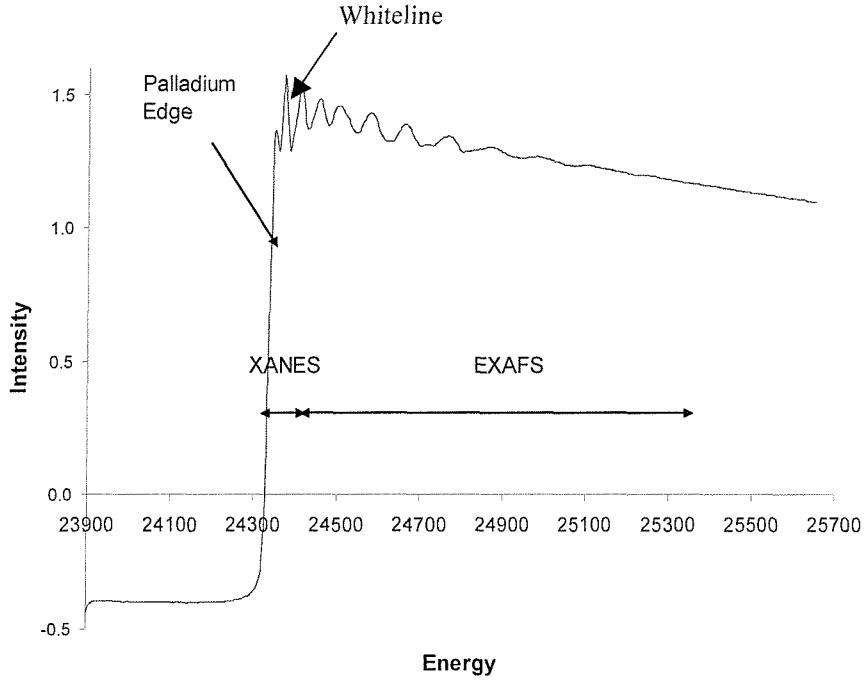

Figure 2.1 XAS of a palladium foil (K edge)

2.2.3 Theory of XAFS

A basic theory of EXAFS was formulated by Stern, Lytle and Sayers, which led to a short range single electron, single scattering theory,[10] there have since been refinements and improvements to the original theory and for practical EXAFS analysis the theory is described by Poltorak and Boronin.[11]

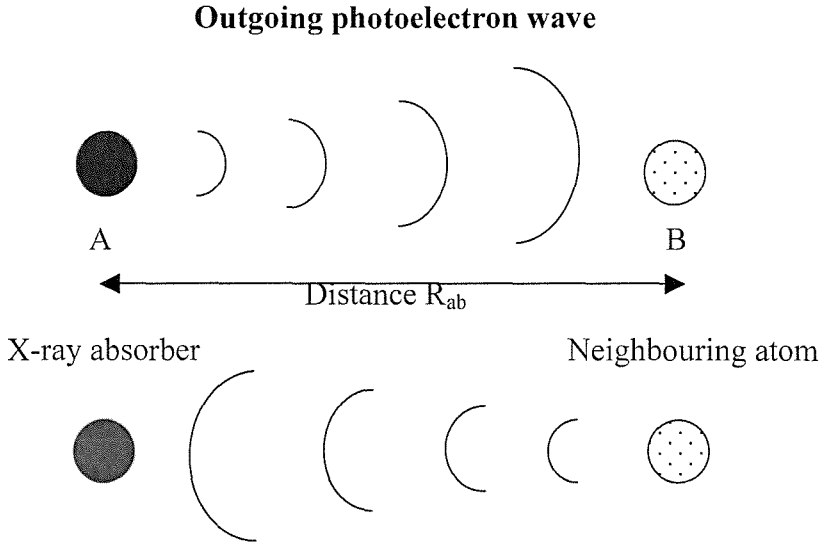

Figure 2.2 The photoelectron wave emitted from the X-ray absorber and its backscattered portion.[12]

The oscillations in figure 2.2 are due to constructive and destructive interference between the outgoing photoelectron and its backscattered proportion. The ejected photoelectron can be represented as an outgoing spherical wave originating from the X-ray absorbing atom. This backscattered electron wave may travel back through, and therefore interfere with, the excited absorbing atom resulting in the sinusoidal variation of the absorption coefficient, μ (Equation 2.1). The total absorbance $\mu(E)_x$ is represented as the following:

$$\mu(E)_x = [\mu(E)_s + \mu(E)_m + \mu(E)_0 + \mu(E)_{EXAFS}]_x \qquad \textbf{Equation 2.1}$$

where $\mu(E)_s$ is the sloping spectrometer baseline, $\mu(E)_m$ is the absorption due to the matrix in which the absorbing atom is imbedded, $\mu(E)_0$ is the absorption that would be observed for a free atom, and $\mu(E)_{EXAFS}$ is the modulation in the absorption about $\mu(E)_0$. To be able to examine the EXAFS oscillations only, it is therefore necessary to isolate the EXAFS intensity $\chi(E)$ by subtraction of the background components and normalise it with respect to the free atom absorption:

$$\chi(E) = \mu(E)_{EXAFS}/\mu(E)_0 = [\mu(E)/\mu(E)_0] - 1 \qquad \textbf{Equation 2.2}$$

The frequency of the oscillations gives the distance (~1.5 %) between the emitting atom and its neighbours, whilst the magnitude gives the co-ordination number (~15 %).[13]

2.2.4 X-ray Absorption Near Edge Structure (XANES)

Below an energy of ~60 eV the ejected electron can occupy resonant states that correspond to antibonding orbitals arising from the linear combination of atomic orbitals forming the bonds surrounding the central atom. It is these states that give rise to XANES features. Their source is physically distinct to EXAFS (which is caused by scattering effects due primarily to the atomic cores surrounding the absorbing atoms) and yield differing information. The main information that can be deduced from XANES is nonetheless complementary being predominantly due to electronic structure (oxidation states, molecular energy levels etc) rather than physical structure; the position and intensity of pre-edge features can, be related to the symmetry of the co-ordination sphere within which the absorbing atom resides.

The main problem with XANES is interpretation as this requires a detailed understanding of molecular orbital structure (not trivial in itself) which is complicated by the possibility of considerable multiple scattering events.

2.2.5 Multiple scattering

The phenomenon of multiple scattering occurs if the emitted photoelectron encounters more than one backscattering atom before returning to the absorber. If one atom is behind another, relative to the absorbing atom, this will give a significant contribution to the EXAFS. The first neighbour in the system will have a focusing effect on the photoelectron, forward scattering it with increased intensity and a change of phase. This will result in the second backscattering shell giving a greatly enhanced signal. Multiple scattering pathways have been included in an extended description of the curved wave theory,[14] while a further simplification of the theory obtained by an approximation to the wavefunction has enabled multiple scattering calculations to be included in the iterative procedure of EXAFS analysis.[15] Multiple scattering calculations are likely to be required if two different

backscattering shells are bonded to each other with a bond angle of >120 °. As the bond angle increases, the effects of multiple scattering become more pronounced, such that its inclusion in the fitting calculations will be vital for compounds containing CO as a ligand with a bond angle of 180°.

2.2.6 EXAFS / Quick EXAFS (QEXAFS) experimental arrangement

All EXAFS (and QEXAFS) experiments were carried out on Station 9.2 at the SRS operating at 2 GeV (ca. 3.20 X 10^{-10} J) and an average current of 140 mA. In a typical experiment the chosen energy range (figure 2.1) around the absorption edge is scanned and the absorption is measured. QEXAFS uses the same mechanics to obtain an EXAFS spectrum though the movement of the monochromator crystals is optimised to facilitate a rapid scanning of the energy range of interest. This means in real terms that a QEXAFS scan takes ~4-6 minutes, whilst EXAFS ~30 minutes. Unfortunately the signal to noise is reduced, therefore the data is of poorer quality and hence the data range is reduced.

On Station 9.2, the energy is selected by using a double Si(220) crystal monochromator (figure 2.3). The monochromator allows the energy of the X-ray photons passing through to be altered, allowing a set energy range to be scanned, for any given sample. The wavelength of X-rays required is selected according to Bragg's equation ($n\lambda = 2d\sin\theta$) where n is an integer (1 for the fundamental), d is the crystal spacing and θ the angle between the monochromator crystals and the beam. Light reflected off the first crystal contains higher order harmonics in addition to the fundamental. These harmonics can distort the fine structure, and are removed by slightly misaligning the second crystal (harmonic rejection). This misalignment works due to the fact that the rocking curve for higher order harmonics is narrower than that for the fundamental, resulting in a greater loss of intensity for the higher harmonics than for the fundamental reflection.

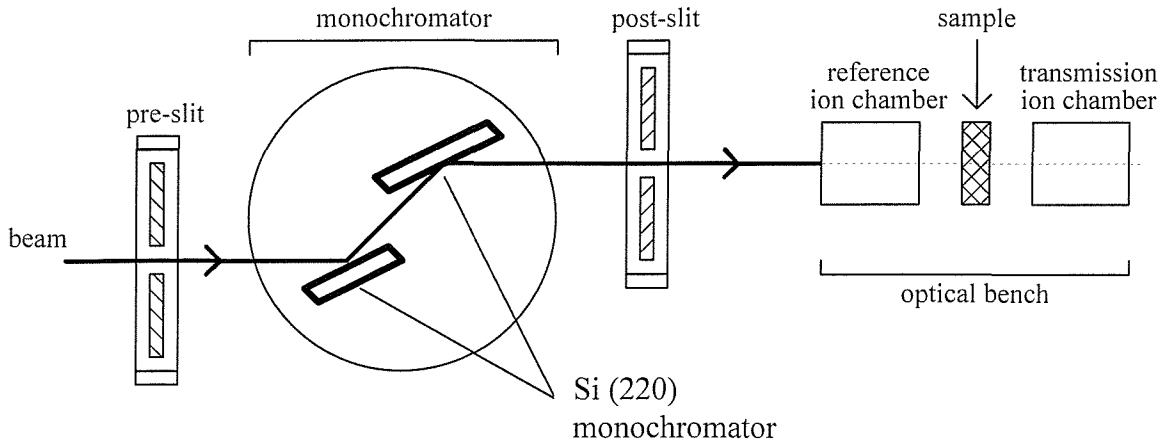

Figure 2.3 Station 9.2 schematic diagram for transmission mode detection (SRS)[16]

There are two main detection modes employed for EXAFS (fluorescence and transmission). The above figure shows the setup for transmission mode with the reference ion chamber and the transmission ion chamber in the line of the beam. In a fluorescence experiment, the sample is angled 45° incident to the beam and transmission ion chamber is replaced by a fluorescence detector which is moved perpendicular to the beam, so it can detect the fluorescence from the sample. Fluorescence detection is generally used if the metal concentration is under 25 mM, since the lowest concentration used in this thesis was 40 mM, all experiments were undertaken in transmission mode.

Therefore for a transmission experiment: the beam travels through the pre-slit, used to reduce the energy range hitting the monochromator, the double monochromator selects the correct energy and reduces the harmonics and the post-slit blocks any other energies, so ensures that only the required energy hits the sample. The beam then travels through the reference ion chamber, the sample, then the transmission ion chamber from which the change in the absorption coefficient can be calculated.

In EXAFS spectroscopy, μ, the absorption coefficient, is defined by the equation 2.3:

$$\ln (I_0 / I_t) = \mu t \qquad \textbf{Equation 2.3}$$

where I_t is the transmitted flux, I_0 is the incident flux and t is the thickness of the sample. The ion chambers are filled with different noble gas mixtures in order to get the reference and transmission chambers absorbing respectively ~20% and ~80% of the radiation. The

two electrodes in the ion chambers are connected with a high voltage power supply in order to provide a direct voltage between the two. Thus the beam intensity entering the chamber is proportional to the current generated by the ionized gas. Therefore since t is constant, the ln (I_0 / I_t) allows the measurement of the relative absorbance (μ).

2.2.7 Energy Dispersive EXAFS (EDE)

EDE is a relatively new technique and it is now possible to obtain spectra with a new detector on the millisecond timescale. The reason why the technique is considerably faster is because the double monochromator is replaced by a curved crystal, which focuses all the energies of the required spectral range, simultaneously on one finite point in space (focal spot).

EDE spectra were acquired at ID24 of the ESRF, Grenoble, operating at 6 GeV and an average current of 190 mA. The focal spot can be focussed in each dimension (vertical and horizontal) to 30 μm, but is generally only focused in the vertical plane if high brilliance is essential in the beam. It is required for high pressure experiments, but not needed for this body of work.

Therefore in a typical transmission experiment the sample is placed in the focal spot and the intensity of the different wavelengths of the beam are measured, after travelling through the sample, and the X-rays hit a phosphor screen that emits visible photons that are detected by a position sensitive Peltier cooled *Princeton* Charge Coupled Device (CCD) camera. However, since there is only one focal spot, I_0 cannot be read simultaneously with I_t. Therefore to obtain a full absorption spectrum I_0 is placed in the focal spot a spectrum is taken, then it is replaced by I_t and another spectrum is taken. As before, the full absorption spectrum is calculated by taking the natural log of I_0 divided by I_t. The experimental set up for ID24 is shown in (figure 2.4).

Since no movement of the monochromator is required, the acquisition time is determined by the X-ray intensity, and the response time of the detector, leading to a 'potential' of a millisecond acquisition timescale.[3]

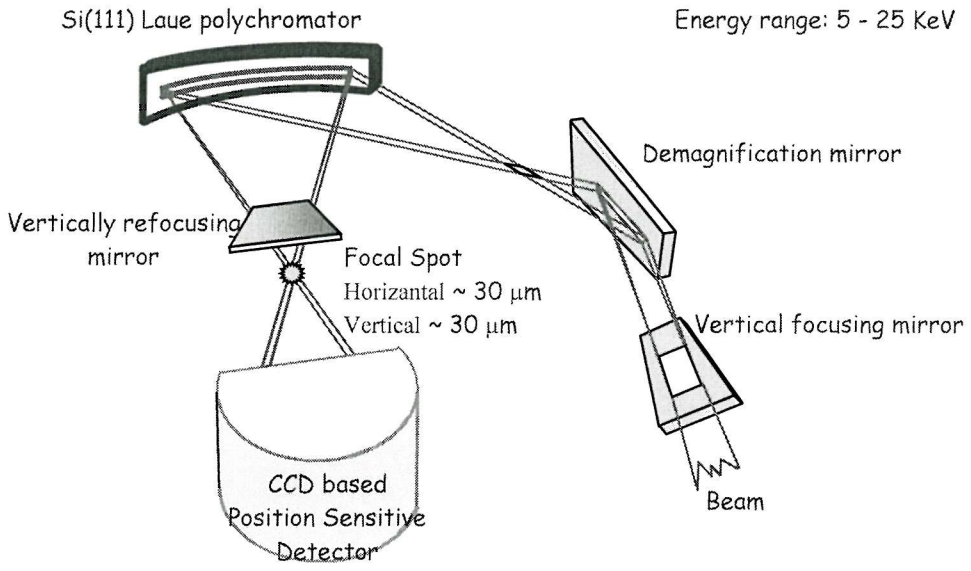

Figure 2.4 The EDE arrangement on ID24 (Grenoble)[17]

2.2.7.1 Advantages and disadvantages of EDE

There are major advantages in using EDE over more traditional scanning XAFS techniques. The main advantage is that the time resolution is only dependent on the readout speed of the detector, currently 18 spectra can be taken in 1.8 ms. Also since there is no movement of optics, the energy scale and focal spot are more stable. Finally, the spot size is considerable smaller, so only small sample volumes are required and also this enables high pressure studies (up to 100 GPa).

As expected these advantages also produce disadvantages. Since the incident and transmitted beam are not measured simultaneously, the results are highly sensitive to beam instabilities. Also fluorescence detection is not possible, so the concentrations have to be kept higher than for scanning XAFS. Finally, due to the small horizontal spot size, results are highly sensitivity to sample inhomogeneities, fortunately this is limited in solution work.

2.2.7.2 Acquisition times

There are two alternative methods of acquiring EDE, which encompass a variety of timescales. The simplest method (Standard EDE scan) yields the best data and is also the

longest. It was the favoured choice for this work, because the reaction times were comparatively long for EDE work. For each spectrum, a scan of I_0 (reference spectrum) is measured followed by I_t (sample spectrum). The CCD camera consists of 18 stripes (generally only 15 of these stripes provided reliable data), so the time taken to measure one scan for a normal experiment, with an integration time of 11 ms (considering each stripe is measured in turn), would be 18 x 11 = 198 ms. But, to improve the signal to noise more scans are taken and averaged. Therefore if 100 scans were averaged, the exposure time would be 19.8 seconds. But, there is also a deadtime of 220 ms, between each scan (CCD readout time), which amounts to 22 seconds, therefore the total time taken for one I_t spectrum would be 41.8 seconds. Then the experimental set up is moved on a motorised table to enable I_0 to be measured. Depending on the sample being measured, I_0 can be air, but for all homogeneous experiments studied in this thesis, it was the solution solvent in an I_0 sample cell. The same number of scans were taken of I_0, but collection time was slightly quicker since the integration time was ~1.3 ms (total I_0 time is 24.3 seconds, 22 seconds of this time is due to the CCD readout). The total time for the detector readout was 66.1 seconds, but overall time of each spectrum measured was 160 seconds due to the motors of the stage interchanging I_0 and I_t. This method of data acquisition was acceptable for most of the experiments studied since collection of I_t lasted only 41.8 seconds (generally the integration time was faster) and the reactions being studied were typically conducted over two hours. The beauty of the EDE technique compared with the XAFS, is that since the sample is radiated with all energies of the beam simultaneously, even if the structure changed over the collection time it would not invalidate the spectrum, compared with normal energy scanning techniques.

Some of the reactions measured by EDE only had a timescale of thirty minutes. Using Standard EDE techniques, only 10 spectra could be obtained which obviously would not yield much information on the reaction. Therefore a second data acquisition mode was employed, called Time Resolved EDE. In this method only two I_0 spectra were taken, one at the start and one at the end of the reaction. Therefore the sample can be 'held' in the beam for the duration of the reaction and time is not 'lost' due to the motors interchanging I_t and I_0. Generally 50 scans were measured for each spectrum, which took ~20 seconds, therefore 100 scans can be measured in 33 minutes. When the absorption spectra are calculated from I_0 and I_t, linear interpolation is made between the initial and final measured I_0 and an I_0 is calculated for every I_t. Data quality is generally noisier than for the first technique and is

greatly affected by beam instability. This was shown by a decrease in the length of the analysable data set.

2.2.8 Sampling arrangement

Figure 2.5 shows the sampling arrangement used to conduct EDE experiments at ID24. The arrangement was the same for XAFS experiments on Station 9.1, except the I_0 cell was not required.

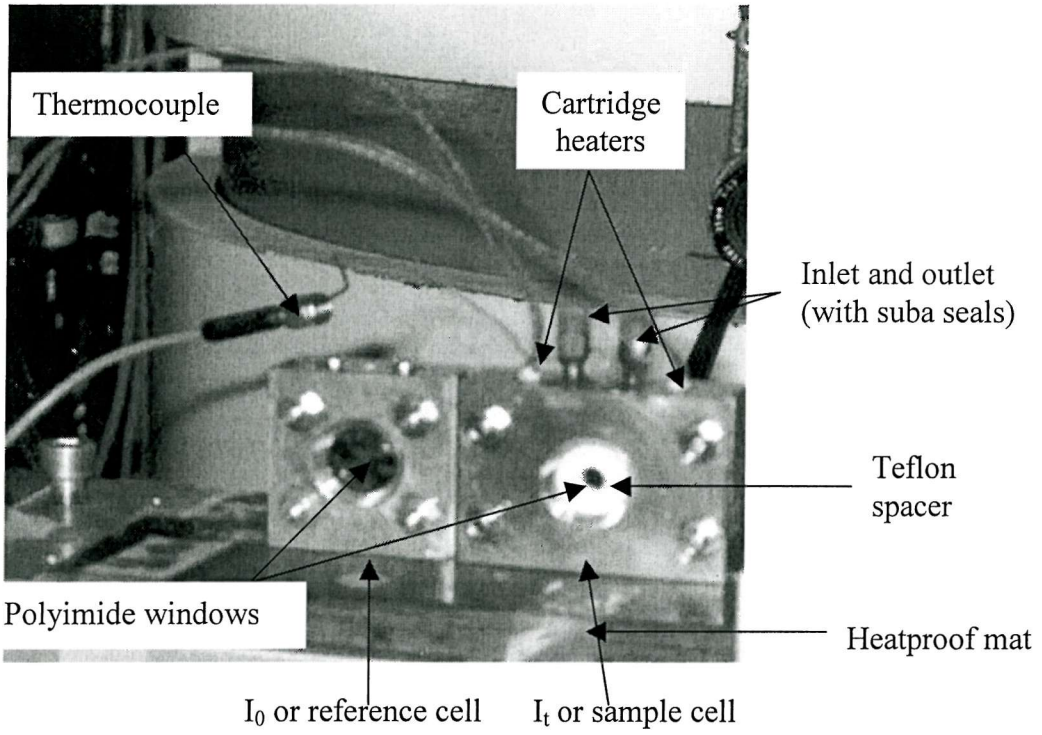

Figure 2.5 EDE cells arrangement on ID24

The cells are made from stainless steel and are built up from three sections; the main body of the apparatus and two plates, which hold the teflon spacers and polyimide (kapton) windows (0.05 mm thickness) in place. The two plates hold the windows in place, by screwing them to the central section. Both cells have a solution inlet and outlet situated on the top of each cell which are sealed with NMR suba seals or teflon plugs. Both cells are similar but the sample cell is more complex. It has two cavities to accommodate two RS cartridge heaters (0.25 x 2 inch, 240V 50W), and a third cavity for a K type thermocouple.

The heaters and thermocouple are connected to a Digi-Sense temperature controller for work in the laboratory or to a Eurotherm for work conducted in Grenoble. The sample cell also has a teflon spacers, which are used to reduce the path length from 10 mm to 5 mm. These spacers are used when the sample being studied contains iodobenzene since iodine atoms are strong absorbers of X-rays, therefore not all the beam is absorbed by the sample. The spacers, the central metal plate and the spacers all have grooves for rubber o-rings to prevent leakage.

The two cells are mounted onto a heat proof mat, which is securely attached to a motorised jack, which can be remotely moved in the x,y and z directions. With this arrangement the beam can be directed through either cell and data collected.

Prior to conducting an experiment, new polyimide windows and clean o-rings were placed in the cell (the spacer was aligned if used) and it was screwed together. The suba seals were placed in the inlet and outlet ports and the cell was pumped and flushed (with nitrogen) four times. If required, the cell was preheated prior to syringing in the sample. Generally, in a disposable glove bag, the suba seals were replaced by teflon caps to prevent any loss of solution through the suba seals during the heating process.

2.2.9 Procedural differences

Due to the experimental setup, the EDE experiments were slightly different to the experiments undertaken in the laboratory.

The main experimental problem was during the transfer of solution to the cell. The laboratory was in a different room to the experimental hutch where the EXAFS work was undertaken. The cell was preheated, but cooled during solution transfer and whilst transferring the cell to the hutch and interlocking the hutch. Also the syringe used to transfer the solution from the reaction vessel to the cell was not preheated, so this would have added to the cooling down process. Experiments were conducted in house, prior to the beamtime, to establish if cooling the solution affected the results; it was discovered this was not the case.

The other main difference was due to the different experimental procedures, i.e. NMR experiments were carried out in a flask with stirrer bar, whilst the XAFS experiments were carried out in the cell (kapton, Teflon or stainless steel container walls), with no stirrer, but a smaller reaction volume. The time lag between the thermocouple reading and the actual solution temperature was calculated, but compensation for not stirring the solution, was considerably harder.

2.2.10 Data analysis

The analysis took place in three stages: calibration, background subtraction and model refinement. The initial stage was slightly more complicated for EDE results, but the latter stages were very similar.

2.2.10.1 I_0 and I_t

For normal scanning XAFS, a Daresbury program EXCALIB[18] is used to calibrate the spectrum. The natural log is taken of (I_0 / I_t) to yield the absorption (y axis) and it also converts the monochromator angle into energy (x axis). The signal to noise ratio can also be improved by averaging spectra.

The process is slightly more complicated in EDE experiments As mentioned earlier in an EDE experiment two spectra are taken, one of the sample solution (I_t) and one of the reference (solvent) solution (I_0) (a typical I_0 and I_t are shown in figure 2.6). These are taken from the end of a typical Heck reaction experiment (Pd K edge, 50 mM). The results are recorded as intensity versus pixel number.

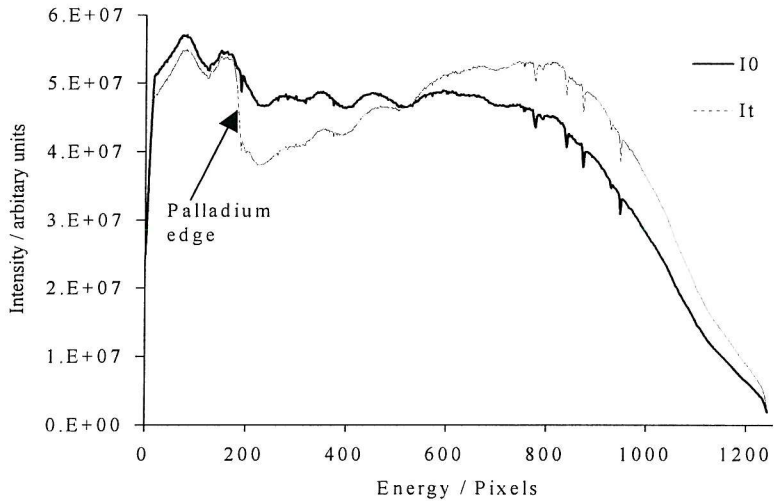

Figure 2.6 I_0 and I_t for a typical homogeneous palladium experiment (50 mM)

The natural log is taken of (I_0 / I_t) to yield an absorption spectrum of intensity versus energy (pixels). A Daresbury program (CalibX[19]) is used to calibrate each EDE spectrum of a palladium foil (taken after every beam change) to a standard EXAFS spectrum of a palladium foil. To improve accuracy the calibration is carried out on the background subtracted spectrum (see next section). The values calculated are used to correct the offset of the edge jump and to convert the pixel number to the photon energies; these are then incorporated in a calibration file. The appropriate file is then used with the final calibration program (proc16 or proc17 dependent on the EDE run[20]) to convert the corresponding EDE data file into the calibrated data file. The data is now present in the format of intensity versus energy and a typical palladium foil spectrum is shown in figure 2.1.

2.2.10.2 Background subtraction

Program for Analysis of X-ray Absorption Spectra (PAXAS)[21] is used to subtract the background from the calibrated absorption spectra. It also includes the facility to average data sets (easiest method to average EDE data), edit the data length and in very extreme cases can be used to edit glitches, which can arise due to inhomogeneity in the monchromator. Care has to be taken, since editing could change the raw data and hence alter the EXAFS spectra. The background subtraction process is carried out in a number of stages and the process for an EDE palladium foil spectrum is shown in figure 2.7.

Pre-edge background subtraction (figure 2.7)

The first subtraction step is the pre-edge background subtraction. The programme defines polynomials by 2 points; L1 and U1 at the beginning and end of the pre-edge region respectively, and an extra point, P1, is chosen at the end of the post edge region. Usually P1 is weighted and its y-coordinate is adjusted to achieve good pre-edge subtraction. The background-subtracted absorption (bsa) is approximately horizontal beyond the edge, or sloping gently downward.

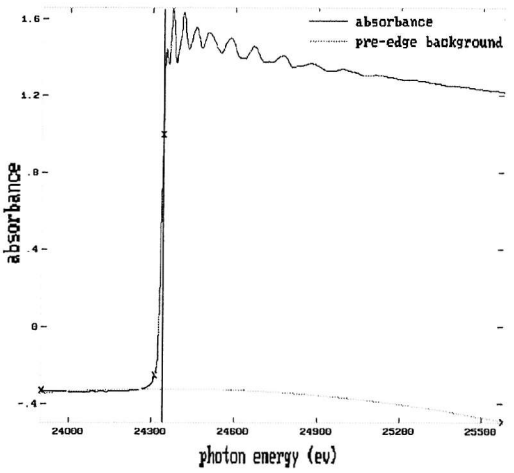

Figure 2.7 Pre-edge background subtraction

Post-edge background subtraction (figure 2.8)

Three points define the post-edge background subtraction, L2, P2 and U2. These points are fitted with high order polynomials of 6, 7 or 8. The polynomial order is chosen to minimise unwanted features observed below distances of 1 Å (too small to be interatomic distances) in the Fourier transform spectrum.

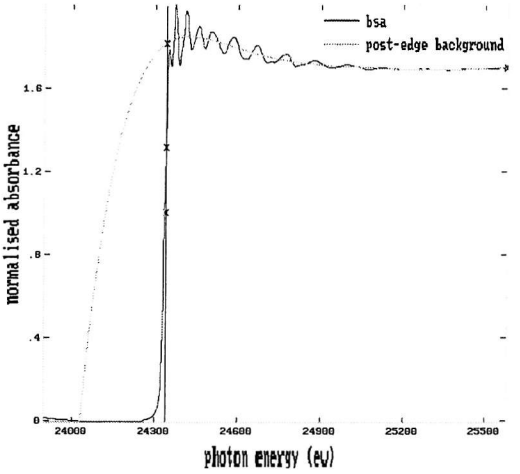

Figure 2.8 Post-edge background subtraction

k^3 χ(k) data (figure 2.9)

After background subtraction the EXAFS is then k weighted to a power 1, 2 or 3 (i.e. k^1, k^2 or k^3), so the higher k values can be used for analysis. The shape of the EXAFS curve gives information on the nature of the backscattering atoms. If the curve has large amplitude at high k values then the backscatter's are high z atoms (i.e. palladium

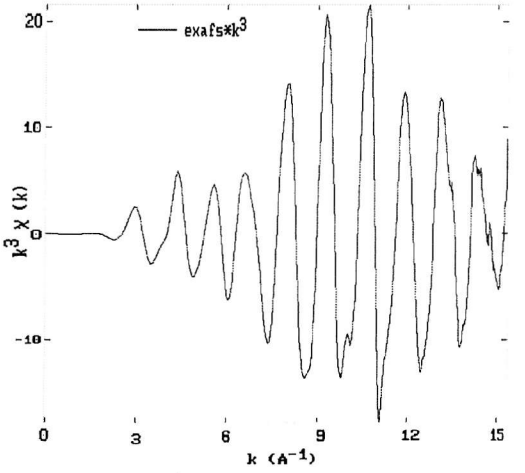

Figure 2.9 $k^3.\chi(k)$ data

and iodine) and if the peaks have high amplitudes at low k values the backscatters are low z atoms (i.e. carbon and oxygen). Therefore if analysing light atoms, the k weighting would be 1 or 2 to emphasis the low k data, whilst a weighting of 3 is normally used for large backscatters.

Fourier transform and back transform (figure 2.10)

The Fourier transform of the k weighted EXAFS data is then calculated, to yield a spectrum of radial atom distance versus intensity. After obtaining the Fourier transform, the back transform between the window limits in r space (containing structural information) may be compared to the EXAFS. This depicts which peaks in the Fourier transform are formed by the different peaks in the EXAFS.

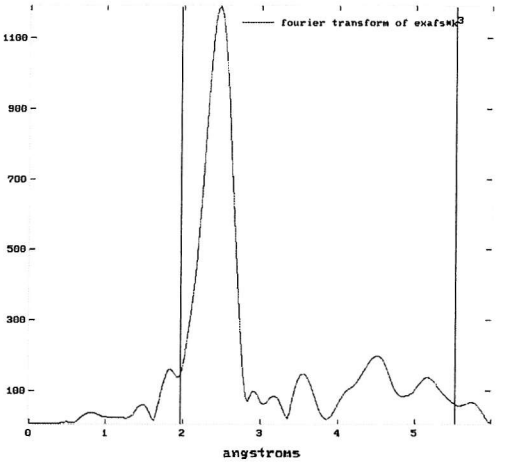

Figure 2.10 Fourier transform and back transform

To obtain the best result, differences between the EXAFS and back transform are minimised by iteration and refinement.

2.2.10.3 Model fitting

The final stage of the analysis is to design a model, calculate the EXAFS and Fourier transform arising from this model, then visually and with a least squares iterative refinement process, adjustments are made to the model until there is high correlation between the experimental and the theoretical curves. These tasks are all achievable with the aid of a program called EXCURV98.[22]

The model is constructed by defining shells, where each shell contains a unique or a number of equivalent atoms (w.r.t. to the absorbing atom). Each shell is generated using a number of structure dependent parameters:

C.N. - The number of atoms in the shell (coordination number)

Atom - The type of atom in the shell

a - The Debye-Waller factor for the shell, expressed as $2\sigma^2$, where σ is the mean square variation in interatomic distances. Debye-Waller factors should lie between 0.003 and 0.03 $Å^2$. However, as Debye-Waller factors include contributions from the lattice and thermal effects, their values will be higher on experiments performed at higher temperatures. Debye-Waller factors and co-ordination numbers are highly correlated and should not be refined simultaneously.

r - Interatomic distance

The model is constructed shell by shell, after the addition of each shell the parameters are refined (including E_f (below)), then the next shell was added. For this work the shells were constructed in the order of radial distance from the absorbing atom (shortest first).

E_f - The difference between the calculated Fermi level energy and the known values for the element, typically –15 to 5eV

Other factors taken into consideration when refining models were:

afac -The energy independent amplitude factor which accounts for the reduction in amplitude to multiple excitations occurring at the central atom.

Emin -The minimum energy used to calculate the theoretical spectrum

Emax -The maximum energy used to calculate the theoretical spectrum

When fitting models with normal single scattering effects the model is one dimensional. But, if multiple scattering effects are present, which arise due to the geometry of the atoms, a three dimensional model must be constructed, either by using polar coordinates or by reading crystal structures into the program.

Fitting parameters

The number of parameters refinable (N_{ind}) for a specific data set is dependent on the *k* range

(Δk) obtained and r range (Δr) between the shortest and longest shell. N_{ind} is calculated using equation 2.4.[23]

$$N_{ind} \approx 2\Delta k \Delta R/\pi \qquad \textbf{Equation 2.4}$$

There are two measures of the 'goodness' of the fit, between experimental and theoretical spectra. The first is called the fit index (FI) and calculates the fit between the experimental and theoretical curve. FI in a k^3-weighted EXAFS can be calculated as follows:

$$FI(EXAFS) = \Sigma_I [(k_i)^3(\chi_i^T - \chi_i^E)^2] \qquad \textbf{Equation 2.5}$$

The sum of the square of the differences between the theoretical and experimental data points has to be below 5×10^{-4} to produce a good fit. However, FIs of less than 8×10^{-4} are acceptable.

A second parameter, known as the R-factor[24] is calculated to estimate the quality of the fit:

$$R(EXAFS) = = \frac{[\int |\chi_i^T(k) - \chi_i^E(k)| \, k^3 \, dk] \times 100\%}{[\int |\chi_i^E(k)| \, k^3 \, dk]} \qquad \textbf{Equation 2.6}$$

The R-factor is a percentage calculating the total sum of all the errors between all the data points. An R-factor below 30 % constitutes a good fit although for EDE spectra, due to the lower signal to noise ratio, a value of 40-50 % is acceptable.

Sine transform

The k weighted data can be shown as a sine transform rather than as the Fourier transform. This appears more complex, but can be a useful tool in determining which atom is in a shell, especially useful if the atoms are a similar size. The Fourier transform is the square root of the Sine transform squared, which ensures that the amplitude is always positive in the transform, but can cause some information to be lost.

Statistical significance test

Joyner *et al*[35] have concluded that addition of any extra parameters should decrease in fit index at 4% or more. This statistical significance test, which is available in the EXCURVE program can be used to determine the good fit spectra. The criteria for shell error evaluation were given in terms of

$$FI_{n+1} / FI_n < 0.96 \qquad (2.11)$$

where n is the number of shells. If a reduction in the fit index is satisfied (the ratio is less than 0.96) then the new shell is significant. This assumes that each data point is an independent observation, and there are 200 data points in the spectrum. This is an optimistic assessment of the number of independent parameters.

Correlation Coefficient

This matrix of coefficients for each pair of parameters shows the correlation for each of them, where the coefficients vary from –1 to 1. Highly correlated parameters will give a coefficient of higher than $|0.8|$, which should indicate that one of the shells is not reasonable in the fit. Highly correlated phenomena usually happen when 2 shells of similar atomic number backscatterers are being fitted at similar distances, e.g. Pd-O and Pd-C at ca. 2.1 Å.

Fit index contour maps

The map function of fit index values against two fitting parameters is also used in this research in order to give indication of well defined correlation between two parameters in the coordination sphere. The contour plots for well defined parameters should result in spherical contours with a steep increment between them as displayed in Figure 2.11A. Poorly or wrongly defined parameters will give a shallow minima, meanwhile the contours are elongated in one direction in the case of parameters of different importance in the fit (Figure 2.11B).

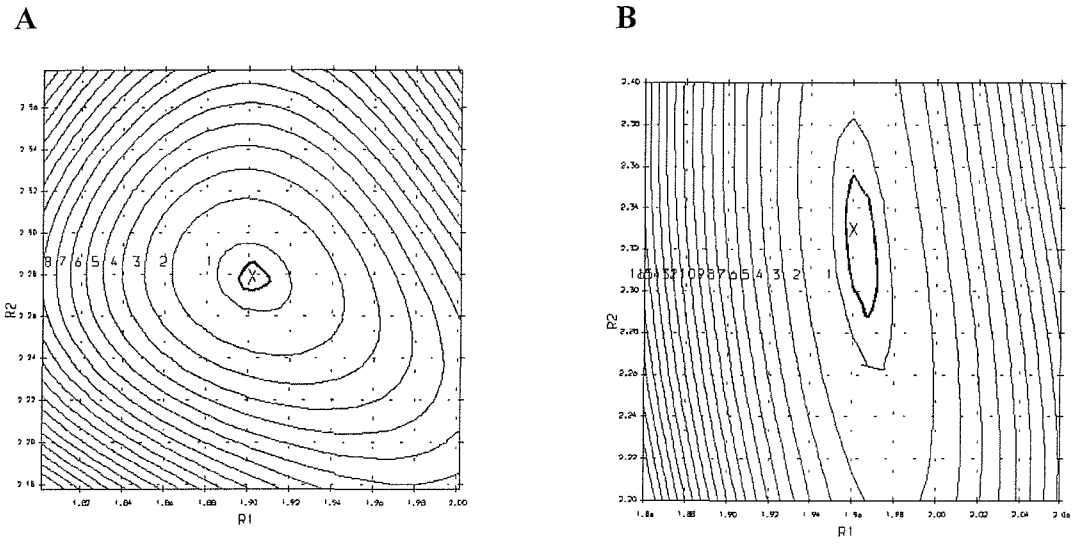

Figure 2.11 Two-dimensional map of the fit index plotted of two parameters derived from curve fitting, showing a good refinement with a spherical contour (A) and poorly defined variables with contours elongated in one direction (B).

Model fitting for an EDE spectrum of a palladium foil

A model was then fitted to a palladium foil which had been background subtracted in section 2.2.9.2. Figure 2.12 shows the background subtracted k^3 EXAFS data, the Fourier transform and the sine spectrum for the palladium foil. It is fitted to four shells and the corresponding model table is also shown in the figure

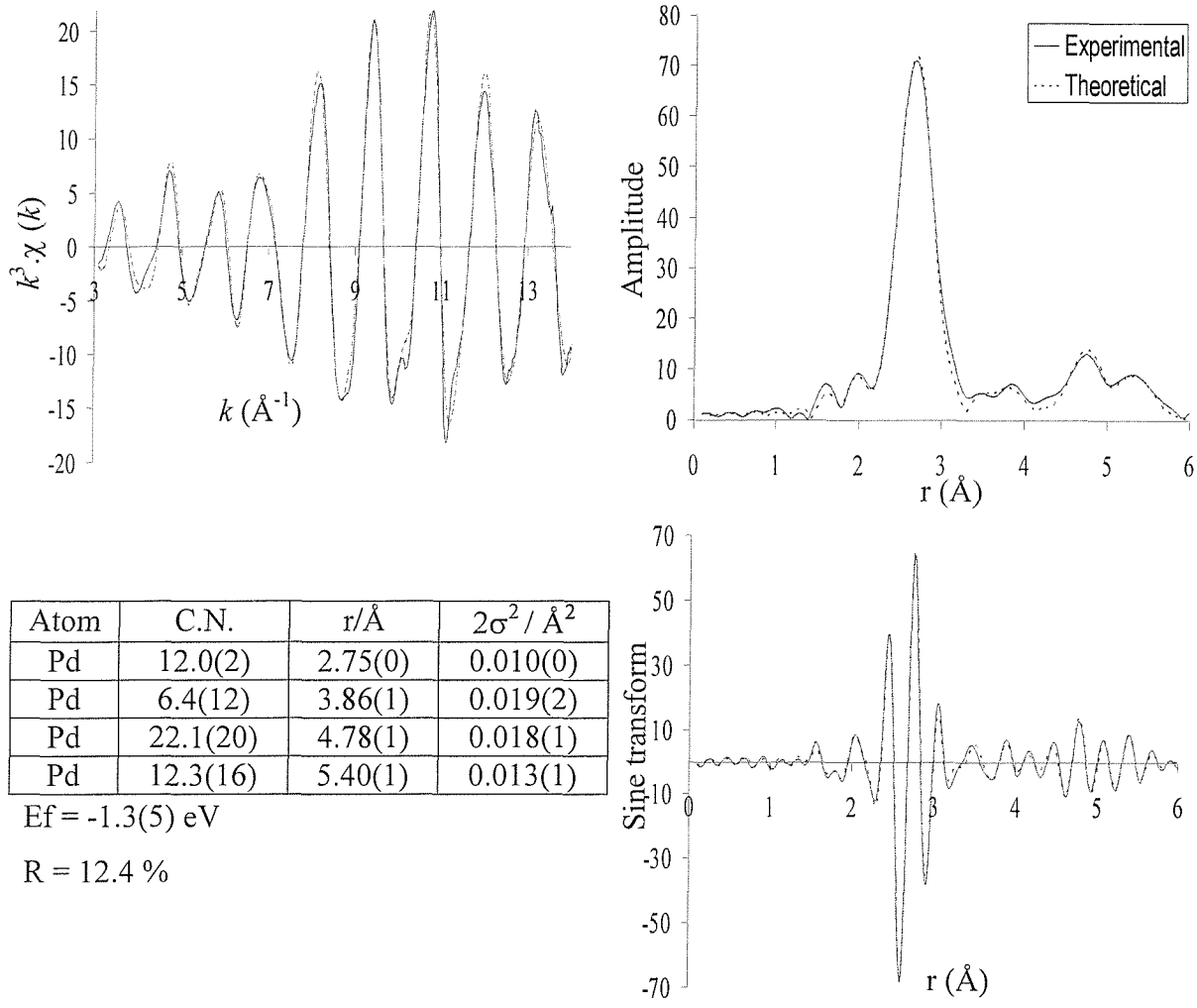

Atom	C.N.	r/Å	$2\sigma^2$ / Å^2
Pd	12.0(2)	2.75(0)	0.010(0)
Pd	6.4(12)	3.86(1)	0.019(2)
Pd	22.1(20)	4.78(1)	0.018(1)
Pd	12.3(16)	5.40(1)	0.013(1)

Ef = -1.3(5) eV

R = 12.4 %

Figure 2.12 The palladium K-edge k^3-weighted EXAFS data, Fourier transform and sine transform for an EDE palladium foil at room temperature and pressure (RTP).

The results refine very well to the model for bulk palladium. The metal is face centred cubic so the coordination number for the different palladium shells is 12, 6, 24, 12. So within the standard errors (in brackets) the EDE results agree. The interatomic distances are also very close to the reported distances, they are all within 0.08 Å, with the first and third shell being only 0.01 Å different. The Debye-Waller terms are all reasonable values and the errors are low. The R factor is extremely low and the fit index is 0.117. The quality of the fit can also be observed visually since the theoretical curve constructed from the model maps the experimental curve very closely. The data quality of the background subtracted spectrum is also very good, noise is at a minimum and data range is 14 k. The reason why this spectrum is so good is because the concentration of palladium and the homogeneity is extremely high compared with normal samples.

2.3 Matrix Assisted Laser Desorption/Ionisation (MALDI)[25]

MALDI is a relatively new mass spectrometry technique that allows high molecular weight compounds to be analysed with high sensitivity. Ions are formed by a pulsed laser beam that is directed onto a sample which is dissolved in a solid matrix. The matrix is a non-volatile solid material that absorbs the laser radiation causing vaporisation of the matrix and the sample which is embedded in the matrix. It absorbs the majority of the energy from the laser radiation minimising the damage to the sample. The matrix also ionises the sample molecules when in the gas phase. The charged species are then directed into a time-of-flight (TOF) mass analyser. This analysis is based on the fact that the ions are accelerated towards a detector with the same amount of energy, but as the ions have a different mass, they reach the detector at different times. Smaller ions reach the detector first because they have greater velocity and the heavier ions take longer. The mass-to-charge ratio (m/z) is determined from the ions' arrival time.

There are many advantages of using this technique (works for a large mass range, very sensitive (low picomole possible), little fragmentation is observed, tolerance of salts) and it was the only mass spectral technique where it was possible to observe the palladium complexes in solution. But inevitably there are also disadvantages: the analysis was not completed under a nitrogen atmosphere, there was also a possibility of photodegradation by the laser and it is possible that the matrix background interfered with the results.

2.4 Experimental

All manipulations were carried out under a nitrogen atmosphere using standard Schlenk techniques. Anhydrous NMP, chlorobenzene, bromobenzene, 2-methyl-prop-2-en-1-ol, palladium acetate and all phosphines were used directly. Iodobenzene and tributylamine were dried over calcium hydride and distilled prior to use. All chemicals were obtained from Aldrich Chemicals, Lancaster and Strem.

Unless otherwise stated, all Heck reactions were 4 ml in total volume and preparation for NMR, MALDI and XAFS experiments was identical. A 50 ml three necked round bottom flask, with a condenser in one neck, a suba seal in another (for sample collection) was connected to a vacuum line via the third neck. The apparatus was pumped and flushed three times and the palladium catalyst (50 mM per palladium) and phosphine (150 mM if applicable) was added. The halobenzene (1000 mM), methallyl alcohol (1200 mM) and tributylamine (1200 mM) were syringed into the reaction vessel. These concentrations had been used before[26] and the large concentration of palladium was chosen to enable analysis of the palladium using XAFS techniques. These same conditions when then consequently used in the NMR and MALDI experiments, to ensure that the same species were present in all the reactions and to ensure that a change of concentration did not affect the results. The solution was then heated in an oil bath and samples were taken at an appropriate time, dependant on the reaction and the spectroscopic technique being utilised.

2.4.1 NMR analysis

For *ex situ* NMR analysis the samples were taken at a predetermined stage in the reaction, chosen as a fixed temperature, or a fixed time at the reaction temperature. The NMR samples were syringed directly from the reaction mixture into a 5 ml NMR tube which was sealed with an NMR suba seal and had been pumped and flushed with nitrogen four times. An external reference was used, which was C_6D_6 or $CDCl_3$ in a sealed glass capillary tube in the NMR tube. ^{1}H, ^{13}C and ^{31}P nuclei experiments were then run on the samples in a Bruker AC 300. *In situ* experiments were measured in a Bruker AM 360 spectrometer and the solution was syringed (after dissolving the catalyst) into a 10 ml Young's NMR tube (under nitrogen), which was heated in the spectrometer. The experiments were run unlocked

and referenced against known ^{31}P peaks.

2.4.2 MALDI analysis

MALDI experiments were very similar, except a drop of the reaction mixture was spotted on a metal plate and spectra were taken. Note that this was not under an inert atmosphere. The experiments were run on a Micromass TOF Spec 2E instrument run in reflectron mode.

2.4.3 XAFS analysis

A range of XAFS techniques (EXAFS, QEXAFS and EDE) and experimental conditions were used. The two main distinctions between the experiments were *ex situ* and *in situ* (analogous to the NMR experiments). For *ex situ* experiments, the reaction mixture was injected directly from the reaction flask into the XAFS cell (section 2.2.7) and the spectrum was measured at room temperature and pressure (RTP) or 40 °C, depending on solubility. As for the NMR experiments the samples were taken at a predetermined stage in the reaction, chosen as a fixed temperature, or a fixed time at the reaction temperature. Generally, these were chosen as spectra of the initial and final solution. But, also included catalytic samples for one of the reactions. Due to time constraints it was not possible to extend this to further reactions. For *in situ* XAFS analysis, once the catalyst was soluble in solution (or as a fine suspension) i.e. after heating to ~50 °C, it was syringed into the XAFS cell, which was heated to the reaction temperature and held for a fixed length of time. QEXAFS and EDE (standard and time resolved) spectra were then taken over the duration of the experiment.

2.5 References

1 D.C. Koningsberger, R. Prins *X-ray absorption, principles, applications, techniques of EXAFS, SEXAFS, and XANES*, Wiley Interscience, New York, **1988**.

2 D. Burnaby, PhD Thesis, University of Southampton, **2000**.

3 M.A. Newton, A.J. Dent, J. Evans, *Chem. Soc. Rev.*, **2002**, *31*, 83.

4 http://www.esrf.fr/

5 http://www.srs.ac.uk/srs/

6 J. Evans, *Catalysis*, **1989**, *8*, 1.

7 B.K.Teo, *EXAFS: Basic Principles and Data Analysis,* Springer Verlag, Berlin, **1986**.

8 H. Bertagnolli, T.S. Ertel, *Angew. Chem. Int. Ed.,* **1994**, *33*, 45.

9 P.A. O'Day, J.J. Rehr, S.I. Zabinsky, G.E. Brown, *J. Am. Chem. Soc*, **1994**, *116*, 2938.

10 D.E. Sayers, E.A. Stern, F.W. Lytle, *Phys, Rev, Lett,*. **1971**, *27*, 1204.

11 O.M. Poltorak, V.S. Boronin, *Russian J. Phys. Chem.*, **1996**, *40*, 1436.

12 J. M. Corker, PhD Thesis, University of Southampton, **1991**.

13 J.M. Corker, J. Evans, H. Leach, W. Levason, *J. Chem. Soc. Chem. Comm.*,**1989,** 181.

14 S.J. Gurman, N. Binsted, I. Ross, *J. Phys.C*, **1986**, *19*, 1845.

15 S. J. Gurman, *J. Phys. C*, **1988**, *21*, 3699.

16 M.B.B. Abdul Rahman, PhD Thesis, University of Southampton, **1998**.

17 S. Pascarelli, ID24, E.S.R.F., Grenoble

18 *EXCALIB*, SERC Daresbury Laboratory Program, **1990**.

19 A. Dent, *CalibX*, SERC Daresbury Laboratory Program, **1997**.

20 A. Dent, *proc16 (proc17)*, SERC Daresbury Laboratory Program, **1999 (2000).**

21 N. Binsted, *PAXAS* (*Programme for the Analysis of X-ray Absorption Spectra*), University of Southampton, **1988**.

22 N. Binsted, S. Gurman, J.W. Campbell, *EXCURV98,* SERC Daresbury Laboratory Program, **1998**.

23 S.S. Hasnin, (Editor), *X-ray Absorption Fine Structure*, Ellis Horwood, New York, **1995**, 195.

24 S. Brandt, *Statistical and Computational Methods in Data Analysis*, North Holland, Amsterdam, **1970**.

[25] G. Siuzdak, *Mass Spectrometry for Biotechnology*, Academic Press, **1996**.

[26] V.L. Kambhampati, PhD Thesis, University of Southampton, **1998**.

Chapter 3

Reactions of palladium acetate with trialkyl and triarylphosphines

3.1 Introduction

In this chapter, **1** was synthesised and characterised using XAFS (solid and solution state), to establish if the nature of the monomer / dimer equilibrium (figure 3.1) shown by phosphorus NMR (chapter 1) can be investigated using these techniques. This also allowed a direct comparison between the quality of the data obtained through the different XAFS techniques.

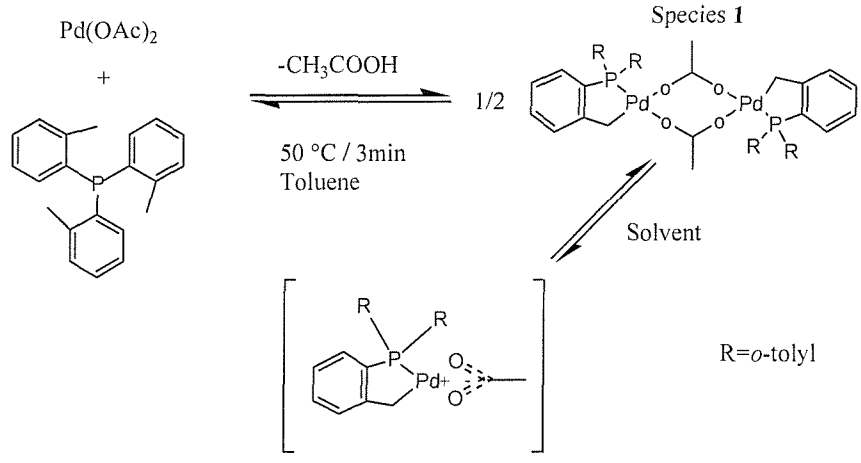

Figure 3.1 Formation of species 1 and its possible monomeric structure in solution.

The mechanism of the formation of **1** from palladium acetate and tri-*o*-tolylphosphine (figure 3.1) was then investigated using time resolved EDE and *in situ* NMR techniques. In respect to the XAFS technique this was not an easy objective, since the local environment (up to 2.5 Å) around the central palladium atom only changes marginally (2 oxygen atoms are replaced by 1 phosphorus and 1 carbon atom). Therefore the results acquired from XAFS analysis of **1** was used as a 'fingerprint' to facilitate this work.

The final portion of this chapter was devoted to XAFS analysis of other reactions of palladium acetate with some alkyl and arylphosphines. In these reactions cyclopalladation does not occur, but again there is coordination of phosphorus to the palladium metal.

During this chapter the usefulness of white line analysis is shown. Since it can be an excellent tool (dependent on the system being analysed) to pinpoint specific points during the reaction to analyse . This facilitates analysis and is especially important in time resolved runs where 100 spectra were obtained in 30 minutes.

3.2 Preparation and characterisation of species 1

Palladium acetate ($Pd(OAc)_2$) was reacted with tri-*o*-tolylphosphine ($P(o\text{-tolyl})_3$) to form **1** and recrystallised from toluene and petroleum ether (see experimental section 3.8). It was characterised using ^{13}C, ^{31}P NMR and Matrix Assisted Laser Desorption Ionisation (MALDI) mass spectroscopy.

The ^{31}P NMR of **1** in solution gives a broad peak at $\delta = 35$ ppm. This logically suggests that there is an equilibrium present in the solution. Hermann has suggested that it is present in the form of a monomer / dimer equilibria (figure 3.1) and participation of coordinating solvents favour bridge splitting of the dimer.[1]

MALDI work was carried out on **1**. This was undertaken to characterise the palladacycle and also to test the accuracy of this relatively new mass spectrometry technique on these systems. The matrix used was 2-5-dihydroxybenzoic acid and the main peaks detected were due to the parent ion, the parent ion minus a methyl group, the parent ion minus two acetate groups, the parent ion minus two acetate groups and a palladium atom and the parent ion minus two acetate groups, a palladium atom and a tolyl group.

3.2.1 XAFS analysis of species 1 in solution

As for the MALDI work, XAFS analysis was undertaken on a standard compound, which had similar structure and similar conditions to the sample **1**. Palladium acetate was chosen as an appropriate standard, since it has a similar environment (4 oxygen atoms) around the palladium atom as for **1** (2 oxygen, 1 carbon and I phosphorus atom). The crystal structure of palladium acetate is trimeric,[2] but in solution it is monomeric or trimeric dependent on solvent and temperature.[3] For the XAFS model the only difference between the monomer and trimer is the inclusion of a Pd...Pd non-bonding shell at 3.15 Å. QEXAFS (6 x 5 minutes (averaged)) analysis of palladium acetate (70 mM) in NMP by Evans *et al.*[4] showed no inclusion of a palladium shell, which suggests that the monomer model is correct. Especially since in the case of the linear trimer in $[Ni(acac)_2]_3$ in toluene, the non-bonded Ni...Ni distance could be modelled.[5] The QEXAFS model for the palladium acetate gave a

Pd-O bond length of 2.00 Å, which is very close to the crystal structure of 1.973-2.014 Å. For this thesis EDE spectra (100 scans averaged, I^t = 2.1 ms) of palladium acetate (50 mM) in NMP also showed the same results with a bond length of 2.00(1) Å, a coordination number of 3.86(33) and a Debye-Waller value of 0.008(2) σ^2. Since QEXAFS and EDE agreed closely with the X-Ray crystal structure, this enforces just how accurate these techniques are.

The palladacycle (**1**) was then studied in solution using EXAFS, QEXAFS and EDE techniques. The best quality spectra obtained was from EXAFS data. So initially this was examined to calculate a good model for the palladacycle in solution.

3.2.1.1 Background subtraction

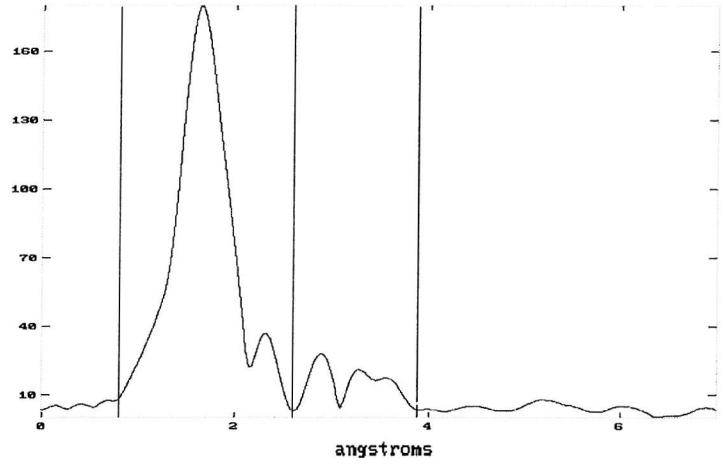

Figure 3.2 The Fourier transform of the Pd K edge EXAFS (2 x 30 minutes averaged) of species 1 (50 mM) in NMP at room temperature and pressure (RTP), with no phase shift correction.

Figure 3.2 shows the Fourier transform of the Pd K edge EXAFS of **1** (50 mM in NMP at RTP). Three EXAFS transmission scans, with a sample path length of 10 mm, were taken and averaged. The three vertical lines in the spectra are the limits used to examine the k^3 back transforms and to compare them with the k^3 EXAFS data. The lower limit was kept at 0.80 A, whilst the upper limit was varied from 2.16 to 3.88 A.

Figure 3.3A compares the k^3 EXAFS spectra with the k^3 back transform. The limits used were 0.80 and 2.60 Å and were measured from the Fourier transform without any phaseshift correction. The spectra shows a very good fit at high k values, but the fit deteriorates as k

reduces to low values. This suggests that the peaks in the Fourier transform where R is larger than 2.60 Å are integral to the fit and are not noise.

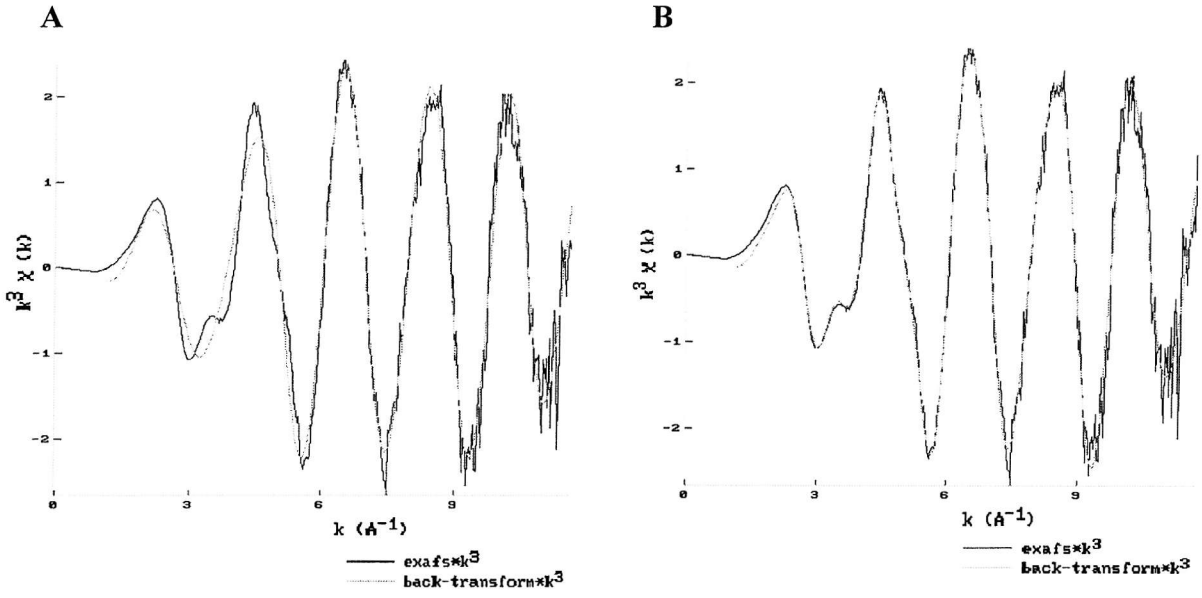

Figure 3.3 Comparison of k^3 data with k^3 back transformed data for species 1, with back transform limits of 0.80 to 2.60 Å^{-1} (A) and 0.80 to 3.88 Å^{-1} (B).

The higher limit for the back transform was then increased to include each new peak and then compared with the k^3 weighted EXAFS. For every new peak included, the back transform fit improved at low k. It was only after the higher limit was increased to 3.88 Å, that the inflection at 3.7 Å^{-1} in the k weighted data was correctly fitted, shown in figure 3.4b. Hence this shows that all of the Fourier transform peaks present in that window are actual peaks and not attributed to noise.

3.2.1.2 Curve fitting

The background subtracted EXAFS data for **1** was then curve fitted in Excurv98 and various models were fitted to the data, to attain the best fit (figure 3.4).

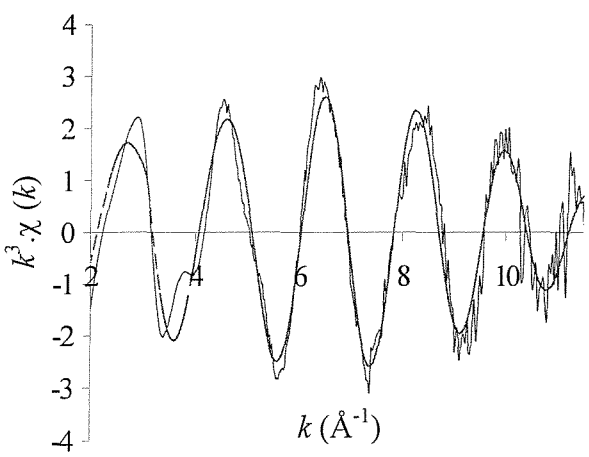

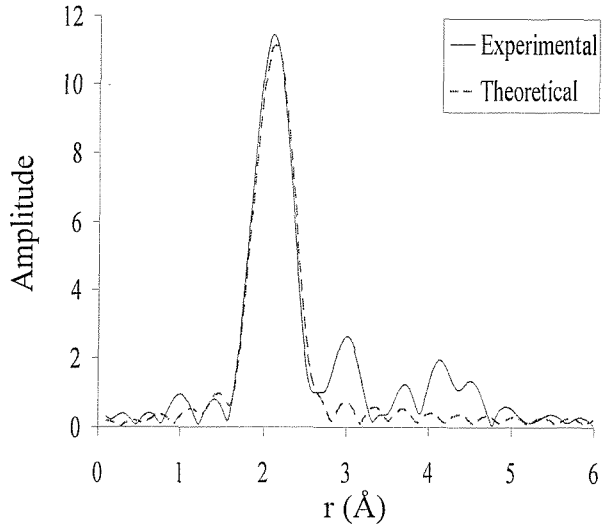

Atom	C.N.	r / Å	$2\sigma^2$ / Å^2
C	1.2(3)	2.02(2)	0.001(5)
O	1.9(5)	2.16(2)	0.023(10)
P	1.0(1)	2.25(1)	0.004(3)

E_f = -0.13(86) eV

R = 27.4 %

Figure 3.4 The palladium K-edge k^3-weighted EXAFS data (2 x 30 minutes) and Fourier transform of species 1 in NMP (RTP).

PAXAS showed that to give a good fit the first four Fourier transform peaks have to be fitted in the model. But, due to the complexity of the structure (i.e. in the crystal structure there are 20 atoms within 4.5 Å of a palladium atom)[6] and therefore the large number of variable parameters that need to be fitted, this can not be justified.

Therefore the model was constructed initially by including only the palladium bonding interactions. The model gives a fairly good result with a substantial decrease in R factor with the addition of each shell. The interatomic distances are also very close to the crystal structure (carbon 2.02 Å, oxygens (average) 2.11 Å and 2.15 Å and phosphorus 2.22 Å). The EXAFS fit at high k values is good, whilst the fit at low k is poor. This suggests that there is a problem with the model for the lighter atoms, since they have the greatest effect at low k. This is probably due to carbon atoms not being fitted since there are over 15 carbon atoms within 5 Å of the central atom. These are not possible to fit; because there are too many shells to be fitted with the k range available, there is greater flexibility in solution so the interatomic distances could vary and the shells overlap so they cannot be defined as

discrete.

Phosphorus NMR gives a broad peak suggesting that there is an equilibrium process in action, which is likely to be an equilibrium between the monomer and dimer species. In the monomer there would be no Pd...Pd interaction so a palladium shell was fitted at 3.15 Å (calculated from crystal data), the R factor increased slightly but the Fourier transform did not fit the shell. Due to the flexibility of the acetate ligands this distance was increased up to 5 Å, but did not give a good fit. But an EDE spectrum of $[Pd_2I_6][NEt_3H]_2$ with 13 *k* of excellent quality data does not show the nonbonding Pd…Pd interaction at 3.83 Å.[7]

Since a palladium atom could not be fitted, this suggests that the species may be predominately monodentate, therefore it was decided to try to fit the central carbon atom of the acetate group. Searching the CDS database there were no crystal structures for palladium with a bidentate acetate ligand bonded directly to the palladium atom. So the search was widened to include rhodium, this search gave two references for appropriate molecules.[8,9] Carbon rhodium distance are 2.49 Å and 2.52 Å respectively and this be very similar in the palladium case (since the palladium single bond covalent radii is only 0.03 Å longer[10]). The Rh-O bond length in $\{Rh(Cl)[\mu\text{-}(OC(CH_3)O)]_2\}_2$ is 2.01 Å,[11] which is slightly larger than the Pd-O bond length in $Pd(OAc)_2$ In the crystal structure the smallest palladium carbon distance is 2.02 Å, with the next palladium carbon distance at 3.02 Å. Therefore if a carbon shell could be fitted between 2.5 and 2.7 Å, this should prove that the catalyst is a monomer in solution. A carbon shell was fitted to the previous EXAFS data but the Debye-Waller was pushed up to 0.09 when refined, which means it is not present at that distance. But, if it is present it should be fitted since a Ni…C shell was fitted by EXAFS at a non bonding distance of 2.90 Å in the complex $Ni(H_2NCH_2CH_2NH_2)_2Cl_2$.[12]

Therefore it is still inconclusive what the correct structure is since the palladium shell can not be fitted in the case of a dimer and the central carbon of the bidentate acetate ligand cannot be fitted to prove that it is a monomer. Since a Pd...Pd interaction cannot be fitted in $Pd_2I_6^{2-}$ (at 3.83 Å), then it is not surprising that the palladium interaction at 3.15 Å is not observable in the dimer or the carbon at 2.7 Å in the monomer (it has a shorter length but the carbon atom is considerably smaller). Therefore neither structure can be discounted.

Multiple scattering effects were then considered to see if this could shed any new

information on the species present. The crystal structure for the dimer[6] was obtained from the crystal structure database. This was then edited to give a model, which contained two palladium atoms, both bridging acetate ligands and one of the five membered palladated rings. The geometry around the palladium atoms is very close to square planar (figure 3.5).

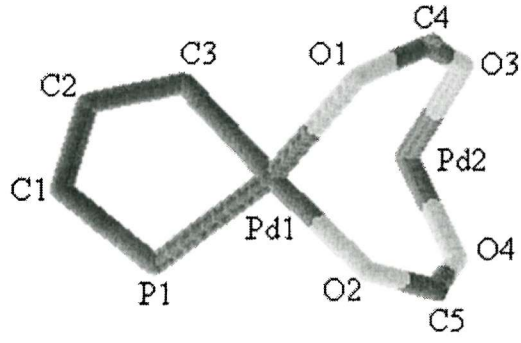

Figure 3.5 Model used to calculate multiple scattering path lengths in the dimer.

In Excurv98 the model was treated as a cluster (symmetry defined as C1). Units (used to keep the integrity of a ring etc.) were not used, since multiple scattering pathways are not calculated between different units (i.e. if the cyclopalladated ring is defined as one unit and the two acetate bridging ligands as another unit, the Pd1-C3-Pd1-O2-Pd1 multiple scattering pathway would not be considered). The maximum number of atoms to be considered in any one multiple scattering path was set at four. The main multiple scattering paths are listed in the order, atoms in path (relative magnitude, 0.5 x pathlength); Pd1-O1-C4-O1-Pd1 (0.107, 3.37 Å), Pd1-O1-Pd1-P1-Pd1 (0.059, 4.33 Å), Pd1-C3-Pd1-O2-Pd1 (0.048, 4.17 Å), Pd1-O2-C5-Pd1 (0.046, 3.20 Å), Pd1-C3-C2-Pd1 (0.031, 3.27 Å), Pd1-P1-C1-Pd1 (0.028, 3.61 Å), Pd1-C3-O2-Pd1 (0.026, 4.17 Å), Pd1-O1-P1-Pd1 (0.025, 4.31 Å), Pd1-O1-C4-O1-C4-Pd1 (0.023, 4.50 Å) and Pd1-O2-C5-O2-C5-Pd1 (0.021, 4.45 Å). (Note that the pathlength is twice the interatomic distance, because the photoelectron wave travels from the X-ray absorber to the neighbour atom and is backscattered to the absorber).

There is a mixture of multiple scattering pathways, with the biggest due to the acetate group. The next major contributions are due to paths encompassing both units, the pathways being almost linear, this again is known to be a large multiple scattering pathway in square planar complexes.[13] The remainder of the main pathways are due to multiple scattering pathways either in the palladated ring or the acetate bridging ligands (with the latter providing the greatest contribution). The amplitude of the experiment was 67.6, since the

largest contribution provided by multiple scattering is only 0.107, this can not be regarded as very significant to the fit,[14] the same rule applied to the overall total of the multiple scattering pathways.

So an 'approximate' model of the monomer was constructed, in order to calculate if this species would have any significant multiple scattering contributions. This was achieved by coordinating a carbon atom to O1 and O2, eliminating the remainder of the bridging ligands from the model and varying the angles in the ring to obtain a likely Pd...C non bonding distance (~2.5 Å). This showed that any multiple scattering effects decreased rather than increased, so this avenue of work was closed.

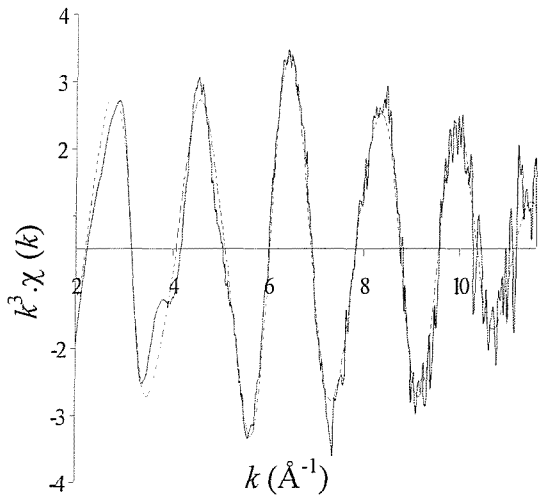

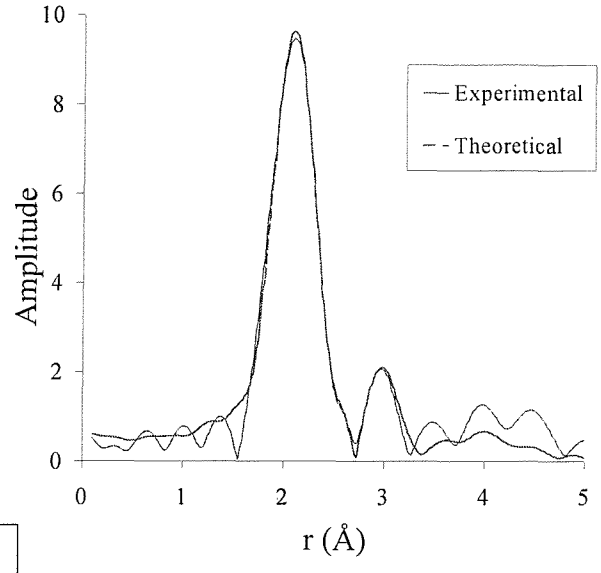

Atom	C.N.	r / Å	$2\sigma^2$ / Å^2
C	1.03(1)	2.02(3)	0.001(4)
O	1.00(6)	2.13(12)	0.017(65)
O	1.00(7)	2.16(13)	0.017(64)
P	1.02(0)	2.24(1)	0.004(3)
C	1.02(0)	3.03(3)	0.001(4)
C	1.02(5)	3.12(7)	0.015(26)

E_f = -0.15(91) eV

R = 20.3 %

Figure 3.6 The palladium K-edge k^3-weighted EXAFS data and Fourier transform of species 1 in NMP (RTP), considering multiple scattering effects.

To test the hypothesis that the contribution of the multiple scattering to the fit was negligible, a smaller model of the dimer was constructed (than used for calculating the path

lengths) in an effort to reduce the number of shells to a realistic number. Since it is not known if the species is a monomer, dimer or mixture, only the oxygen atoms of the acetate ligands remained in the model. The palladated ring was left intact and the model with fit is shown in figure 3.6.

The results look very good but the errors in the Debye-Waller terms are very large for some of the atoms, which is due to high correlation between very similar shells (i.e. the two oxygen shells are almost identical). The values for the coordination numbers are very good as are their errors. The interatomic distances are also very close to the crystal structure data. All of the values are within 0.02 Å, except for the final shell, which is only 0.06 Å different.

A palladium atom was fitted at 3.15 Å, but the Debye-Waller factors rose above 0.03 Å and the Fourier Transform did not fit it, suggesting it is an invalid shell. Then a carbon at 2.5-2.7 Å was fitted, the R factor did not increase but the Debye-Waller factors, coordination number and interatomic distance gave very reasonable values. This data could indicate that the catalyst is a monomer in solution.

The main multi scattering path lengths are Pd-C1-Pd-O-Pd (0.058, 4.16 Å), Pd-C1-C2-Pd (0.033, 3.27 Å), Pd-C1-C2-C1-Pd (0.047, 3.53 Å), Pd-P-Pd-O-Pd (0.051, 4.48 Å). Again the total contribution of multiple scattering pathways to the total back scattering is very low since the amplitude of experiment is 72.4.

The fit has improved and the R value has decrease from 27.4% to 20.3%. This could be due to multiple scattering (which theoretically is too small), or the other possibility is that the fit has improved because another four shells (12 parameters) have been added to the model, so the fit improves marginally for each refinable variable.

3.2.2 XAFS analysis of species 1 in the solid state

Due to the difficulties in fitting a suitable model to the solution spectra of the palladacycle, XAFS analysis was carried out on the palladacycle in the solid state, since it is known that it is a dimer. The spectra were recorded on Station 9.2 (SRS) in single bunch mode. Neat palladacycle was packed into a sample holder with a path length of 2.5 mm. Six transmission QEXAFS runs (12 minutes per scan) were measured (RTP) with an average

beam current of 20.7 mA and lifetime of 15.5 hours. Harmonic rejection was set at 70% and gave an edge jump of 0.8.

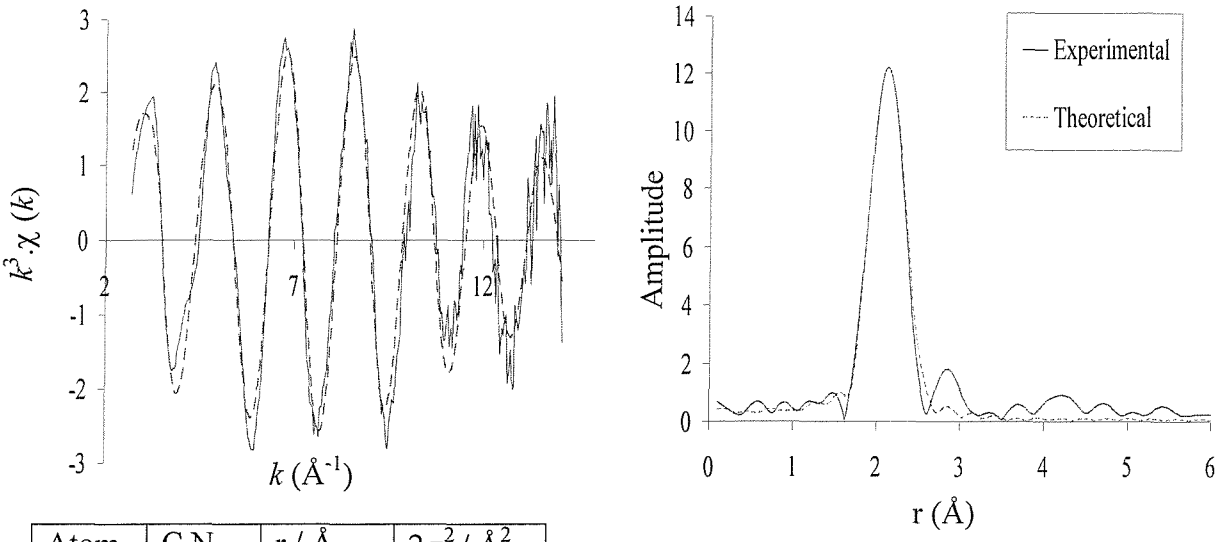

Atom	C.N.	r / Å	$2\sigma^2$ / Å^2
C	0.9(1)	2.04(1)	0.004(3)
O	1.7(3)	2.18(1)	0.023(6)
P	1.0(1)	2.26(1)	0.006(1)

E_f = -1.11(80) eV

R = 26.42 %

Figure 3.7 The palladium K-edge k^3-weighted QEXAFS (6 x 12 minutes, averaged) and Fourier transform for the solid state species 1 in NMP (RTP).

Figure 3.7 shows the fit for the solid state **1**. The result yields 14 Å^{-1} of data and is very good quality. It fits very well to the crystal model with 1 carbon, 2 oxygens and 1 phosphorus atom. The bond lengths are also very close to the X-Ray diffraction values and are very similar to the fit for **1** in solution.

If a palladium shell with a bond length of 3.15 Å is added to the model, the Debye-Waller value for the oxygen shell increases to 0.08 Å^2 and the R value increases to 28.0 %. As for the solution state work, the theoretical data line does not fit to the experimental feature around 4 Å^{-1}. Again this feature located at low k, can be shown to be formed from photoelectron wave interference due to atoms at a distance between 3 and 5 Å from the emitting palladium atom. The same multiple scattering models were applied to this data set, but again it was shown that multiple scattering effects provided only a minimal contribution to the fit, so have not been included.

Since it is know that **1** is a dimer at RTP in the solid state, this clearly demonstrates that even with 14 $Å^{-1}$ of data the palladium shell at 3.15 Å cannot be observed. Hence this information does not yield any further information on whether the palladacycle is a monomer in solution. Therefore it was decided to directly compare the background subtracted data for both spectra (solid and solution state).

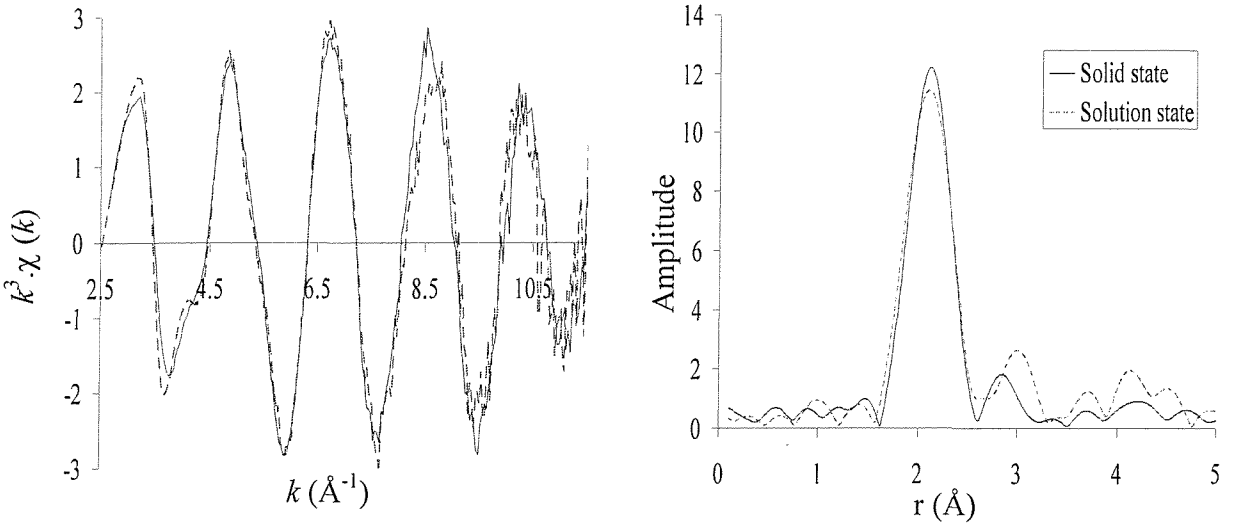

Figure 3.8 The palladium K-edge k^3-weighted QEXAFS (6 x 12 minutes, averaged) of the solid state species 1 compared with the EXAFS (2 x 30 minutes) for the solution state species 1 in NMP (RTP).

Figure 3.8 clearly shows the data quality is better in the solid state experiment (especially over 10 $Å^{-1}$), which is because the concentration (w.r.t. palladium) is considerably larger. The other main differences are at 4 $Å^{-1}$ the inflection in the solution experiment is more pronounced and there is variation in the peak intensity at high k, excluding these differences the spectra are almost identical and have the same frequency.

These results indicate the solid state and solution samples are essentially indistinguishable on the EXAFS scale obtained. The similar frequencies indicate that overall the bond lengths are the same. Since the palladium atom in the dimer (solid state) cannot be modelled, this would not considerably effect the data shown. But if a monomer had formed in the solution phase the bidentate acetate ligand with a shell of 1 carbon at a distance of 2.7 Å might needed to be considered as an influence on the spectra. Conversely if a palladium shell at 3.15 Å is not observable, the monodentate carbon could also have an insignificant effect on the results. Therefore this information does not help to decide on the monomer/dimer hypothesis.

Investigating the differences could yield some conclusions. Above 8 $Å^{-1}$ there is a slight shift, to higher *k* for the palladacycle in solution, which could mean an overall average smaller interatomic distance in solution

The Fourier transform of the spectra were both phaseshift corrected for carbon. As expected from the EXAFS data the Fourier transforms are similar. The main peak centred at 2.1 Å is very similar in both experiments. It is slightly less intense and broader in the solution case, which could be due to experimental error or due to greater freedom of movement in solution. Considering that the atoms bonded to the palladium atom are the same in both scenarios, this is the expected result. This part of the spectra cannot be fitted to the model and could be attributed to noise from the EXAFS. It is unlikely it is due to noise because by back transforming the data for both experiments, the peaks up to 5 Å are required to produce the inflection feature in the *k* weighted data at 4 $Å^{-1}$. Hence the difference is due to production of the monomer, but could also arise due to greater freedom of movement of the palladacycle in solution. The monomer production is favoured, since the difference in the Fourier transforms are too great at large distances, hence the differences must be due to changes of the environment around the metal centre.

In an attempt to assign the second peak (~2.9Å) in the Fourier transform (figure 3.8) the peak was Fourier filtered. In both cases the Fourier filtered peak was modelled as a palladium shell, but could not be fitted. In both cases it could be modelled as a carbon shell with varying success. In the solution the carbon shell could be best fitted as C.N. = 1.24(4), r = 3.04(0) Å, a = 0.002(1) $Å^2$, R = 18.3 %, in solid state the model fitted was C.N. = 0.88(4), r = 2.97(0) Å, a = 0.002(1) $Å^2$, R = 22.0 %, the data sets both had a *k* range from 3 to 12. Unfortunately this shell is not the carbon atom in the acetate ligand since the interatomic distance is too large. The crystal structure shows that the two carbon atoms in the palladated ring are 3.02 and 3.08 Å, so this Fourier transform peak could be due to the influence of these two carbons, since the Debye-Waller factor in both refinements is low.

3.2.3 Conclusions

Overall, with the data obtained it is very difficult to conclude on the exact structure of the palladacycle in solution. All the atoms directly bonded to the central palladium give a good single scattering model. The broad phosphorus NMR peak suggests that there is a monomer / dimer equilibrium, but could also be due to solvation (e.g. a monomer with a monodentate acetate group and an NMP molecule coordinated to the palladium, to keep the square planar symmetry). But from the data of the solution state sample it is difficult to establish what it is. Multiple scattering contributions were included, but theoretically all contributions were negligible and improvements to the fit were due to fitting more parameters, rather than fitting multiple scattering pathways.

Analysis of the solid state sample shows that the palladium-palladium interaction is not observable with the EXAFS data obtained, which does not rule out the presence of the dimer in solution. But, the subtle differences in the EXAFS between the solution and solid phase support a difference in the structure, hence production of monomer. It has been shown that the feature at 4 $Å^{-1}$ (more defined in solid state) is formed by interference of the atoms in the photoelectron wave at a distance of 3 to 5 Å from the central palladium atom. This could be caused by either a change in the molecular structure due to the formation of monomer, or due to changes in the interatomic distances in the molecule due to greater degrees of freedom in solution.

3.3 Comparison of the different XAFS techniques for species 1

A single scan for standard EXAFS (30 minutes), QEXAFS (4 minutes) and EDE (I^t = 2.2 ms) spectra were compared for **1** in solution (figure 3.7).

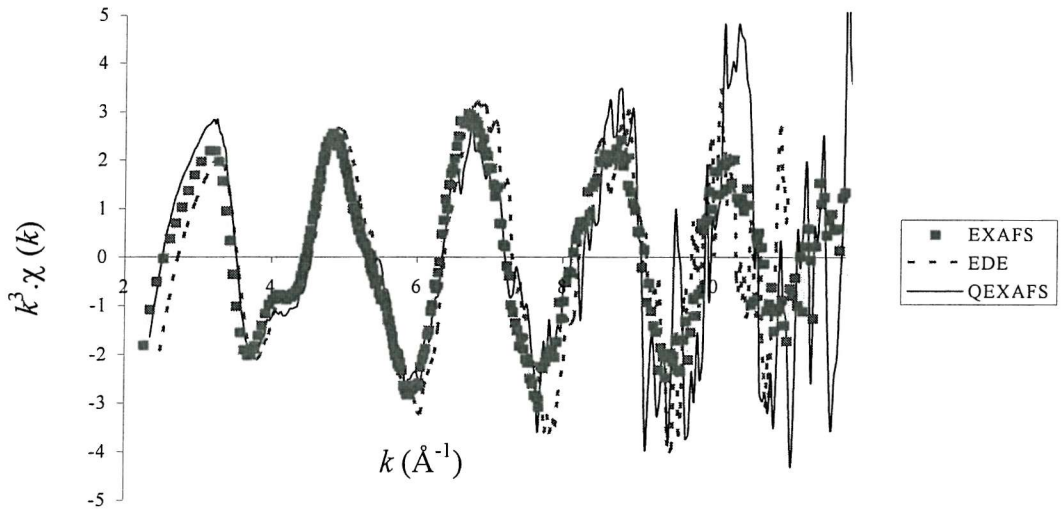

Figure 3.9 The palladium K-edge k^3-weighted spectra for species 1 (in solution) comparing spectra quality for EXAFS (1 x 30 minutes), QEXAFS (1 x 12 minutes) and EDE (100 scans, 1.4 ms).

The figure shows that the data quality for the standard EXAFS is definitely the best. Not surprisingly the QEXAFS data also has less noise than the EDE data, but for values of k equal to 9 and above the QEXAFS data is actually noisier and diverges more from the EXAFS data than the EDE spectra. It has a large spike at k = 9.3 Å^{-1} and the data quality for k > 10 Å^{-1} is so poor it would be unwise to include it into any further analysis. For the EDE spectra this upper limit could be slightly extended to k = 10.5 Å^{-1}, whereas the full data set can be used from the standard EXAFS experiment.

Another factor which needs to be considered, when comparing the spectra accuracy is the number of data points taken in the scan. For the spectra shown, the number of data points measured between k = 2.2 Å^{-1} and k = 11.1 Å^{-1} was calculated. For standard EXAFS 309 data points were measured, with 238 points measured for QEXAFS and only 207 measured for EDE. This factor explains why the EDE spectrum is smoother than the QUEXAFS

spectrum.

These spectra show that to obtain the best results for investigating the experiments conducted in this thesis, a synergy of techniques is best. Standard EXAFS can be used to investigate the pre and post catalytic species. It can also be used to investigate the 'quenched' catalytic solution, but generally this is prohibitively expensive in regards to time, since an average of three scans for one sample takes 90 minutes. Also, with the experimental apparatus used, it is only possible to 'quench' down to RTP, which can raise two arguments:

1) Is the catalytic solution properly quenched?
2) Is the catalytic species still stable at RTP?

The results from the *in situ* and *ex situ* ^{31}P NMR results tend to suggest that that the species could be stable and quenched. But obviously the NMR study was only on one reaction, so in some reactions the species could be more unstable.

3.4 Heating species 1

As mentioned in section 3.2, the nature of the equilibrium investigated in the previous section could be far more complex than a simple monomer / dimer equilibrium. The equilibrium could also involve monodentate acetate ligands and solvent molecules. EXAFS analysis of the palladacycle in solution is not able to determine the precise nature of the equilibria. Therefore to try to answer this question and to investigate the effect of heat on the palladacycle, it was heated to 130 °C.

One EXAFS scan was taken of the palladacycle (50 mM in NMP, path length of 1mm) at 50, 70, 90, 110 and 130 °C.

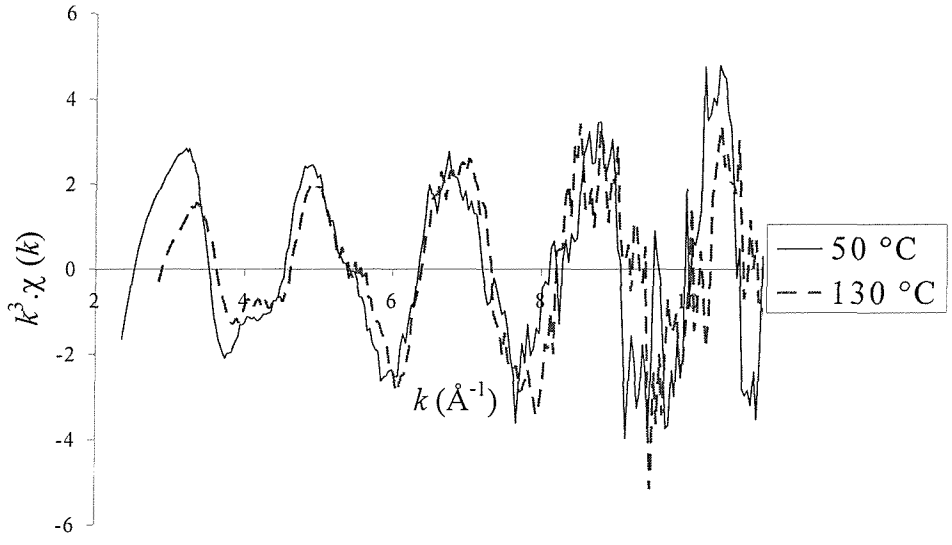

Figure 3.10 The palladium K-edge k^3-weighted EXAFS (1 x 30 minutes) of the solution state species 1 NMP (heating).

Figure 3.10 shows that at low k the intensity of the k^3 data decreases with increasing temperature. In the figure only the lowest and highest temperature spectra is shown for simplicity, but it is a trend of all five spectra. A plot of the normalised white line against temperature shows this trend very clearly (figure 3.11A). There is a linear decrease in the white line intensity as the palladacycle is heated. Since the white line intensity changes this is indicative that there is a change in the species concentration in the sample. It is very unlikely that it would change due to heating so suggests that there is a change in the equilibrium shifts. To investigate further the k^3 EXAFS data was Fourier transformed and phaseshift corrected (figure 3.11B).

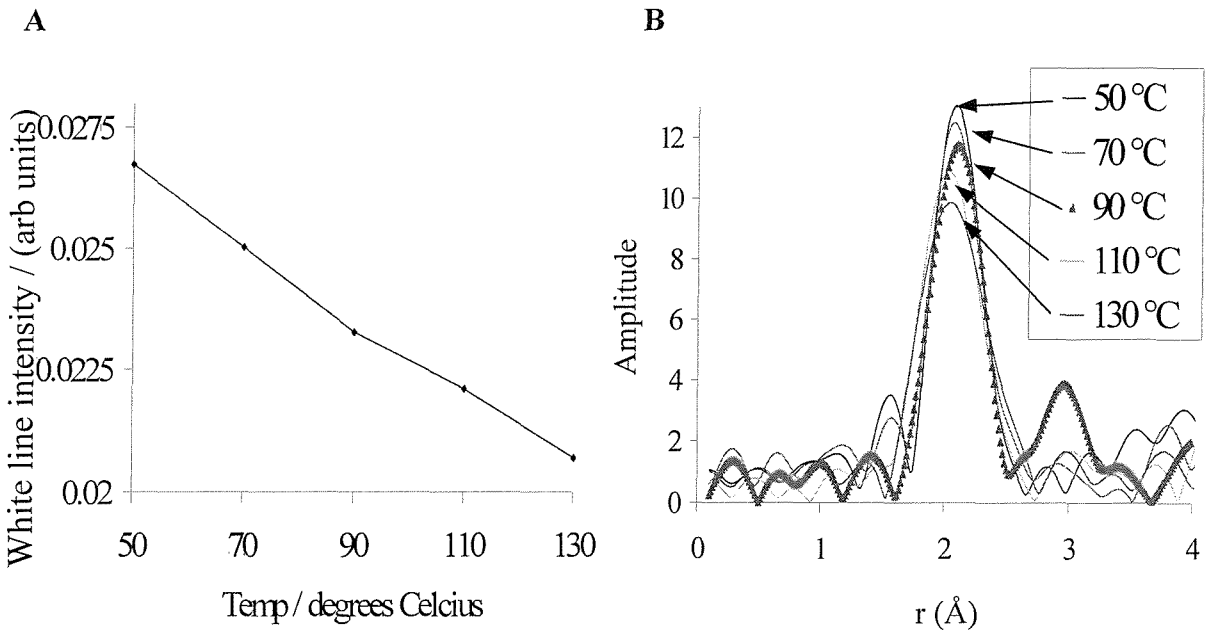

Figure 3.11 Graph of the normalised white line intensity for species 1 against temperature (A) and the palladium K-edge k^3-weighted QEXAFS and Fourier transforms (1 x 12 minutes) (B) for species 1 on heating to 130 °C.

This figure clearly shows that as the palladacycle is heated the intensity of the Fourier transform peak decreases and broadens. This could be because of the greater vibrational amplitudes due to the increase in thermal motion. It could also be caused by an increase in the interatomic distances in the species present. The overall distance is very similar, so the model would contain a similar ligand set. It does not yield any further clues to whether the equilibrium changes. But there is also a slight decrease of the r value for the maximum peak intensity. This suggests that there is an overall decrease in the interatomic distances as the palladacycle is heated. Considering that any change in the P-C ring distances would be very small, they can be discarded. Therefore the only changes are due to a change in the equilibrium. By examining the proposed equilibria this shows that the monomer dimer equilibria shifts towards more production of the monomer.

Models were then fitted to the five spectra to see if any further information on the structure during heating could be deduced. The results were all very similar, with the interatomic distance of the carbon / oxygen shell ranging from 2.06-2.09 Å (see section 3.5.2) and the carbon phosphorus bond length ranged from 2.20-2.23 Å, but there were no overall trends.

3.5 Formation reaction of species 1

It is thought that phosphine palladacycles form by the coordination of the phosphine and followed by closure of the palladated ring (chapter 1). To test this theory the formation of **1** was investigated with XAFS and *in situ* NMR techniques.

3.5.1 *In situ* NMR

Palladium acetate (50 mM) was stirred at room temperature with tri(*o*-tolylphosphine) (150 mM) in toluene until homogeneous, then transferred into a 5 ml Young's NMR tube. The solution was heated to 80 °C and ^{31}P NMR spectra were measured throughout the reaction. The samples were run unlocked and referenced against a standard sample of tri-*o*-tolylphosphine. The results acquired from the experiment are shown in figure 3.12.

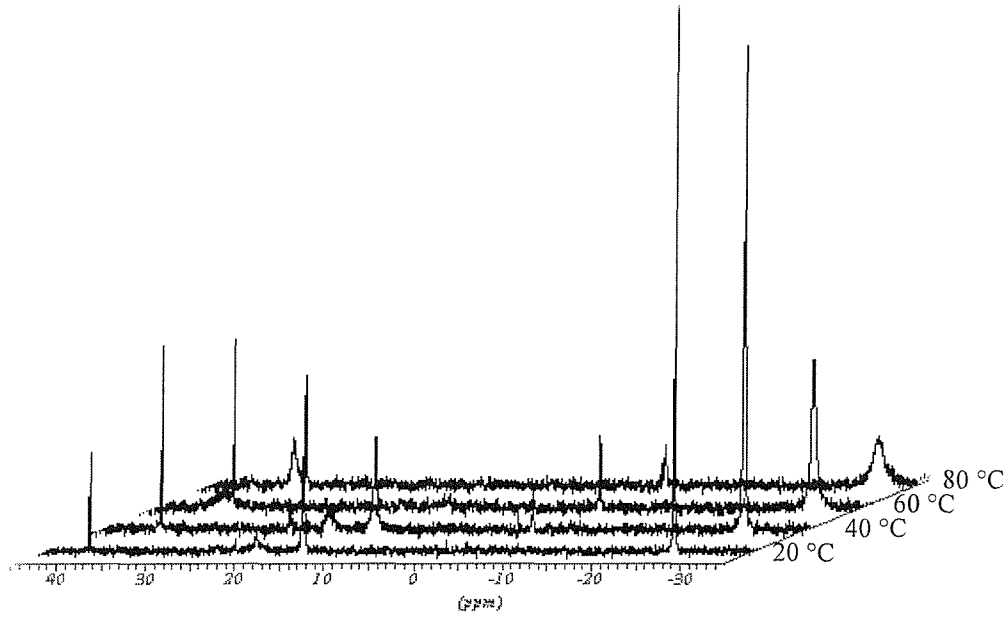

Figure 3.12 $^{31}P\{^{1}H\}$ NMR spectra for the formation of species 1.

The results show at 20 °C, 66% of the phosphorus species is present as tri-*o*-tolylphosphine (-29.5 ppm) and 34% is present as a peak at 12.2 ppm. After heating to 40 °C, there was still no formation of **1**. After heating another 20 °C the peak at 12.2 ppm had disappeared, 72% of the phosphorus was present as the starting material, 25% was present as **1** (35.2 ppm) and there was a small amount of by product at -5.8 ppm. At the final temperature the ratio of reactant to product was 2:1, which shows that the yield is almost 100 % (w.r.t. the

palladium acetate). At this temperature the peaks due to tri-*o*-tolyphosphine and **1** are both very broad (**1** is normally broad), which shows that in the reaction solution there is an exchange process of the phosphine ligand, between coordination to palladium and free ligand.

The peak at 12.2 ppm is likely to be the intermediate species with the phosphine ligand coordinated to palladium, but before cyclisation commences. The bridging acetate compound $[Pd(PPh_3)(CH_3COO)(\mu\text{-}CH_3COO)]_2$ has been reported,[15] so the intermediate present could be the *o*-tolyl analogue.

Monitoring the concentration of the free phosphine shows there is fluxionality since the concentration increases then decreases during the reaction. Note that the peak at 36.1 ppm is $O{=}P(o\text{-tolyl})_3$ and remained constant in concentration throughout the reaction. The experiment was repeated *ex situ* and the results were very similar and the same species were observed.

3.5.2 EDE study of the formation of species 1

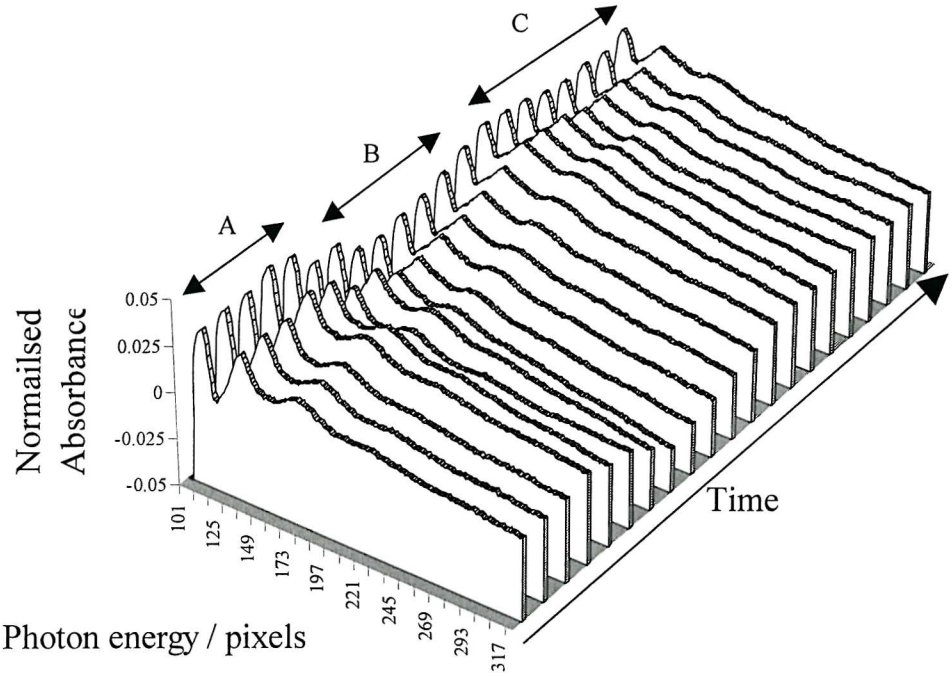

Figure 3.13 Pd K edge time resolved EDE spectra for the formation reaction of species 1 (showing every five spectra).

The formation reaction was repeated and followed with *in situ* EDE techniques. The reaction mixture was stirred at RTP and transferred into the XAFS cell. The reaction mixture was heated to 130 °C and a hundred time resolved spectra (50 scans, I^t = 1.2 ms) were measured in thirty three minutes. The XAS around the palladium K edge for the reaction is shown in figure 3.13, with every five spectra being plotted to aid clarity.

The temperature was considerably higher then for the analogous NMR experiment to aid mixing of the solution through convection currents (not required in the NMR experiment due to spinning of the sample in the spectrometer).

From the XAS plot it can be seen that there are three distinct regions in the plot (A, B and C), but it is very difficult visually to ascertain any further information, so a white line plot was calculated and is shown in figure 3.14. It confirms the observation in the previous diagram that there are three main distinct areas, it is also considerably clearer and shows at what times during the experiment the transitions occur.

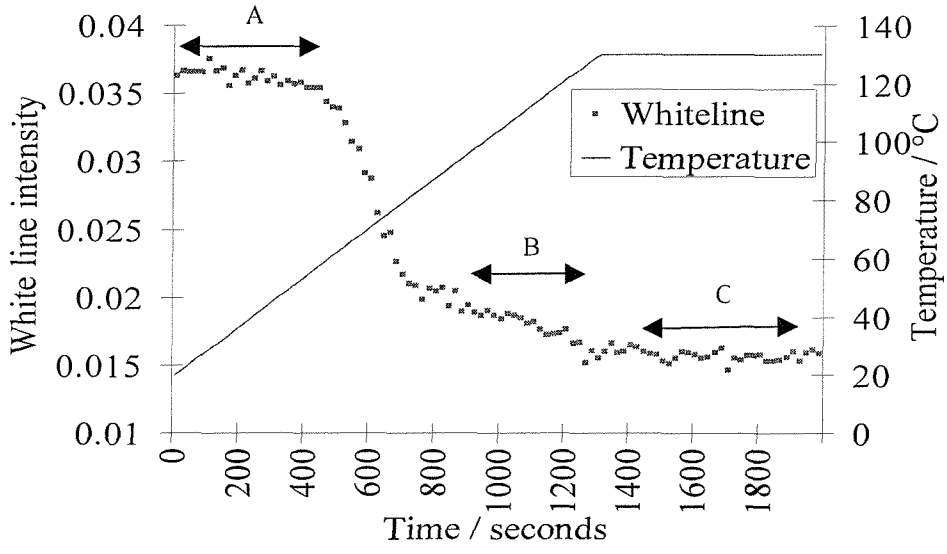

Figure 3.14 Plot of white line intensity and temperature against time, for the formation of species 1.

From this figure it was decided to analyse spectra at 0, 812, 1010 and 1960 seconds. They were chosen since they appear in each of the three main marked areas, 812 seconds was chosen since it appears as a little step, just before the start of section B. The Fourier transforms (with models) are shown in figure 3.15A for each of these spectra.

These four Fourier transforms show exceptionally well the different stages in the reaction. At 0 seconds palladium acetate is present in solution, which fits very well to a model of 4 oxygen atoms. After 820 seconds the Fourier transform has shifted to higher r values, which is due to coordination of the phosphorus ligand. Due to the EDE data having a shorter *k* range than for the EXAFS data (see section 3.2.1), it is not possible to keep the oxygen and carbon shell discrete. Therefore the mixed shell is modelled as 2.7 oxygens at 2.08 Å, (i.e. 2 oxygens and 1 carbon atom (the carbon atom is smaller) at a mixture of bond lengths (carbon at 2.02 Å and oxygen ~2.14 Å)). A very similar model is applied to the spectrum taken at 1020 seconds and the Fourier transforms are very similar. The graph of **1** being heated (figure 3.11) shows that the Fourier transform should decrease in intensity during the heating process, since this trend is not shown for these two Fourier transforms in figure 3.15 and because the white line has changed this could suggest that some other change has occurred which is not just due to heating. This change could be attributed to the formation of the Pd-C bond. The final species (1980 seconds) also refines well to the model of the palladacycle. The Fourier transform shows the same trends as for when **1** was heated, so is probably the palladacycle at higher (130 °C) temperatures.

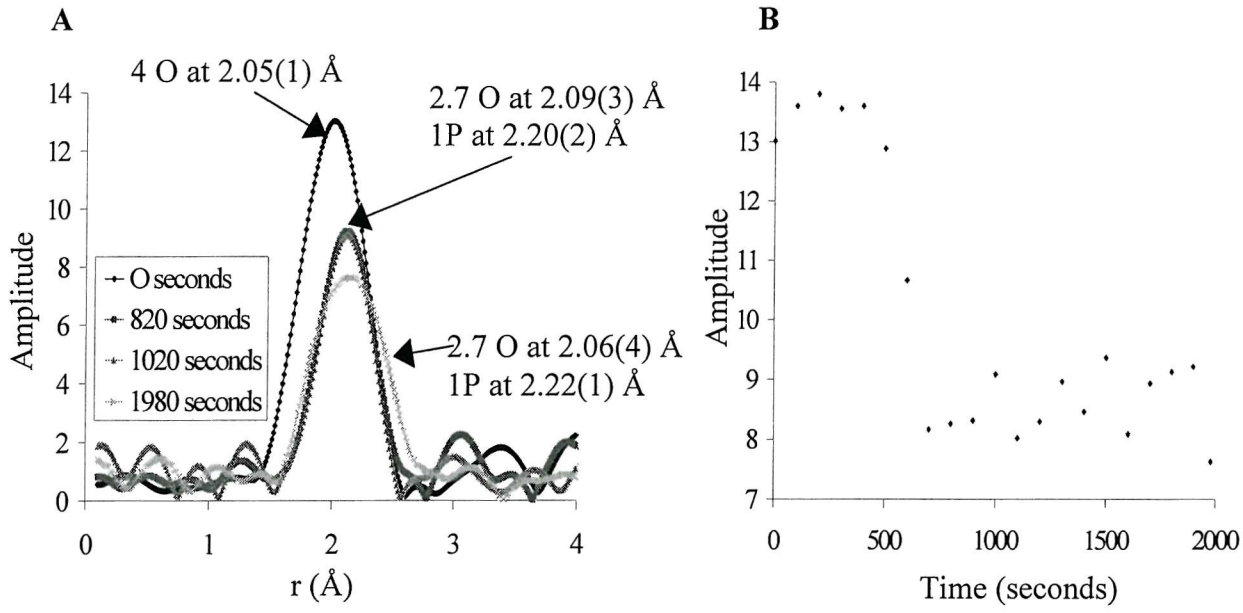

Figure 3.15 The palladium K-edge Fourier transforms for selected times during the formation of species 1 (A) and the Fourier transform peak heights (showing every five spectra) for the same reaction (B).

Figure 3.15B shows the Fourier transform peak heights during the formation reaction of **1**.

This figure corroborates the trend (decrease in peak intensity) shown in figure 3.15A. But, also shows that the data is noisier than predicted by figure A, especially towards the end of the experiment. The plot shape is very similar to the shape of the white line plot in figure 3.14. This depicts the strong correlation between the change in white line features and the change in the environment around the palladium metal.

To confirm the observations made by the previous figure, the *k* weighted data for the same selected points during the reaction were compared (figure 3.16A). The results show there is a considerable difference between the palladium acetate at 0 seconds and the palladium species coordinated to phosphorus at 820 seconds. The spectra taken after this are all very similar, which agrees with the hypothesis that there is no major change of the environment around the palladium atoms.

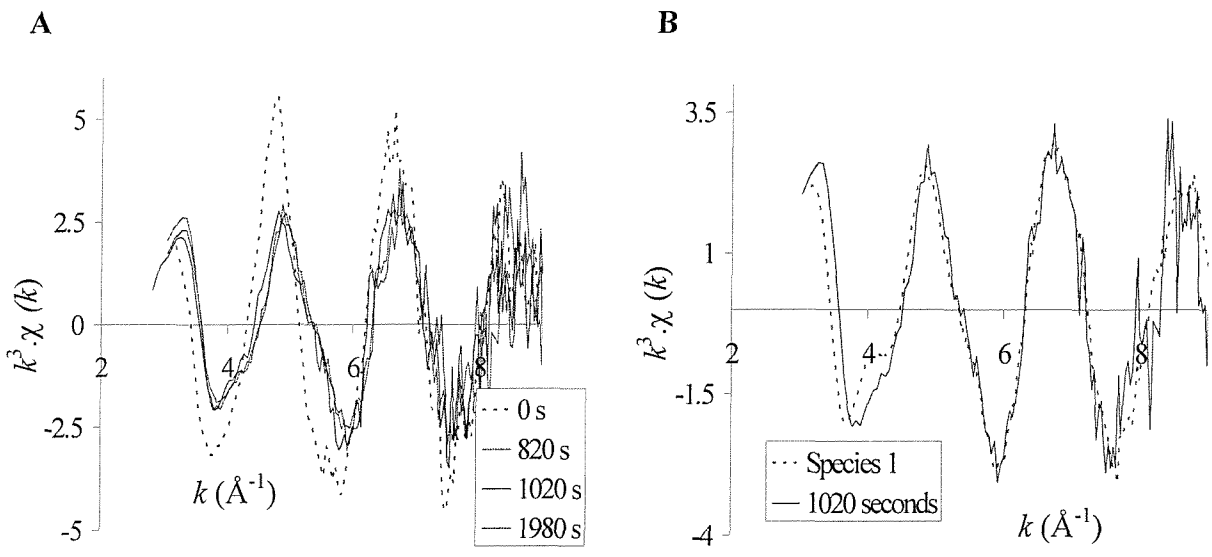

Figure 3.16 The palladium K-edge k^3-weighted EDE spectra (50 scans, I_t = 1.2 ms) for the formation of species 1 (A) and the comparison of EDE scan (t = 1020 seconds) with an EXAFS scan of solution state species 1.

Figure 3.16B shows the scan at 1020 seconds overlaid the EXAFS scan of **1** in solution. The spectra are very similar indicating the species are very similar (i.e. the palladacycle has formed). The main difference is that the inflection at 4 Å^{-1} is more defined for the preformed catalyst. The lack of definition in the reaction spectrum could be due to the phosphine exchange process indicated by the broad phosphorus NMR peaks (figure 3.12).

3.5.3 EDE study of the formation of species 1 with a reduced phosphine concentration

The previous study was repeated with the same palladium concentration (50 mM) but the tri-*o*-tolylphosphine concentration was reduced to 100 mM. The reaction was heated from 22 °C to 50 °C at a rate of 10°C/2min and held. Time 0 was taken as the initial time of heating. The time resolved EDE collection time took 32 minutes and 100 spectra were taken. Each was an average of 50 scans. A plot of the white line intensity (every 2 spectra) against the reaction scan number is shown in figure 3.17.

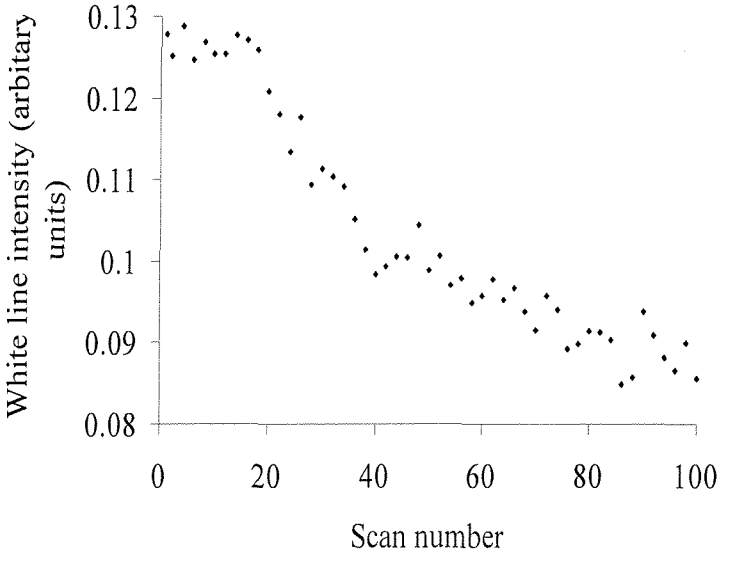

Figure 3.17 White line intensity for formation of species 1 (2:1 ratio of tri-*o*-tolylphosphine to palladium acetate).

The white line intensity shows the same trends as the 3:1 experiment (figure 3.14). Due to the reduced temperature in the 2:1 reaction the same features appear but later on in the experiment. The little step in the 3:1 graph prior to the start of section B, has been expanded in the 2:1 experiment as the area between scan 40 and 65. This area relates to the palladium species with phosphorus coordinated, but before internal metallation occurs. From figure 3.17 the section where **1** is formed starts at scan number 80 (section B in the 3:1 experiment). Obviously section C is not reached in the 2:1 experiment, because the maximum temperature reached is only 50 °C.

3.6 Reactions between $Pd(OAc)_2$ and other tertiary phosphine ligands

The previous experiment was extended to investigate the reaction of $Pd(OAc)_2$ with tri-tert-butylphosphine (P^tBu_3), tricyclohexylphosphine (PCy_3) and triphenylphosphine (PPh_3). XAFS techniques were used and the procedure was very similar to the P(*o*-tolyl)$_3$ reaction, with a palladium concentration of 50 mM and a phosphine concentration of 150 mM. The solutions were stirred under nitrogen at room temperature until the reactants had dissolved, then injected into the XAFS cell. The cell was then ramped to 130 °C (at a rate of 5 °C / min) and held, whilst 100 time resolved EDE scans were taken (1 every 24 seconds).

3.6.1 Reaction between $Pd(OAc)_2$ and PCy_3

The first study was the reaction between $Pd(OAc)_2$ and PCy_3. ^{31}P NMR analysis of the reaction solution after heating to 100 °C showed that 45 % of the total amount of phosphorus remained unreacted as the free ligand (10.8 ppm), 30 % formed $O{=}PCy_3$ (48.0 ppm)[16] and 23 % formed $Pd(PCy_3)_2$ (22.7 ppm).[17] There was no formation of $Pd(PCy_3)_3$ at 37.9 ppm.[17]

Since the ratio of phosphorus to palladium is 3:1, 35 % of the palladium in solution is coordinated as $Pd(PCy_3)_2$ and which means 65 % is present as $Pd(OAc)_2$. The corresponding EXAFS model for palladium would be an oxygen shell with coordination number of 2.6 and a phosphorus shell with coordination number of 0.7.

As before the reaction was heated to 130 °C and held and time resolved XAFS was taken. The temperature was ramped as before but for this experiment the heating was started after 90 seconds. The white line plot is show in figure 3.18.

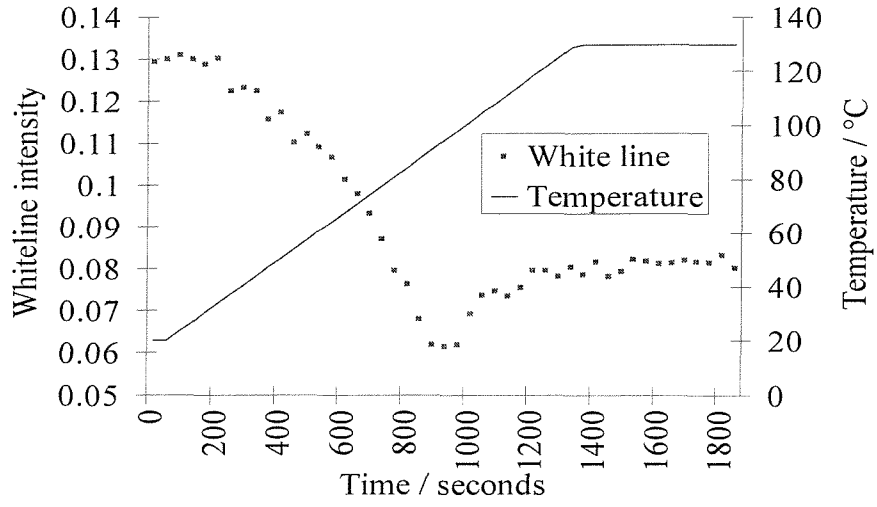

Figure 3.18 The palladium K-edge white line plot of the reaction between $Pd(OAc)_2$ and PCy_3 (1:3).

The results show two trends over the reaction, first there is a decrease in the white line height, which achieves a minima at 850 seconds, which then increases slightly towards the end of the reaction. This minima could be due to the end of the formation reaction of $Pd(PCy_3)_2$ and the increase in the white line intensity (afterwards) could be due to the species degrading due to the extreme reaction conditions. Using the figure as a guide spectra were analysed from specific points during the reaction (0, 860 and 1980 seconds).

Figure 3.19 shows the EDE data acquired from the very start of the $Pd(OAc)_2$ and PCy_3 reaction at RTP. The data is of reasonable quality considering it is time resolved and it fits well to a model of $Pd(OAc)_2$, with four oxygen atoms coordinated to the palladium atom. This shows that there is negligible phosphorus coordination to palladium at this temperature.

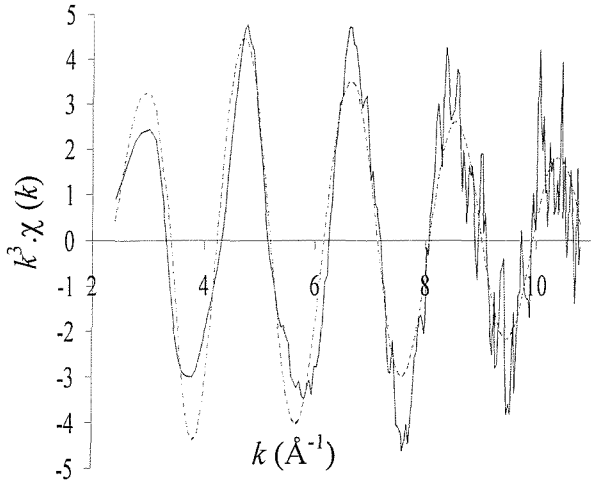

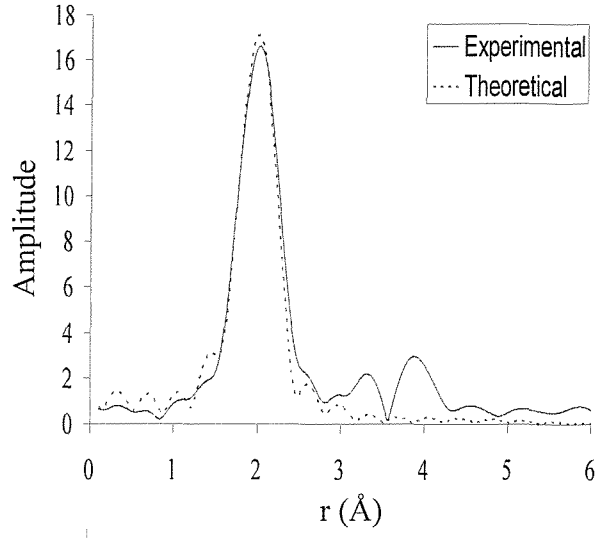

Atom	C.N.	r / Å	$2\sigma^2$ / $Å^2$
O	3.8(2)	2.05(1)	0.010(1)

E_f = -5.2(13) eV

R = 39.3%

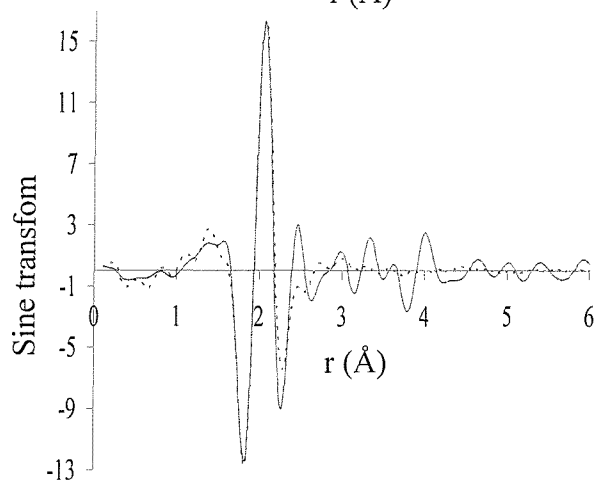

Figure 3.19 The palladium K-edge k^3-weighted EDE data (I^t = 2.2 ms), Fourier transform and sine transform for the reaction between $Pd(OAc)_2$ and PCy_3 (1:3) (0 seconds).

The EDE spectrum taken after 860 seconds was then analysed and is shown in figure 3.20. The model calculated from the NMR reaction at the start of this section (2.6 oxygen atoms and 0.7 phosphorus atoms) fitted fairly well to the experimental data.

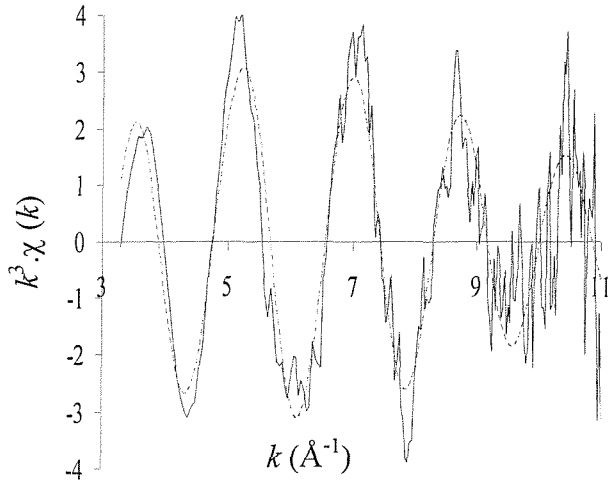

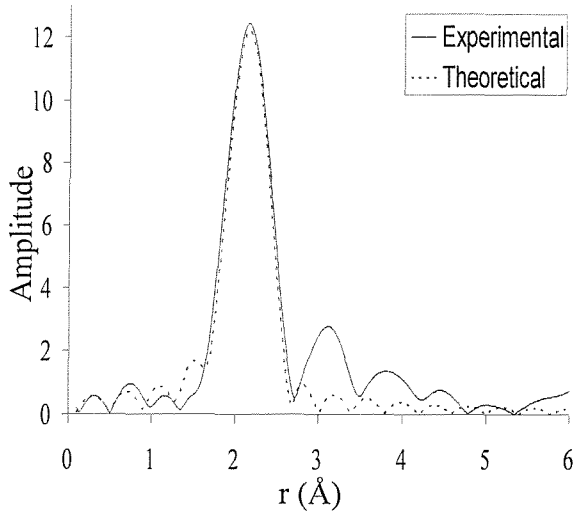

Atom	C.N.	r / Å	$2\sigma^2$ / $Å^2$
O	1.5(8)	2.07(3)	0.021(6)
P	1.0(3)	2.26(1)	0.007(4)

E_f = 4.3 (63) eV

R = 42.4 %

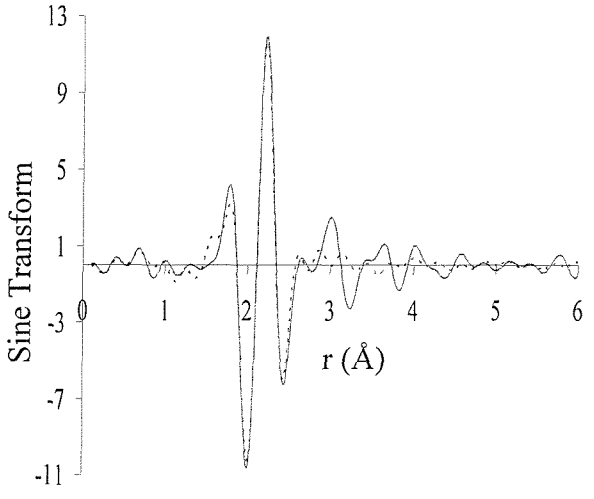

Figure 3.20 The palladium K-edge k^3-weighted time resolved EDE data (I^t = 2.2 ms), Fourier transform and sine transform for the e reaction between $Pd(OAc)_2$ and PCy_3 (860 seconds).

The refined model has large errors on the oxygen shell, with large oxygen Debye-Waller terms. This shows that in the XAFS sample there was greater formation of the Pd-P species, compared with the NMR sample. This shows that from the white line graph it is possible to choose points of interest and then analyse the selected spectra. Whereas in the choice of NMR samples, it normally has to be conducted by choosing appropriate temperatures, times or colour changes (if applicable). The QEXAFS scan at the end of the reaction (1980 seconds) was analysed, but the results were poor due to some precipitation of palladium black.

3.6.2 Reaction between $Pd(OAc)_2$ and P^tBu_3

This study was then expanded to include the reaction of $Pd(OAc)_2$ and P^tBu_3 (1:3). Figure 3.21 shows the XANES plot of the normalised white line against the EDE scan number. Heating was started at 20 °C and at 1320 seconds the reaction temperature reached 130 °C.

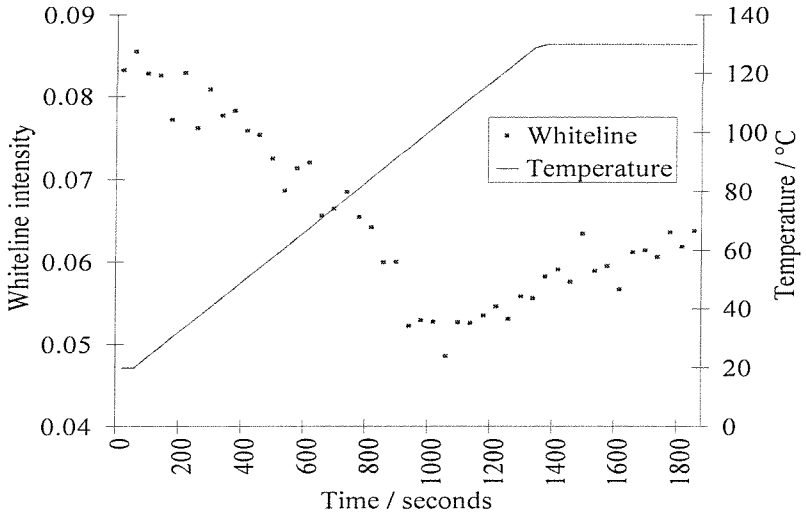

Figure 3.21 The palladium K-edge white line plot taken during the reaction between $Pd(OAc)_2$ and P^tBu_3 (1:3).

The plot is very similar to the previous one with PCy_3 as the ligand. In both cases the acetate ligands are being replaced by phosphine ligands, but unlike the PCy_3, the P^tBu_3 ligand could cyclopalladate. This is unlikely to occur because it would create a four membered ring rather than a five membered ring, which are not as energetically favourable due to stain in the ring due to steric congestion. But the cyclopalladated species $(PdCl(C_4H_8P(^tBu)_2)(P(^tBu)_3)$ has been reported, synthesised by reacting the free phosphine with palladium (II) chloride ($PdCl_2(P^tBu_3)_2$ was also formed).[18]

The results show two trends over the reaction, first there is a decrease in the white line height, which achieves a minima at 1056 seconds, which then increases slightly towards the end of the reaction (corresponding to a slight decrease in edge jump, which indicates some palladium degradation). Using the figure as a guide spectra were analysed from specific points during the reaction (0, 704, 1056 and 1804 seconds).

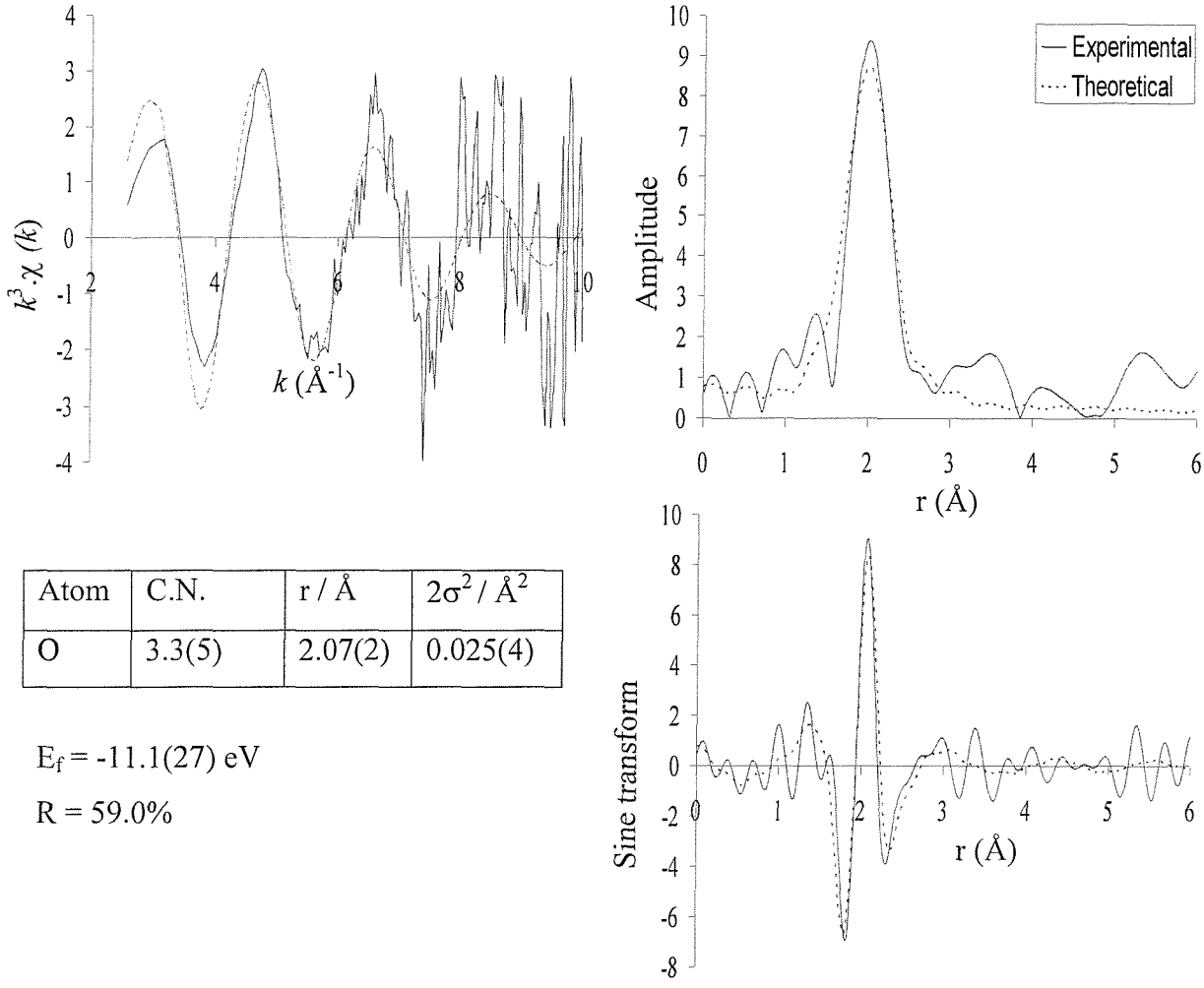

Atom	C.N.	r / Å	$2\sigma^2$ / Å^2
O	3.3(5)	2.07(2)	0.025(4)

E_f = -11.1(27) eV

R = 59.0%

Figure 3.22 The palladium K-edge k^3-weighted EDE time resolved data (I^t = 2.2 ms), Fourier transform and sine transform for the reaction between $Pd(OAc)_2$ and P^tBu_3 (1:3) (0 seconds).

Figure 3.22 shows the starting spectra for the reaction. The data refines fairly well to the expected fit for $Pd(OAc)_2$, with a good bond length, but lower than expected coordination number which also manifests itself as a higher than expected Debye-Waller term. This suggests that product formation had already commenced. The errors are all with acceptable limits, but the R value is very high which is caused by the very noisy data between 8 and 10 Å^{-1}.

The final scan was then analysed and the result is shown in figure 3.23. Again the data is not of the highest quality, but refines well to a model of 2 phosphorus atoms, with a bond length that agrees with the X-ray crystal structure[19] reported in 1992. The coordination number and Debye-Waller values calculated agree that the species formed has two rather

than three phosphine ligands coordinated.

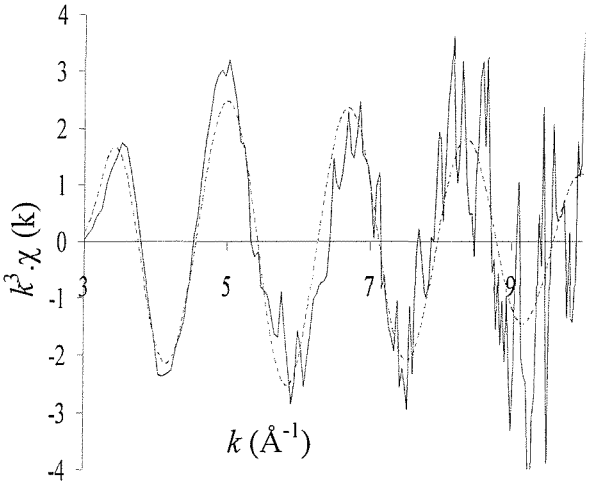

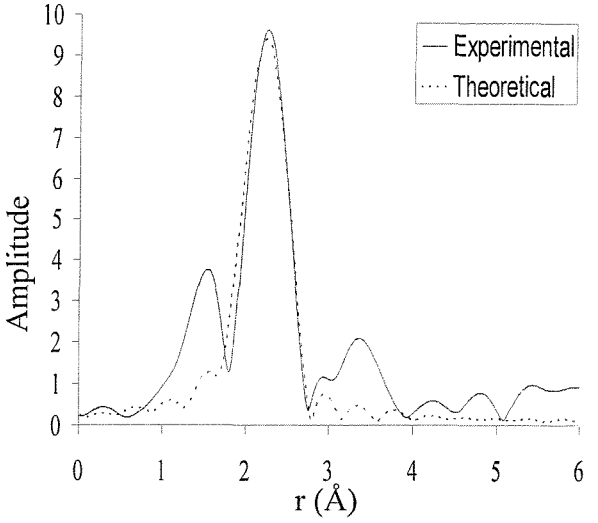

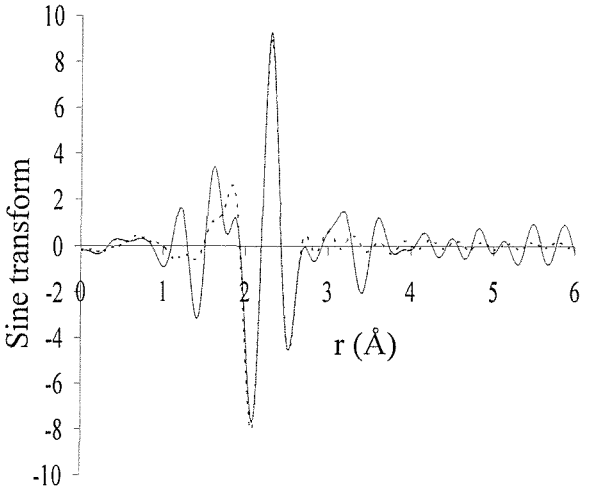

Atom	C.N.	r / Å	$2\sigma^2$ / Å^2
P	2.0(2)	2.29(2)	0.015(2)

E_f = -8.5(28) eV

R= 52.8%

Figure 3.23 The palladium K-edge k^3-weighted EDE time resolved data (I^t = 2.2 ms), Fourier transform and sine transform for the reaction between $Pd(OAc)_2$ and P^tBu_3 (1:3) (1804 seconds).

Analysis of the EDE data from 704 seconds (halfway between shortest and longest white line) and 1056 seconds (shortest white line) gives a very similar result to the model for scan 100. The coordination number refines to 2(2) and a Debye-Waller value for 704 seconds at 0.017(2) σ^2 and for 1056 seconds at 0.015(2) σ^2. The only main difference is the average bond length which refines to 2.23(2) Å for both scans. Due to the low data range it is very difficult to be precise and to say exactly when the palladium phosphine species has formed and this problem is exacerbated since the EXAFS changes between starting and finishing materials is not large.

To yield further information the EXAFS data and the XANES region of the XAS were directly compared (figure 3.24).

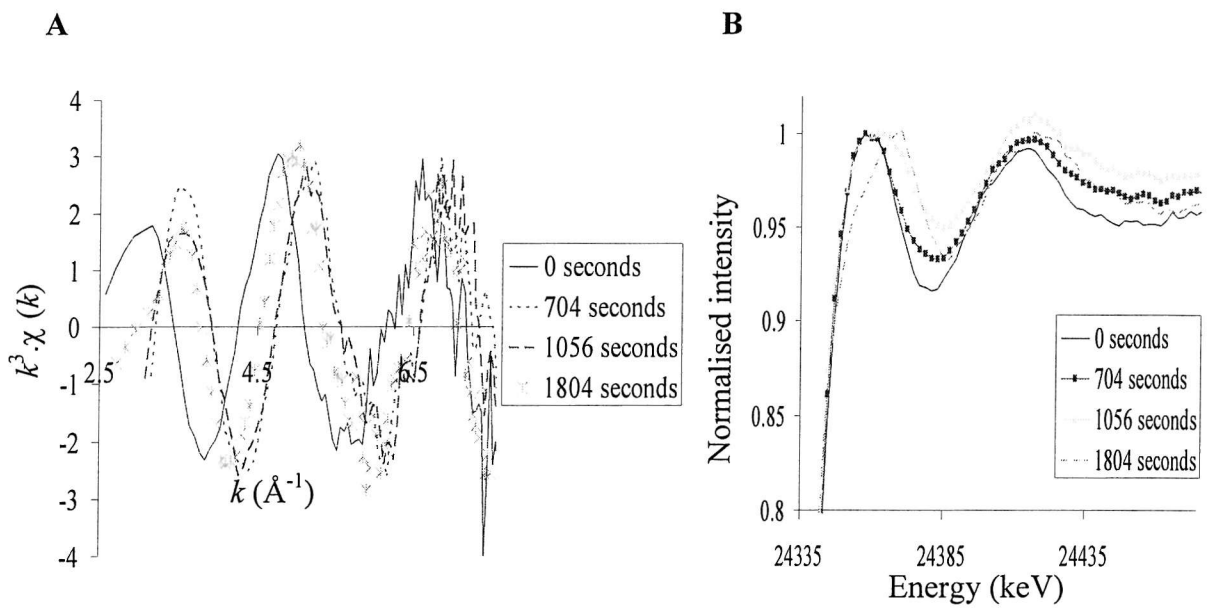

Figure 3.24 Comparison of the EXAFS region (A) and the normalised XANES region (B) for selected scans from the reaction of $Pd(OAc)_2$ and P^tBu_3 (1:3).

Comparison of the low k EXAFS region shows that there is a noticeable difference between 0 seconds and 704 seconds, no change between 704 and 1056 seconds and then a change in the frequency between 1056 and 1804 seconds. Since the Fourier transform shows that scan 1 is the $Pd(OAc)_2$, it appears as if the $Pd(P^tBu_3)_2$ species has formed at 704 seconds, which disagrees with the white line spectrum, which shows that the species has not completely formed until 1056 seconds. The EXAFS refinements for 1056 and 1804 seconds gave the same model, but the comparison of the k weighted data shows there is a significant change between the data sets. This is presumably due to the deterioration of the palladium species under the extreme temperature conditions and interference in the EXAFS from precipitation of solid palladium. This was not evident in the Fourier transform, but was depicted by a slight reduction in the XAS step, caused by a reduction in the absorption of the X-rays due to a decrease in the amount of absorber present.

Analysis of the normalised XANES section of the XAS (figure 3.24B), shows that the XANES region is different for all four scans, this agrees with the white line plot that all four spectra are all different. There is considerable difference between the XANES for 704 and 1056 seconds (i.e. not just a difference in the white line height), this shows that even though the EXAFS data is very similar, the electronic configuration between the two species are

very different.

Therefore using the EXAFS and XANES information together this shows that at the start of the reaction the main palladium species present is $Pd(OAc)_2$ and the product is formed at 1056 seconds, which is unstable at high temperatures and some decomposes to solid palladium. EXAFS shows that at 704 seconds the main species present is the palladium (0) complex, but there is still a large electronic difference between 704 and 1056 seconds.

^{31}P NMR spectroscopy was not used to analyse the experiment, so it is not possible to conclude what the oxidised species in the reaction is, to account for the reduction of the palladium. It is known from the $Pd(OAc)_2$ and PCy_3 reaction that $O{=}PCy_3$ is formed, so it is very likely the $O{=}P^tBu_3$ is formed in this reaction, but obviously cannot be directly detected using XAFS.

3.6.3 Reaction between $Pd(OAc)_2$ and PPh_3

The study was finished by investigating the reaction of $Pd(OAc)_2$ with PPh_3. Again the white line was plotted as the reaction progressed and is shown in figure 3.25A and the corresponding Fourier transform calculated from specific points during the reaction are shown in figure 3.25B. For this reaction the heating ramp commenced at the start of scan 5.

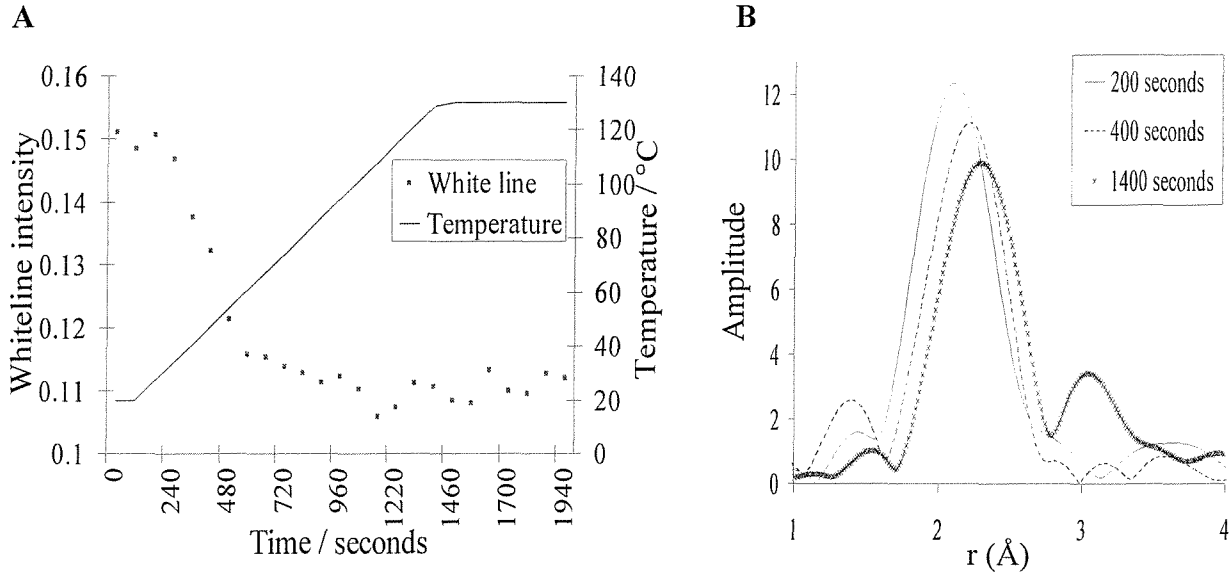

Figure 3.25 The palladium K-edge EDE (I^t = 2.2 ms) white line plot (A) and the corresponding Fourier transform after 200, 400 and 1400 seconds (B).

As before the white line quickly decreases, but after reaching a minimum it does not increase again. This suggests that the palladium phosphorus species formed are more stable at high temperatures, since they do not decompose at the same reaction conditions, as for the previous two experiments.

The Fourier transform plot (figure 3.25B) shows scans from the beginning (200 seconds), middle (400 seconds) and end (1400 seconds) of the reaction. At the start is the $Pd(OAc)_2$, at the end is probably a mixture of $Pd(OAc)_2(PPh_3)_2$, $Pd(PPh_3)_3$ and in the middle is a mixture of all species. This is depicted in the figure since there is a shift of the Fourier transform peak to higher R values due to the longer phosphorus palladium bond. There is also a decrease in the Fourier transform intensity, which could be due to a reduction in the coordination number and also due to the heating process increasing the molecular vibrations in the complexes.

As before without the phosphorus NMR data it is very difficult to establish chemically what is happening. The EDE results show that the amount of phosphorus coordinated to palladium increases during the reaction and again presumably the oxidised species present is $O{=}PPh_3$.

3.7 Conclusions

Phosphorus NMR gives a broad peak for **1** and it has been hypothesised that this is due to a monomer / dimer equilibrium.[6] XAFS analysis was used to characterise the catalyst and in an attempt to establish more details on this equilibrium. It was discovered that **1** fitted very well to a simple model of 1 carbon, 2 oxygen and 1 phosphorus atom coordinated to the palladium atom with bond lengths similar to the crystal structure. Any attempts to improve the model were unsuccessful. It was discovered that multiple scattering effects provided negligible contributions to the fit. It was not possible to detect any contributions to the experimental data from a palladium atom (dimer model) or the central carbon of the bidentate acetate ligand. Analysis of the solid state form of **1** (known to be a dimer), showed very similar XAFS results and therefore showed that it is not possible to include the palladium-palladium interaction in the model.

Therefore from these systems no further information could be elucidated on the equilibrium. But, by heating the preformed palladacycle in solution there was a slight shift of the Fourier transform peak to lower r values, which suggests a slight decrease in the average interatomic distance around the central palladium atom. This could be caused by a shift in the equilibrium towards production of more monomer species.

The formation of **1** was investigated, which showed an intermediate product formed in the *in situ* ^{31}P NMR and was also observed in the white line plot of the reaction. The intermediate was hypothesised to be a palladium species with coordinated phosphine, but before intramolecular metallation occurs (i.e. $[Pd(P(o\text{-tolyl})_3)(CH_3COO)(\mu\text{-}CH_3COO)]_2$. Analysis showed that this species then disappeared and **1** was formed. Repeating the analysis with *ex situ* ^{31}P NMR analysis showed that the same species were formed and the intermediate was stable at room temperature. The white line plot showed the ease of choosing EDE spectra to analyse from the multitude of spectra collected.

The chapter was completed by investigating the reactions of a variety of phosphine ligands with palladium acetate. In the PCy_3 reaction the palladium was reduced from $Pd^{II}(OAc)_2$ to $Pd^0(PCy_3)_2$ species. It was shown by ^{31}P NMR that this was achieved by the free ligand, which was oxidised to $O{=}Pcy0._3$. Very similar results were obtained from the EDE results

of the other reactions studied, but the results are not as definitive due to the lack of NMR data. Again, white line plots were extremely useful in pinpointing changes in the palladium environment.

3.8 Experimental

Preparation and characterisation of *trans*-di(μ-acetato)-bis[*o*-(di-*o*-tolylphosphino) benzyl] dipalladium (II) (species 1)

Under nitrogen, $Pd(OAc)_2$ (1.92g, 8.55mmol) was dissolved in dry toluene (240ml). Tri-*o*-tolylphosphine (3.42g 11.2mmol) was added and stirred for one minute, then the whole reaction mixture was then stirred for three minutes at 50°C (the solution changed from dark to light orange). The solution was rapidly cooled to room temperature and reduced under vacuum until it turned slightly turbid. Crystals were precipitated with the addition of anhydrous, cold petroleum spirit (370ml), and collected by filtration.

The crystals were purified by dissolving them in dry toluene (280ml), filtering through celite and recrystallising out with the addition of anhydrous petroleum spirit (300ml). This solution was filtered and dried in vacuo to yield yellow crystals (2.8g, 2.99mmol). This reaction gave a 70% yield w.r.t palladium.

NMR studies were conducted at -70 °C due to hydrogen exchange at room temperature. The results agreed with previous work .[20]

^{1}H NMR (360 MHz, -70 °C, CD_2Cl_2): δ = 7.28 (m, 4 H, H_{tolyl}), 7.18 (m, 2H, H_{tolyl}), 7.10 (m, 6H, H_{tolyl}), 7.09 (t, 2H, H_{benzyl}, ^{3}J (H,H) = 7.5 Hz), 6.89 (m, 4H, H_{tolyl}), 6.67 (t, 2H, H_{benzyl}, ^{3}J(H,H) = 7.5 Hz), 6.54 (t, 2H, H_{benzyl}, ^{3}J (H,H) = 8.7 Hz), 6.34 (dd, 2H, H_{benzyl}, ^{3}J (H,H) = 7.9 Hz, ^{4}J (P,H) = 12.4 Hz), 2.98 (s, 6H, CH_3), 2.79 (dd, 2H, CH_aH_b, ^{2}J(H_a,H_b) = 14.1 Hz, ^{3}J(P,H) = 4.3 Hz), 2.38 (dd, 2H, CH_aH_b, ^{2}J(H_aH_b) = 14.1 Hz, ^{3}J(P,H) = 1.0 Hz), 2.08 (s, 6H, CH_3).

^{13}C{^{1}H} NMR (90.6 MHz, -70 °C, CD_2Cl_2): δ = 179.8 ($CH_3\mathbf{C}O_2$), 32.1 ($\mathbf{C}H_2$), 25.5 ($\mathbf{C}H_3CO_2$), 24.2 ($\mathbf{C}H_3$), 23.5 ($\mathbf{C}H_3$) and aryl carbons

^{31}P{^{1}H} NMR (121 MHz, 20 °C, CD_2Cl_2): δ = 34.9

Infra red studies yielded a very similar result to previous work.[20]

3.9 References

1 W.A. Herrman, V.P.W. Bohm, C. Reisinger, *J. Organomet. Chem.*, **1999**, *576*, 23.

2 A.C. Skapski, M.L. Smart, *Chem. Comm.*, **1970**, 658.

3 D.D. Kragten, R.A. van Santen, M.K. Crawford, W.D. Provine, J.J. Lerou, *Inorg. Chem.*, **1999**, *38*, 331.

4 J. Evans, L. O'Neill, V.L. Kambhampati, G. Rayner, S. Turin, A. Genge, A.J. Dent, T. Neisus, *J. Chem. Soc., Dalton Trans.*, **2002**, 2207.

5 J. M. Corker, J. Evans, *J. Chem. Soc., Chem. Commun*, **1991**, *1104*; J. M. Corker, PhD Thesis, University of Southampton, **1990**.

6 W.A. Herrman, C. Brossmer, C. Reisinger, T. Riermeier, K. Ofele, M. Beller, H. Fischer, *Angew. Chem. Int. Ed. Engl,*. **1995**, *34*, 1844.

7 S. Chem, S.M. Lee, Z. Lin, W.T. Wong, *J. Organomet. Chem.*, **1996**, *510*, 219.

8 L. Dahlenburg, C. Prengel, N. Hock, *Z. Naturforsch Teil B,* **1986**, *41*, 718.

9 Y. Wakatsuki, M. Maniwa, H. Yamazaki, *Inorg. Chem.*, **1990**, *29*, 4204.

10 J.G. Stark, H.G. Wallace, *Chemistry data book*, John Murray (publishers) Ltd., London, **1982**.

11 V.M. Miskowski, W.P. Schaefer, B. Sadeghi, B.D. Santarsiero, H.B. Gray, *Inorg. Chem.*, **1984**, *23*, 1154.

12 J. Evans, W. Levason, R.J. Perry, *J. Chem. Soc. Dalton. Trans.*, **1992**, 1497

13 N.A. Young, *J. Chem. Soc. Dalton. Trans.*, **1996**, 249.

14 Personal communication with A.J. Dent, **2001**, Daresbury Laboratory

15 T.E. Busigyna, V.K. Polovnyak, N.S. Akhmetov, *J. Gen. Chem. USSR (Engl. Transl.)*, **1984**, *54*, 249.

16 J.A. Davies, S. Dutremez, A.A. Pinkerton, *Inorg. Chem.*, **1991**, *30*, 2380.

17 B.E. Mann, A. Muscoc, *J. Chem. Soc. Dalton. Trans.*, **1975**, 1673.

18 R.G. Goel, R.G. Montemayor, *Inorg. Chem.*, **1977**, *16*, 2183.

19 M. Tanaka, *Acta Cryst. C,*. **1992,** *48*, 739.

20 W.A. Herrman, C. Brossmer, C. Reisinger, T. Riermeier, K. Ofele, M. Beller, *Chem. Eur. J.*, **1997**, *3*, 1357.

Chapter 4

The Heck reaction using preformed palladacycles

4.1 Introduction

In this chapter, XAFS and NMR techniques were used to investigate the Heck reaction between chlorobenzene, bromobenzene or halobenzene and methallyl alcohol catalysed by species **1** and **3b**.

Carbon NMR was used to monitor the start of catalysis and phosphorus NMR was used to determine which phosphine species were present in the reaction. Various XAFS techniques were used to investigate the coordination sphere around the palladium atoms in the reaction.

The first set of Heck reactions to be investigated were catalysed by **1**, the preformed palladacycle investigated in chapter 3. This was them complemented by investigating the same reactions catalysed by **3b**, the bromine bridged derivative of **1**.

4.2 XAFS standards

Some standard XAFS spectra were taken of samples which were deemed likely to be present in the reactions investigated. Species **1** was investigated in chapter 3. In this chapter the investigation was extended to the same family of palladacycles, but containing iodine, bromine or chlorine ligands (**3b, 4a, 4b**, or **4c**). Hermann showed[1] that by reacting **1** with a tetrabutylammonium halide the acetate ligands are substituted by the halide atoms to form the corresponding species **3a, 3b** or **3c**. With the addition of excess halide species **4a, 4b** or **4c** are formed (figure 4.1). The species **2a, 2b** or **2c** are also easily formed by coordinating a solvent molecule to the palladium.

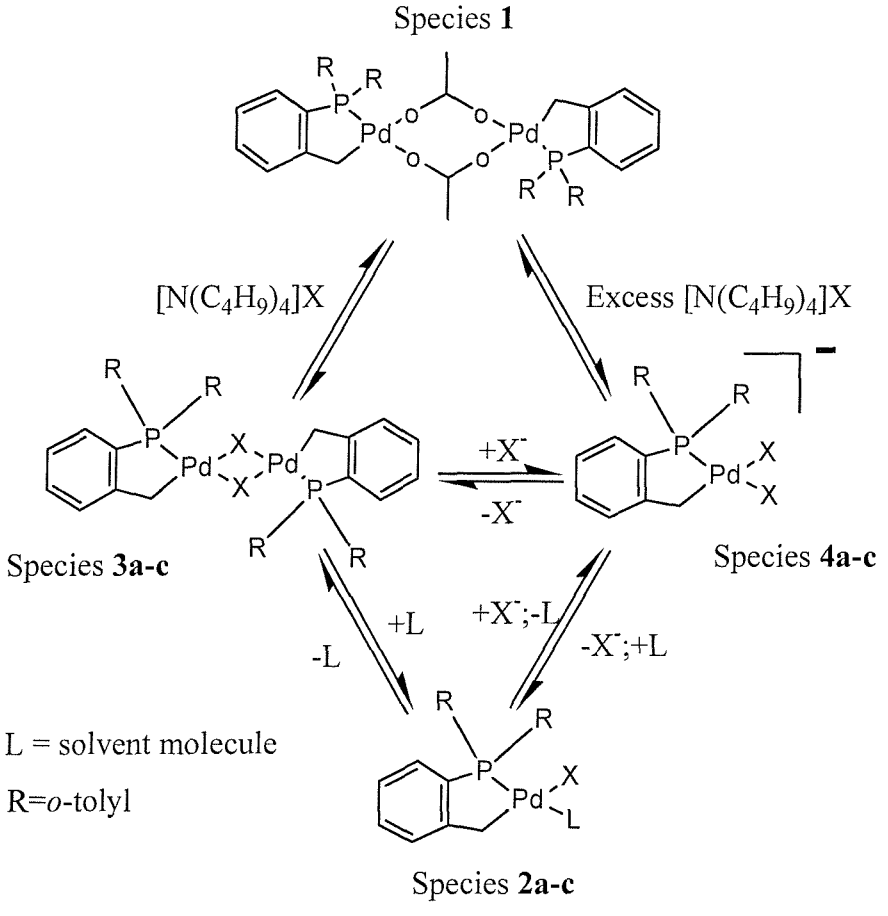

Figure 4.1 The reaction of species 1 with tetrabutylammonium halide.

^{31}P NMR results showed that in excess tetrabutylammonium halide there was almost 100% conversion in under a minute. A broad peak at 35.4 ppm (**1**) disappeared to form a sharp peak at 44.6 ppm (iodide (**4a**)), 41.9 ppm (bromide (**4b**)) or 39.2 ppm (chloride (**4c**)).

4.2.1 Synthesis and EXAFS analysis of species 3b (*trans*-di(*u*-bromo)-bis[*o*-(di-*o*-tolylphosphino) benzyl] dipalladium (II))

Species **3b** was synthesised by reacting **1** with tetrabutylammonium bromide[2] and recrystallised. Due to poor solubility, 3 standard EXAFS scans were recorded and averaged, of the catalyst (45 mM) in NMP at 130 °C. The results are depicted in figure 4.2.

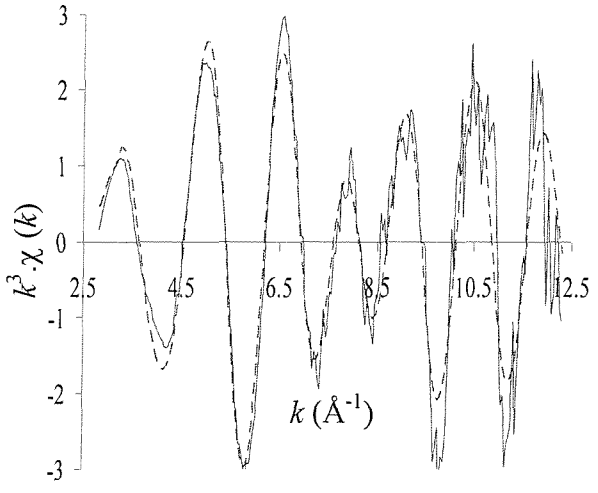

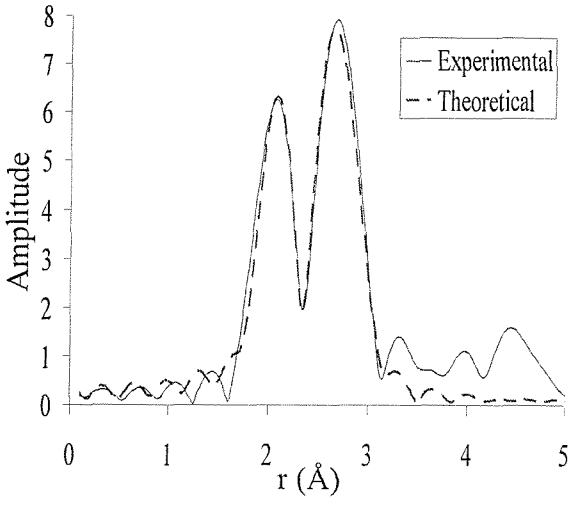

A

Atom	C.N.	r / Å	$2\sigma^2$ / Å^2
C	0.9(2)	2.02(2)	0.001(2)
P	0.9(1)	2.28(1)	0.005(2)
Br	1.9(1)	2.56(1)	0.016(1)

E_f = -3.8(22) eV, R = 29.9 %

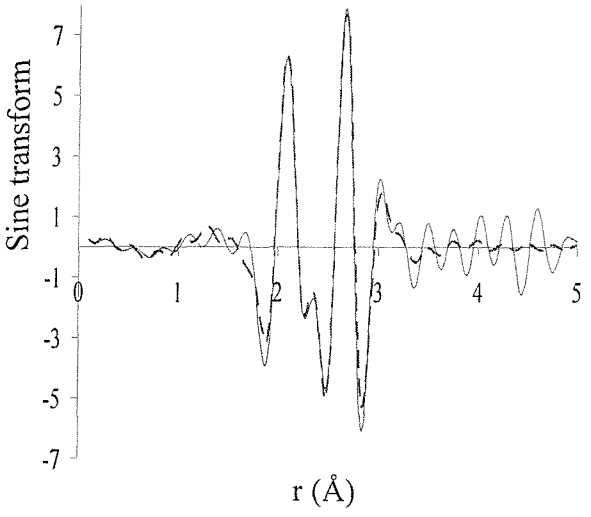

B

Atom	C.N.	r / Å	$2\sigma^2$ / Å^2
C	0.8(2)	2.05(2)	0.001(6)
P	1.1(3)	2.21(4)	0.015(11)
Br	1.0(1)	2.58(1)	0.001(2)
Br	0.9(2)	2.44(2)	0.004(4)

E_f = 0.6(22) eV, R = 25.2 %

Figure 4.2 The palladium K-edge k^3-weighted EXAFS data (3 x 30 minutes averaged), Fourier transform, and sine transform of species 3b in NMP (130 °C). The experimental fit is calculated from table A.

The spectra fits the $k^3\chi(k)$, Fourier transform and sine transform very well to a simple model of three shells, with only a slight discrepancy at low k values. The model in table A has refined coordination numbers close to the expected values of 1 carbon, 1 phosphorus and 2

bromine atoms, the refined coordination numbers are correct within the standard errors. The Debye-Waller terms have values which indicate they are integral to the fit and the bond lengths (within the errors) are the same as a similar reported crystal structure[3] {[(*o*-tolyl)$_3$P]Pd(Ar)(Br)]$_2$} (Pd-C 2.01 Å, Pd-P 2.29 Å, Pd-Br (trans to P) 2.53 Å and Pd-Br (trans to C) 2.58 Å). The average palladium bromine bond length to 2 decimal places is 2.56 Å, which is the same value as the refined EXAFS model. This is not a palladated species but the crystal structure[4] for **1,** gives the bond lengths for Pd-C (2.02 Å) and Pd-P (2.22 Å). This suggests that the presence of the ringed species decreases the palladium phosphorus bond length. Therefore with this new data the phosphorus shell's interatomic distance might be expected to refine to under 2.28 Å. But the Pd-P bond length[7] for **3a** is 2.27 Å, so by substituting acetate ligands for iodine atoms, this increases the phosphorus bond length, so overall the refined model (table A) is very good.

The model was then extended to establish if improvements could be introduced to the fit. A palladium shell was added at 3.80 Å to fit the non bonded palladium palladium distance[3] (the non bonded palladium palladium distance was investigated and two structures with very similar structures compared with **3b** gave distances of 3.64 and 3.80 Å,[5,6] with the variation due to the R groups present). The shell fitted with r = 3.87(3) Å and a = 0.021(7) Å^2, which are viable results, but the R value increased, so it was omitted. Then a fit of the 2 benzylic carbons in the palladated ring was attempted. A shell of 2 carbons was fitted[7] at 3.1 Å, but the Debye-Waller term increased to over 0.05, so this was also excluded.

A model was proposed (table B in figure 4.2) where two separate bromine shells were constructed, this was to establish if the two bromine atoms could be resolved separately, since they are not equivalent. The R factor decreased by over 10 %, which could indicate the extra shell is integral to the fit, or could be due to fitting more parameters. Unfortunately the errors for the phosphorus shell increase considerably in the revised model. Also the bond lengths change, the carbon increases, whilst the phosphorus and the second bromine distance decreases considerably (by 0.08 Å and 0.09 Å respectively), compared with the crystal structure mentioned before. Hence it was decided not to include this model, also with the additional shell, the number of theoretical independent parameters was exceeded.

Finally, a square planar model was constructed in Excurv98 to investigate multiple scattering effects. A square planar model was constructed using information obtained from

the crystal structure of **3a**.[7] Since the Pd_2I_2 rhombus (with angles of 90±5 °) is situated around an inversion centre that requires strict planarity and the symmetry around the palladium atoms are also square planar. Therefore the model designed had two cis bromines, a carbon and a phosphorus atom around the palladium central atom. The model was square planar with all angles at 90°. The model was refined and multiple scattering paths were calculated for paths involving up to four different atoms. As expected the largest contributing paths were the linear paths involving a bromine atom and the lighter atom trans to it. The largest path was the Pd-Br-Pd-P-Pd (4.71 Å) but only contributed 0.23 % to the total experimental amplitude and the sum of the multiple scattering paths only contributed 0.54 % to the total experimental amplitude. The refined model was very similar to the 4 shell model, except the Pd-P interatomic distance refined to 2.27 Å (closer to the hypothesised bond distance). The R factor decreased to 23.5 %, which was due to the theoretical curve making a better fit in the Fourier transform at 4.5 Å. Even though the R factor had improved, multiple scattering effects were deemed not to be integral to the fit, since the total contribution of the multiple scattering path lengths to the total amplitude of the experiment was too low.[8]

Therefore the most valid model to be fitted to the data was the first and simplest proposed model, with only 3 shells (1 carbon, 1 phosphorus and 2 bromines) and excluding multiple scattering.

4.2.2 QEXAFS analysis of species 4b

Species **4b** was synthesised *in situ* by stirring **1** (50 mM) with excess tetrabutylammonium bromide[2] in NMP at room temperature under nitrogen for one hour. (10 x 6) minute QEXAFS scans (RTP) were taken and averaged (figure 4.3).

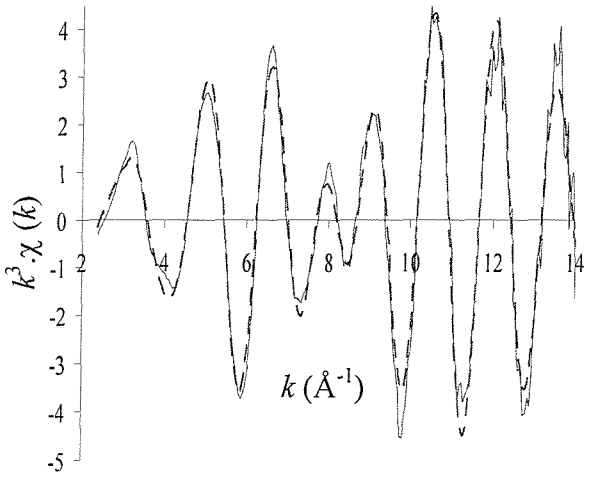

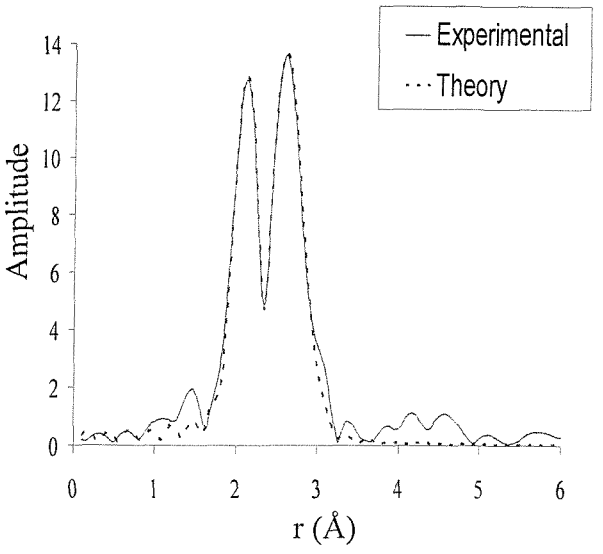

Atom	C.N.	r / Å	$2\sigma^2$ / Å^2
C	1.2(2)	2.07(1)	0.008(2)
P	0.9(1)	2.23(0)	0.002(1)
Br	2.0(1)	2.54(0)	0.012(0)

E_f = -8.6(14) eV

R = 18.8 %

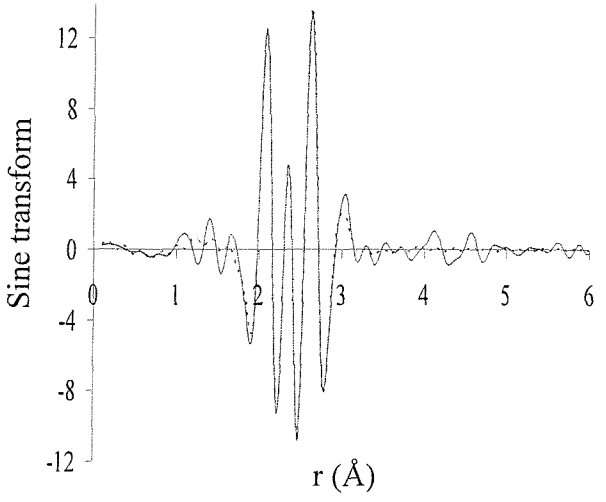

Figure 4.3 The palladium K-edge k^3-weighted QEXAFS data (10 x 6 minutes averaged), Fourier transform and sine transform for species 4b (RTP).

The model fitted very well to a simple model for **4b**. It has a very low R factor and very low errors on the refined values. Again multiple scattering paths were calculated, and again they were deemed too small to be significant to the overall fit. Analysis of the peaks in the Fourier transform between 4 and 5 Å^{-1}, shows that the intensity for the peaks is smaller for **4b**. This could be attributed to a greater number of atoms in the dimer contributing to shells at this distance from the palladium, or could be due to noise caused by the poorer data quality and length.

The model for **4b** shows the carbon bond length has increased whilst the phosphorus and bromine have decreased (compared with **3b**), presumably caused by changes in the species

from monomer to dimer. Crystal structures for chlorine dimer analogues gives an average palladium chlorine bond length of 2.45 Å for $[Pd(P((C_6H_2)(CH_3)_3)_2C_6H_2(CH_3)_2CH_2)Cl]_2$[9] and 2.41 Å for $[Pd(P(O(2,4\text{-}Bu^t{}_2C_6H_3))_2OC_6H_2(Bu^t)_2)Cl]_2$.[10] But, the average chlorine bond length decreases for monomers, for cis $[PdCl_2(C_3H_7N)(C_{18}H_{15}P)]$ the average length is 2.36 Å and an average length of 2.36 Å for a similar palladacycle monomer.[11] Hence there is an average bond length decrease of 0.07 Å. Therefore armed with this information, the palladium bromine average bond length should decrease for the monomer. The model fitted for **4b** is only 0.02 Å shorter, but could be indicative of monomer formation.

4.2.3 Comparison of the XAFS for species 3b and 4b

The background subtracted XAFS for **3b** and **4b** were overlaid (figure 4.4), to see if a visual comparison could yield any further information.

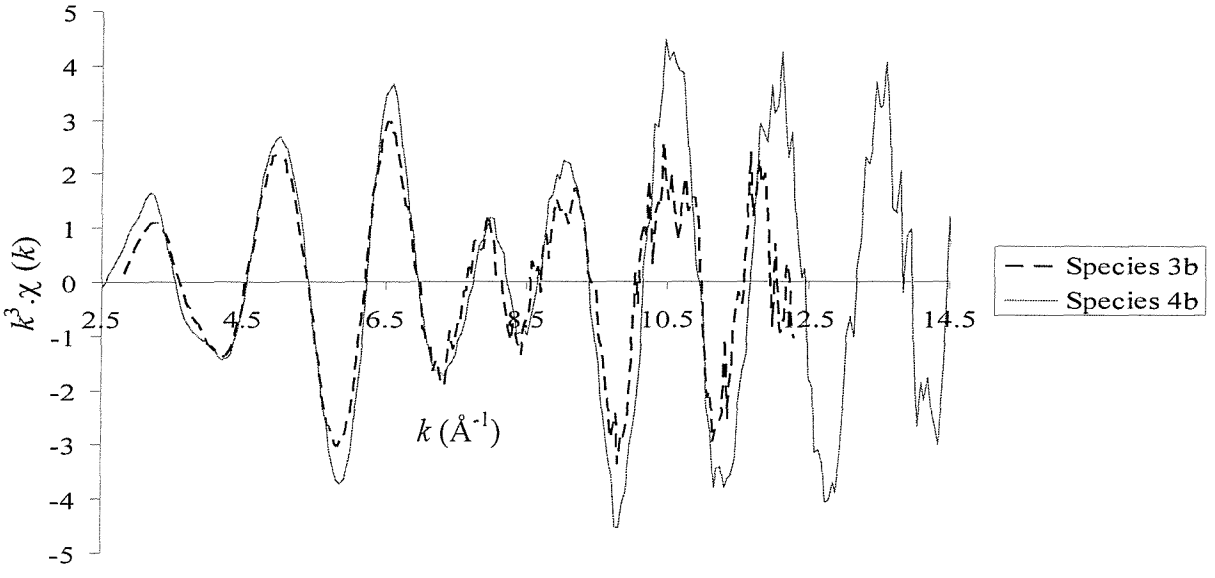

Figure 4.4 Comparison of the k^3 EXAFS data for species 3b (130°C) and species 4b (RTP).

As expected for the comparable regions the spectra are similar, since the XAFS models are nearly identical. The frequency is the same, except for high k, where the data quality is poor. This depicts that the bond lengths and chemical environment around the emitting atom are the same. The only real difference in the spectra is the peak intensity. There are slight differences in the peak intensity at low k, but there are large differences at high k.

The lower intensity is indicative of smaller coordination numbers or larger Debye-Waller

factors. Hence, the differences at high *k* suggests that the number of large backscatterers (palladium and/or bromine) is smaller for **3b**. But, if there is a slight contribution from palladium (even if it cannot be fitted as a shell) in the dimer, then **3b** should have greater intensity compared with the monomer. Therefore the difference observed is probably exacerbated due to the poor data quality at high *k*.

Otherwise there is no major difference in the spectra, but this is hardly surprising since the only difference is the presence of a palladium-palladium interaction, but this can not be fitted, with the data range shown.

4.2.4 QEXAFS analysis of species 4a

The study was then widened to include analysis of the iodine monomer **4a**. The species was synthesised by reacting **1** (50 mM) with excess tetrabutylammonium iodide in NMP, for one hour. (5 x 5) minute QEXAFS scans were recorded and averaged, of the resulting solution at RTP (figure 4.5).

The crystal structure for **3a** was reported in 1984.[7] Selected bond lengths are Pd-C 2.08(7) Å, Pd-P 2.27(2) Å, Pd-I (trans to C) 2.72(1) Å and Pd-I (trans to P) 2.67(1) Å and the non bonding palladium-palladium is interaction is 3.93(1) Å.

The result shown in figure 4.5 gives a very good fit with the predicted model of 2 iodine, 1 phosphorus and 1 carbon atom bonded to the palladium. Obviously since it is a monomer the non bonded palladium distance is not present so there was no attempt at adding this shell, also there is no observable peak at the correct distance. Again a model for multiple scattering was constructed, but again there was no appreciable contribution to the fit, so multiple scattering has been excluded for the remainder of this chapter.

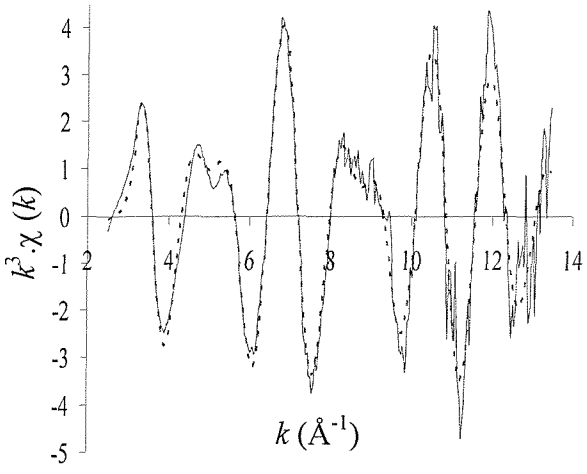

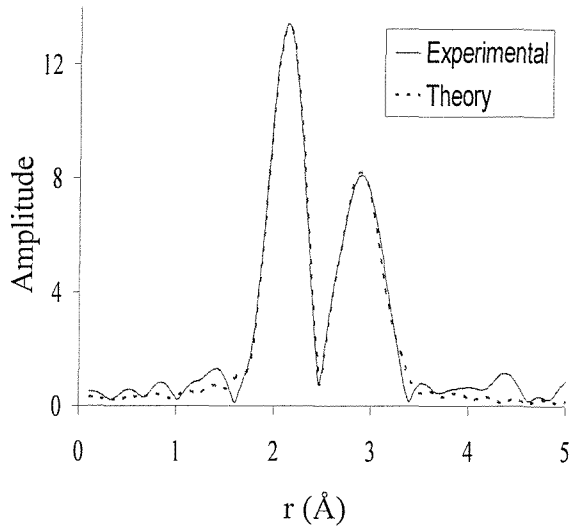

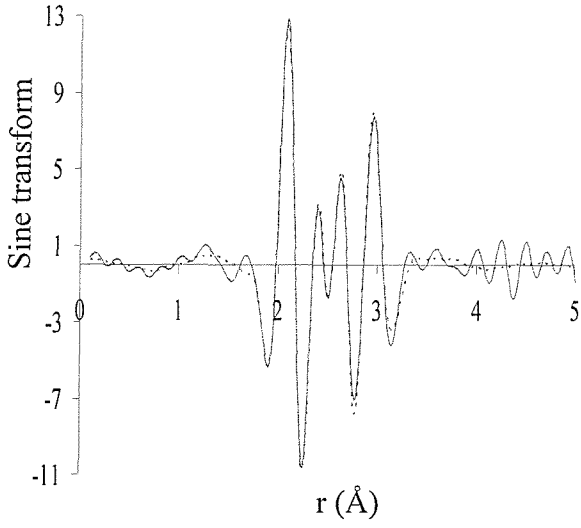

A

Atom	C.N.	r / Å	$2\sigma^2$ / Å^2
C	0.9(2)	2.05(1)	0.001(2)
P	1.0(1)	2.24(1)	0.004(1)
I	1.9(1)	2.69(1)	0.016(1)

E_f = -6.8(8) eV, R = 23.6 %

B

Atom	C.N.	r / Å	$2\sigma^2$ / Å^2
C	1.0(2)	2.06(1)	0.002(2)
P	1.0(1)	2.24(1)	0.004(1)
I	1.0(13)	2.70(11)	0.013(4)
I	0.8(13)	2.66(11)	0.018(14)

E_f = -6.7(13) eV, R = 20.3 %

Figure 4.5 The palladium K-edge k^3-weighted QEXAFS data (5 x 5 minutes averaged), Fourier transform and sine transform for species 4a in NMP at RTP (modelled on table A).

Table A and table B both give very good results, with a greater then 10 % reduction in the R factor for the addition of the fourth shell. For both tables, the bond lengths are very close to the analogous crystal structure, the coordination numbers refine very closely to the predicted result and the Debye-Waller terms give sensible values. But, after the addition of the fourth shell the errors for the third and fourth shell increase drastically and exceed the actual values of the coordination numbers. So again the 4 shell model was omitted, but this time because the errors were too large, rather than not being able to fit the halogen bond lengths correctly. Again this is due to the shells being too stongly correlated.

Another important point to be noted is that NMR studies indicate that there is 100 % conversion. The XAFS model indicates that there is 100 % conversion, but the background subtracted data shows a loss of structure between 8 and 10 $Å^{-1}$, this is probably due to destructive photoelectron wave interference. This phenomenon manifests itself in the Fourier transform, since the iodine shell peak is less intense than the phosphorus and carbon peak. But species **4a** should be more intense, since the halogen peak is more intense for **4b** and since iodine is a larger backscatterer this feature would be reinforced. Therefore this suggests that there is still a small amount of the starting palladium species present **1**. The C.N. value refines to 1.9 not 2.0, which is only a small difference but the bromine shell for **4b** refines to 2, so this could indicate that the average number of iodines has not reached 2. To compound this fact, the Debye-Waller value for **4b** is 0.012 $Å^2$, whilst the value refined for **4a** is 0.016 $Å^2$. Since they are very similar compounds, it could be concluded that they should have very similar Debye-Waller terms. This again suggests that the coordination number for **4a** should be reduced. Species **3b** (130 °C) shows a Debye-Waller value of 0.016 $Å^2$, but this is a slightly different structure and Debye-Waller terms increase with temperature, due to the increased molecular vibrations, since they are a measure of the uncertainty of the location of a particular atom.

4.2.5 QEXAFS analysis of species 4c

To complete the halogen investigation species **4c** was synthesised (same method as for **4a** and **4b**) and (10 x 6) minute QEXAFS scans were recorded (RTP) and averaged, see figure 4.6.

The experimental data fits very well (*k* weighted, Fourier and sine transform) to the predicted model of 1 carbon, 1 phosphorus and 2 chlorine atoms. The errors are very low and the R factor is only 24 %. Section 4.2.2 suggested that the chlorine bond length should be closer to 2.36 Å, but the actual crystal structure for **4c** has not been published. The reported crystal structure for an analogous dimer $[Pd(P((C_6H_2)(CH_3)_3)_2C_6H_2(CH_3)_2CH_2)Cl]_2$ gives an average palladium chlorine bond length of 2.45 Å, it is highly unlikely that the extra methyl groups on the phenyl ring would effect the bond length so it can be hypothesised that the average chlorine bond length in the chlorine dimer (**3c**) is also 2.45 Å. Therefore it can be argued that the reduction in 0.04 Å agrees with the NMR data that species **4c** has formed. The palladium carbon distance (from the same crystal structure) is

2.03 Å and the palladium phosphorus bond length is 2.24 Å. These results are in excellent agreement with the refined model. The quality of the data and no real loss of structure in the background subtracted data suggests that there is approximately 100 % conversion from **1** to **4c** unlike the iodine reaction (previous section).

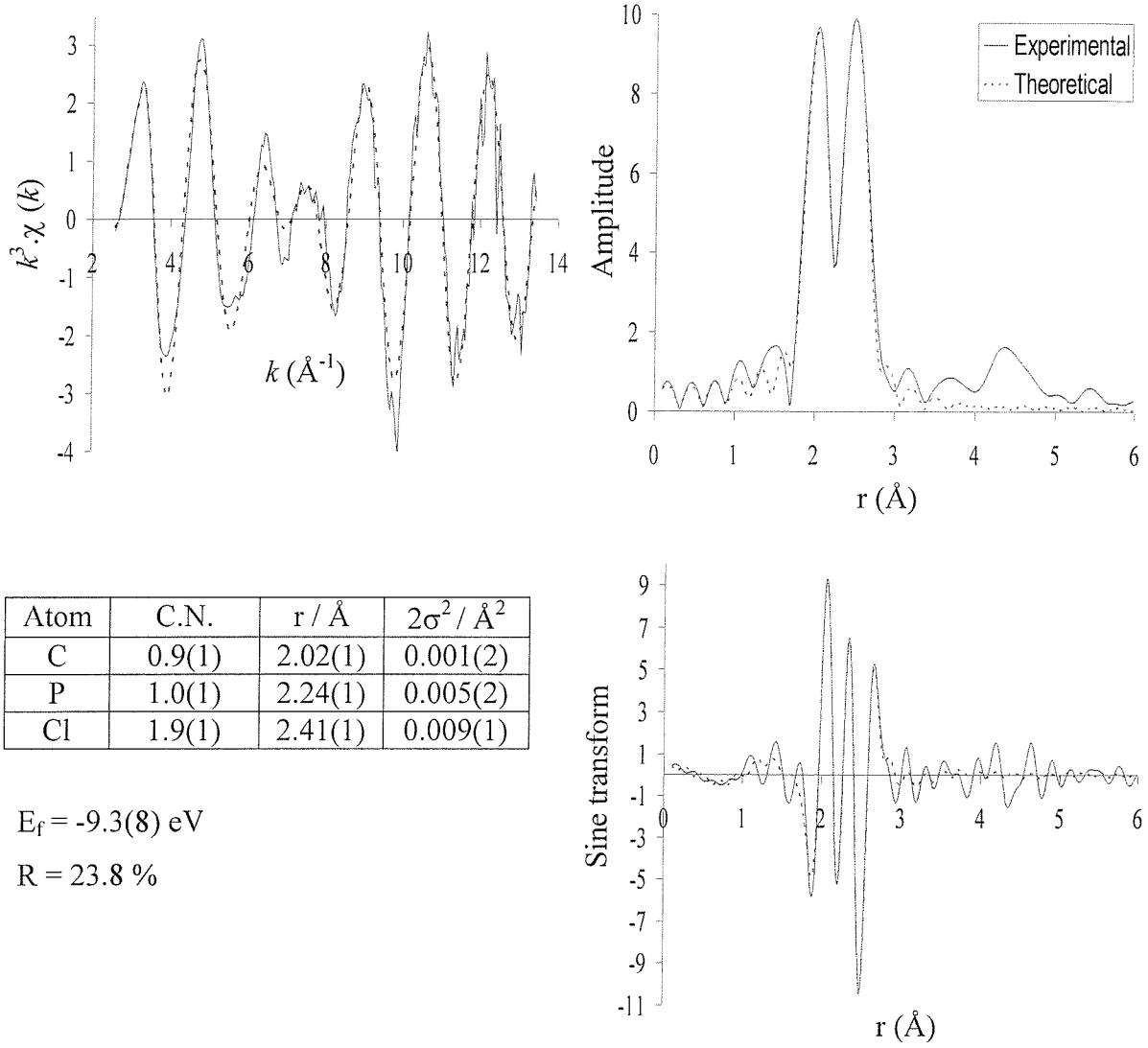

Atom	C.N.	r / Å	$2\sigma^2$ / Å^2
C	0.9(1)	2.02(1)	0.001(2)
P	1.0(1)	2.24(1)	0.005(2)
Cl	1.9(1)	2.41(1)	0.009(1)

E_f = -9.3(8) eV

R = 23.8 %

Figure 4.6 The palladium K-edge k^3-weighted QEXAFS data (10 x 6 minutes averaged), Fourier transform and sine transform for species 4c in NMP at (RTP).

4.2.6 Summary

The sample spectra shown in this section reinforce the usefulness of the XAFS technique. The spectra fit very well to the proposed models, with bond lengths close to crystal structures of related compounds. Also because all the ligands are different sizes, the problem that occurred when modelling **1**, is not present.

All four examples fit well to a three shell model, but generally it is not possible to add a fourth shell, in an attempt to distinguish the different halogen environments. But, the reason seems to change for every model (R factor increases, bond lengths decrease or errors increase). It is also not possible to improve the model by introducing a shell to fit the benzylic carbons at 3.05 Å, since the Debye-Waller terms are pushed too high. Finally, multiple scattering models were constructed, but it was discovered that any multiple scattering paths, were only a minor contribution and not integral to the fit.

The technique is not a good method to distinguish between **3b** and **4b**. The XAFS is very similar due to the same palladium environment. There is a slight difference at high *k*, which could due to the different long range structure. But, **3b** shows reduced amplitude at high *k*, which is the opposite result expected, since there should be contributions from large backscatterers at high *k*, so the only difference in the spectra could be due to the quality of data. But the method was useful in the iodobenzene experiment, to establish that the reaction had not gone to completion.

4.3 Investigation of the Heck reaction between halobenzenes and 2-methylprop-2-en-1-ol, catalysed by species 1

The Heck reaction between halobenzene (iodo-, bromo- and chloro- benzene) and 2-methylprop-2-en-1-ol (methallyl alcohol) catalysed by **1** was examined with NMR and XAFS spectroscopy. The equation is shown in equation 4.1 and the experimental procedures and reactant concentrations (unless otherwise stated) are described in chapter 2.

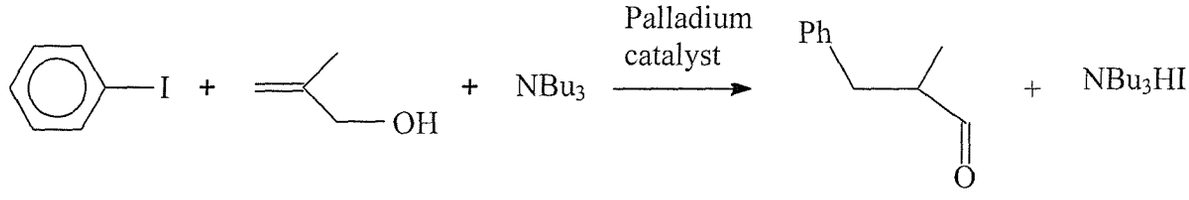

Equation 4.1 The reaction between iodobenzene and methallyl alcohol, with species 1 as catalyst.

4.3.1 Investigation of Heck reaction between methallyl alcohol and iodobenzene, catalysed by species 1

The first reaction of the three to be studied was between iodobenzene and methallyl alcohol.

4.3.1.1 NMR analysis

NMR spectroscopy was used to follow the Heck reaction between methallyl alcohol and iodobenzene. The reaction was heated up to 115 °C and held for 2 hours at that temperature. NMR samples were collected at specific points during the reaction and ^{1}H, ^{13}C and ^{31}P NMR spectra were taken at RTP. The experiment was carried out four times, whilst varying the catalyst concentration or solvent. Results from analysis of the spectra obtained are shown in table 4.1. The table expresses the integration values of the phosphorus NMR peaks as a percentage of all the phosphorus peaks present. It also shows the integration value of the product peak at 205 ppm, as a percentage of the solvent peak at 174 ppm (NMP) or 169 ppm (DMA).

^{31}P NMR shifts for the Heck Reaction									Prod**
Temp °C	Time at 115 °C	Expt	^{31}P NMR shift (ppm) and integration value*						
			-29.3 P(o-tolyl)$_3$	33.9	35.4 **1**	39.3	42.0 **2a**	44.6 **4a**	45.3 **3a**	
60		a		38	47	3	2		10	0
		b		17	44	10	6	5	18	0
		c		19	48	9	5		19	0
		d		21	60	7	3		9	0
90		a					20	24	56	0
		b					22	25	53	0
		c		18			21	19	42	0
		d					15	23	62	0
115	0	a					19	33	48	0
		b					18	58	24	0
		c					37	29	34	0
		d					14	35	51	0
115	30	a					9	67	24	1
		b					4	62	34	4
		c					15	68	17	3
		d					6	60	34	4
115	60	a					6	94		4
		b					6	94		3
		c					7	93		6
		d					4	70	26	4
115	120	a	5					95		1
		b	1				8	91		7
		c					5	95		12
		d	1				22	77		6

a=40mM, b=50mM, c=50mM dma, d=60mM

* ^{31}P integration values expressed as a percentage of total phosphorus integration

** Product (1-phenyl-2-methyl-propanal) (205 ppm (^{13}C NMR)) integration value expressed as a percentage of the solvent solvent signal at 174 ppm (value of 100) in NMP or 169 ppm in DMA.

N.B. Assignments **2a** and **3a** made due to agreement with research conducted by Hermann[1]

Table 4.1 Showing the ^{31}P NMR shifts for different stages during the Heck reaction.

The general trend for all the reactions is shown by the table that at 60 °C the two main peaks are at 33.9 and 35.4 ppm (**1**). The peak at 33.9 ppm could not be assigned as O=P(*o*-tolyl), because its chemical shift is 36 ppm. So it could be an impurity in the catalyst or

another possibility is coordination of the amine in the reaction mixture to the palladium, which splits the bridging acetate ligands. The next largest contribution is at 45.3 ppm due to initial production of **3a**. There are also small contributions to the phosphorus NMR at 39.3 ppm (unassigned) and 42.0 ppm (**2a**). This shows that there are a mixture of phosphorus species present and there is already some coordination of iodine to the palladium centre.

At 90 °C the original precursor and the other peaks at 33.9 and 39.3 ppm have disappeared (except for experiment c). The concentrations of the iodine containing species (**2a** and **3a**) have all increased. There is also the formation of a new peak at 44.6 ppm (**4a**), observed in the Hermann paper[1] and confirmed by NMR analysis in house (section 4.2).

Once the solution reaches 115 °C, there is still no product formation and there are only three phosphorus species present (**2-4a**). All species are coordinated to palladium and the palladium is coordinated to iodine (1 or 2 atoms), the species are also a mixture of monomers and a dimer. Generally the concentration of **2a** and **3a** has fallen, whilst **4a** has increased.

After heating at the reaction temperature for 30 minutes, there is some product formation. Species **2a** has fallen to a low proportion, **3a** has decreased and **4a** has increase. Therefore one of these species could be the active catalytic species.

After 60 minutes at the reaction temperature, generally there is further production of product, hence catalysis has continued. Species **3a** has disappeared, suggesting that is not the catalytic species. **4a** has continued increasing in concentration and **2a** has continued to dwindle.

Finally after heating the reaction at 115 °C for 2 hours, the reactions have finished, emphasised by the fact that the catalyst has degraded, depicted by production of free phosphine at -29.3 ppm. There has been further catalysis, so this agrees with the earlier observation that **2a** or **4a** are the active species. Since **4a** is by far the most abundant species (generally over 90 %), this indicates that this is the active species. Since the concentration of **2a** has depleted over time and there was no catalysis when this species was most concentrated, this is indicative that this is not the species.

Comparisons can also be made between the different experiments (a-d). As previously stated all the experiments show similar trends. Firstly investigating the three experiments conducted in NMP with varying concentrations. During the heating process, **2a** is less concentrated for higher catalyst concentrations, but at the end of the reaction the trend is reversed and the 60 mM palladium experiment has the greatest concentration of **2a**. For **3a** the maximum concentration produced is very similar for the three experiments, which reach a peak of 58 % (±5) at 90 °C. The concentration then reduces to zero, but takes longer for the 60 mM experiment. Finally, analysis of **4a** shows again in the 60 mM experiment the production of the phosphorus species is slightly slower, but the amount of species present at the end of the reaction is markedly lower. These results lead to the conclusion that at the end of the experiment there is on average 1.76 iodines per palladium rather than 1.9 (40 and 50 mM experiments). This is because after 60 minutes at 115 °C, it is the only experiment to contain **3a**, which only has 1 iodine atom per palladium, rather than 2 (**4a**). With time the majority of this species forms **2a** rather than **4a**, which suggests that **2a** is more stable than **4a** and that there is not enough free iodine in the solution to form close to 100 % of **4a**. Another possibility is that the reaction has not finished, but the phosphorus NMR shows that there is degradation of catalyst since free phosphine has formed, which indicates the reaction has finished.

Analysis of the carbon NMR integration value for the product production, indicates that the 40 mM experiment is slower and produces less product. The latter statement is difficult to verify since the amount of product present appears to decrease over the last hour of heating.

Comparison between using the two different solvents shows more marked results. Iodine uptake by the palladium is slower at the start of the heating process (DMA experiment), but once it reaches the 30 minute stage at reaction temperature both experiments are the same. This is shown in the results, since at 90 °C, 18 % of the phosphorus is still present in a form uncoordinated to iodine. Also when the solution reaches 115 °C, the amount of high iodine content species (**4a**) is considerably lower. These results could indicate that the iodine containing species are less soluble in DMA, so need greater energy for them to form in the solution.

4.3.1.2 Palladium K-edge QEXAFS analysis

A QEXAFS study was then conducted on the previous experiment (50 mM). The reaction was heated to 115°C and held for 1.5 hrs. Samples were taken from this solution at various times during the reaction (50°C, 80°C, 115°C, 0.5 hrs (at 115°C) and 1.5 hrs (at 115°C)) and injected into the XAFS cell. (10 x 6 minute) QEXAFS scans were taken and averaged of each solution at 40°C.

A) 50°C

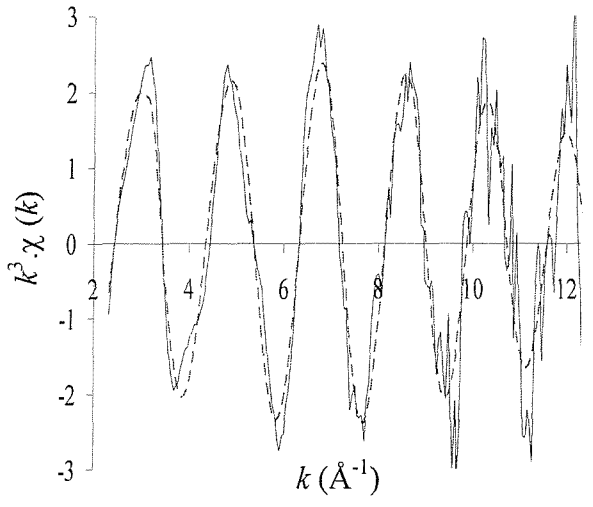

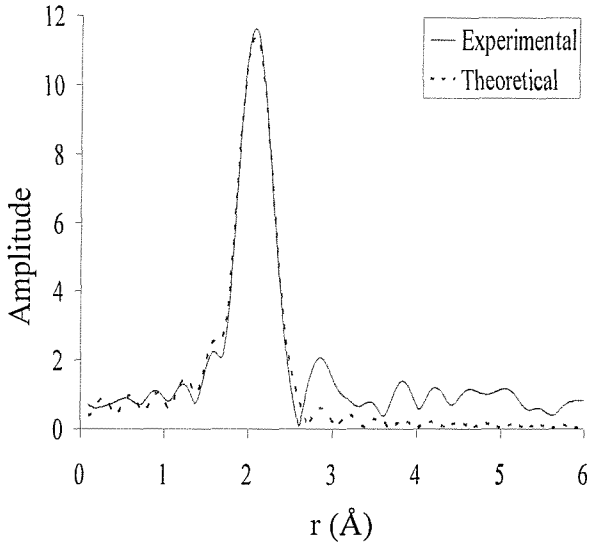

B) 80°C

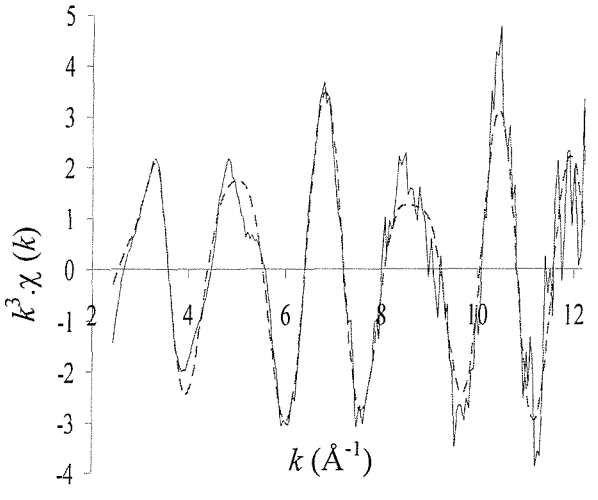

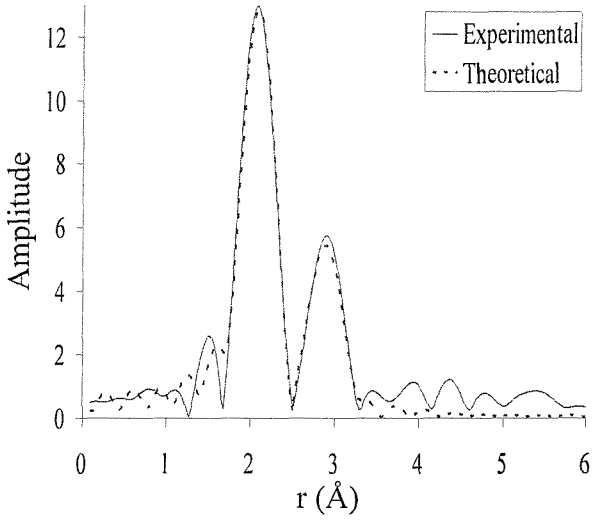

C) 115°C

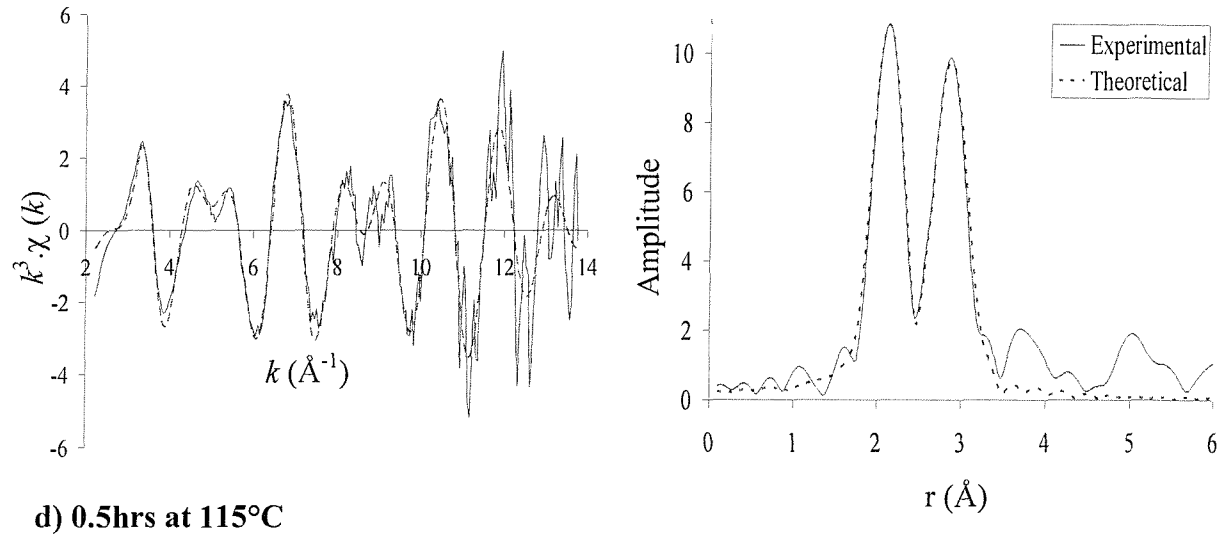

d) 0.5hrs at 115°C

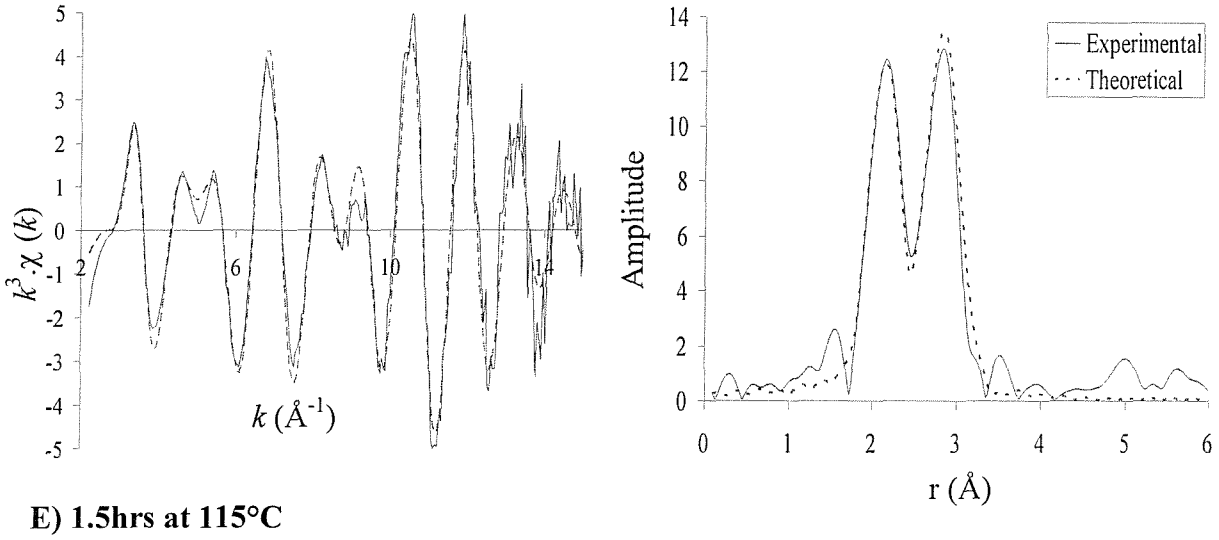

E) 1.5hrs at 115°C

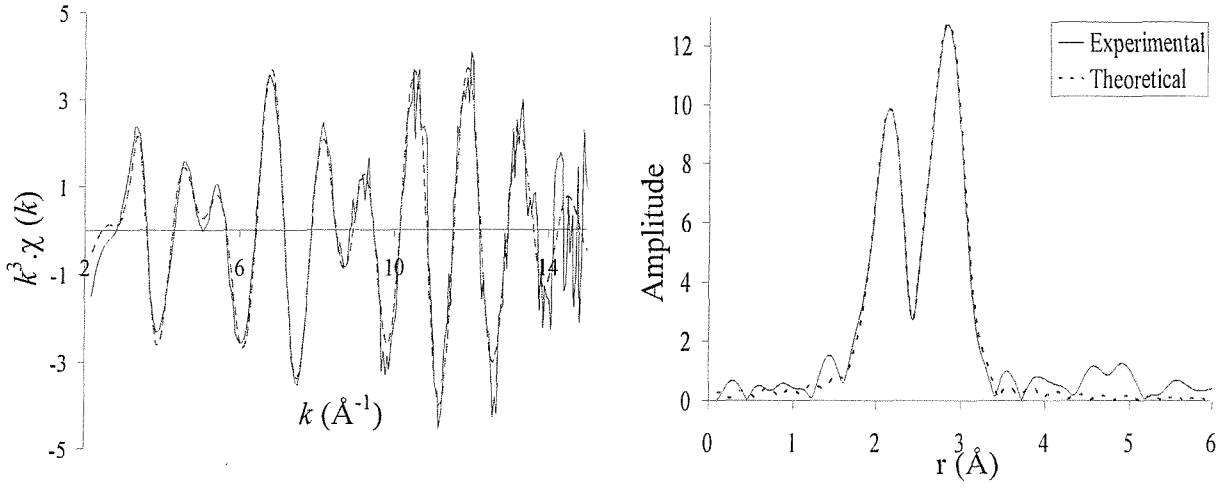

Figure 4.7 The palladium K-edge k^3-weighted QEXAFS data and Fourier transform of the reaction between iodobenzene and methallyl alcohol, with species 1 as catalyst (50 mM).

Table 4.2 Model tables for figure 4.7

SAMPLE	1st shell				2nd shell				3rd shell				R / %	E_F / eV
	Atom	C.N.	r / Å	$2\sigma^2$ / Å^2	Atom	C.N.	r / Å	$2\sigma^2$ / Å^2	Atom	C.N.	r / Å	$2\sigma^2$ / Å^2		
A	O	2.6(4)	2.10(2)	0.020(5)	P	1.0(1)	2.23(1)	0.005(1)	-	-	-	-	32.4	-10.3(16)
B	C	1.6(4)	2.08(2)	0.005(1)	P	1.2(3)	2.23(1)	0.011(6)	I	1.0(1)	2.70(1)	0.013(2)	30.2	-6.9(14)
C	C	0.9(3)	2.07(2)	0.002(3)	P	1.1(2)	2.25(1)	0.008 (3)	I	1.9(2)	2.71(1)	0.015(1)	35.7	-7.8(16)
D	C	1.0(2)	2.07(1)	0.003 (3)	P	1.0(1)	2.24(1)	0.005(1)	I	1.9(1)	2.70(0)	0.012(0)	28.8	-8.5(9)
E	C	0.9(2)	2.09(2)	0.007(3)	P	1.0(1)	2.25(1)	0.008(1)	I	2.0(1)	2.69(0)	0.012(0)	20.6	-8.8(8)

At 50 °C, the palladium species modelled was the initial catalyst (**1**). The background subtracted data is very similar to the spectrum shown for the catalyst in solution (chapter 3). The Fourier transform is also very similar and there is no formation of an iodine peak. There is a small peak around 2.8 Å, but this cannot be fitted as an iodine shell, since the Debye-Waller values are pushed to a high value above 0.03 Å. Table 4.2 shows that the refined model fits well to the experimental data. The coordination number for the first shell (oxygen) refines to 2.6, this is a reasonable value since this includes the palladated carbon. The Debye-Waller and interatomic distance are also reasonable values. The errors are all within the expected limits. The second (phosphorus) shell also fits very well and again the refined values and errors are the correct size.

At 80 °C there is some iodine coordination visible in the Fourier transform. The model fitted is 2 carbons, 1 phosphorus and 1 iodine atom. It fits fairly well to the k^3 data, but there are problems fitting at low k. The first two shells fit well to this model, except for the coordination numbers. The coordination number for phosphorus is too high, since there can only be 1 phosphorus per palladium atom (only phosphorus source is the initial catalyst). The coordination number for carbon is lower than hypothesised, but this is probably affected by the phosphorus. The problem with resolving these coordination numbers is shown by the slightly higher than expected errors (the error is 3 times the value for the phosphorus shell, compared with sample A, D and E). The iodine shell fits very well, with low errors. These results indicate that if there was only 1 species present in the solution and it had retained the palladated ring, then the species present would be the oxidative addition product of iodobenzene to **1** to form **2a**.

When the reaction reached 115 °C the palladium containing species had considerably more iodine coordinated. The model was now fitted with 1 carbon, 1 phosphorus and 2 iodine atoms. The carbon and phosphorus shells fit well and the problem with resolving the coordination numbers has improved, the errors are still slightly high, but the refined values are closer to the target values. The iodine shell fits well, but the Debye-Waller value is slightly higher than for the halo analogues, **4c** = 0.009, **4b** = 0.012 and **3b** = 0.016 (but is at 130 °C and the Debye-Waller values increase with increasing temperature due to greater vibrational motion). Therefore with the slightly higher Debye-Waller value and the fact the coordination number refines to less than 2, this suggests the average iodine coordination is under 2. This theory is reinforced since the iodine intensity in the Fourier transform is lower

than the phosphorus and carbon intensity (see section 4.2.4) and finally the k^3 spectrum (figure 4.7) shows a reduction in the definition of the curve between 8 and 9.5 $Å^{-1}$, which suggests a mixture of species present (**2-4a**).

After heating at 115 °C for 30 minutes the iodine peak is now the most intense peak in the Fourier transform. The *k* weighted data is very well defined and the experiment fits very well (R factor of 28.8 %), with lower errors to the proposed model of 1 carbon, 1 phosphorus and 2 iodine atoms (model for **3a** and **4a)**. But there are ill fitting points at 5 and 9 $Å^{-1}$, which could mean that the final palladium species has not been totally formed. The coordination number for iodine refined to 1.9 not 2.0, but this target value is within the error. This suggests that **2a** and **4a** are the main species left in solution, but there might be a small amount of **2a** present.

Finally after heating for 90 minutes at the reaction temperature, the palladium species appears to have reached its final form. The ill fitting areas in the *k* weighted data, now fit to the experimental data. This is shown in the Fourier transform by the iodine theoretical peak now fitting the experimental peak better, compared with the previous spectrum. This explains why the R factor has shot down to 20.6 Å. The proposed model in the table refines very well to the proposed model, all parameters refine to sensible values with low errors. The only slight glitch is the palladium carbon bond length of 2.09 Å, this is longer than the distance quoted for the crystal structures for the chlorine and acetate dimers. But, analysis of the EXAFS for **3b** and **4b** (section 4.2.1 and 4.2.2 respectively) show that the palladium carbon distance is 0.05 Å longer in the monomer. Also the bond length is longer for bromine species compared with chlorine (2.07 Å : 2.02 Å), therefore the 2.09 Å calculated is a very reasonable refined length. Therefore it could be concluded that the final species present is **4b**, rather than **3b**.

Analysis of the bond lengths for iodine and carbon bond lengths agree with the suggested mechanism above. The carbon / oxygen bond length is long at the start of the reaction, but this is due to the longer oxygen bond contribution. Over the next couple of samples the length decreases due to the loss of the oxygen and formation of the dimer, then as the concentration of dimer diminishes and the monomer increases the bond length increases again (last two experiments). Analysis of the iodine bond length also agrees with the mechanism. Between sample b and c the iodine bond increases slightly, due to the influence

(concentration) of **2a** (monomer) falling and the concentration of **3a** (dimer) increasing. The bond length rises to 2.71 Å, whilst the average bond length for the crystal structure of the dimer is 2.73 Å. Finally as the concentration of **3a** decreases and **4a** (monomer) increases, the bond length decreases to 2.69 Å.

Analysis undertaken on the experiment to form **4a**, by reacting **1** with tetrabutylammonium iodide (section 4.2.4) can be used to corroborate the statements made in the previous experiment. Analysis of the Heck reaction shows that during the experiment the main features that change in the *k* weighted data is loss of intensity for the peak between 4.3 and 5.6 *k* to form a double peak and the same situation occurs between 7.8 and 9.2 $Å^{-1}$. By correlating these results with the results from section 4.2.4, it can be observed that the *k* weighted and Fourier transform data from 4.2.4 fits nicely between the spectra for the previous experiment between 80 and 115 °C (figure 4.7b).

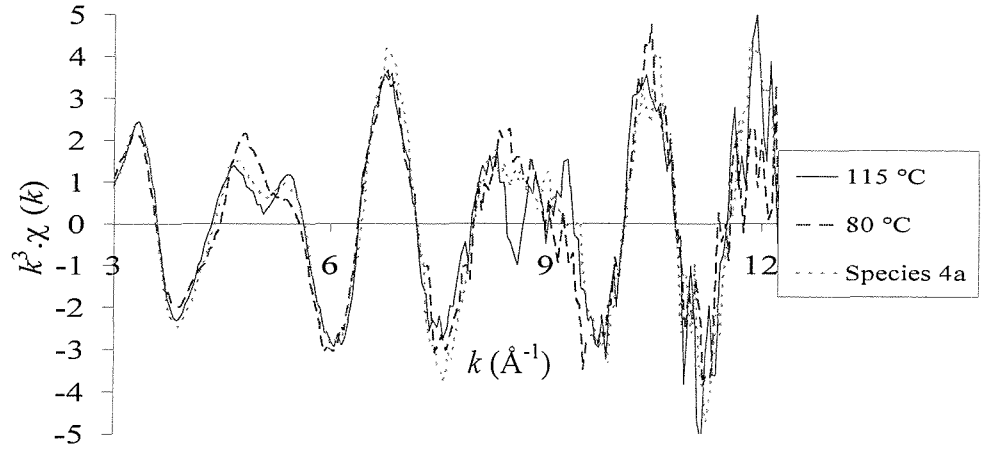

Figure 4.7b The palladium K-edge k^3-weighted EXAFS data, comparing species 4a with the reaction solution at two stages during the reaction.

This observation is qualified since the first double peak (5 $Å^{-1}$) is more pronounced in the formation reaction compared with 80 °C, but the second double peak (9 $Å^{-1}$) is less defined than for the sample at 115 °C. Due to being able to fit this spectrum into the reaction scheme, it helps to reinforce the proposed models. Since, we know the palladated ring remains intact and we know light scatterers (C or O) are replaced by iodine atoms, in the formation reaction, we can hypothesise that this is very similar to the mechanism undertaken in the Heck reaction. But, it is not possible to get more specific, since in the formation reaction there is no source of alkene or phenyl rings, so the formation experiment

spectrum could never exactly fit into the Heck reaction progression.

Summary

The results from the NMR and XAFS experiments can be brought together to reinforce the conclusions so far deduced. XAFS shows the average structure of all the species present, but ^{31}P NMR shows the solution is far more complex and consists of a mixture of species (up to a maximum of 6) present at any one time.

XAFS of the catalyst as soon as it is soluble (50 °C) shows it is still present as **1**. After heating to 60 °C the catalyst is mainly present in its original form, but there is some coordination of iodine (**2-3a**). Then after heating another 20 °C QEXAFS shows that there is an average 2 carbons, 1 phosphorus and 1 iodine around the palladium. Which without the NMR data could be assigned as **2a**, but is a mixture of the original catalyst and **2-4a**.

At 90 °C NMR shows that all the palladium species are now coordinated to iodine (**2-4a**). Species **3a** is most abundant, whilst **2a** and **4a** are virtually the same concentration.

The NMR and QEXAFS experiments both provide data on the sample at 115 °C. The NMR shows that the same three species are present, but **2a** and **3a** have fallen, whilst **4a** has risen in concentration (this trend propagates throughout the rest of the reaction). The coordination number of iodine around the palladium centre was calculated to be 1.8. This value agrees extremely well with the QEXAFS model of 1.9(2), but as mentioned the Debye-Waller was slightly higher than expected, suggesting that the coordination number is slightly lower (i.e. 1.8). These results show splendidly, that the two techniques are synergetic and that even though the NMR results were measured a few hours after the QEXAFS result (i.e. relative time after the sample has been syringed from the respective experiment), the palladium species formed in the reaction are stable.

After 30 minutes at 115 °C the active palladium species has started to catalyse the reaction. The NMR again shows the concentrations of the palladium species **2a** (2 mM), **3a** (17 mM) and **4a** (31 mM). The calculated iodine coordination number is 2.0 (NMR), whilst the QEXAFS model refines to 1.9(1), so again including errors the results complement each other.

Over the remainder of the reaction NMR data shows that the dominant species is **4a** (46 mM at the end of the reaction), which also suggests that this is the active species. QEXAFS again agrees with this conclusion and refines excellently to **4a**. XAFS has therefore proven to be an excellent tool and even though it gives an average result, it can be used to validate the NMR assignments made.

Overall, these results show that by 90 °C the precursor peaks have all gone and that all the phosphine complexes contain iodine and palladium and the P-C ring integrity is maintained, in all the species. Iodine coordination is very fast to the palladium and increases slowly towards the end of the reaction. Species **2a** and **3a** form initially, their concentration reaches a maximum then **4a** forms. From this point the concentration of **4a** increases, whilst **2a** and **3a** falls. Catalysis only seems to occur after the concentration of **4a** reaches a certain level, since the concentration of **2a** and **3a** are decreasing, it would appear that **4a** is the active species.

4.3.1.3 Iodine K-edge QEXAFS analysis

The reaction between iodobenzene and methallyl alcohol (catalysed by **1**) was repeated and followed using iodine K-edge QEXAFS. The reaction conditions were identical to the previous experiment, except the iodobenzene concentration was reduced to 150mM (3:1 w.r.t. palladium). This work was undertaken to confirm the conclusions made from the previous experiment and to elucidate more information on the reaction The iodobenzene concentration was reduced because otherwise the ~1000 mM iodobenzene XAFS would dominate over the ~50 mM iodine bonded to palladium XAFS. The iodine edge was calibrated with lithium iodide hydrate and gave a K edge at 33.158 keV.

4.3.1.3a Reaction start

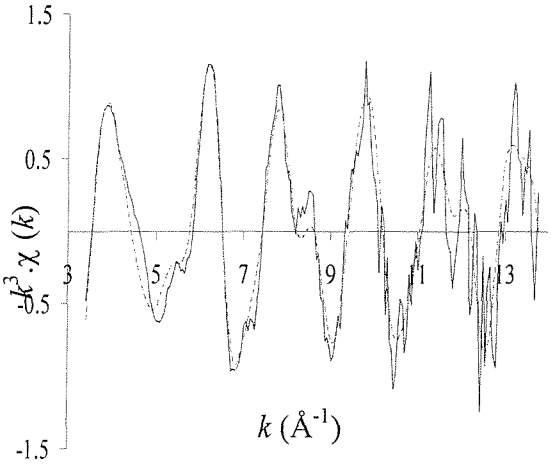

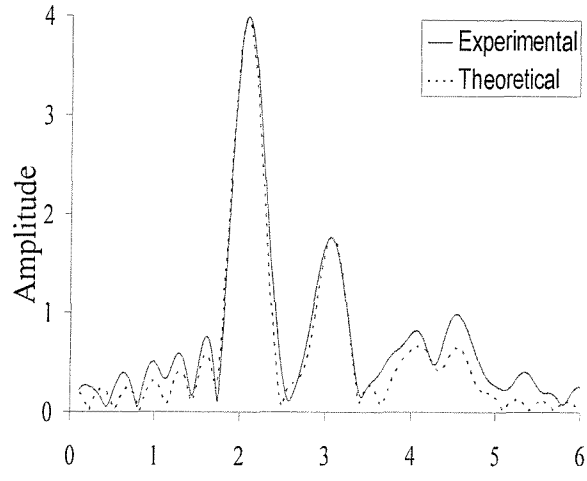

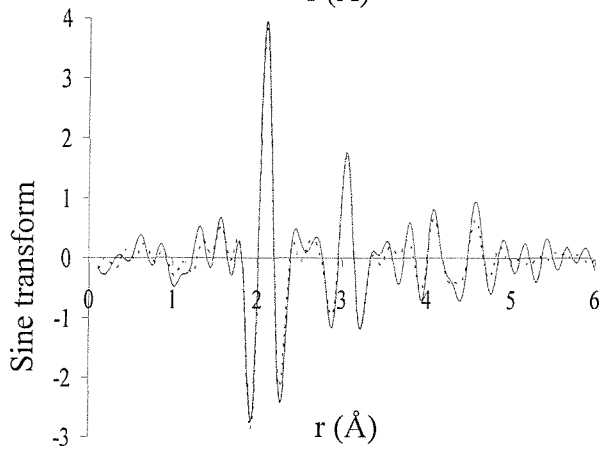

Atom	C.N.	r / Å	$2\sigma^2$ / Å^2
C	1.0(1)	2.10(1)	0.002(1)
C	1.8(2)	3.05(1)	0.007(1)
C	2.3(8)	4.10(2)	0.008(5)
C	1.6(7)	4.58(2)	0.002(6)

E_f = -7.0(11) eV

R = 35.1 %

Figure 4.8 The iodine K-edge k^3-weighted QEXAFS data (4 x 6 minutes averaged), Fourier transform and sine transform of the PhI Heck reaction, catalysed by 1 (40 °C), after heating to 50 °C.

The catalytic mixture was heated to 50°C to make the solution homogeneous, (4 x 6 minute) QEXAFS scans were taken at 40°C and averaged, the results are shown in figure 4.8.

The results give a very good fit for iodobenzene. The model created was originally 4 shells of carbon atoms (1 ipso, 2 ortho, 2 meta and 1 para from the iodine atom). The number of independent parameters which can be modelled is 16. So the refined model (with 13 refined parameters) is within this limit. When fitting each additional shell the R value decreased by over 10 % indicating that each additional shell was integral to the fit. For the closer shells the error values are very low and increase considerably for the outer shells, but the refined coordination numbers are all within the error values for the iodobenzene model. This is also shown by the Fourier transform of the two outer shells, which are fitted but poorly. Examination of the sine curve for the model shows the same frequency and phase for the four fitted shells which is also indicative that the Fourier transform peaks are not attributed to noise and they are correctly assigned as carbon atoms. Also, the Debye-Waller terms are all low, which suggests that each shell is integral to the fit. Finally the crystal structure for iodobenzene has been reported[12] and the reported distances of the carbons atoms from the iodine atom are: ipso 2.11 Å, meta 3.04 Å, ortho 4.33 Å and para 4.86 Å. These distances for the closest two shells are only 0.01Å different from the X-ray results, but this increases to 0.28 Å for the furthest shell.

These results confirm that in the initial solution formed at 50°C, the predominant iodine species present is iodobenzene. This shows there is no immediate coordination of iodine or the phenyl ring, to the palladium catalyst. The errors for the outer shells are quite high, but the data quality is quite poor and was only collected over a timescale of 24 minutes. The reason why a carbon shell can be fitted to 4.58 Å, but a palladium shell can not be fitted to the palladacycles investigated earlier in this chapter, could be due to the increased concentration of the absorbing atom, since the iodine concentration is three times the concentration of the palladium in the other samples.

4.3.1.3b Reaction end

The solution examined in the previous QEXAFS study was heated in the EXAFS cell for 120 minutes at 115°C, the solution was cooled to 40°C and (10 x 6) minute QEXAFS scans were taken and averaged (figure 4.9).

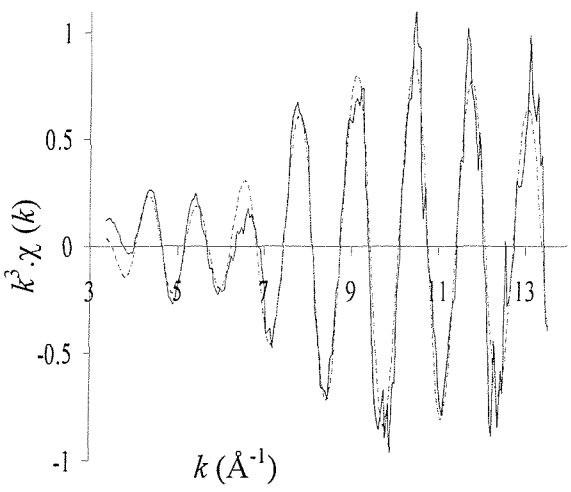

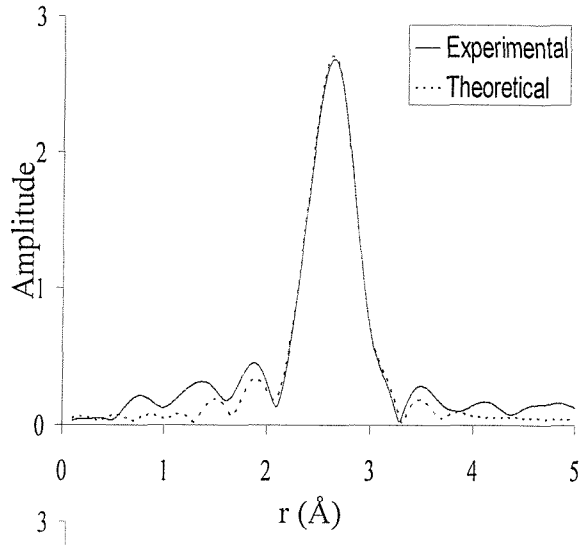

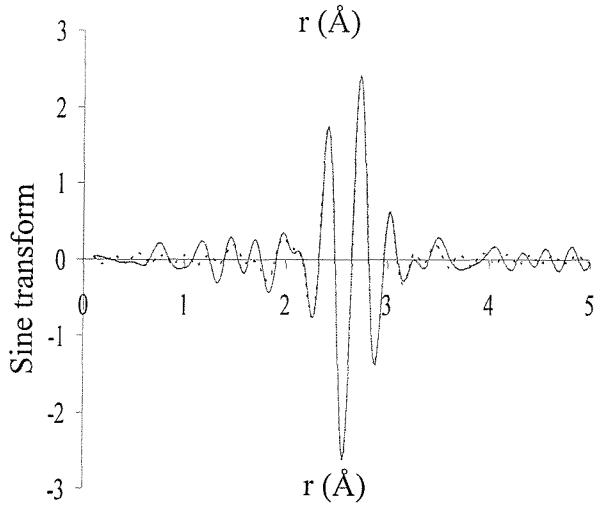

Atom	C.N.	r / Å	$2\sigma^2$ / Å^2
Pd	0.6(0)	2.71(1)	0.012(0)

E_f = -5.6(15) eV

R = 31.2 %

Figure 4.9 The iodine K-edge k^3-weighted QEXAFS data (10 x 6 minutes averaged), Fourier transform and sine transform showing the Heck reaction after heating at 115 °C for 2 hours (RTP).

The experiment fits very well to the proposed model of an average of each iodine atom, being bonded to two thirds of a palladium atom (**3a** or **4a**). The errors are very low, for example only 6 % for the coordination number. The sine curve also gives a very close theoretical curve compared with the experimental. If an iodine atom is fitted in an attempt to improve the model (in the iodine bridged palladacycle the I...I non bonded distance[7] is 3.78 Å), the model refines to r = 3.78(5) Å, C.N. = 0.28(21), a = 0.018(8) Å^2 and R = 30.2 %. Therefore the added shell fits to the correct values for **3a** (1/3 iodine), but the errors are large and the R fit does not improve by over 10 %, hence it cannot be argued that it is a valid shell. If the coordination number is increased to 0.66 (**4a**), the Debye-Waller rises to 0.04 Å^2, which is indicative that the coordination number is too high.

The fit for the first shell is very good and agrees with the previous EXAFS results of iodine bonded to palladium and gives the same bond length at 2.70 Å. But with the model refined it is very difficult to establish which possible species is predominant (figure 4.10), the two possibilities are:

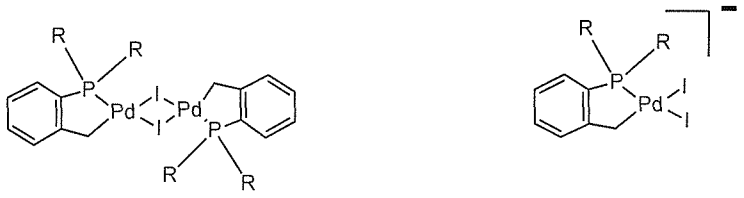

Species **3a** Species **4a**

Figure 4.10 The probable iodine containing molecules at the end of the reaction.

Considering at the start of the reaction there are three iodine atoms to every palladium atom and hypothesising that at the reaction end all the iodine atoms are either coordinated as one of the above proposed species or as I^-. This means that if species **3a** is formed as the final product, 1/3 of the iodine containing species is species A, and 2/3 is I^-. Therefore on average each iodine atom is surrounded by 2/3 of a palladium atom (2 palladium atoms bonded to each iodine). The result is the same for species **4a**, since 2/3 of the iodine atoms will be coordinated in species B and in this scenario each iodine atom is coordinated to only 1 palladium. Hence, EXAFS gives the same result for the first shell for both species.

One method to distinguish which species is present would be to fit an iodine shell. This distance would be ~3.8 Å.[7] The coordination number would be 1/3 for **3a** and 2/3 for species **4a**. But the Fourier transform does not show this peak and the shell cannot be included in the model. This is not surprising since 13 $Å^{-1}$ of high quality palladium K edge data for $Pd_2I_6^{2-}$(70 mM) has been reported[13] and the palladium palladium distance was not observable.

4.3.1.3c *In situ* QEXAFS experiments on the PhI system

Whilst the previous solution was being heated in the EXAFS cell for 120 minutes at 115°C, 6 minute QEXAFS scans were taken. Two main factors meant the quality of the results was fairly poor. The first reason was, because the reaction was proceeding the scans could not be

averaged, so the data quality was poor and secondly there was dampening of the EXAFS due to interference due to the mixture of species present. Therefore fitting any models to the data was very difficult. Therefore to aid analysis the white line was analysed and is shown in figure 4.11.

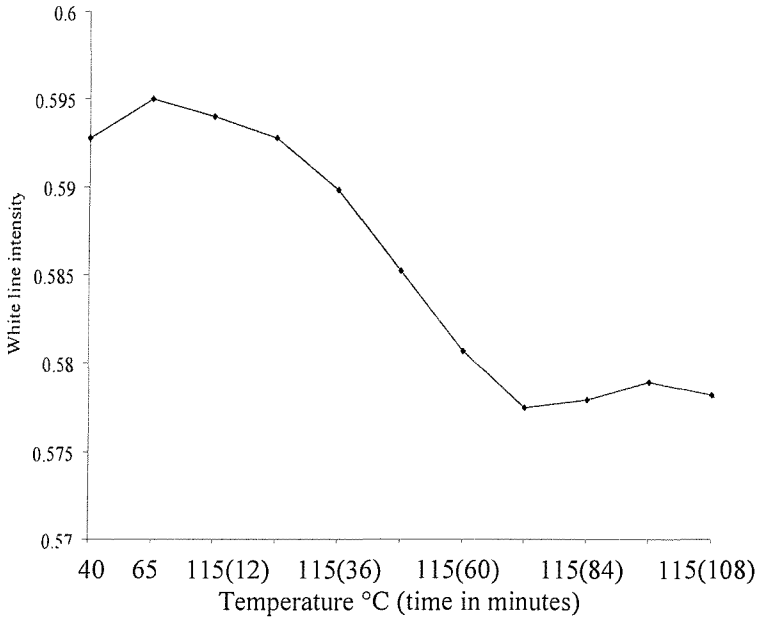

Figure 4.11 White line plot for the *in situ* PhI reaction catalysed by species 1, followed by iodine K-edge QEXAFS (1 x 6 minute).

The figure shows a general trend which is a reduction in the white line intensity with time. The two main areas of interest from the graph are the 65 °C spectrum and the spectrum taken after heating the solution for 72 minutes at 115 °C. These were chosen because they occur at changes in the trend of the graph.

Figure 4.12 shows the spectrum for the sample which was started at 65 °C (the sample reached 115 °C during this scan). The *k* weighted data is poor and the QEXAFS is seriously dampened around 9.5 $Å^{-1}$. It was very difficult trying to fit a reasonable model. The sample starts at only 15 °C above the starting spectrum (figure 4.8), but the QEXAFS has changed considerably, which informs us that the environment around the iodine has changed. The logical conclusion is that at this stage there is substantial coordination of the iodine to palladium. From the NMR data (table 4.1) a very approximate model can be calculated. Since the spectra is obtained from a sample being heated from 65 °C to 115 °C, the average environment around the palladium can be assumed to be the NMR data taken at 90 °C, this

is obviously not the case, but gives an approximate area to start the calculations.

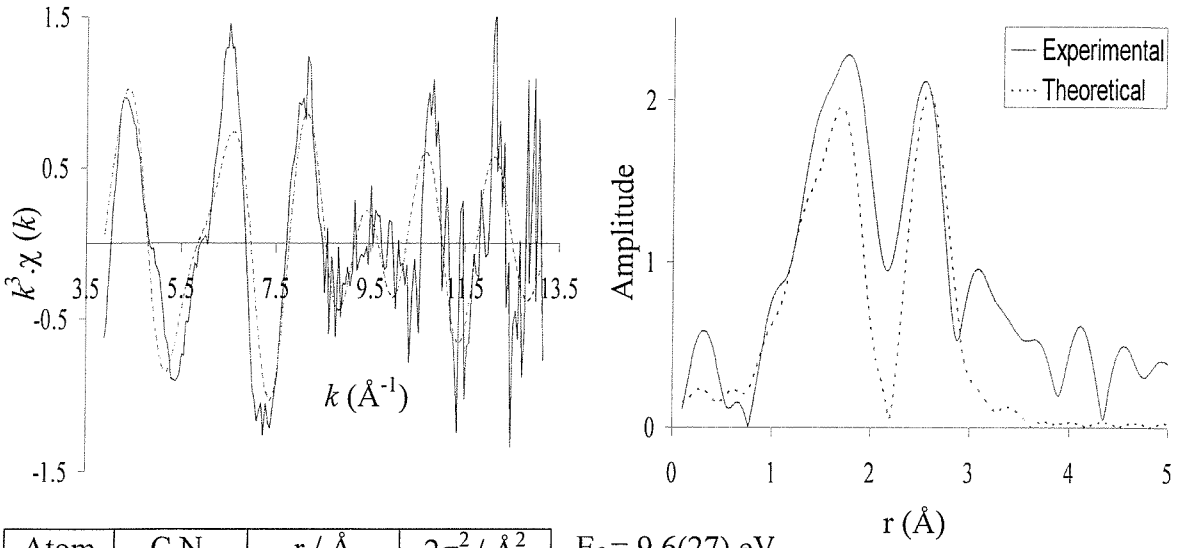

Atom	C.N.	r / Å	$2\sigma^2$ / Å^2
C	0.8(2)	2.01(2)	0.006(3)
Pd	0.6(1)	2.64(1)	0.016(2)

E_f = 9.6(27) eV

R = 59.2 %

Figure 4.12 The iodine K-edge k^3-weighted (1 x 6 minute) QEXAFS data and Fourier transform of the Heck reaction (the scan was started when the reaction was at 65 °C which heated to 115 °C during the duration of the scan).

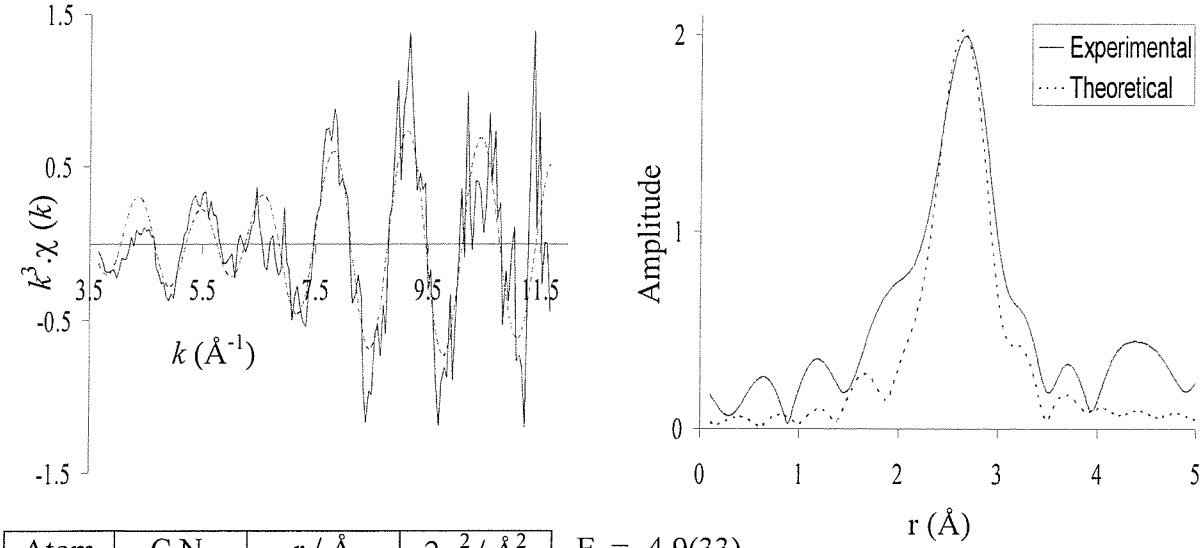

Atom	C.N.	r / Å	$2\sigma^2$ / Å^2
Pd	0.7(1)	2.71(1)	0.014(1)

E_f = -4.9(33)

R = 59.2 %

Figure 4.13 The iodine K-edge k^3-weighted (1 x 6 minute) QEXAFS data and Fourier transform of the Heck reaction (after heating the sample for 72 minutes at 115 °C).

At the start of the reaction the concentration of palladium is 50 mM, whilst the iodobezne is 150 mM. Assuming all the iodine is either coordinated as iodobenzene or palladium species, then the iodine containing species present are iodobenzene, or **2-4a**. The ^{31}P NMR data shows that of the palladium species 22 % is **2a**, 53% is **3a** and 25 % is **4a**. Therefore the 'concentration' of iodine (from iodobenzene) used to coordinate to these species is 11 mM (**2a**), 27 mM (**3a**) and 25 mM (**4a**, 2 iodines per palladium, not 1). Therefore the 'concentration' of iodobenzene used to coordinate iodine to palladium was 63 mM, which means the concentration of iodobenzene remaining is 87 mM (150–63 = 87). Therefore the average coordination number for carbon (in iodobenzene) is 87/150*1 = 0.58. The average coordination for palladium is (11 (**2a**) + 53 (**3a**) + 25 (**4a**))/150*1 = 0.59 (N.B. Species **3a** is coordinated to 2 palladium atoms (hence the value is doubled).

This model was applied to figure 4.12 and it can easily be observed from the Fourier transform, that the palladium shell fits quite well, but the carbon shell does not. The model refines well to the calculated coordination number for palladium of 0.6, gives reasonable values for the other refined values and sensible errors. But, the carbon shell has a less intense theoretical peak in the Fourier transform, which can be observed in the k^3 data, by the poor fitting at low k. The coordination number refines to 0.2 higher than the calculated value and has low Debye-Waller terms, which suggests that the coordination number should be increased. If the coordination number is increased to 1, the theoretical peak is still less intense than the experimental and the model refines to 1.1. Obviously chemically this is impossible, since the maximum coordination for carbon is 1. Since there is palladium coordination then this number must be reduced. Therefore it is not possible to fit this spectrum well to any model. The reason is that the species in the sample has changed considerably over the data collection time, which means the start of the k weighted data describes 1 sample, whilst the end describes a different sample, therefore it is not possible to obtain quantitative results. But the data shows us that palladium is coordinated early on in the reaction to iodine (slightly high Debye-Waller), which agrees with the earlier results and the palladium shell refines to 0.6.

The second point of interest in the white line graph was at the point of inflection. This spectrum was measured at 115 °C after the solution had been heated at this temperature for 72 minutes (figure 4.13). The spectrum is similar to the final result shown for this reaction

and a palladium shell fits well with a coordination number of 0.7 (as expected), but a slightly higher than expected Debye-Waller and bond length, compared with previous results, but as this is not the final spectrum these discrepancies can be expected. A carbon shell was fitted but the bond length refined to 2.2 Å, considerably too long to be incorporated into the fit. Analysis of spectra before this result, showed that this is the first spectrum where a carbon shell can not be included, so reinforces how useful white line plots can be at pinpointing structurally important stages in a reaction.

Summary

Iodine QEXAFS complements the results so far obtained on this reaction. It agrees that at 50 °C there is little or no bonding of iodine to the metal and it shows at the end of the reaction, that the large majority of the palladium is bonded to iodine. But, it cannot determine if the final palladium species is **3a** or **4a**.

In situ work shows that there is very quick addition of the iodine to palladium and this occurs soon after the heating process commences. The white line then gives extra additional information and shows that after heating the solution for 72 minutes at 115 °C there is no additional coordination of iodine to palladium.

4.3.1.4 The Heck reaction excluding methallyl alcohol or iodobenzene

To complete the investigation on the Heck reaction already studied, the reaction was carried out as usual but one of the reactants was omitted.

4.3.1.4a NMR studies

NMR studies were undertaken to investigate the **1** by excluding the alcohol or iodobenzene. The reaction was carried out as usual, except the alcohol or iodobenzene was excluded and replaced by additional NMP to keep the concentrations the same (table 4.3).

A

^{31}P NMR shift/ppm	Temperature / °C		
	70	90	110
36.3 **O=P(*o*-tolyl)$_3$**			12
35.4 **1**	70	73	16
33.9	30	24	26
26.7		3	16
-29.3 **P(*o*-tolyl)$_3$**			30

B

^{31}P NMR shift/ppm	Temperature / °C		
	55	110	115 (120min)
45.3 **3a**		12	54
44.6 **4a**			27
42.0 **2a**		6	19
39.3		7	
35.4 **1**	72	59	
33.9	28	16	

Table 4.3 ^{31}P NMR shifts for the Heck reaction but excluding iodobenzene (A) or methallyl alcohol (B) in NMP.

Shaw[14] has suggested that in the first step the alcohol adds to the palladium metal to form a Pd^{4+} complex. Therefore the first experiment was to heat the reaction mixture without the iodobenzene. ^{31}P NMR shows that after slow heating to 90 °C (33 min.) **1** (35.1 ppm) was in solution unreacted and there was production of a very small peak (26.4 ppm). After heating to 110 °C (75 min.) phosphorus NMR shows the catalyst had degraded to P(*o*-tolyl)$_3$ (-29.3 ppm) and O=P(*o*-tolyl)$_3$ and the signal at 26.4 ppm had increased. Therefore due to the instability of the catalyst in this solution, it is unlikely that the first step involves the alcohol.

The Heck reaction was then repeated, but the alcohol was excluded rather than the

iodobenzene. ^{31}P NMR shows that at 110 °C there is still some unreacted **1**, **2a**, **3a** and a new peak at 39.3 ppm have formed. The final solution at 115 °C (120 min) shows **2, 3** and **4a** are all present in varying amounts. This could also lead to a small amount of biphenyl formation (difficult to establish due to the large number of carbon peaks with similar chemical shifts in the region of 120 to 140 ppm). ^{13}C NMR does show reduction in the intensity of the iodobenzene peaks, assuming there was no loss of iodobenzene through evaporation, this was due to coordination of iodine to palladium.

These results show that as before, at any one time there is a mixture of phosphorus species present. The phosphorus species observed are the same as found in the full Heck reaction, but appear later during the heating process. At 110 °C in the full Heck reaction (table 4.1) only **2-4a** are present The concentration of the three species in the above reaction, is more or less identical to the NMR results from the full Heck reaction at 90 °C.

Therefore it appears as if there is coordination of the iodobenzene before the alcohol, since the same phosphorus species form and in the same concentrations. But there must be involvement by the alcohol at an early stage, since the rate of addition of iodine to the palladium is slowed down. Then at a certain stage it stops, but the species are stable in the solution.

4.3.1.4b XAFS analysis of the Heck reaction excluding alcohol

The experiment was undertaken for XAFS analysis. The usual concentrations of reagents were used and stirred at 50 °C to dissolve the catalyst. The solution was transferred to the EXAFS cell, 6 x 4 minute QEXAFS spectra were measured and averaged. The solution was then heated in the cell and more spectra were taken, to follow the reaction *in situ*.

The ^{31}P NMR spectra show that after heating and holding the sample at 90 °C for 16 minutes the palladacycle spectra had not changed. The solution was then heated to 115°C and held. An iodine atom can be included in the model after 40 minutes, with a Debye-Waller value of 0.021(5) $Å^2$. As mentioned previously this is slightly high, so the coordination number is probably lower than the refined value of 1. The iodine shell becomes more integral to the fit with time and comes to a constant (Debye-Waller value of 0.011(2) $Å^2$) after another 24 minutes. The final spectrum is shown in figure 4.14.

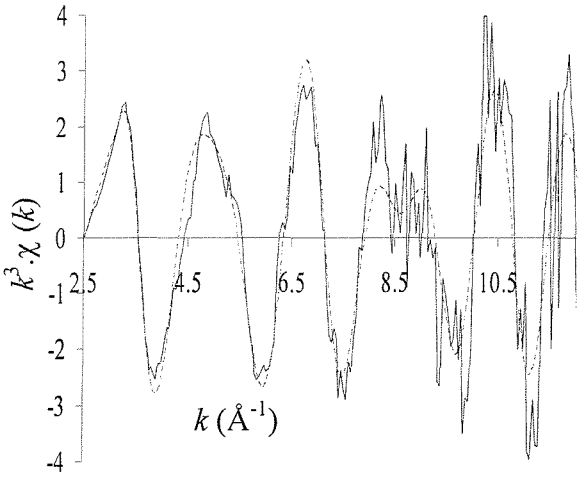

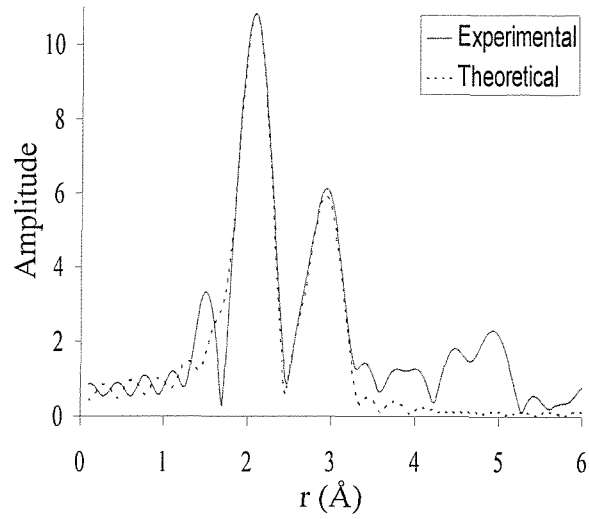

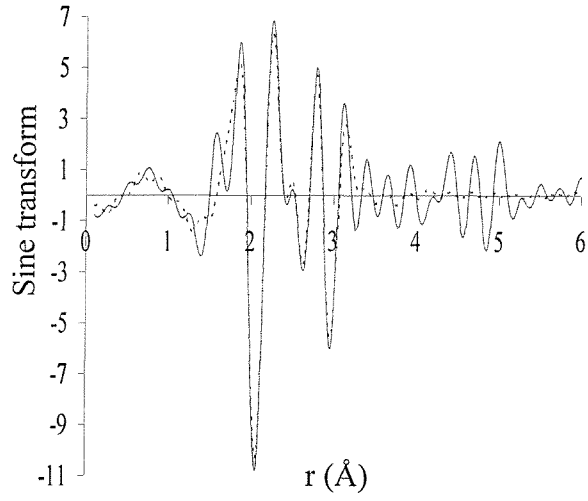

A - All parameters refined

Atom	C.N.	r / Å	$2\sigma^2$ / Å^2
C	1.4(6)	2.08(3)	0.008(5)
P	1.4(5)	2.27(2)	0.015(8)
I	1.1(2)	2.72(1)	0.011(2)

E_f = -5.0(26) eV , R = 40.4 %

B - C.N. for phosphorus not refined

Atom	C.N.	r / Å	$2\sigma^2$ / Å^2
C	1.9(3)	2.09(2)	0.008(5)
P	1*	2.27(2)	0.015(8)
I	1.0(2)	2.72(1)	0.011(2)

E_f = -6.8(15) eV, R = 40.7 %

*Coordination number is unrefined.

Figure 4.14 The palladium K-edge k^3-weighted QEXAFS data and Fourier transform for the Heck reaction, excluding methallyl alcohol (model from table B), after heating for 40 minutes at 115 °C.

The results shown are very good, considering it is a 4 minute QEXAFS spectrum with no averaging. The experimental spectrum fits to a model of 2 carbons, 1 phosphorus and 1 iodine. Table A shows the results for the model with all parameters refined. The Debye Waller terms have values indicative of being important to the fit and have errors of the normal magnitude. The interatomic distances are of the correct length with low errors. The only slight problem with the fit is the coordination number refinement. The refinement for the iodine shell is good, with low errors. The refined coordination numbers for the carbon and phosphorus are just within the proposed model, using the errors calculated. But, the

coordination numbers have been refined to approximately the same value and the errors are large (44 % for the carbon shell). This indicates that the data range is too short and of insufficient quality to differentiate the coordination numbers between the two shells, even though the Debye-Waller and interatomic distance terms refine to two different shells.

In the initial palladium species there is only 1 phosphorus atom per palladium and no other source of phosphorus is present in the solution. Therefore the coordination number for palladium cannot exceed 1. Hence this was fixed at this value (since the refinement increased this coordination number to 1.44) and all the other parameters were refined (table B). The iodine shell is discrete so remains unaffected. For the carbon and phosphorus shells the Debye-Waller and interatomic distance terms are very similar, but now the coordination number for the carbon shell is much closer to the proposed 2 carbons and the errors are considerably smaller.

Therefore by using the knowledge that the phosphorus coordination number cannot exceed 1, the data obtained which is not of the highest quality, can still yield very good results. The refined model agrees closely with the proposed model of 2 carbons, 1 phosphorus and 1 iodine atom bonded to the palladium.

Therefore these results shown that the same palladium species form in solution as for the reaction with the alcohol included. But, the rate of formation is slower and **1** is still present in the final solution.

4.3.1.4c Using this information to facilitate analysis of the Heck reaction

The QEXAFS results shown can be used to facilitate analysis of the QEXAFS data from the Heck reaction being studied so far. The QEXAFS spectrum for the final solution of the Heck reaction without methallyl alcohol (figure 4.14) was compared against the spectra obtained for the same reaction with the alcohol included (figure 4.7) The closest fit was when the Heck reaction solution was at 80 °C and the comparison is plotted in figure 4.15.

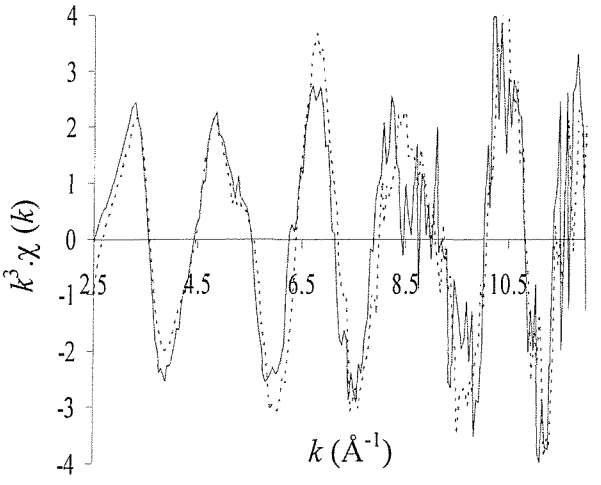

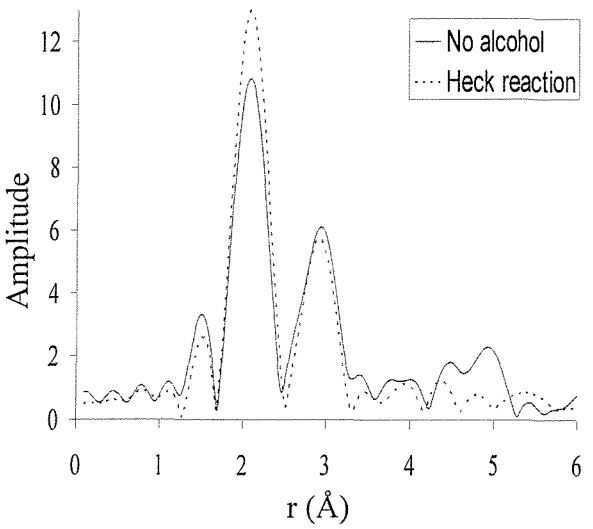

A - Heck Reaction

Atom	C.N.	r / Å	$2\sigma^2$ / Å^2
C	1.6(4)	2.08(2)	0.005(1)
P	1.2(3)	2.23(1)	0.011(6)
I	1.0(1)	2.70(1)	0.013(2)

E_f = -6.9(14) eV, R = 30.2 %

B- Heck reaction excluding alcohol

Atom	C.N.	r / Å	$2\sigma^2$ / Å^2
C	1.9(3)	2.09(2)	0.008(5)
P	1*	2.27(2)	0.015(8)
I	1.0(2)	2.72(1)	0.011(2)

E_f = -6.8(15) eV, R = 40.7 %

*Coordination number is unrefined.

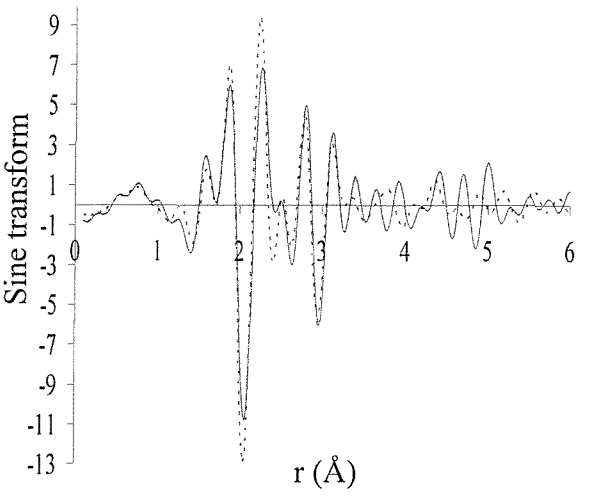

Figure 4.15 The palladium K-edge k^3-weighted EXAFS data, Fourier transform and sine transform comparing the experimental QEXAFS spectra of the Heck reaction at 80 °C against the Heck reaction excluding the methallyl alcohol at 115 °C after 64 minutes.

The spectrum for the solution with alcohol is considerably better (depicted by lower noise in the k^3 graph and lower R factor from table A) due to the fact that it was calculated from an average of 10 QEXAFS scans rather than just one. Otherwise the two spectra are very similar. The only difference is in the greater peak intensity for the reaction with alcohol between 6 and 7 Å^{-1}, which manifests as a more intense peak at ~2.10 Å in the Fourier transform.

These results show that the spectra are very similar. The bond lengths are the same and the

coordination numbers are very similar. The iodine shells are almost identical and indicate that in both cases the palladium has 1 iodine atom coordinated. The 2 smaller shells are also very close, with the difference in intensity being due to coordination of the alcohol, or due to experimental error. Since the spectrum with the alcohol included has an abnormally high intense Fourier transform peak at 2.10 Å, compared with the same peak for the other Fourier transforms from the rest of the experiment (figure 4.7), it is more likely that the difference between the two spectra is due to experimental error.

Therefore figure 4.15 shows that the environment around the palladium metal centre for the reaction of methallyl alcohol with iodobenzene catalysed by **1** at 80 °C, is the same as the identical reaction with the alcohol omitted after being at 115 °C for 65 minutes. The model proposed is an environment of 2 carbon, 1 phosphorus and 1 iodine atom, which has been shown by the NMR to be a mixture of signals. In this case it is a mixture of **1** and **2a, 3a** and **4a**. These results show that iodobenzene adds oxidatively to the initial palladacycle, before any involvement of the alcohol, but the process is considerably quicker when the alcohol is present. NMR results also showed that if the iodobenzene is omitted instead of the alcohol, the catalyst degrades and tri-*o*-tolylphosphine is formed.

4.3.1.5 Conclusions

All the results from the investigation on the reaction between iodobenzene and methallyl alcohol with **1** as catalyst work closely together to give a very detailed picture. Especially concerning the environment around the palladium edge and the phosphorus content in the reaction solution.

They show that immediately the solution becomes homogeneous at the start of the reaction, **1** is still present in its original form. After heating only 10 °C more, there is already coordination of iodine to palladium and when the solution has reached reaction temperature the average number of iodines coordinated to palladium is 1.6. During the heating process **2a** and **3a** form first followed by **4a**. During the catalysis there are only three phosphorus species present and all are coordinated in palladium iodide complexes and the P-C ring is intact. Catalysis commences after a fixed concentration of **4a** is reached and the concentrations of **2a** and **3a** are decreasing, showing that **4a** is likely to be the catalytic species.

Iodine QEXAFS agrees with the above hypothesis very closely. It shows that at the start of the reaction all the iodines are coordinated as iodobenzene, followed by very rapid coordination of iodine to palladium. Then towards the end of the reaction, it can pinpoint at which stage the influence on the XAFS from the iodobenzene contribution is negligible.

Finally by conducting the experiment without one of the reactants, more information can be obtained. By excluding the alcohol, the catalyst very quickly deteriorates suggesting that catalysis does not start by a Pd^{2+}/Pd^{4+} step (i.e. by the alcohol adding to the precursor). By excluding the alcohol in the reaction, the same phosphorus species are formed as in the reaction, but the rate of formation is slower and the concentrations only reach a level equivalent to heating the full Heck reaction to 90 °C. This shows that none of the species observed in the Heck reaction have olefin coordinated.

4.3.2 Investigation of the Heck reaction between methallyl alcohol and bromobenzene, catalysed by species 1

To further the investigation on the Heck reaction, **1** was used to catalyse the reaction between methallyl alcohol and bromobenzene. Again XAFS and NMR studies were used to investigate the phosphorus and palladium species present during the reaction. The same procedures and concentrations were used except bromobenzene replaced the iodobenzene.

4.3.2.1 NMR analysis

The NMR reaction between bromobenzene and methallyl alcohol with **1** as catalyst was investigated.

Temperature / °C	^{31}P NMR shift/ppm						Amount of x present*		
	42.4 **3b**	41.9 **4b**	38.9 **2b**	35.6 **1**	33.9	-29.3 PR_3	OH[a]	PhBr[b]	Prod[c]
60			5	71	24		100	100	0
90	14		21	49	16		85	86	0
115 (0 min)	69	15	16				56	80	5
115 (15 min)	51	39	10				35	65	15
115 (30 min)	36	55	9				20	53	25
115 (60 min)	15	80	5				3	35	40
115 (120 min)	5	90	4			1	0	8	100

*Amount of x present is the ^{13}C carbon NMR product integration value at [a]alcohol peak at 108ppm, [b]bromobenzene peak at 132 ppm and [c]product peak (1-phenyl-2-methyl-propanal) at 204 ppm, relative to the solvent signal at 174 ppm.

Table 4.5 ^{31}P and ^{13}C NMR results for the Heck reaction between bromobenzene and methallyl alcohol, with species 1 as catalyst (NMP as solvent).

The table shows (as before) the phosphorus peaks present (with assignment), as integration values, as a percentage of the total phosphorus integration. Carbon NMR was run directly before the phosphorus NMR, therefore the relative amount of reactant and product for the same sample is shown, so these can be directly related to the phosphorus species. The

relative amounts of product or reactant present was calculated by comparing the carbon integration for one of the peaks against a standard (solvent peak). This value was taken as 100 % for the reactants from the first sample and 100 % for the product from the final sample. The table is also shown in graphical form in figure 4.16.

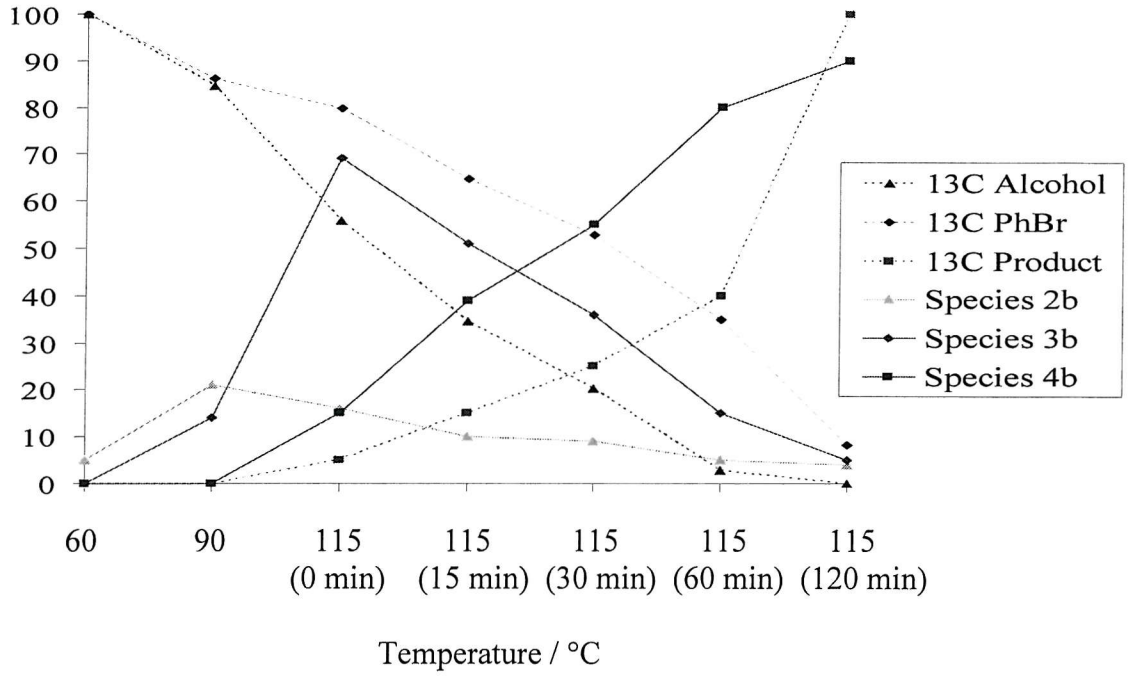

Figure 4.16 Species present in the solution during the reaction of bromobenzene with methallyl alcohol.

Table 4.5 and figure 4.16 can be used together to investigate what is happening to the phosphorus coordination as well as showing the amount of reactants and product present in the same sample.

At 60 °C, the majority of the phosphorus species is in the original form, in addition there is a peak at 33.9 ppm, which was present for the reaction when iodobenzene was excluded from the Heck reaction, therefore the species is not coordinated to a halogen (earlier was assigned as coordination of the amine). There is also a small peak at 38.9 ppm, which is likely to be the logical oxidative addition product (**2b**) of bromobenzene to catalyst **1**.

After heating to 90 °C, the two peaks at 33.9 and 35.6 ppm have decreased, consistent of them being related to the precursor. The peak at 38.9 ppm has increased and a new peak has

formed at 42.4 ppm, which is consistent with the formation of (**3b**). This shift also agrees with the ^{31}P NMR shift reported by Hermann.[1] These results agree with the results found in the iodobenzene experiment, but the formation of the bromine adducts is slower in comparison with the iodine analogues. Assuming this reaction follows the same trends, it can be hypothesised that **4b** will have formed in the next sample (115 °C).

There is some reduction in the amount of reactants present, which could be due to reactants being in the vapour phase. Bromobenzene has a higher boiling point (156 °C) than chlorobenzene so there would be a higher concentration in the solution, but since there is some formation of the halogenated palladacycle complexes, both reactants have decreased by the same percentage.

When the reaction temperature reaches 115 °C, there is already some initial production of product. The methallyl alcohol peak reduces considerably quicker due to reactant refluxing. The bomobenzene reduces due to refluxing and the formation of more bromine palladated species. The precursor peaks have disappeared and the amount of **3b**, is at its maximum. The amount of **2b** is now reducing at a fairly constant rate. There is also the production of a new peak at 41.9 ppm (**4b**).

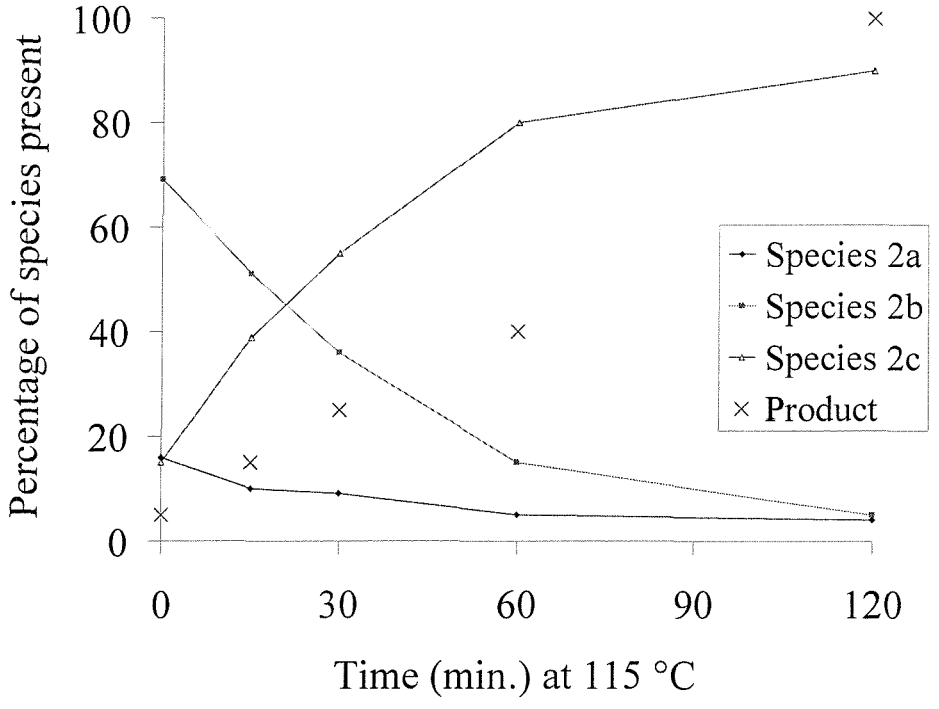

Figure 4.17 The abundance of species present whilst holding the reaction at 115 °C.
N.B Product = 1-phenyl-2-methyl-propanal

Figure 4.17 shows similar information to the previous figure, but shows the amount of the different species present during the catalysis and presents the data in real time with a fixed temperature.

Whilst the reaction solution was heated at 115 °C, the amount of reactants falls as the product forms. Due to the exchange processes going on between the liquid and vapour phases, due to condensation on the glass and due to formation of the product, it is very difficult to analyse the data quantitatively. This is shown by the fact that in theory there is only 3 % of the alcohol left after 60 minutes (at 115 °C), but at the same time only 40 % of the product has formed. This is due to the reactants refluxing at the reaction temperature, so the actual concentrations in the refluxing mixture is higher than the NMR samples from the solution.

During the reaction species **2b** and **3b** decreases, whilst species **4b** increases. At the end of the reaction after all the alcohol has been consumed, 90 % of the phosphorus species present are in the form of **4b**. There is still a small amount of **2b** and there is 1 % present as tri-*o*-tolylphosphine, formed due to degradation of the palladated species.

The assignments of the species **2b, 3b** and **4b** are justified because the ^{31}P NMR shift for **4b** agrees with the NMR shift of **4b** synthesised from **1** and tetrabutylammonium bromide. This value also agrees with Hermann[1] and follows the same trends as the analogous iodine complexes, but with a slightly smaller chemical shift.

Knowing that there was an excess of 20 fold of bromine to palladium and using the ^{31}P NMR integration values, then the amount of bromine coordinated to the palladium can be calculated at any one time. The final species **4b**, has two bromines for every palladium, therefore at a maximum, 10 % of the total bromine atoms present in solution can be coordinated to palladium. Therefore a graph was plotted (figure 4.18), showing the number of bromine atoms coordinated to palladium, expressed as a percentage of the total possible number of bromine atoms coordinated to palladium.

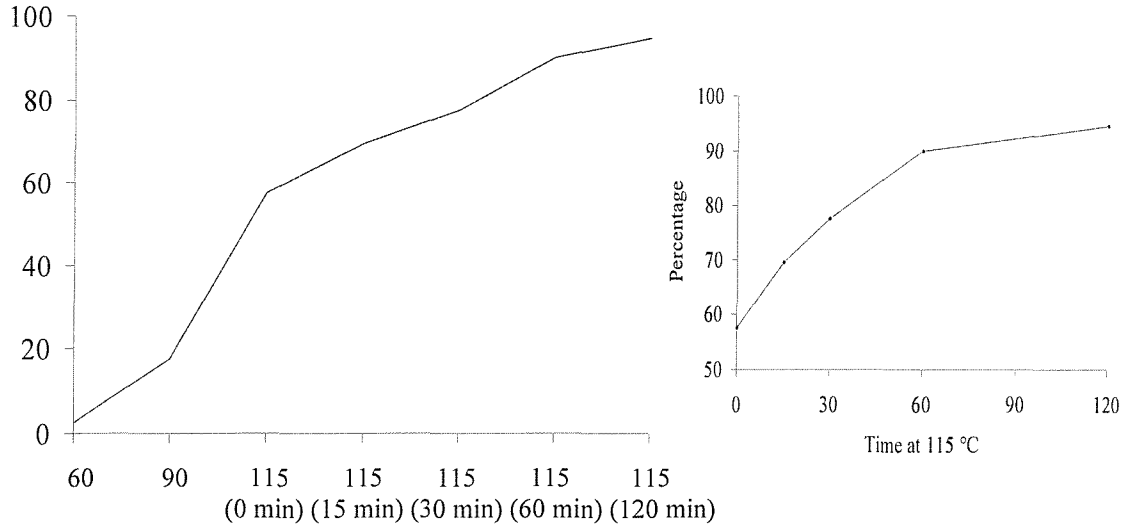

N.B. Insert shows the same information, but in real time and at a fixed temperature.

Figure 4.18 The number of bromine atoms coordinated to palladium, as a percentage of the total possible number of bromine atoms (i.e. two) coordinated to palladium.

These calculations show that when the temperature is 90 °C, only 20 % of the total amount possible of coordinated bromines, are already coordinated to the palladium. This jumps rapidly to almost 60 % as the solution is heated a further 25 °C. As the reaction proceeds at 115 °C the rate of addition of bromine to the palladium decreases with time (see insert). The amount of bromine coordinated finishes 5 % lower than the theoretical maximum of two bromines per palladium atom.

4.3.2.2 QEXAFS analysis

The XAFS experiment was carried out as usual. (5 x 5 minute) QEXAFS scans were taken of the initial solution at RTP after dissolving the catalyst in the reaction mixture at 50 °C. Analysis of these results showed that the catalyst was still in its initial form.

After heating for 2 hours at 115 °C the solution was cooled to RTP and (5 x 5 minute) QEXAFS scans were taken and averaged and the results are shown in figure 4.19.

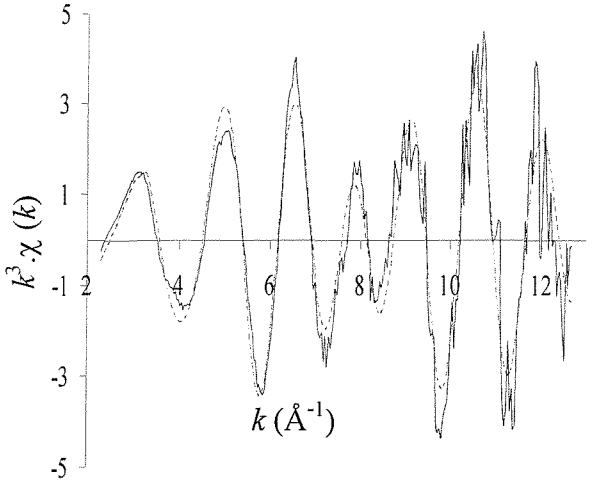

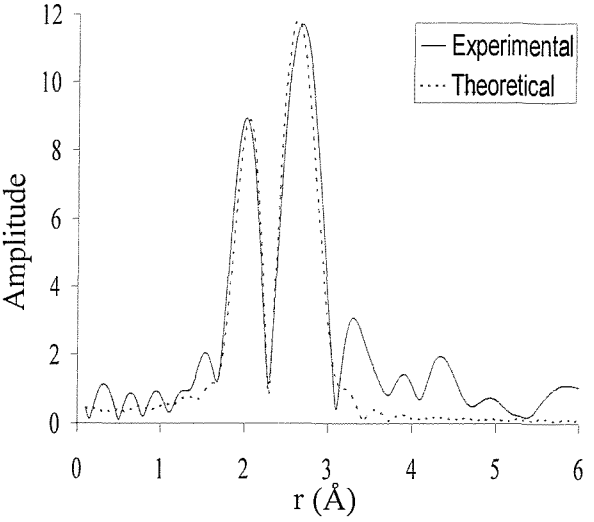

Atom	C.N.	r / Å	$2\sigma^2$ / Å^2
C	1.3(3)	2.05(2)	0.002(3)
P	0.8(3)	2.28(5)	0.008(3)
Br	2.0(1)	2.56(1)	0.013(1)

E_f = -11.3(2.5) eV

R = 34.2 %

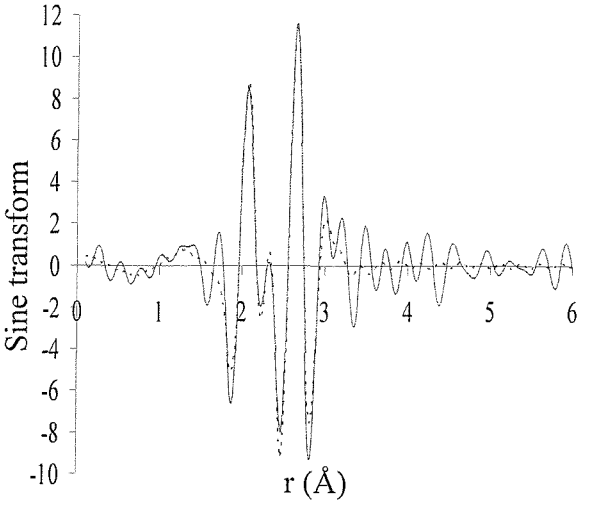

Figure 4.19 The palladium K-edge k^3-weighted QEXAFS data (5 x 5 minutes averaged), Fourier transform and sine transform showing the end of the reaction between bromobenzene and methallyl alcohol with species 1 as catalyst (after heating for 2 hours at 115 °C).

These results give a very good fit for a model of 1 phosphorus, 1 carbon and 2 bromine atoms (**4b**). The fit has low errors for the bromine shell (error on coordination number is 7 %). The errors for the coordination numbers of the other two shells are considerably larger (29 % w.r.t. phosphorus), but this is probably again due to difficulties resolving them into two discrete shells. The NMR data shows that 99 % of the phosphorus is still coordinated to the palladium, therefore the refined phosphorus coordination number is too low. Therefore in an attempt to resolve this problem a map was drawn for the coordination numbers of carbon against phosphorus (figure 4.20).

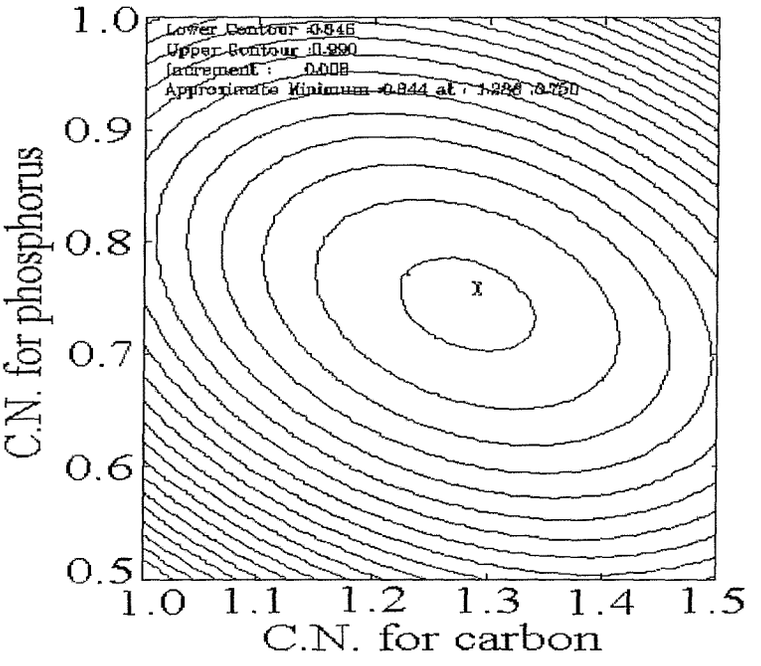

Figure 4.20 Map of the fit index for coordination number of carbon against phosphorus, for the end solution of the Heck reaction between methallyl alcohol and bromobenzene, with species 1 as catalyst.

The map shows a well defined minima with the values for the model depicted by an X inside the minima. The minima is more defined for the phosphorus coordination number. A trough in the contours travels in the direction and encompasses the proposed values of 1 carbon and 1 phosphorus atom. This trough travels along the line where the total coordination number of both shells equals two. Hence, the last figure depicts nicely the problem with resolving the coordination numbers for the two shells, even though the other refined parameters are discrete.

The refined model (figure 4.19) suggests that the palladium species present (1 carbon, 1 phosphorus and 2 bromines) are **3b** or **4b**. The QEXAFS data is almost identical to the QEXAFS spectra obtained by reacting **1** with tetrabutylammonium bromide, but since the spectra for **3b** and **4b** are very similar this is not surprising. Therefore the sine transform for these experiments were compared (figure 4.21) to try to determine which palladium species is present.

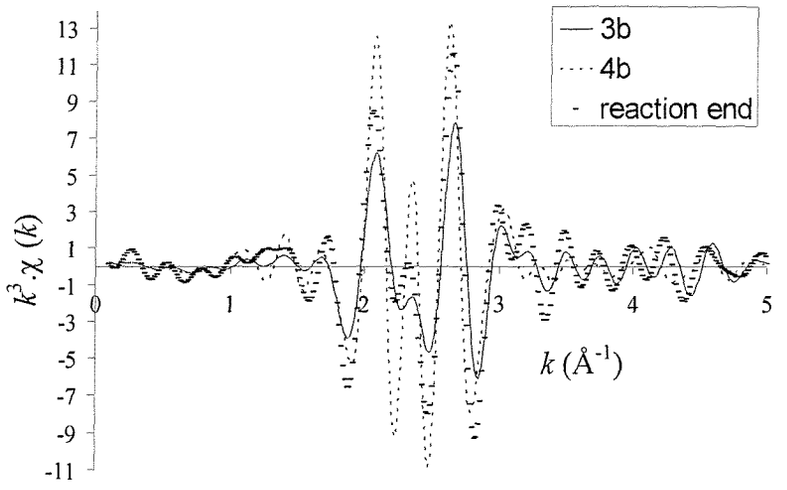

Figure 4.21 The palladium K-edge sine transform data comparing species 3b and 4b with the end of the reaction between bromobenzene and methallyl alcohol.

The figure shows that the intensity for some of the sine peaks is very varied between the different samples. Part of this variation was attributed to poor data quality, since **3b** had poor solubility and a lower concentration in solution. Assigning one of the species to the solution at the end of the reaction, is very difficult, since the species was only 90 % abundant, meaning there are contributions from other species. Observation of the above figure, would suggest that the 'reaction end' spectrum is closer in character to **4b**, since they have closer intensity and a similar phase between 2.7 and 3 Å, compared with **3b**. Between 2.2 and 2.5 Å, the 'reaction' sine wave is considerably lower in amplitude than **4b**, which is probably due to dampening by **2b** and **3b**. These results then agree well with the NMR results.

4.3.2.3 Summary

Species **1** catalyses the PhBr reaction and the palladium phosphorus species that form during the reaction are the bromine analogues of the PhI reaction. The species are also formed in the same chronological order starting with **2b**, followed by the formation of **3b** and the end species present is **4b**. Again there are no palladium phosphorus complexes which are attributed to containing the olefin.

4.3.3 Investigation of the Heck reaction between methallyl alcohol and chlorobenzene, catalysed by species 1

To complete the investigation on the Heck reaction with **1** as catalyst, the reaction between methallyl alcohol and chlorobenzene was examined,

4.3.3.1 NMR results

NMR spectroscopy was used to follow the Heck reaction between chlorobenzene and methallyl alcohol.

^{13}C NMR showed that there was no formation of product or biphenyl. The only new carbon peaks formed are between 126 and 132 ppm and are very weak. They are probably due to the production of phosphine species with aryl carbons or slightly different palladacycle species, with substitution of the acetate groups by chlorine atoms. Therefore the only loss of reactants is due to evaporation or coordination to the palladium species. A graph was plotted (figure 4.22) showing the reduction in the concentration of reactant present, since this might yield further information on how much chlorobenzene is consumed, to coordinate chlorine to palladium.

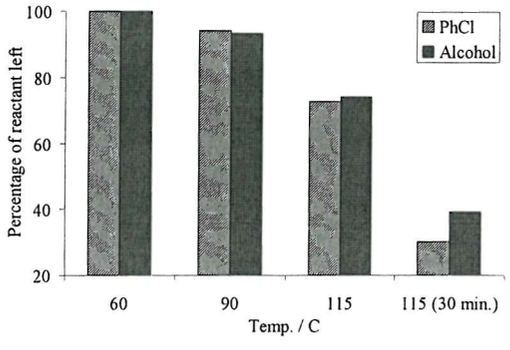

Figure 4.22 The percentage of chlorobenzene or methallyl alcohol present during the reaction.

As previously, the amount of reactant present was determined by ratioing, the integration value for one of the reactant carbons with one of the solvent carbons. This value for the first spectrum was assigned as 100 % for each reactant, afterwards the reduction in the

integration value over time could be plotted as a percentage of the original value.

The alcohol peak at 108 ppm reduces by 61 % (relative to the solvent peak 174 ppm) with time and the chlorobenzene peak at 131 ppm decreases by 70 % over the course of the reaction. The boiling point for the alcohol is 113-115 °C and for chlorobenzene is 132 °C. This is a huge decrease in reactant considering there was no product formation. This loss was therefore due to evaporation through the bubbler, reaction with the catalyst or condensation on the reaction vessel. Much evaporation is unlikely, since the reaction temperature was only 115 °C, a condenser was used and there would be a greater loss of the lower boiling alcohol. Condensation is likely to account for some loss in the peak intensities. During the heating process there will be reactant vapour in the vessel, so there would be a lower concentration in the solution since the solvent and amine has a high boiling point (202 and 216 °C respectively). There is also condensation on the glass which reduces the reactant concentration in the solution. The final NMR sample was taken after cooling the solution down to room temperature therefore all the reactant vapour would have condensed on the vessel walls or back in the solution. Therefore for the scenario described above, it is likely the peak intensity reduction is due to condensation on the vessel, which would affect both reactants and the greater chlorobenzene loss could be due to reaction with the catalyst. This agrees with figure 4.20 because during the heating process, the reductions in the amount of both reactants is equal. The only difference appears for the final result where there is a greater 8 % 'loss' of chlorobenzene compared with the alcohol, relative to the initial concentration.

^{31}P NMR spectra were analysed for the same reaction and are shown in table 4.7

Temperature / °C	^{31}P NMR shift/ppm								
	39.8 **3c**	39.2 **4c**	37.4 **2c**	36.7	35.5 **1**	33.9	30.4	26.7	-29.3
60				6	71	23			
90				6	72	22			
115	6		6	6	60	16		3	3
115 (30 min)	38	9	31	3			16		3

N.B. The integration values shown, are calculated as a percentage of the overall integration area per spectrum.

Table 4.7 Shows the ^{31}P NMR shifts for the reaction between chlorobenzene and methallyl alcohol with species 1 as a catalyst (NMP).

The results show that after initially dissolving the catalyst and heating to 90 °C, only the peak at 33.9 ppm (thought to be amine coordination to **1**), **1** (35.5 ppm) and the peak at 36.7 (O=P(*o*-tolyl)$_3$) are visible. Comparison of these results with the analogous halobenzene experiments shows that for the other experiments, at the same stage in the reaction there is already formation of halogenated palladium complexes.

Comparison of the phosphorus integration for the 60 °C and 90 °C samples shows that the precursor has not changed over the temperature range. These two results also show how accurate a tool the phosphorus integration technique is, since the results are only 1 % different.

After heating to 115 °C the initial species concentrations have both reduced and there is some degradation (formation of P(*o*-tolyl)$_3$ at -29.2 ppm) of the initial catalyst. Other phosphine species have formed. A peak at 26.7 ppm is present which formed when iodobenzene was excluded in the Heck reaction (section 4.3.1.4), hence this does not have halogen coordinated. Finally there is the initial production of two peaks at 37.4 and 39.8 ppm, assuming the reaction follows a similar trend to the halogen reactions then it can be hypothesised that these are **2c** and **3c**. The trend in the change in the chemical shift from the iodine to bromine coordinated palladium complexes, follows for the chlorine examples, since both species have shifted downfield.

For the last spectra the initial species have all reacted or degraded to form other species,

leaving a very small amount of oxidised tri-*o*-tolylphosphine. There was no further production of tri-*o*-tolylphosphine, but there was a large increase in the amount of chlorine containing species. Species **2c** increased to account for 31 % of the phosphorus species, whilst **3c** for 38 %. There was also formation of **4c** (9 % of species) at 39.2 ppm. The only other peak formed was a broad peak at 30.4 ppm.

Calculations using the ^{13}C NMR integration data, suggested that assuming there was no bonding of the alcohol to any palladium species then 8 % of the original chlorine atoms (as chlorobenzene) were bonded to phosphine species. Therefore 80 % of the palladium phosphorus species should have two chlorines coordinated According to the phosphorus results 47 % of the phosphorus species contain 2 chlorines and 31 % contain 1 chlorine. This means if all the palladium phosphorus species had two chlorines coordinated, 63 % would be this species. This value is lower than calculated, but considering that a conservative error value for the carbon NMR integration is ± 1 % (calculated from result 2 and 3 from figure 4.20) and the concentration of palladacycle is very low compared with the chlorobenzene, this means that the value could be between 70 and 90 %.

4.3.3.2 XAFS analysis

The above reaction was then studied using QEXAFS. (5 x 6 minute) QEXAFS scans were taken at RTP of the solution after dissolving the catalyst at 50 °C. The k^3 background subtracted data was the same as for **1** and gave a model consistent for this compound.

The solution was heated to 100 °C and (10 x 6 minute) QEXAFS scans were taken at RTP The results were averaged and are shown in figure 4.23.

These results fit very well for the model of **1**, 2.7 carbon atoms and 1 phosphorus. If a chlorine shell at 2.4 Å is added, the Debye-Waller value rises to over 0.04, indicating this is not a valid shell. The inflection at 4 $Å^{-1}$ in the background subtracted graph, is also indicative that **1** is still in its initial form (chapter 3). These results show that at 100 °C the catalyst is still in its initial form.

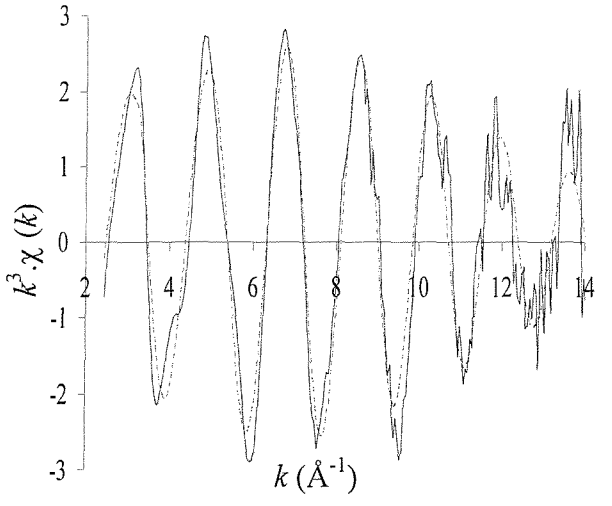

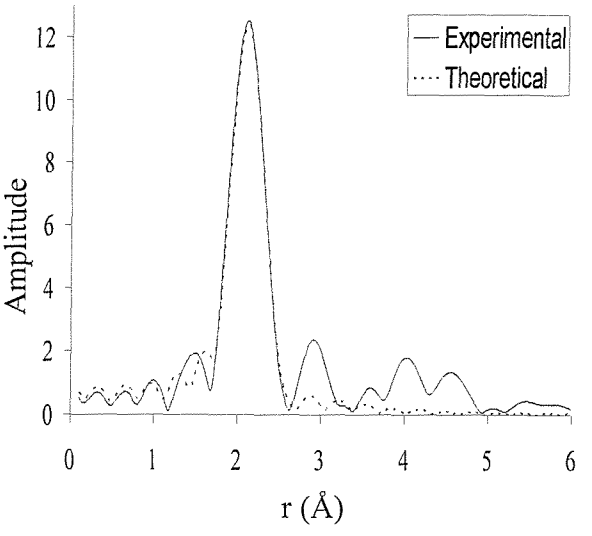

Atom	C.N.	r / Å	$2\sigma^2$ / Å^2
C	2.7(4)	2.12(1)	0.009(6)
P	0.9(2)	2.22(1)	0.010(6)

$E_f = 2.4(10)$ eV

R = 28.2 %

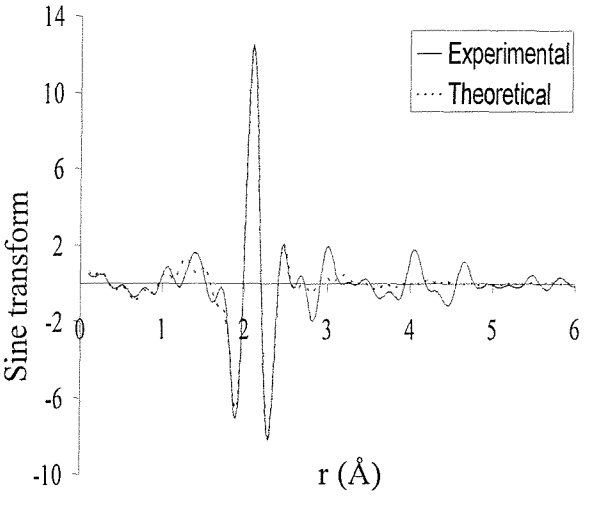

Figure 4.23 The palladium K-edge k^3-weighted QEXAFS data (10 x 6 minute averaged), Fourier transform and sine transform of the chlorobenzene reaction (RTP) after heating to 100 °C.

The results show that **1** does not catalyse the previous experiment with chlorobenzene. Chlorine coordinates to the palladium, but considerably slower than for the other reactions. QEXAFS shows that at 100 °C there is no chlorine coordination and NMR shows that at 115 °C there is only minimal coordination (12 % of the species). At the end of the heating process, species **2-4c** are all present, but **4c** has only formed in low concentrations (9 %), which could be the reason why no catalysis occurs.

4.3.4 Conclusions

Species **1** catalyses the Heck reaction with iodobenzene and bromobenzene, but not chlorobenzene. In each reaction three halogenated species coordinated to palladium are formed **na-c** (n=2,3,4). Each species maintains the integrity of the P-C ring and has 1 or 2 halogen atoms coordinated. They have been shown to form in the order of **2a-c**, followed very closely by **3a-c** (in some reactions this time scale is not discernable) and finally **4a-c** is formed. For the reactions where catalysis occurs, after initial production of **4**, **2** and **3** reduce in concentration, whilst **4** increases (to almost 100 %). The maximum concentration of **3** observed is 69 %, whilst the maximum concentration of **2** is only 21 %. Catalysis commences after **4a** is 58 % abundant, but before **4b** is 15 % abundant. Since catalysis occurs when **3a** is absent and at very low concentrations of **2** and **3a-b**, it is likely that **4a-b** are the catalytic species.

In all the reactions species **a** forms before **b**, which forms before **c** (in relation to time and temperature). In the chlorobenzene reaction, only 9 % of **4c** is formed, which suggests that if the concentration was higher, then catalysis might occur. Again it is unlikely that **2-3c** are catalysts, since they are present in quantities greater than 30 % concentration of the total palladium species present.

Species **2-4b** have been assigned by Hermann and species **4a-c** have been confirmed by in house NMR. The other assignments have been deduced from the information known. These assignments have been reinforced by NMR data, especially for the chlorobenzene experiment, because it is known that the chlorobenzene is not used to form product, a rough quantitative analysis can show how much is 'used up' in bonding to the palladium complexes.

4.4 Analysis of the Heck reaction with the bromine bridged palladacycle (3b) as catalyst

The reactions studied were extended to investigate the same Heck reaction, but the catalyst was changed to the bromine bridged palladacycle (**3b**), which had been synthesised from **1** and tetrabutylammonium bromide and then recrystallised. NMR and XAFS studies were carried out as usual, except that the catalyst was considerably less soluble in the reaction solution and needed to be heated to 130 °C with a concentration of only 40 mM, the reaction was then carried out at this temperature.

4.4.1 Analysis of the reaction between iodobenzene and methallyl alcohol with species 3b as catalyst

Again the first reaction to be investigated was between iodobenzene and methallyl alcohol.

4.4.1.1 NMR

NMR analysis was taken of samples (RTP) during the reaction (130 °C) and the results are shown below in table 4.8.

From earlier results (sections 4.3 and 4.4) the peaks already assigned are 42.0 (**2a**), 44.6 (**4a**), 45.3 (**3a**) 38.9 (**2b**), and 42.4 ppm (**3b**). As mentioned there is a shoulder to the peak at 42.0 ppm. For the first 2 spectra, the shoulder has a small peak at 41.9 ppm. It is not possible to resolve the peaks, but could contribute up to 20 % of the integration value. On the third spectrum this shoulder peak, is undefined from the main peak and the shoulder has completely disappeared for the remaining spectra.

The unassigned peak at 44.3 ppm, could be attributed to a variant of species **4** with a bromine and iodine coordinated to the palladium. This assignment is reinforced by the fact that the chemical shift appears in between the values for **4a** and **4b**.

Time / min.	^{31}P NMR shift/ppm									Amount of x*		
	45.3 **3a**	44.6 **4a**	44.3	42.4 **3b**	42.0 **2a****	38.9 **2b**	23.5	22.4	-29.4	OH[a]	PhI[b]	Prod[c]
0	14	13	5	26	23	19				100	100	0
5	15	12	7	20	28	18				87	96	0
10	21	17	7	14	28	13				72	93	0
20	21	33	8	17	13	8				65	92	35
45		81		13	6					20	76	60
90		85		1	2		2	1	9	2	1	100
120		81		1			3	1	14	1	1	42

*Amount of x present is the ^{13}C carbon NMR product integration value at [a]alcohol peak at 108 ppm, [b]iodobenzene peak at 138 ppm and [c]product (1-phenyl-2-methyl-propanal) peak at 204 ppm, relative to the solvent signal at 174 ppm (value of 100).

This peak has a shoulder at 41.9 ppm (first 3 spectra), presumably **4b.

Table 4.8 ^{31}P and ^{13}C NMR results for the Heck reaction between iodobenzene and methallyl alcohol, with 3b as the catalyst.

The table shows that after **3b** has dissolved into the solution, there is a wide range of species present, including **2a, 3a** and **4a** and **2b, 3b,** and **4b**, all in substantial concentrations. These species are all present (except **4b**) at the start of catalysis. As expected over this period the bromine species are decreasing whilst the iodine species are increasing. The main noticeable difference between the spectra which represent just before and after commencement of catalysis, is that the concentration of **4a** has doubled.

After 45 minutes, 60 % of the total measured synthsised product has been produced. Only three species are left, 13 % is attributed to the original catalyst, 6 % to **2a** and the majority is species **4a**. After 90 minutes the reaction has finished and there is a considerable amount of biphenyl formed. The main species left is **4a** (85 %), a very small amount of **2a** and **3b**, and some decomposition of the catalytic species to tri-o-tolylphosphine (-29.4 ppm) and species at 22.4 and 23.5 ppm. Heating for another 30 minutes, degrades the product formed and ^{31}P NMR shows that there is further degradation of the catalyst to form tri-o-tolylphosphine and palladium metal. There is considerably greater degradation of the palladium species, compared with any of the other reactions, studied so far in this report.

These results show that at the start of the reaction there is a broad mixture of palladium

species present, all halogenated. When catalysis commences the only marked change in the phosphorus NMR is a large increase in the proportion of **4a** present. During catalysis this species increases in concentration, whilst the remaining species decrease. Since the remaining species are present in lower concentrations during the catalysis than before catalysis, species **4a** must be the active catalytic species.

The results also show that the reaction time is quicker using **3b** compared with **1**, but it must be remembered that the reaction temperature is 15 °C higher. There is also greater degradation of palladium species which could also be due to the more extreme reaction conditions. Another point worth noting is the formation of biphenyl, this presumably formed after the alcohol was consumed in the reaction or lost due to evaporation.

4.4.1.2 QEXAFS analysis - Start of reaction

(5 x 6 minute) QEXAFS scans were taken (RTP) and averaged, of the reaction solution after dissolving the catalyst into solution at 125 °C (figure 4.24). After transferring the sample into the XAFS cell, it was observed that there was a suspension in the solution, indicating that the catalyst had not fully dissolved in the solution.

The results show that the data quality obtained is very high, considering that the sample was not homogeneous. 14 $Å^{-1}$ of data was recorded and only has one spike (at 13.7 k), this is a very long data set, considering the acquisition time was only 30 minutes.

Analysis of the k^3 data, refines a model close to the initial catalyst **3b**. Again there are problems with resolving the coordination numbers for carbon and phosphorus, depicted by a lower phosphorus coordination number (not possible since the NMR results show it is all coordinated to palladium at the start of the experiment) and large errors on the refined values. The bromine coordination number is slightly lower than the expected value of 2, but is within this value, when taking the errors into account. By comparing the k^3 spectrum with the spectrum of **3b** in solution (figure 4.2), it is noticeable that most of the structure between 8 and 9.2 $Å^{-1}$ has been dampened out (depicted in the Fourier transform with a reduction in the intensity of the bromine peak), this is indicative of destructive photoelectron wave interference. This is caused by a proportion of the bromine atoms being substituted by

iodine atoms. This agrees with the lower coordination number calculated for bromine (by 10 %). Since the reduction is small, the contribution due to the coordination of iodine atoms, is not observable and it is not possible to fit an iodine shell. To investigate further to see if any iodine atoms were contributing to the largest shell, the sine curve was analysed. Since the curve shows a very good fit up to 3 Å, this reinforces the fact that the contributions to the longer Fourier transform peak are due to bromine and not iodine atoms.

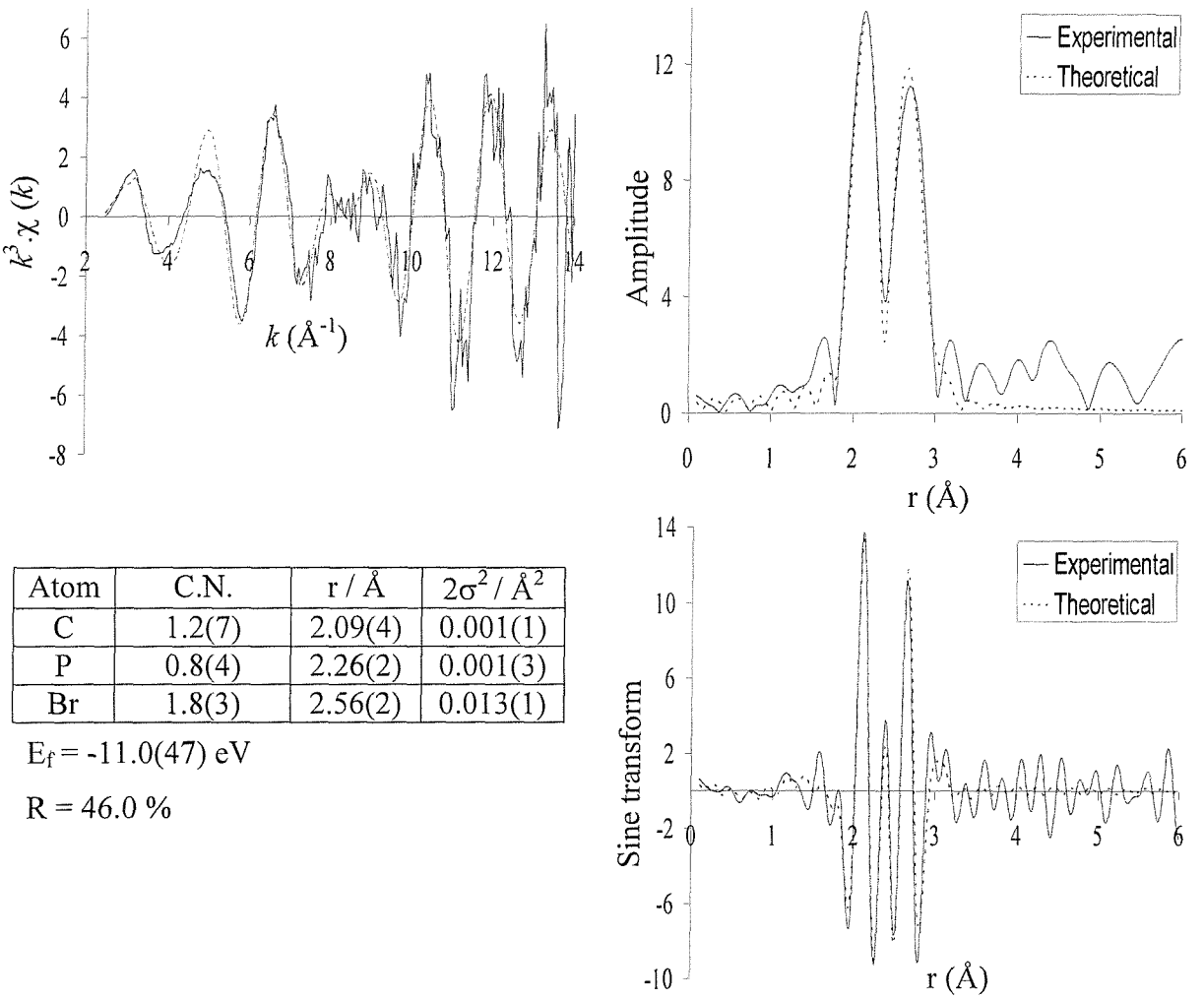

Atom	C.N.	r / Å	$2\sigma^2$ / Å^2
C	1.2(7)	2.09(4)	0.001(1)
P	0.8(4)	2.26(2)	0.001(3)
Br	1.8(3)	2.56(2)	0.013(1)

E_f = -11.0(47) eV

R = 46.0 %

Figure 4.24 The palladium K-edge k^3-weighted QEXAFS data (5 x 6 minutes averaged), Fourier and sine transform for the reaction between iodobenzene and methallyl alcohol with species 3b as catalyst (RTP), after heating to 125 °C.

These results are as expected since some of the catalyst is in suspension, the model refined is very close to the initial catalyst **3b**. But, the loss of structure in the k^3 spectrum, suggests that once the catalyst is in solution, it very quickly forms a mixture of species (bromine and iodine containing), which agrees with the NMR data taken from a sample at 130 °C, that a number of species are present.

4.4.1.3 QEXAFS analysis - End of reaction

After reacting the solution for 2 hours at 130 °C, (10 x 6) minute QEXAFS spectra were taken and averaged (figure 4.25).

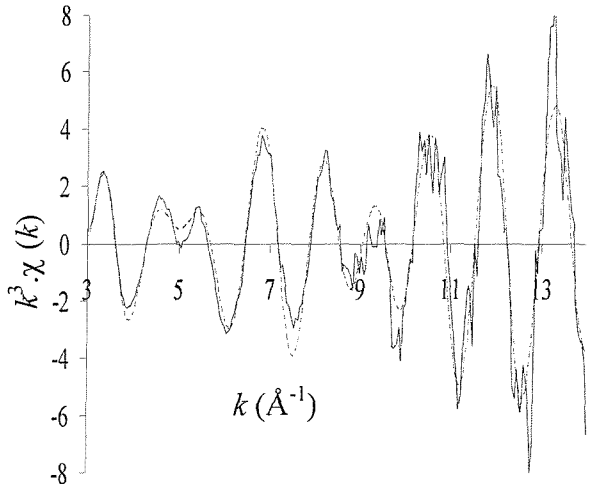

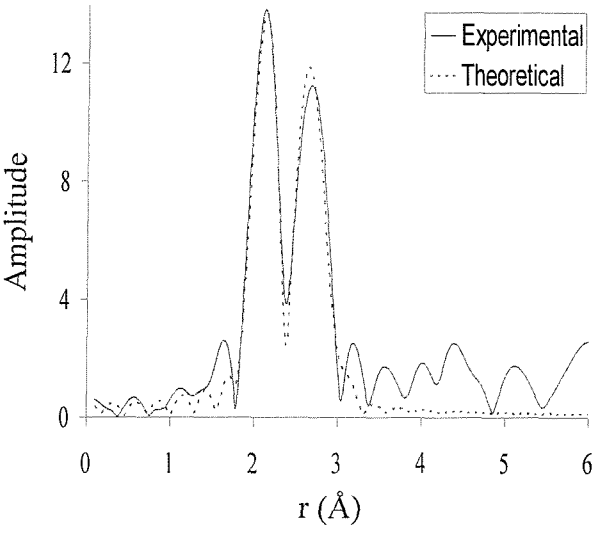

Atom	C.N.	r / Å	$2\sigma^2$ / Å^2
C	0.8(5)	2.03(8)	0.025(20)
P	1.0(1)	2.25(1)	0.001(1)
I	1.9(1)	2.68(1)	0.010(1)

E_f = -6.7(14) eV

R = 34.7 %

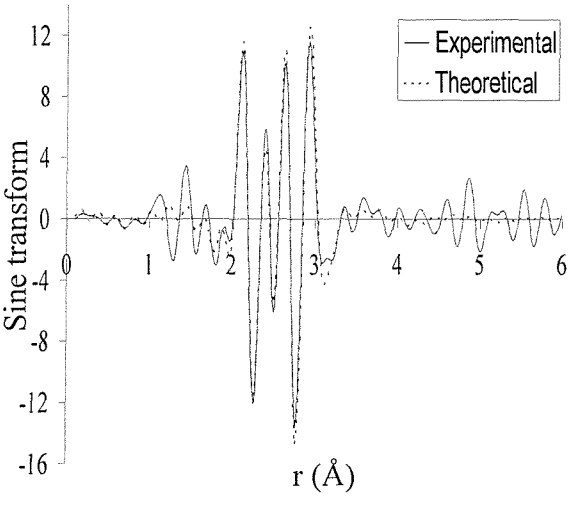

Figure 4.25 The palladium K-edge k^3-weighted QEXAFS data (10 x 6 minutes averaged), Fourier transform and sine transform for the reaction between iodobenzene and methallyl alcohol with species 3b as catalyst (RTP) after heating for 2 hours at 130 °C.

These results give a very close fit to the model of **4a**. The results are very close to expected values, but the carbon shell has large errors and a high Debye Waller value of 0.025 Å^2. The

k^3 spectrum fits very well, except for at 5 $Å^{-1}$. The Fourier transform and sine curve, fits very well in the region modelled.

These results agree nicely with the NMR results, that the final species present is **4a**. After two hours there is approximately 81 % present, whilst the majority of the remainder is degradation products (mainly tri-o-tolyphosphine and palladium deposits), which could explain the errors present in the carbon shell.

The *k* weighted data is very similar to the data for the end of the same reaction with **1** as catalyst. The phase is the same for both reactions, but the intensity for this reaction is lower at 9 *k* than for the reaction studied earlier in the chapter, this is a very important part of the spectrum, since this area had the greatest changes over the course of the reaction. This section of the spectrum has greater resemblance to the spectrum taken after 0.5 hrs at 115 °C, but before concluding that the previous sample is more similar to 0.5 hr sample, than the 1.5 hr sample the area between 4 and 6 $Å^{-1}$ needs to be investigated, since this was the other area of great change. Careful analysis of this area shows that the 1.5 hr sample is closer in character to the last spectrum, since for both of these the peak at 4.5 $Å^{-1}$ is more intense than the peak at 5.5 $Å^{-1}$, whilst this observation is reversed for the 0.5 hr spectrum. Since NMR showed that there is a lot of catalyst degradation present, there could be small palladium particles present. Since palladium is a large backscatterer, if it were to effect the XAFS then it would have a greater influence at high *k*. Therefore using the lower *k* data as a 'fingerprint', it can be concluded that the final spectrum for both reactions (**1** and **3b** as catalyst) is very similar and has the same main species present **4a**.

4.4.2 Analysis of the reaction between bromobenzene and methallyl alcohol with species 3b as catalyst

To continue the investigation of this family of experiments, catalyst **3b** was used to catalyse the reaction between bromobenzene and methallyl alcohol.

4.4.2.1 NMR results

The results from the experiment are shown in table 4.9.

Time / min.	^{31}P NMR shift/ppm					Amount of x*		
	42.4 **3b**	41.9 **4b**	38.9 **2b**	36.6 O=P(*o*-tolyl)$_3$	-29.4 P(*o*-tolyl)$_3$	OH[a]	PhBr[b]	Prod[c]
0	29	52	17	2		100	100	2
5	30	53	15	2		88	97	6
15	21	67	10	2		68	83	14
30	8	86	5	1		38	66	45
60		95	3	1	1	26	46	68
90		90	7	2	1	10	24	100

*Amount of x present is the ^{13}C carbon NMR product integration value at [a]alcohol peak at 108 ppm, [b]iodobenzene peak at 132 ppm and [c]product peak (1-phenyl-2-methyl-propanal) at 204 ppm, relative to the solvent signal at 174 ppm (value of 100).

Table 4.9 ^{31}P and ^{13}C NMR results for the Heck reaction between bromobenzene and methallyl alcohol, with 3b as catalyst.

Table 4.9 shows that after dissolving the catalyst in solution at 130 °C, there is very quick formation of product. Species **2-4b** are all present in solution in large concentrations. Species **4b** is present in the largest concentration, whilst the initial catalyst (**3b**) is present as only 29 % of the phosphine species. There is also a very small peak at 36.6 ppm (O=P(*o*-tolyl)$_3$).

During the reaction **2b** decreases with time and **3b** decreases and disappears, at the same time **4b** increases and reaches a maximum of 95 % of the total phosphine species present. This occurs after the reaction had been proceeding for 60 minutes. At this stage only 68 %

of the total product formed, had been produced, hence this suggests in this reaction that **4b** is the active catalytic species.

After 90 minutes, there was still some reactants present, but **4b** had started to decompose, so it was likely that the reaction had finished.

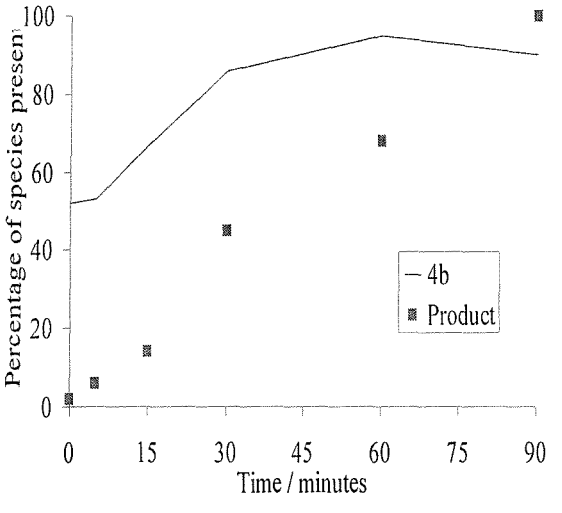

Figure 4.26 The amount of product and species 4b present during the reaction between bromobenzene and methallyl alcohol (130 °C).

Figure 4.26 shows that the product (1-phenyl-2-methyl-propanal) forms linearly with time, as the reaction is held at 130 °C. Species **4b** is present in high concentration (over 50 % of the palladium species) at the start of the reaction and this quickly reaches a maximum ~35 minutes into the reaction.

4.4.2.2 QEXAFS analysis

(10 x 6) minute QEXAFS scans were taken (RTP) of the solution after heating the reaction for 45 minutes at 130 °C and transferring to the XAFS cell (figure 4.27).

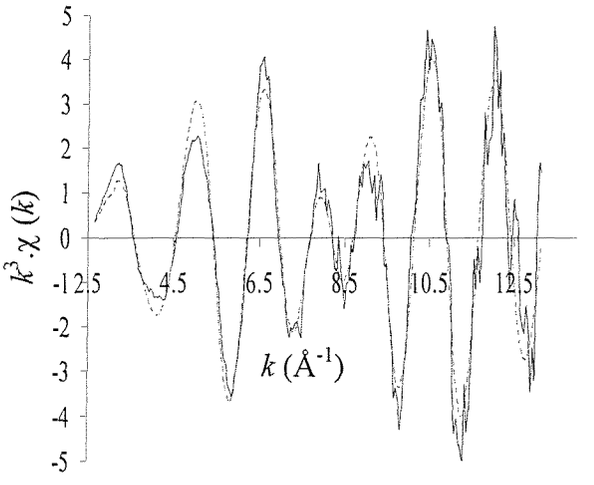

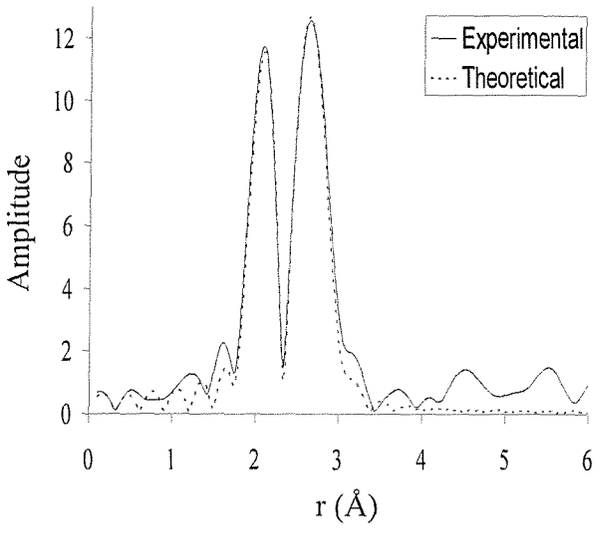

Atom	C.N.	r / Å	$2\sigma^2$ / Å^2
C	1.1(2)	2.07(1)	0.001(4)
P	1*	2.24(1)	0.007(3)
Br	2.0(1)	2.55(0)	0.013(1)

E_f = -7.8(11) eV

R = 28.3 %

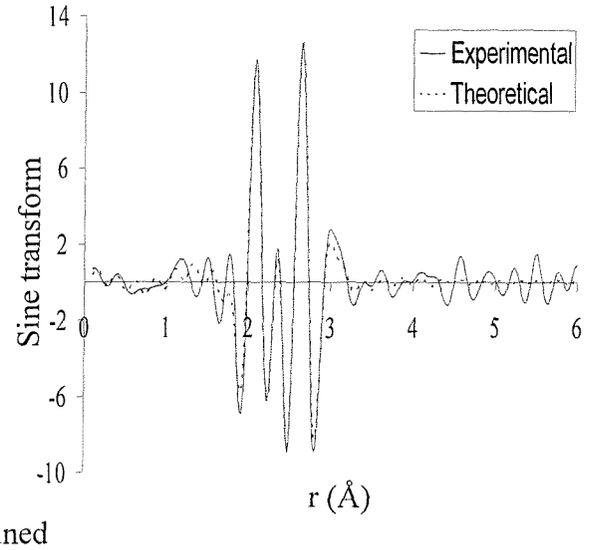

*Phosphorus coordination number was not refined

Figure 4.27 The palladium K-edge k^3-weighted QEXAFS data (10 x 6 minutes averaged), Fourier transform and sine transform for the reaction between bromobenzene and methallyl alcohol with species 3b as catalyst (RTP) after heating for 45 minutes at 130 °C.

The $k^3\chi(k)$, Fourier transform and sine spectra are very similar to the spectra obtained for **4b**. The appropriate model refines very closely to the experimental data, with very low errors on the refined parameters and a very low R value. As before there were problems resolving the carbon and phosphorus shells in relation to coordination number (when refined the coordination number for phosphorus was pushed above 1 (impossible) and carbon below 1, the errors on the refined values were also extremely high), therefore the phosphorus coordination number was fixed at 1. The validity of this method can be argued, since the refined Debye-Waller value for the phosphorus shell yielded a sensible result and

the k^3 data is very similar to the spectrum obtained for **4b** and the spectrum at the end of the same reaction with **1** as catalyst. In figure 4.27 the k^3 weighted peak at 9 *k* is slightly less intense than for the spectra of **4b**. This is probably due to interference from other palladium species, since figure 4.26 predicts that at the 45 minute mark, there is approximately 92% of **4b** present.

Therefore the NMR and XAFS data agree that the final species present in the reaction is **4b**. The NMR data shows that **4b** is formed very quickly (52 % of the phosphorus species present at the start of the reaction) and increases in concentration over time. Initial formation of product is very quick since there is a small amount produced in the first sample.

^{31}P NMR data shows that there is formation of **2b** during the reaction, which decrease in concentration with time during the reaction, but it is not possible to model this in the previous spectrum.

4.4.3 Analysis of the reaction between methallyl alcohol and chlorobenzene with species 3b as catalyst

To finish the investigation of using preformed palladacycles to catalyse the Heck reaction, **3b** was used to catalyse the reaction between chlorobenzene and methallyl alcohol.

4.4.3.1 NMR results

Carbon NMR data shows that there are no new peaks, indicating that there was no product formation. Quantitative results calculated from integration of the reactant peaks is not viable here due to the higher reaction temperature, this is shown in the results, since integration of the alcohol peak is larger at the end of the reaction. This is because the final NMR sample is collected from the reaction mixture at room temperature, hence the alcohol vapour has condensed back into the solution. The difference is not as marked for the chlorobenzene integration, but this could be due to the higher boiling point of the liquid rather then reaction with the palladium catalyst.

The ^{31}P NMR results from the experiment are shown in table 4.10.

Time / min.	^{31}P NMR shift/ppm					
	42.4 **3b**	41.4	38.9 **2b**	37.5 **2c**	36.6 **O=P(*o*-tolyl)$_3$**	-29.4 **P(*o*-tolyl)$_3$**
0	35	25	38		2	
10	34	25	35	3	3	
60	25	22	42	6	3	2

Table 4.10 ^{31}P and ^{13}C NMR results for the Heck reaction between chlorobenzene and methallyl alcohol, with 3b as catalyst (130 °C).

At the start the main species present is the initial catalyst **3b**, species **2b** and a new species at 41.4ppm. Following previous arguments the new species could be a cyclopalladated complex with 1 chlorine and 1 bromine atom coordinated (**3b** appears at 42.4 ppm and **3c** at 39.9 ppm). The only other species present is a minute amount of oxidised tri-*o*-tolylphosphine.

After 10 minutes the only important change in the palladium species present is the formation of a very small amount of **2c,** formed due to a reduction in the amount of brominated species present. After a further 50 minutes, there is some formation of tri-*o*-tolylphosphine, the amount of **3b** and the peak at 41.4 ppm has decreased whilst **2b** and **2c** increased.

These results show that there is no catalysis present in the reaction. There is only a small amount of **2c** formed and no **3c** or **4c**. The other peak of interest is at 41.1 ppm, which could be the palladacycle with one bromine and one chlorine coordinated. Therefore if **4c** would be the catalytic active species, then there is no catalysis.

4.4.3.2 XAFS analysis

(5 x 6 minute) QEXAFS scans were taken at RTP after heating the reaction solution for 10 minutes at 130 °C. Initial observation of the background subtracted data, is similar to the spectrum for species **3b**. The experimental spectrum is noisy and the data quality is reflected by the lower *k* range fitted. Trying to fit the EXAFS model of **3b** to the spectrum, produces an R factor of 44 % and a poorly fitting Fourier transform for both peaks. Therefore the NMR results obtained (table 4.10) were used to elucidate the model.

The results show that after 10 minutes, the phosphorus species hypothesised are 34 % **3b**, 25 % (41.4 ppm), 35 % **2b**, 3 % **2c** and 3 % tri-*o*-tolylphosphine oxide. Therefore assuming that the palladium metal formed due to the phosphine oxide production is not injected into the XAFS cell, the actual palladium species concentrations are 35 % **3b**, 26 % (41.4 ppm), 36 % **2b**, 3 % **2c**. Assuming that the species at 41.4 ppm has 1 bromine and 1 chlorine atom coordinated to the palladacycle centre, the average environment around the palladium centre in the solution is 1.4 carbons, 1.0 phosphorus, 0.3 chlorines and 1.3 bromine atoms coordinated. A model similar to this was constructed, refined in Excurv98 and the results are shown in the table in figure 4.28. The refined fit, is close to the experimental data (EXAFS, Fourier transform and sine), with an R factor of 31.4 %. Most importantly it is not possible to fit a chlorine shell (with a coordination number of 0.3) to the data. When attempted, the refined interatomic distance increased from 2.45 Å to 2.75 Å, so it was excluded from the model. The large errors on the coordination numbers and Debye-Waller terms for carbon and phosphorus could be due to problems resolving the different shells

(observed before), but the problems could be exacerbated due to the chlorine atoms presence, since they are similar in size to phosphorus. Therefore even though the shell cannot be modelled, the chlorine presence still affects the XAFS.

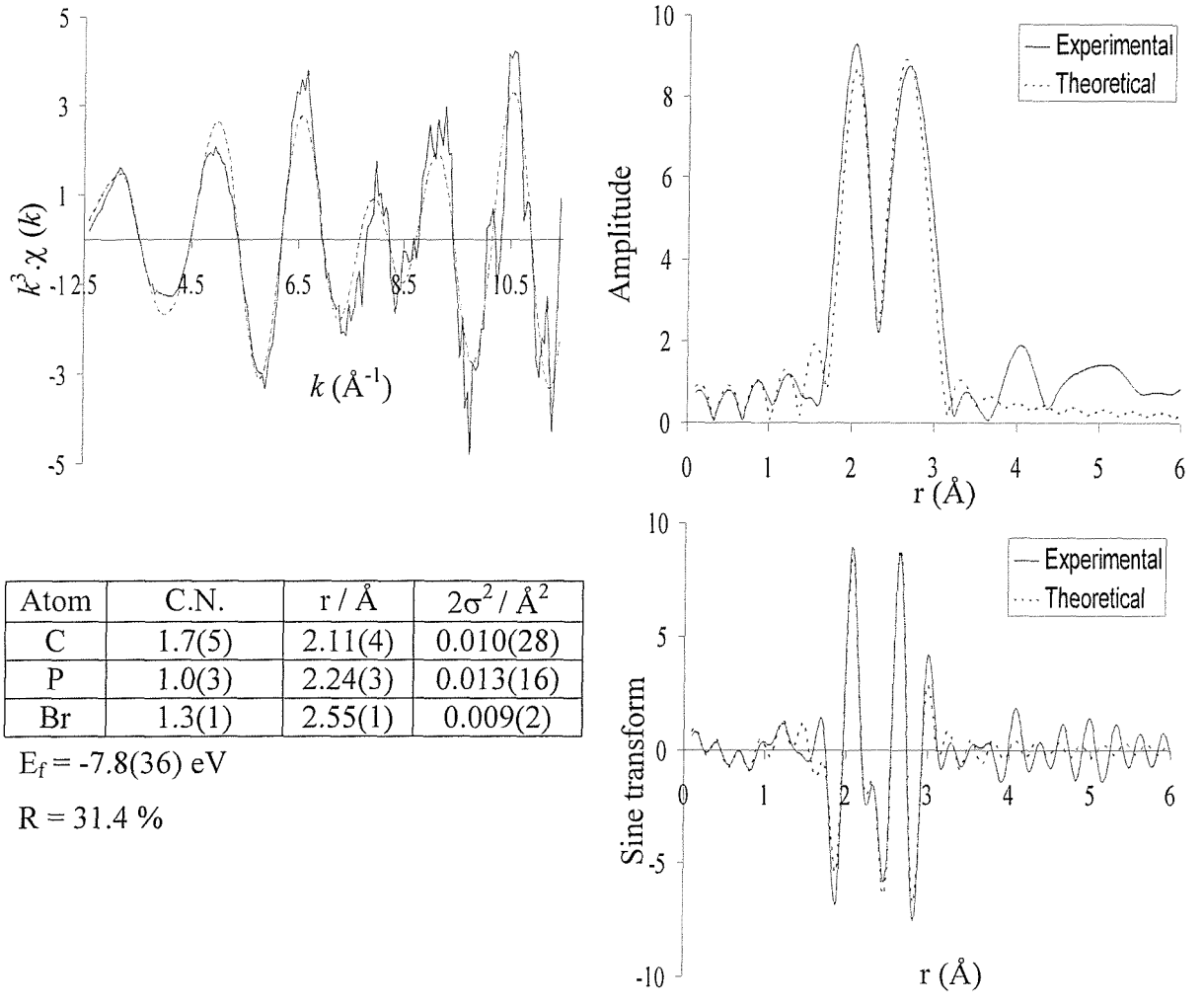

Atom	C.N.	r / Å	$2\sigma^2$ / Å^2
C	1.7(5)	2.11(4)	0.010(28)
P	1.0(3)	2.24(3)	0.013(16)
Br	1.3(1)	2.55(1)	0.009(2)

E_f = -7.8(36) eV

R = 31.4 %

Figure 4.28 The palladium K-edge k^3-weighted QEXAFS data (5 x 6 minutes averaged), Fourier transform and sine transform of the chlorobenzene reaction catalysed by 3b (RTP), after heating for 10 minutes at 130 °C.

Therefore again the XAFS and NMR information agree very well. In this scenario the XAFS is not quantitative, but shows there is some chlorine coordination. Since **2c** is only present as 3 %, this adds fuel to the argument that the phosphorus peak at 41.4 ppm, has 1 chlorine atom coordinated to the palladium.

4.4.4 Summary from the Heck reactions using species 3b as catalyst

Species **3b** catalyses the PhI and PhBr Heck reactions. The palladium species formed are very similar to the species formed in the same reactions, with **1** as catalyst. In the PhBr reaction the main species present at the start of the reaction is **4b**, there is still a substantial amount of precatalyst present **3b** and a significant concentration of **2b** present. The concentrations of **2b** and **3b** decrease over the course of the reaction, whilst **4b** increases.

In the PhI reaction there is a wide range of species present during the reaction. At the start of the reaction bromine species (**2b** and **3b** (the prectalayst)) are present. So are also the iodine species formed when **1** was the precatalyst (**2a**, **3a** and **4a**). There is also a peak which could be assigned to a complex including bromine and iodine (44.3 ppm). During the reaction the bromine complexes decrease in concentration and the iodine increase (**4a** is the main species present at the end of the reaction).

Species **3b** does not catalyse the PhCl reaction. Species **2b** and **3b** (brominated species) are present in solution in large concentrations. Chlorinated species are present in solution (**2c**) is present as 6 % of the total phosphorus species. It was hypothesised that a mixed halogenated species was formed (41.4 ppm) in large concentrations (22 % of the phosphorus species).

During all the reactions the metallated ring was intact. The catalytic species are likely to be of similar structure to **2a**, **2b**, **4a** and **4b**. The monomer allows easier coordination of the olefin to the palladium, due to less steric congestion in the dimer. Hermann's suggestion of a very reactive, two coordinate palladium (0) intermediate is a possible structure for the active catalyst. But, catalysis in the PhBr experiment started earlier than for the PhI experiment, which is probably due to the precatalyst being closer to the catalytic structure in the PhBr reaction. This means the active catalyst has halogen coordinated to the palladium metal.

4.5 Conclusions

Two preformed palladacycles (**1** and **3b**) were used to catalyse the Heck reaction. They both catalysed the PhI and PhBr reactions, but did not catalyse the PhCl reaction. The reaction condition were slightly different due to the poor solubility of **3b**, but the reactions showed very similar trends with regards to palladium phosphine complexes formed and the order of formation. The species formed all had the Pd-C ring intact and the majority of phosphine complexes formed also contained iodine.

For reactions catalysed by **1** the first species to form is **2a** or **2b** (dependent on halobenzene), followed by **3a** or **3b** and the final species formed is **4a** or **4b**, which is the main species present at the end of the reaction. Reactions catalysed by **3b** show very similar trends, with a slight variation at the start of the reaction due to initial coordination of bromine. This is shown in the results since **3b** is formed before **2b** (PhBr reaction) and there are a wide variety of species (brominated, iodated and possibly a mixture of both) present at the start of the PhI reaction. As the reactions proceed, the same trends appear in the results pertaining to the relative concentrations of the species present.

The catalytic species are likely to be of similar structure to **2a**, **2b**, **4a** and **4b**. The monomer allows easier coordination of the olefin to the palladium, due to less steric congestion in the dimer. Hermann's suggestion of a very reactive, two coordinate palladium (0) intermediate is a possible structure for the active catalyst. But, catalysis in the PhBr experiment started earlier than for the PhI experiment, which is probably due to the precatalyst being closer to the catalytic structure in the PhBr reaction. This means the active catalyst has halogen coordinated to the palladium metal.

Experiments conducted whilst excluding one of the reactants (alcohol or halobenzene) shows that when the halobenzene is excluded from the reaction, the precatalyst does not form any new complexes and then decomposes, shown by production of free phosphine. When the alcohol is excluded, the same palladium species are formed (as for the PhI Heck reaction) but in lower concentration. This shows that one of the early steps in the reaction cycle is coordinating the iodobenzene to the metal. This suggests that the Pd^{II}/Pd^{IV} mechanism suggested by Shaw is unlikely to be a dominating factor in these experiments. It

again points to the formation of a Pd^0 species with a similar formation to Hermann's two coordinate reactive palladacycle.

As stated chlorobenzene experiments were not catalysed, which was due to the small concentration of chlorine palladium complexes formed. A mixed halogen palladium species was formed when **3b** was the catalyst, but coordination of the bromine hindered any catalysis.

These results show how XAFS and NMR techniques can be combined to yield information on different catalytic systems. ^{31}P NMR is very specific (quantitatively and qualitatively), but XAFS is used to confirm the assignments.

4.6 Experimental

4.6.1 Preparation and characterisation of *trans*-di(μ-bromo)-bis[*o*-(di-*o*-tolylphosphino) benzyl] dipalladium (II) (species 3b)

Under nitrogen, tetrabutylammonium bromide (1.61g, 5.00mmol) was added to $[Pd_2(OAc)_2\{o\text{-}CH_2C_6H_5P(o\text{-}tol)_2\}_2]$ (0.24g, 0.26mmol) in dry DCM (20ml), to give a yellow solution. This was stirred at room temperature for one hour. The solvent was removed in vacuo and the organic residue was washed in dry methanol (30ml) to dissolve any unreacted tetrabutylammonium bromide.

The mixture was filtered and washed in dry methanol (2x20ml), followed by dry petroleum ether (2x20ml). After drying in vacuo, the reaction afforded 0.133g of yellow crystals, to give a 53% yield with respect to palladium.

4.7 References

1 W.A. Herrmann, C. Brossmer, K. Ofele, M. Beller, H. Fischer, *Angew. Chem. Int. Ed. Engl.*, **1995**, *34*, 1844

2 W.A. Herrman, C. Brossmer, C. Reisinger, T. Riermeier, K. Ofele, M. Beller, *Chem. Eur. J.*, **1997**, *3*, 1357

3 F. Paul, J. Patt, J.F. Hartwig, *J. Am. Chem. Soc.*, **1994**, *116*, 5969

4 W.A. Herrman, V.P.W. Bohm, C. Reisinger, *J. Organomet. Chem.*, **1999**, *576*, 23

5 A.M. Aarif, F. Estevan, A. García-Bernabé, P. Lahuerta, M. Sanaú, M.A. Ubeda, *Inorg, Chem.*, **1997**, *36,* 6472

6 F. Paul, J. Patt and J. F. Hartwig, *Organometallics*, **1995**, *14*, 3030

7 A.J. Rheingold, W.C. Fultz, *Organometallics,* **1984**, *3*, 1414

8 Personal communication. A.J. Dent, Daresbury Laboratory

9 E.C. Alyea, G. Ferguson, J. Malito, B.L. Ruhl, *Organometallics*, **1989**, *8*, 1189

10 D.A. Albisson, R.B. Bedford, S.E. Lawrence, P.N. Scully, *Chem. Commun.*, **1998**, 2095

11 P. Kocovsky, S. Vyskocil, I. Cisarova, J. Sejbal, V. Langer, *J. Am. Chem. Soc.*, **1999**, *121*, 7714

12 K. Nakano, K. Sada, Y. Kurozumi, M. Miyato, *Chem. Eur. J.*, **2001**, *7*, 209

13 J. Evans, L. O'Neill, V.L. Kambhampati, G. Rayner, S. Turin, A. Genge, A.J. Dent, T. Neisus, *J. Chem. Soc., Dalton Trans.*, **2002**, 2207

14 B.L. Shaw, S.D. Perera, E.A. Staley, *Chem. Commun.*, **1998**, 1361

Chapter 5

The Heck reaction catalysed by palladium acetate and triaryl and trialkylphosphines

5.1 Introduction

The previous chapter investigated the Heck reaction (chlorobenzene, bromobenzene and iodobenzene) catalysed by preformed palladacycles. This chapter focuses on the same reactions, but they are catalysed by palladium acetate and a variety of phosphine ligands, of which the majority are mentioned in chapter 3. The ligands were chosen to cover a wide area of catalytic activity; from a phosphine ligand that promotes catalysis in the most demanding (chlorobenzene) reaction, to a phosphine ligand that prevents catalysis for all three halobenzene reactions. The ligands also vary in size, cone angle and include aryl and alkyl phosphines. Also, some of the ligands have the steric ability to form palladacycles.

The chapter begins with investigating the catalytic properties of palladium acetate without the aid of phosphine ligands to stabilise and promote catalysis. Work had been conducted on the iodobenzene reaction, so this was extended to the other halobenzene reactions.

This was then extended to the palladium acetate and triphenylphosphine system, again the iodobenzene experiment has been investigated, but this initial research has been extended and also the other two halobenzenes have been added to the previous work.

The next body of work was on the palladium acetate and tri-*o*-tolylphosphine system. For these reactions they were not added to the reaction as a preformed palladacycle, but as separate entities. This was performed to see if the same catalytic species formed, or if the reaction followed a different catalytic path.

Then reactions aided or hindered by tri-*t*-butylphosphine and tricyclohexylphosphine (respectively) were investigated, to try to establish the variety in catalytic activity since they have similar cone angles and are both bulky phosphine ligands.

The work was then completed by investigating the effect of tri(1-naphthyl)phosphine and tris(*o*-methoxyphenyl)phosphine on the reaction, since these phosphine ligands both have the possibility of forming five membered palladated rings.

5.2 Investigation of the Heck reaction with palladium acetate as catalyst

In the previous chapter, the Heck reaction was catalysed by preformed palladacycles. So it was decided to investigate the same set of reactions, but using palladium acetate ($Pd(OAc)_2$) as the catalyst (same concentration as before) without the addition of any phosphine ligands. Due to the absence of the phosphine ligand the stability of the catalyst was poorer, so the experiments were conducted at 75 °C, to stop early precipitation of palladium metal. The only other experimental change was the use of triethylamine (instead of tributylamine). The PhI experiment has been studied before,[1] so it was decided to further the original investigation and also to include the reactions with PhBr and PhCl.

5.2.1 NMR analysis of the Heck reactions

Obviously, the very useful tool of ^{31}P NMR is not possible with these systems, but ^{13}C NMR was still very useful in determining when catalysis commenced and finished. For the PhBr and PhCl there was no noticeable change in the ^{13}C NMR spectra, showing that catalysis did not occur, but does not rule out the possibility of the catalyst reacting with the alcohol or the halobenzene. The PhI experiment was catalysed by the palladium acetate, consistent with previous results.[1]

5.2.2 X-Ray crystallography analysis of the iodobenzene reaction

Work carried out in conjunction with this thesis and on exactly the same PhI system, isolated $[Pd_2I_6][NBu_3H]_2$ or $[Pd_2I_6][NEt_3H]_2$ (dependent on amine used) at the start of the reaction.[2] The structure consists of an association of two tributylammonium units with a di-anionic Pd_2I_6 unit. The palladium atoms are bridged by two iodine atoms. The structure had been reported before.[3] The bond lengths and angles for the $[Pd_2I_6]$ are within expected values when compared to related complexes.[4] The Pd-I bond distance for terminal iodides (2.611(2)Å and 2.5931(8)Å) and bridging iodides (2.6092(8)Å) are similar indicating no lengthening of this bond through bridging. As expected the I-Pd-I* angle (85.11(4)°) is smaller than the I-Pd-I angle (92.10(4)°), a result of the constraint imposed by the bridging group.

5.2.3 XAFS analysis of the iodobenzene reaction

Only the analysis of the XAFS data (for the PhI reaction) was undertaken for this thesis. EDE analysis was undertaken on the precatalytic species to see if the $[Pd_2I_6]^{2-}$ crystals obtained from the same solution, were present in solution, or if it is just a thermodynamic sink, which the species form when the crystals were obtained. The EDE data of the precatalytic species is shown in figure 5.1.

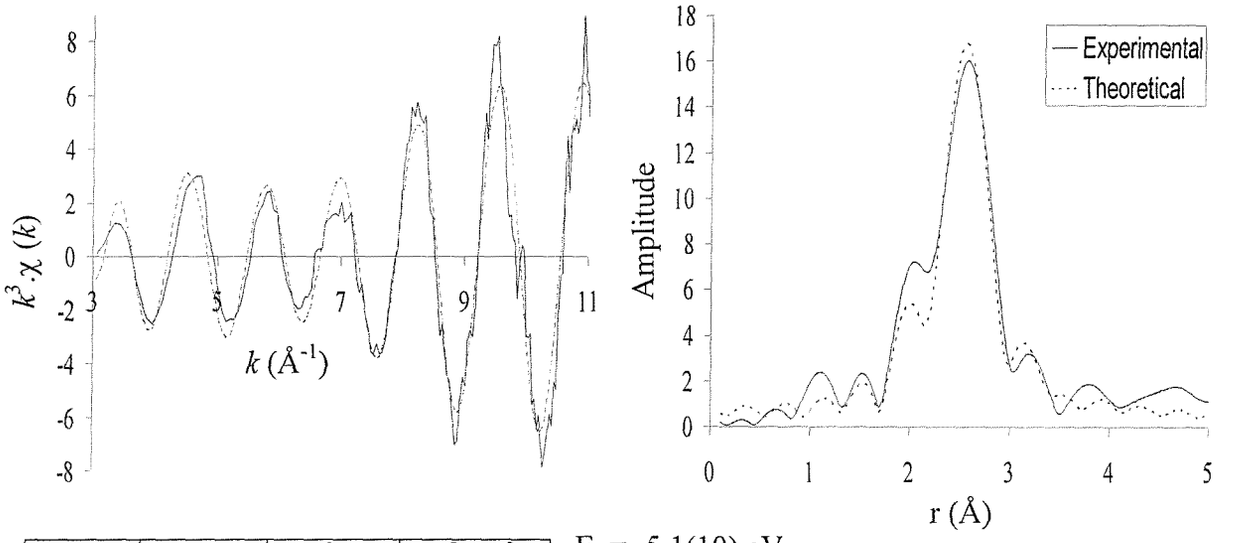

Atom	C.N.	r / Å	$2\sigma^2$ / Å^2
I	3.2(16)	2.62(1)	0.017(0)

E_f = -5.1(10) eV

R = 39.3 %

Figure 5.1 The palladium K-edge k^3-weighted EDE (100 scans, I^t = 6.5 ms) for the precatalytic species (RTP).

The results show a first co-ordination sphere of 3.2 iodines at 2.62 Å. In both experiments a shoulder on this shell is observed at 2 Å. Attempts to fit this shell to carbon, oxygen and even phosphorus resulted in a deterioration of the fit; the Debye-Waller factor for the carbon shell was in the region of 0.058 Å^2. So although this shell may be indicating the presence of a lighter element, there is no definitive information about its nature. It can be concluded that in this red solution oxidative addition of the iodobenzene has probably occurred and the palladium species at this point may be an average of bridged and solvated structures (scheme 5.1).

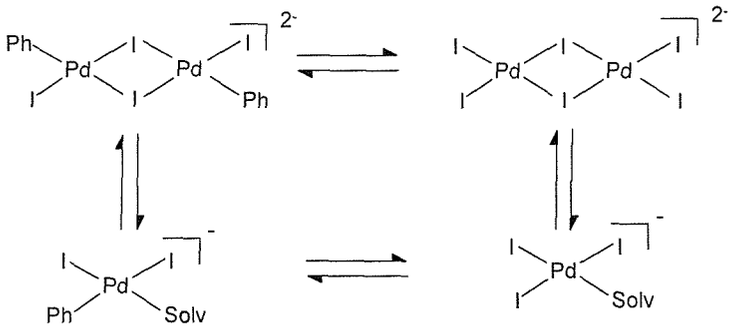

Scheme 5.1 Possible equilibria for the precatalytic solution.

When the red precatalytic solution is heated to 75°C there is a colour change to brown-yellow and catalysis proceeds over an hour. *In situ* ^{13}C NMR of this did not allow observation of the co-ordinated carbon. EDE and QEXAFS experiments utilised for evidence of the palladium species present. QEXAFS spectra were obtained over 50 minutes (10 x 5 minutes) and the average obtained. EDE spectra were obtained by 100 scans and 11 ms integration time. Figure 5.2 shows QEXAFS data and Fourier transform for the solution and gives structural parameters for spectra obtained by EDE and QEXAFS.

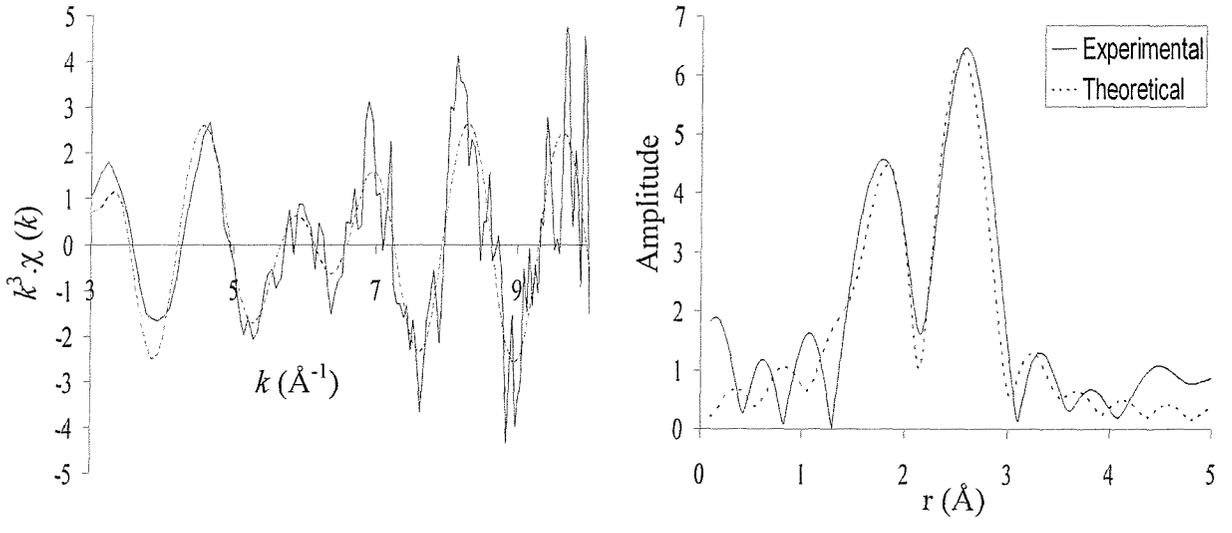

Atom	C.N.	r / Å	$2\sigma^2$ / Å^2
C	1.5(3)	2.06(3)	0.028(3)
I	2.3(3)	2.63(1)	0.028(1)

E_f = -5.1(12) eV

R = 36.2 %

Figure 5.2 The palladium K-edge k^3-weighted QEXAFS data (10 x 5 minutes) and Fourier Transform, of catalytic solution at 75 °C.

The fit is good and shows a first co-ordination sphere of approximately two carbons and second co-ordination sphere of ~ 2 iodines. Possible structures to explain the EXAFS data are given in scheme 5.2. This shows an equilibrium between a dimeric oxidative addition product and the olefin co-ordination complex.

There is no direct evidence to suggest that the oxidative addition product is dimeric. Inclusion of a palladium shell in the EDE or QEXAFS, which would indicate the presence of a Pd..Pd shell, neither improves nor worsens the fit. However, palladium complexes do have a tendency to bridge. It is expected that the low frequency bending vibrations of the $Pd_2(\mu\text{-}I)_2$ unit will provide a high dynamic Debye-Waller factor rendering the Pd...Pd shell difficult to detect at elevated temperatures. The opening of this bridge leaves a free co-ordination site for co-ordination by the olefin before insertion into the Pd-C σ bond, scheme 5.2.

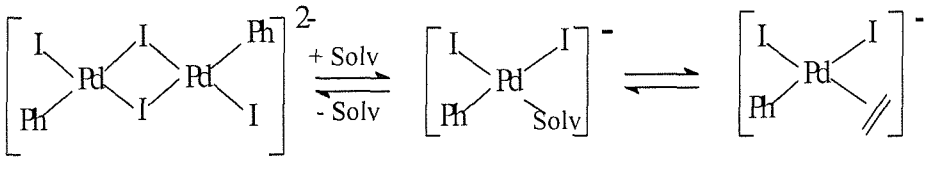

Scheme 5.2 Possible equilibria for catalytic solution.

5.2.4 QEXAFS analysis of the PhCl and PhBr reactions

As stated $Pd(OAc)_2$ did not catalyse the PhBr or the PhCl reaction, but it was decided to undertake XAFS analysis on both reactions to see if the palladium remained unreacted in both experiments.

On heating the PhBr reaction solution to 40 °C it was brown-black in colour and very difficult to determine if the solution was homogeneous. When syringed it appeared to be homogeneous so QEXAFS spectra were measured and are shown in figure 5.3.

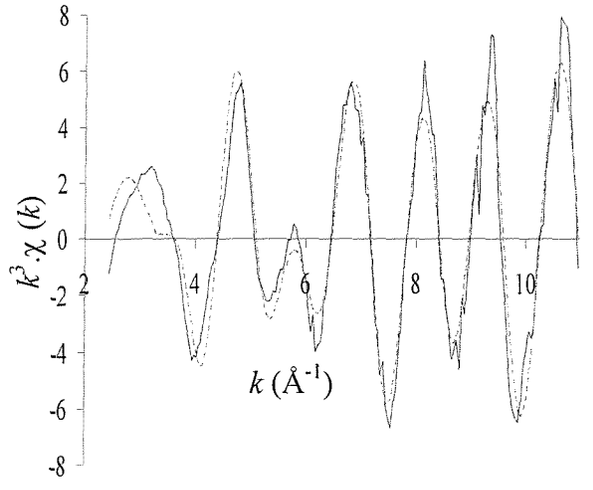

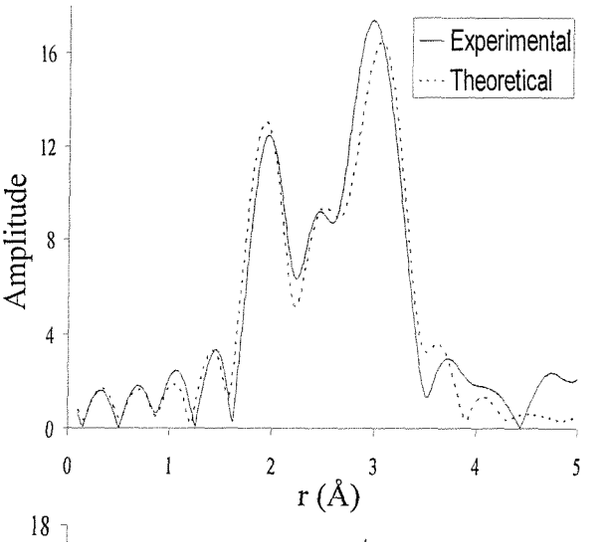

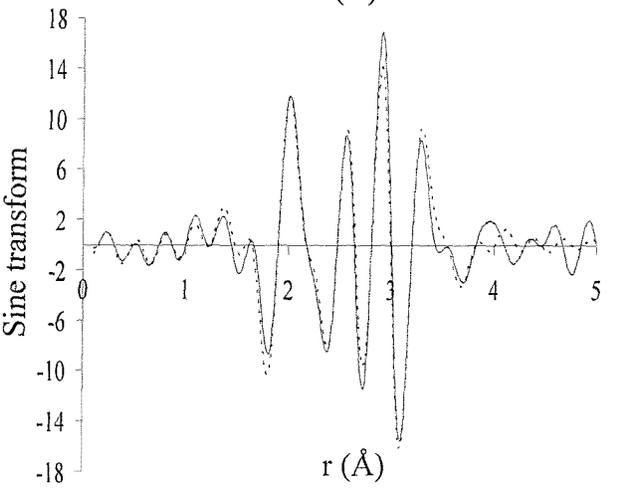

Atom	C.N.	r / Å	$2\sigma^2$ / Å^2
O	2.9(2)	2.02(2)	0.011(2)
Pd	3.0(3)	2.76(1)	0.013(1)

E_f = -4.4(8) eV

R = 30.1%

Figure 5.3 The palladium K-edge k^3-weighted QEXAFS data (5 x 6 minutes averaged), sine and Fourier transform for the PhBr reaction (RTP), after heating to 40 °C.

Two shells (one oxygen and one palladium) fitted very well to the data. The first shell fitted agrees with the Pd-O interatomic distance for $Pd(OAc)_2$ and the second shell has the same Pd-Pd distance as for the first coordination sphere in the bulk metal (chapter 2). Therefore it can be assumed that the black in the solution was due to a fine suspension of palladium metal and there is also unreacted $Pd(OAc)_2$ in solution. A model was created assuming that the mixture was 75 % $Pd(OAc)_2$ in solution and 25 % palladium colloids (i.e. 3 oxygens and 3 palladium atoms), which refined very well to the experimental data.

After heating the reaction in the laboratory to 90 °C the solution was brown green in colour. This solution was analysed using QEXAFS and the results are shown in figure 5.4.

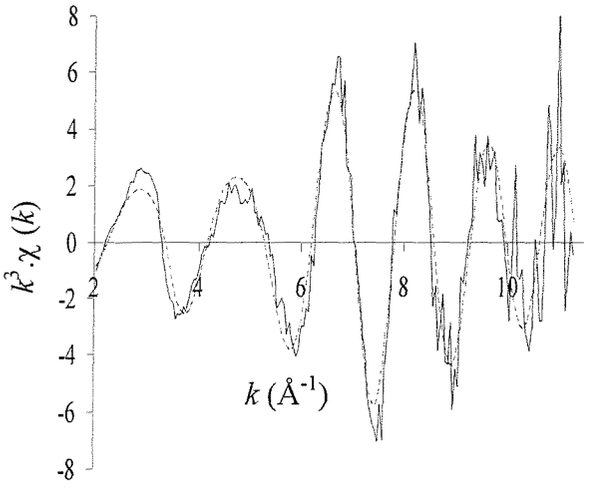

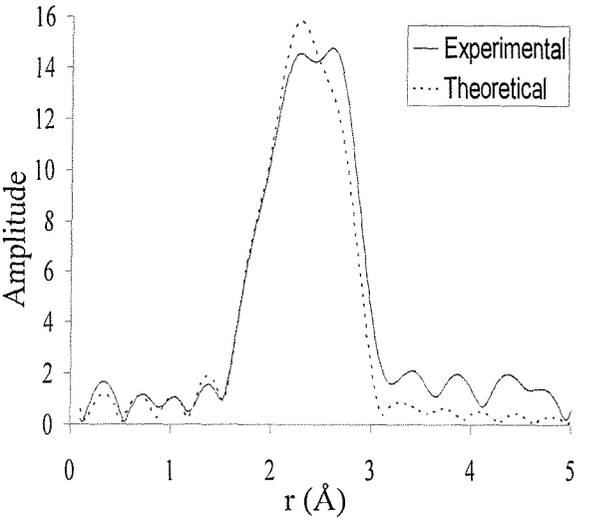

Atom	C.N.	r / Å	$2\sigma^2$ / Å^2
O	1.9(2)	2.06(2)	0.005(3)
Br	2.1(2)	2.46(1)	0.010(1)

E_f = -10.9 (19) eV

R = 34.2 %

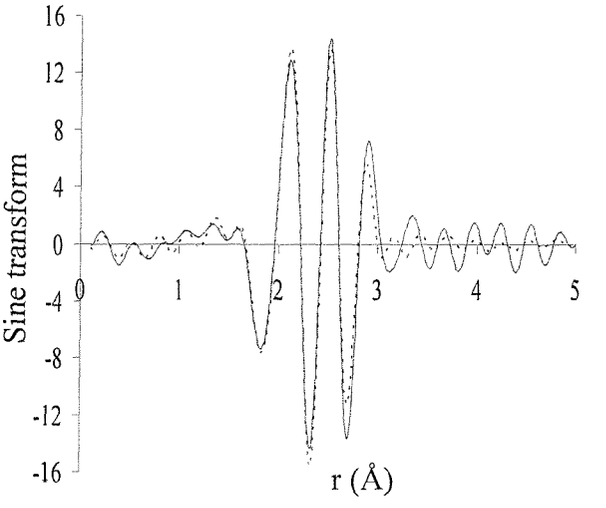

Figure 5.4 The palladium K-edge k^3-weighted QEXAFS data (10 x 6 minutes averaged), sine and Fourier transform for the PhBr reaction (40 °C), after heating to 90 °C.

These results show a bromine shell at 2.46 Å, this is very similar to the reported Pd-Br distance in the dimer $[Pd_2Br_6]^{2-}$ at 2.44 Å.[5] The crystal structure for *trans* $[Br(Ph)Pd(\mu\text{-}Br)]_2^{2-}$ has not been reported, so the Pd-Br bond length is not known. A shell of light atoms (oxygen or carbon) is present and fits well to a shell of oxygen atoms, with a slightly higher than expected bond length for $Pd(OAc)_2$. Again due to a mixture of species being present a mixed model for a half and half concentration of $Pd(OAc)_2$ and $[Pd_2Br_6]^{2-}$ was constructed (i.e. 2 oxygens and 2 bromines) and the experimental data refined very well to this model.

A model of the dimer $[Br(Ph)Pd(\mu\text{-}Br)]_2^{2-}$ was constructed (one carbon atom and three bromine atoms). The XAFS fit deteriorated slightly especially at low k values. The bond

lengths were of appropriate lengths (Pd-Br 2.46 Å and Pd-C 2.09 Å) but the Debye-Waller term for carbon tended towards negative values, suggesting that the carbon coordination number was too low. When refining the coordination numbers the carbon value refined to 2.3.

The start of the PhCl reaction (taken from solution at 40 °C) was the same colour as the PhBr initial solution and gave identical results to the PhBr analysis so have not been included. Analysis was not undertaken of the end solution, so it is not known if there is halogen coordination to the metal as for the PhBr and PhI reactions.

5.2.5 Conclusions on palladium acetate as catalyst

Palladium acetate only catalysed the PhI reaction. $[Pd_2I_6]^{2-}$ was isolated from the start of the PhI reaction, which agreed with EXAFS analysis. As catalysis occurred the iodine coordination around the palladium decreased and enabled the coordination of lighter elements (carbon). This allowed catalysis to occur as shown in scheme 5.2.

5.3 Investigation of the Heck reaction catalysed by palladium acetate and triphenylphosphine

The investigation was extended by investigating the effect of triphenylphosphine (PPh_3) on the catalytic property of $Pd(OAc)_2$. Again this was continuation of an ongoing project and the results are reported in a publication by Evans *et al.*[6] The experimental differences compared with the normal procedure in this thesis was that the ratio of ligand to metal was 2:1, the base chosen was triethylamine (NEt_3) and the solvent was acetonitrile (CH_3CN).

5.3.1 Previous work on the iodobenzene reaction[2]

It was shown that on initial addition of the reagents $Pd(OAc)_2(PPh_3)_2$ precipitated out. Stirring for thirty minutes at 40 °C resulted in a homogeneous solution. Then after heating to 75 °C, crystals of $[(PPh_3)PhPd(\mu\text{-}I)]_2$ precipitated from solution. A crystal structure was taken of these and showed that the structure is a trans centrosymmetric dimer with the iodines bridging between the two palladiums. The Pd_2I_2 metallacycle is a rhombus with considerable difference in the Pd-I-Pd and I-Pd-I angles. Selected bond lengths are Pd-I (trans to the phenyl group) 2.72 Å, Pd-I (trans to phosphorus) 2.66 Å, Pd-C (phenyl group) 2.00 Å and Pd-P 2.27 Å. After heating the reaction for one hour at 115 °C, the mixture can be worked up and crystals of $[(PPh_3)Pd(I)(\mu\text{-}I)]_2$ can be obtained. Again the structure is in a trans conformation with selected bond lengths; Pd-I (trans to the terminal iodine group) 2.61 Å, Pd-I (trans to phosphorus) 2.60 Å, Pd-I (terminal iodine) 2.60 Å and Pd-P 2.21 Å. This shows that by replacing a phenyl group with a terminal iodine atom the Pd-P and Pd-I (average) bond lengths decrease considerably.

In situ ^{31}P NMR (at 100 °C) studies were carried out on the system and showed there was no free ligand in the system at any time and also showed the presence of $[(PPh_3)Pd(I)(\mu\text{-}I)]_2$ (42.5 ppm) at the end of the reaction. To test the hypothesis that *ex situ* ^{31}P NMR measurements taken throughout this thesis are taken of the 'quenched' solution and contain the same species (i.e. the species present in the reaction vessel at the reaction temperature are still present in the NMR tube), the previous experiment was repeated in the reaction vessel (at 100 °C) and samples were taken for *ex situ* measurements at the same reaction time as the *in situ* experiments. The results were similar, with the same ^{31}P NMR peaks

present in both reactions but with variations in the integration values. The variation can be easily explained due to the different nature of stirring the reaction solution and due to the different heating rates of the solutions. Obviously in different reaction solutions some species could change to a more thermodynamically stable species on 'quenching'. But, these results show this is not necessarily the situation and that the *ex situ* experiments yield very similar experiments to *in situ* results.

5.3.2 Phosphorus NMR analysis of the iodobenzene reaction

The experiment was then repeated but with the same Heck experimental parameters as conducted in general for this thesis (i.e. 3:1 ratio of ligand to palladium in NMP). The ^{31}P NMR results are shown for the PhI, PhBr and PhCl reactions in table 5.1.

These results show that there are many phosphorus species present during the reaction. The PhI reaction has the most peaks, followed by the PhBr, and PhCl has the fewest phosphorus species. The peaks show a variety of patterns of behaviour, some are present throughout, others reduce or increase in concentration and appear or disappear with time.

Direct comparison of the three experiments shows that three peaks are present in all the experiments and show similar trends. These therefore do not contain halogen atoms. ^{31}P NMR analysis of $O=PPh_3$ in NMP gave a shift in this region and considering that this species is 72 % abundant in the PhCl reaction, it would have to be a palladium species with three phosphorus atoms coordinated, which is unlikely. Peaks due to $Pd(PPh_3)_3$ and $Pd(PPh_3)_2$ have been reported at 22.6 ppm[7] and 20.4 ppm[8] respectively. Therefore it is possible in the reaction solution they appear just downfield at 23.5 and 21.7 ppm.

For reactions that catalyse the reaction there are peaks in the region 28.9-42.2 ppm. The different experiments show different shifts implying that they could be coordinated to halogen. The peak at 42.2 ppm is known to be $[(PPh_3)Pd(I)(\mu\text{-}I)]_2$ (from the work on the 2:1 system), which suggests that the peak at 40.8 ppm is $[(PPh_3)Pd(I)(\mu\text{-}Br)]_2$. These peaks appear as the reactions progress, which agrees that the level of halogen coordination increases during catalysis.

Table 5.1 ^{31}P NMR table showing the proportion of phosphine species present in the Heck reactions catalysed by palladium acetate and triphenylphosphine.

Expt.	Temp / °C (time/min)	Phosphorus NMR shift / ppm														
		42.2	40.8	32.3	32	31.1	28.9	27.5	26.5* $O=PPh_3$	24.9	24	23.5* $Pd(PPh_3)_3$	21.7* $Pd(PPh_3)_2$	14.8	14.2	14	-4	-4.7
PhI	60								20		25		30		11			14
	90			1					32		52	11	2					2
	115	8		11		7	13		35		6	16	4			19		
	115 (30)	11				8			45			16				32		
	115 (120)	7							39			20						
PhBr	60								31	36		4	29					
	90								46	28		5	8					
	115		5		8				41	24		22					13	
	115 (30)		11		7				32	27		23						
	115 (120)		11		6				33	33		17						
PhCl	60								57			10	14	11				
	90							5	69				5	18				
	115							7	70				3	20				
	115 (30)							9	72				5	13				

The peak at 24.0 ppm corresponds to $(PPh_3)_2Pd(I)(Ph)$, which has been synthesised.[2] The species could also be $[(PPh_3)PhPd(\mu\text{-}I)]_2$, which was determined by crystal structure from the solution at 75 °C. But, the phosphorus to palladium ratio in this complex is 1:1, therefore in the reaction mixture the concentration cannot exceed 33 % of the total phosphorus concentration, but the concentration reached 52 %. This could suggest that in the solution the species is present as $(PPh_3)_2Pd(I)(Ph)$ and crystallises out as the dimer $[(PPh_3)PhPd(\mu\text{-}I)]_2$. This information therefore suggests that the peak at 24.9 ppm is the bromine analogue $(PPh_3)_2Pd(Br)(Ph)$. $(PPh_3)_2Pd(I)(Ph)$ and $(PPh_3)_2Pd(Br)(Ph)$ have also been reported with the phosphorus shift of 22.2 and 22.8 ppm (respectively).[9]

The chlorine reaction shows that $O{=}PPh_3$ is the major species present during the reaction. There is also the formation of two unassigned peaks which could be the formation of Pd-Cl complexes.

5.3.3 QEXAFS analysis of the PhI experiment

The starting solution (taken at 75 °C from the reaction vessel) of the PhI experiment was analysed using QEXAFS (figure 5.5). The spectrum shows that there is already iodine coordination to palladium in the solution. A model was constructed assuming that $(PPh_3)_2Pd(I)(Ph)$ was present as 50 % of the phosphorus species (75 % of the palladium species), since this is the approximate concentration from the ^{31}P NMR data (table 5.1). Ten percent (w.r.t. phosphorus and palladium) is present as $Pd(PPh_3)_3$ and 15 % (w.r.t palladium) is coordinated as $Pd(PPh_3)_2$. This mixture creates the model 0.75 carbon, 2.0 phosphorus and 0.75 iodine. The model refines very well to the data, with the only slight discrepancy due to slightly higher than expected Pd-P interatomic distance.

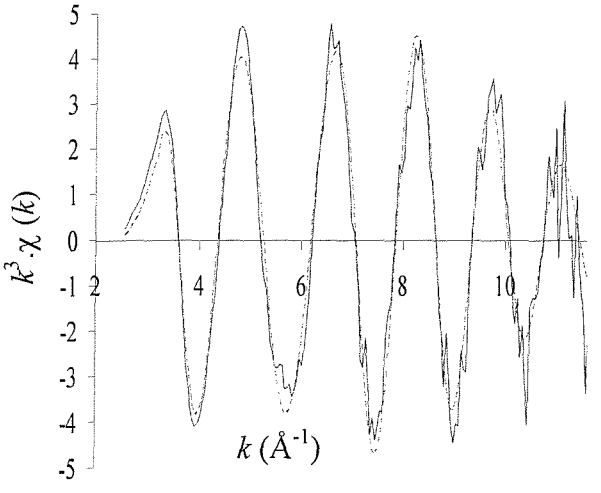

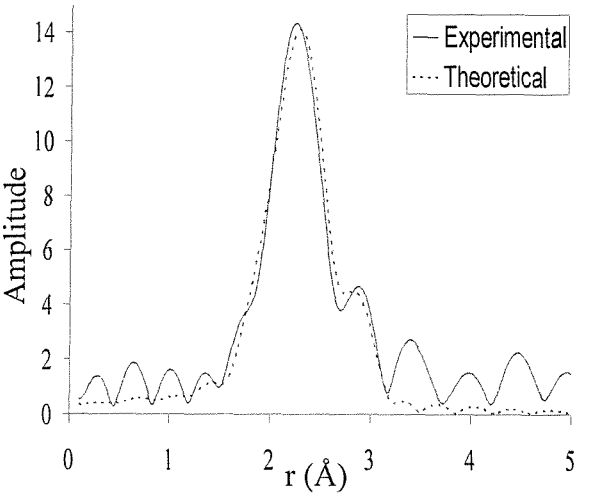

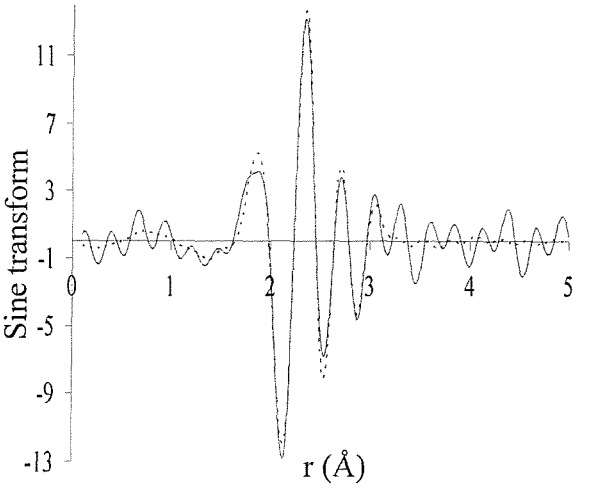

Atom	C.N.	r / Å	$2\sigma^2$ / Å^2
C	0.9(2)	2.01(2)	0.004(4)
P	2.0(1)	2.32(1)	0.006(1)
I	0.7(1)	2.63(1)	0.009(2)

E_f = -7.1 (13) eV

R = 22.4 %

Figure 5.5 The palladium K-edge k^3-weighted QEXAFS data (5 x 6 minutes averaged), sine and Fourier transform for the $Pd(OAc)_2$ / PPh_3 / PhI reaction (40 °C), after heating to 75 °C.

The end of the PhI (after 1.5 hours at 115 °C) reaction was studied with QEXAFS and the results are shown in figure 5.6.

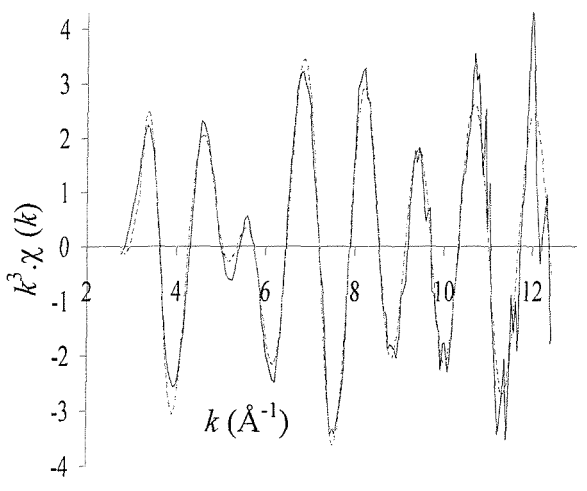

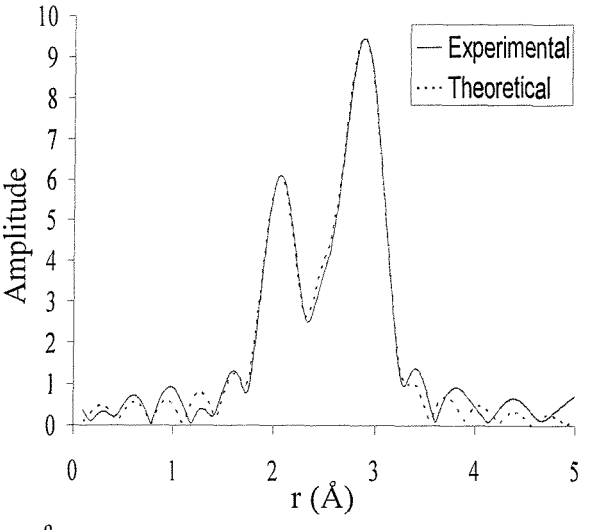

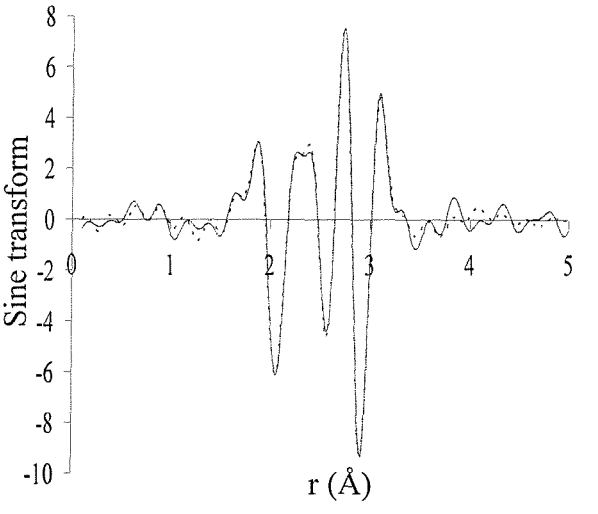

Atom	C.N.	r / Å	$2\sigma^2$ / Å^2
C	0.7(2)	2.06(1)	0.003(5)
P	0.9(1)	2.27(1)	0.010(2)
I	2.4(1)	2.66(0)	0.015(1)

E_f = -8.6 (7) eV

R = 21.2 %

Figure 5.6 The palladium K-edge k^3-weighted QEXAFS data (10 x 6 minutes averaged), sine and Fourier transform for the $Pd(OAc)_2$ / PPh_3 / PhI reaction (40 °C), after heating for 1.5 hours at 115 °C.

The data fitted very well to the model of 0.5 carbons, 1 phosphorus and 2.5 iodines. The carbon shell is intrinsic to the fit, since if excluded the R factor increased to 30 %. X-ray crystallography showed that $[(PPh_3)Pd(I)(\mu\text{-}I)]_2$ was present at the end of the reaction, which would produce an EXAFS model of 1 phosphorus and 3 iodines. The NMR data showed the presence of $Pd(PPh_3)_3$ as a 20 % contribution to the palladium content, which would alter the model to 1.4 phosphorus and 2.4 iodines. If another species was present with carbon coordinated to the palladium, this would make the required model.

5.3.4 QEXAFS analysis of the bromobenzene reaction

The PhBr reaction was undertaken in the normal manner and QEXAFS analysis was undertaken on the reaction solution after heating to 75 °C (figure 5.7).

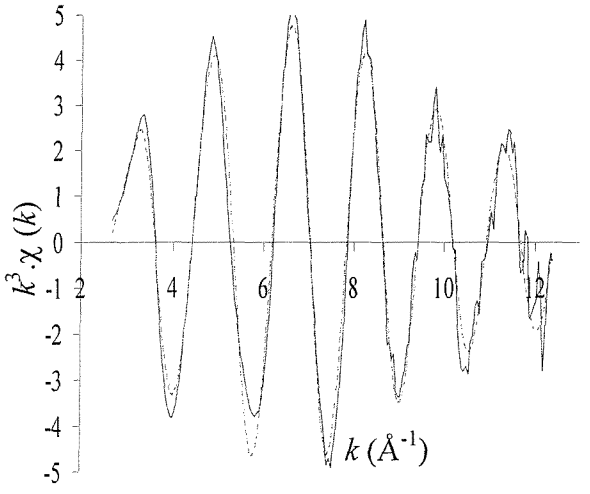

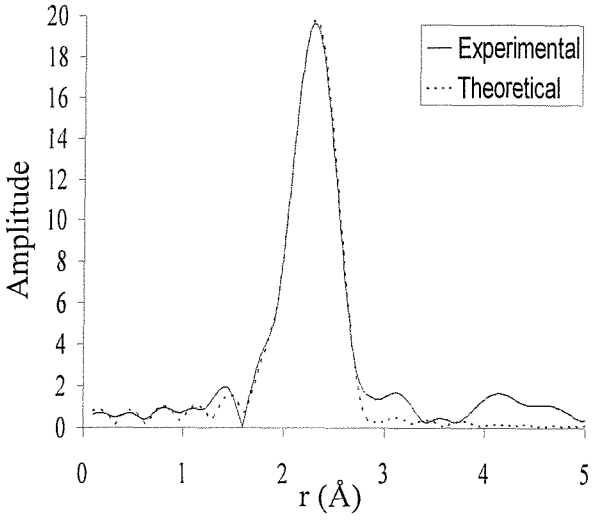

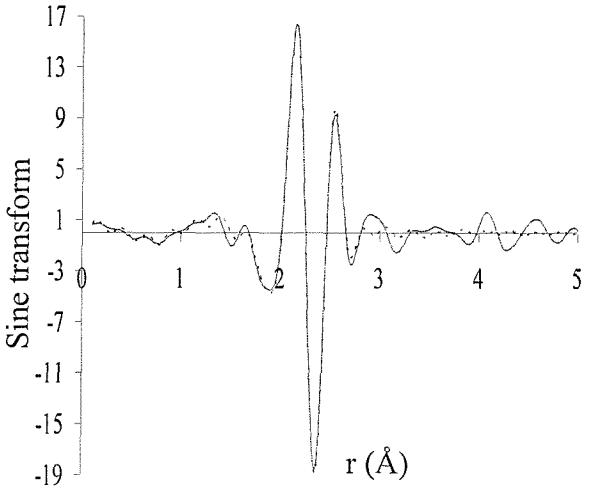

Atom	C.N.	r / Å	$2\sigma^2$ / Å^2
C	1.1(2)	2.06(2)	0.001(3)
P	2.1(1)	2.32(1)	0.005(1)
Br	0.4(1)	2.45(2)	0.012(5)

E_f = -8.2 (12) eV

R = 17.0 %

Figure 5.7 The palladium K-edge k^3-weighted QEXAFS data (5 x 6 minutes averaged), sine and Fourier transform for the $Pd(OAc)_2$ / PPh_3 / PhBr reaction (40 °C), after heating to 75 °C.

The ^{31}P NMR data shows at 75 °C approximately half the palladium species will be coordinated as $(PPh_3)_2Pd(Br)(Ph)$ (24.0 ppm), a very small proportion will be coordinated as $Pd(PPh_3)_3$, approximately 20 % as $Pd(PPh_3)_2$ and the remainder as $Pd(OAc)_2$. This is very similar to the start of the PhI and the data refines well to the model of 1 carbon, 2 phosphorus and 0.5 bromine atoms. This again confirms the assignments made of the phosphine species and shows that bromine is coordinated at an early stage.

The reaction was heated for 1.5 hours at 115 °C and the QEXAFS results (taken at 40 °C) are shown in figure 5.8.

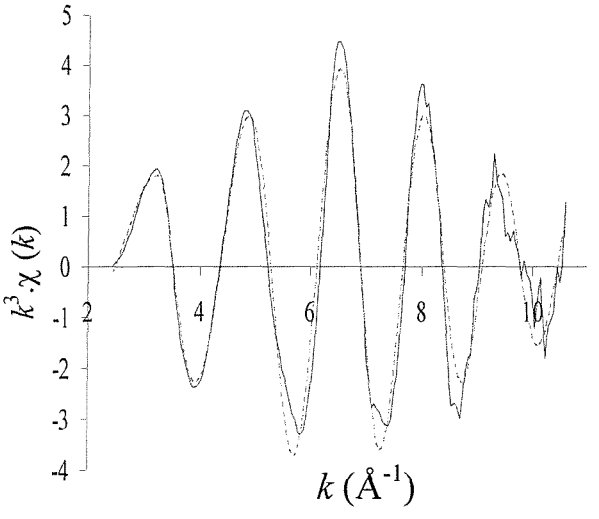

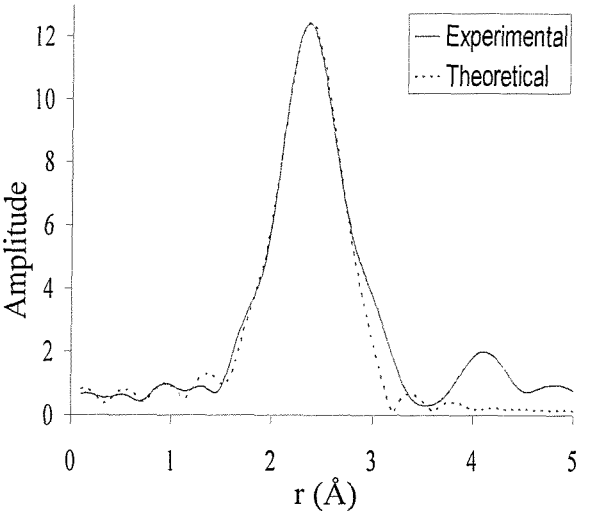

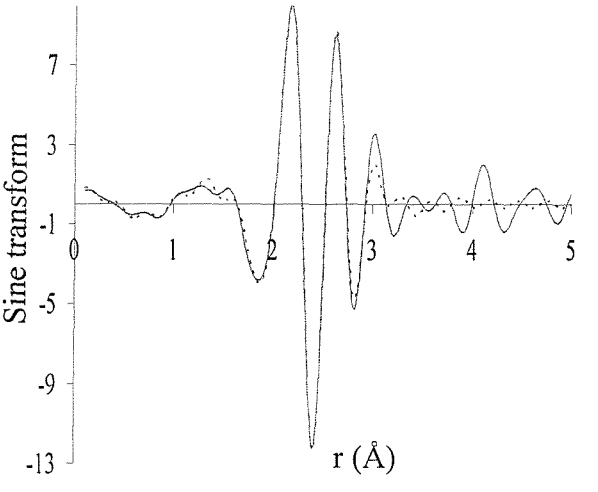

Atom	C.N.	r / Å	$2\sigma^2$ / Å^2
C	1.5(3)	2.01(4)	0.008(8)
P	1.2(2)	2.30(3)	0.008(3)
Br	1.3(2)	2.51(1)	0.013(3)

E_f = -12.6 (20) eV

R = 21.3 %

Figure 5.8 The palladium K-edge k^3-weighted QEXAFS data (10 x 6 minutes averaged), sine and Fourier transform for the $Pd(OAc)_2$ / PPh_3 / PhBr reaction (40 °C), after heating for 1.5 hours at 115 °C.

Phosphorus NMR results indicate that 50 % of the palladium is present as $(PPh_3)_2Pd(Br)(Ph)$, 17 % as $Pd(PPh_3)_3$ and 33 % as $[(PPh_3)Pd(Br)(\mu\text{-}Br)]_2$. This makes a model of 1.5 carbons, 1.2 phosphorus and 1.3 bromines. The experimental data fits very well to this model which again helps confirm the phosphorus NMR assignments.

These EXAFS results show that the average amount of halogen coordinated to the palladium is considerably more for the iodobenzene reaction. This is hard to predict from the NMR data and the low value shown in the NMR experiments (at 42.4 ppm), could be due to degradation of the species during the experiment.

QEXAFS analysis was also undertaken on the PhCl reaction. It was very hard to model due to correlation between the phosphorus and chlorine shells. The Fourier transform shifted slightly to higher R values, indicating smaller atoms being replaced by larger atoms. Since the concentration of $Pd(PPPh_3)_2$ (21.7 ppm) decreases during the reaction (table 5.1), it is likely that chlorine must coordinate to compensate for the reduction in the overall interatomic distance average. Therefore one or both new peaks (14.8 and 27.5 ppm) in the NMR data are due to chlorine species.

5.3.5 Conclusions on palladium acetate and triphenylphosphine as catalyst

Addition of triphenylphosphine to the catalytic system enabled the palladium acetate to catalyse the PhBr reaction, but not the PhCl reaction. It had been shown before that $Pd(OAc)_2(PPh_3)_2$ was present in the reaction solution at 40 °C. On heating to 75 °C $[(PPh_3)(Ph)Pd(\mu\text{-}I)]_2$ could be isolated from the precatalytic solution whilst $[(PPh_3)(I)Pd(\mu\text{-}I)]_2$ had been isolated from the catalytic solution after 1 hour of heating. Phosphorus NMR analysis showed that the initial palladium iodide complex was more likely to be $Pd(Ph)(I)(PPh_3)_2$ in solution, but dimerised on crystallisation. It was also shown that in the PhBr reaction, the brominated analogues also formed. QEXAFS analysis showed that at the end of the reactions there was less bromine coordinated to the palladium than for the iodine reaction. This agrees with the ^{31}P NMR data which shows that $Pd(Ph)(Br)(PPh_3)_2$ is present at the end of the reaction, which is not the case in the PhI experiment.

Phosphorus NMR also shows the presence of $O{=}PPh_3$, $Pd(PPh_3)_2$ and $Pd(PPh_3)_3$ in all three reactions. In the PhI and PhBr experiments the diphosphine appears first. Then as it falls in concentration the triphosphine increases in concentration. Over the course of the reaction $O{=}PPh_3$ is present as approximately a third of the phosphorus species, but varies in actual amount over the course of the reaction. In the PhCl reaction there is only a small amount of palladium phosphorus complexes formed and a much greater concentration of the phosphine oxide. There is reason to believe that there is also a small amount of chlorine coordinated to the palladium phosphine complexes.

5.4 Investigation of the Heck reaction with palladium acetate and tri-*o*-tolylphosphine as catalyst

In chapter 4 the Heck reaction was catalysed by a preformed catalyst (**1**) synthesised from $Pd(OAc)_2$ and tri-*o*-tolylphosphine ($P(o\text{-tolyl})_3$). It was decided to investigate the same reactions but catalysed by adding the phosphine and palladium metal separately (i.e. not preformed), in a ratio of 3:1. It has been noted that a feature of $Pd(OAc)_2$ / $P(o\text{-tolyl})_3$ and PhI catalysed reactions shows the early formation of an orange crystalline complex, the isolated complex has been shown to be **3a**[10] the iodine bridged analogue of **1**.

5.4.1 NMR analysis of the Heck reactions

Carbon NMR analysis showed that the same reactions were catalysed as for **1** (PhI and PhBr), but in a lower yield.

5.4.1.1 Phosphorus NMR analysis of the iodobenzene reaction

^{31}P NMR analysis was carried out as usual on the iodobenzene experiment and the results are shown in table 5.2.

Temp / °C (time / min)	^{31}P NMR shift / ppm								
	45.2 **3a**	41.3	40.5	33.3	28.3	27.5	22.7	16.8	-29.2 $P(o\text{-tolyl})_3$
60					29			9	62
90		2	3	3		22			70
115		8	6	6	7		2		71
115 (30)	1	10	6	7			3		72
115 (60)	1	7	6	6			2		77
115 (120)	1	9	7	6			1		73

Table 5.2 showing selected ^{31}P NMR integration values for the PhI reaction with $P(o\text{-tolyl})_3$ / $Pd(OAc)_2$ as catalyst.

At 60 °C, 62 % of the phosphorus is as free ligand, the other two peaks (28.3 ppm) and (16.8 ppm) were not present in the formation reaction for **1** (chapter 3) so could include

coordination of the PhI ($Pd(Ph)(I)(P(o\text{-tolyl})_3)_2$) or alcohol. They are not $Pd(P(o\text{-tolyl})_3)_2$ since its ^{31}P NMR shift is 6.7 ppm.[11] On heating to 90 °C, carbon NMR shows that there is already a very small amount of product formed. The proportion of free phosphine has increased to 70 % and remains fairly constant over the remainder of the reaction, which means the maximum possible average number of phosphorus atoms coordinated to palladium is fewer than one. The other initial two peaks have disappeared and new ones have appeared at (27.5, 33.1, 40.5, 41.3, 45.2 ppm). The peak at 27.5 ppm is most abundant (22 %), with the other peaks providing only a small contribution to the overall phosphorus content. On heating to 115 °C the peak at 28.3 ppm has reappeared, a new small peak has appeared at 22.7 ppm and the peaks at 33.1, 40.5 and 41.3 ppm have increased in concentration. For the remainder of the reaction the only new peak appears at 45.2 ppm and coincides with the shift of **3a**. The other peaks do not significantly change in concentration. The peaks at 40.5 and 41.3 ppm could be similar to species **2a** and **4a** since they have similar NMR shifts, but they might not be cyclopalladated (i.e. $Pd(P(o\text{-tolyl})_3)_2I_2$, $Pd(P(o\text{-tolyl})_3)_2(I)(Ph)$, $Pd_2(P(o\text{-tolyl})_3)_2I_4$ and $Pd_2(P(o\text{-tolyl})_3)_2(Ph)_2I_2$). It is worth noting that cyclopalladation generally results in a downfield shift. Another point worth noting is that during the reaction there is no formation of **1**.

5.4.1.2 Phosphorus NMR analysis of the bromobenzene reaction

The ^{31}P NMR spectra taken of the PhBr reaction is shown in table 5.3.

Temp / °C (time / min)	^{31}P NMR shift / ppm									
	41.9 **3b**	40.1	39.6	26.2	24.4	22.6	20.0	16.9	12.7	-29.2 $P(o\text{-tolyl})_3$
60							3	5	4	85
90				10	9	9	8			74
115	3	4	3		4	3				70
115 (120)	3	4	4		2	3				69

Table 5.3 showing selected ^{31}P NMR integration values for the PhBr reaction with $P(o\text{-tolyl})_3$ / $Pd(OAc)_2$ as catalyst.

The main species present at 60 °C is the free ligand (85 %). The peak at 12.7 ppm, was present in the formation of **1** and was thought to be a species containing palladium acetate and phosphine ligand. The peak at 16.9 ppm was also present in the PhI reaction so does not include any halogen. Again there is no formation of $Pd(P(o\text{-tolyl})_3)_2$. On heating to 90 °C

the concentration of free ligand has decreased, the earlier peaks have disappeared, except for 20.0 ppm which has increased slightly. Three new peaks have appeared at 22.6, 24.4 and 26.2 ppm. The peak at 22.6 ppm appears in the PhI reaction, so again does not contain halogen, it also was not present at the start of the heating process and after formation remained present through the rest of the reaction. The other peaks are just upfield of two peaks found in the PhI reaction (27.5 and 28.3 ppm) so it could be argued that these are possible halogen containing species. They also show very similar trends. At this stage there is no product formation, unlike the PhI experiment. After heating to 115 °C catalysis has started and there are three new peaks (39.6, 40.1, 41.9 ppm) again these are comparable with the peaks at 40.5, 41.3 and 45.2 ppm in the PhI reaction and probably contain halogen. The peaks at 40.5 and 41.3 are also probably the active catalytic species since they appear when catalysis occurs, which is the same situation occurring in the PhI experiment. The peak at 41.9 ppm has the same shift as species **3b**, so also adds weight to the argument that there is correlation between the PhI and PhBr experiment. The difference in the chemical shifts for analogous species (between the PhI and PhBr reaction) is generally around 1 ppm, but for the peak at 41.9 ppm (PhBr experiment) the shift difference is 3.1 ppm compared with the corresponding peak in the PhI experiment. The extra shift difference could be because species **3a** and **3b** have two halogen atoms in the structure, which suggests that the two peaks at 41.3 and 40.5 ppm only contain one halogen atom.

Again over the whole reaction the amount of free phosphine is very high (~70 %). Again there is no formation of **1**.

5.4.1.3 Phosphorus NMR analysis of chlorobenzene reaction

The $Pd(OAc)_2$ and P(*o*-tolyl)$_3$ mixture did not catalyse the PhCl reaction, but the ^{31}P NMR experiment was undertaken to determine what species did form and the results are shown in table 5.4.

Again at the start of the heating process the peaks at 12.7 and 16.8 ppm appear and do not contain any halogen ligands. The peak at 36.8 ppm appears at the same shift as O=P(*o*-tolyl)$_3$. At 90 °C the palladium metal had started to precipitate out of solution, but no new phosphorus peaks appeared. At 115 °C most of the palladium had precipitated out, but there were two new peaks in very small concentrations at 14.9 and 37.5 ppm, the latter peak could

possibly have chlorine coordinated since it coincides with the chemical shift of species **2c**. At the end of the reaction most of the phosphorus was free phosphine.

Temp / °C (time / min)	^{31}P NMR shift / ppm					
	37.5	36.8	16.8	14.9	12.7	-29.2 P(o-tolyl)$_3$
60		8	9		20	63
90		2	4		2	92
115	1	1		2		96
115 (120)		1		1		98

Table 5.4 showing selected ^{31}P NMR integration values for the PhCl reaction with P(o-tolyl)$_3$.

5.4.2 Conclusions

The P(*o*-tolyl)$_3$ ligand and Pd(OAc)$_2$ system catalyses the same reactions as the preformed catalyst **1** (PhBr and PhI). This preformed catalyst did not form in any of the reactions, which confirms that it is just a precursor. There was also no formation of the phosphine dimer Pd(P(*o*-tolyl)$_3$)$_2$ in any of the reactions (unlike the PPh_3 reaction), but there was formation of peaks due to the palladation reaction in chapter 3. In all the reactions the oxidised phosphine was present in ~70 % yield, which shows that the maximum average P:Pd ratio was under one (it was one for the preformed catalyst).

For the PhBr and PhI reactions for catalysis to start ^{31}P NMR peaks (containing halogen atoms) appeared around ~ 42 ppm. Analogous peaks appeared for both reactions, suggesting the same species (different halogen atom) were present in both reactions. The results also indicated a mixture of the number of halogen atoms present in the complexes. The most likely assignments for these peaks are Pd(P(*o*-tolyl)$_3$)$_2$X$_2$, Pd(P(*o*-tolyl)$_3$)$_2$(X)(Ph), Pd$_2$(P(*o*-tolyl)$_3$)$_2$X$_4$ and Pd$_2$(P(*o*-tolyl)$_3$)$_2$(Ph)$_2$X$_2$ (X = I or Br). At the end of these two reactions there was a very small amount of **3a** and **3b** formed.

In the PhCl reaction the range of halogen NMR peaks was considerably smaller. There was little chlorine coordinated to palladium, depicted by a very small amount of species **2c** being formed.

5.5 Investigation of the Heck reaction with palladium acetate and tri-*t*-butylphosphine as catalyst

The Heck reaction (with PhI, PhBr and PhCl) was studied with palladium acetate and tri-*t*-butylphosphine (P^tBu_3) as catalyst.

5.5.1 Phosphorus NMR analysis on the Heck reactions

NMR analysis was carried out on the three reactions. Initial analysis was carried out on the free ligand (99 % pure) and helped to catalyse all reactions. Unfortunately, due to a change in the hazard classifications of the ligand, the later studies (XAFS and ^{31}P NMR) were conducted with the phosphine, 99 % pure (10 wt% in hexane). The ligand in this reaction did not catalyse the PhCl reaction.

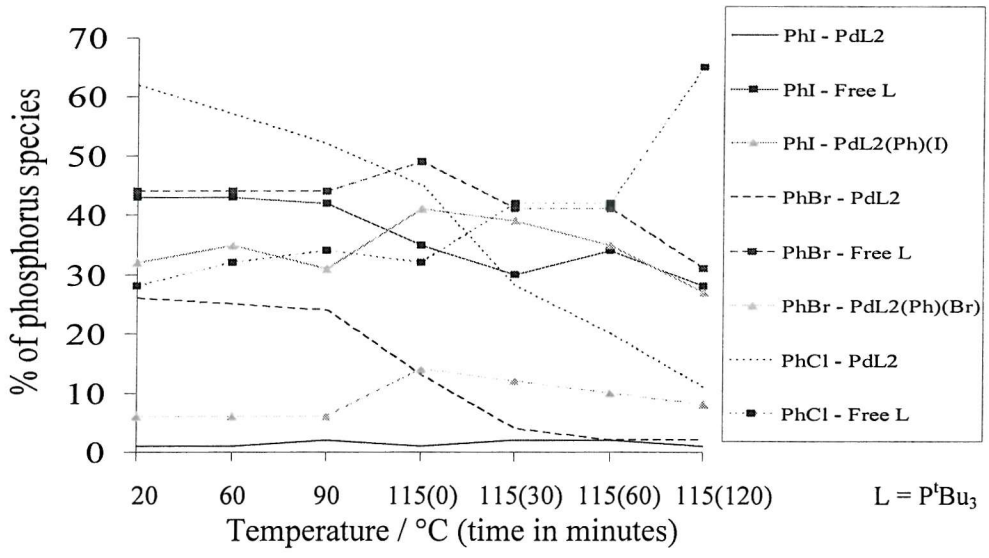

Figure 5.9 The percentage of phosphorus species present in the Heck reactions with $Pd(OAc)_2$ / P^tBu_3 as catalyst.

Figure 5.9 shows the amount of each main phosphine species present in each reaction (PhI (whole line), PhBr (dashed line) and PhCl (dotted line)) as a percentage of the total amount of phosphorus present. The shift for the free ligand (63.4 ppm) was determined in house, the shift for PdL_2 ($Pd(P(t\text{-butyl})_3)_2$) (85.8 ppm) was obtained from literature[12] and the palladium halogen species was deduced (as before) with the Pd-I shift at -6.2 ppm and the Pd-Br shift

(slightly upfield) at -7.1 ppm.

The figure shows that at the start of the PhI reaction 43 % of the ligand is uncoordinated which reduces to a 33 % over the course of the reaction. Therefore towards the end of the reaction the average coordination of phosphine to palladium would be 2, if all the palladium was coordinated to the phosphine. This agrees with the hypothesis that the -6.2 ppm peak is the oxidative addition product of PhI to $Pd(P^tBu_3)_2$ to form $Pd(P^tBu_3)_2(Ph)(I)$. During the whole of the reaction there is only a very small constant amount of the palladium (0) bisphosphine species present. Further investigation on the correctness of this assignment was undertaken by carrying out the reaction but excluding the alcohol. After heating to 115 °C for 15 minutes, the free phosphine was present as 43 % of the total phosphorus species and the peak at -6.2 was present as 44 %, which would give a conversion from $Pd(OAc)_2$ of 66 %, this also shows that this species does not include coordination of the alcohol. Carbon NMR shows that catalysis has started before the reaction reaches 115 °C, which coincides with the maximum concentration of the iodide species, but does not yield any further information.

In the PhBr reaction catalysis proceeds in a very similar way, with initial product formation before 115 °C. But, the phosphorus species are present in very different concentrations compared with the PhI experiment. The amount of free phosphine shows similar trends (but slightly higher in concentration), but the concentration of $Pd(P^tBu_3)_2$ is considerably higher, it accounts for 26 % of the phosphorus containing species, but falls steadily during catalysis and finishes with a 2 % contribution. The amount of $Pd(P^tBu_3)_2(Ph)(Br)$ present is also very small (opposite to the previous reaction), with an initial contribution of 6 % to the phosphine species, this rises to a maximum of 14 % and then finishes with only a contribution of 8 %. This leaves a considerable amount of phosphorus unaccounted and is shown in the NMR spectrum by a multitude of peaks. This shows the difficulty in working with this ligand due to its high sensitivity to air and is probably caused by decomposition in the NMR tube. The assignment of the $Pd(P^tBu_3)_2$ peak was confirmed since crystals were isolated from the PhBr NMR sample (section 5.5.2) of the solution when it reached maximum temperature.

The PhCl reaction was studied with NMR. As stated earlier the catalysis did not occur when the phosphine was dissolved in hexane, which was the situation for this NMR study. Again

the phosphorus trend is very different to the other two reactions. The free phosphine ligand increases in concentration over the reaction from 28 % to 65 %, this shows that there is lability in the phosphine coordination. This was hinted at by the increase of the free ligand concentration during the PhBr reaction, but could be attributed to experimental error, not possible in the PhCl scenario. The other main species of interest is $Pd(P^tBu_3)_2$. At room temperature 62 % of the phosphine is coordinated as this species, which means that 93 % of the palladium is also coordinated as this species. Over the course of heating the solution, the phosphine contribution of this species falls to 11 % (17 % w.r.t. palladium). Over the final stage of heating there was some precipitation of palladium in the reaction vessel, but this does not explain the overall trend of increase in free ligand concentration. Another noteworthy observation, is that there is no formation of peaks ~-8 ppm, to continue the trend shown in the other two experiments. This agrees with the hypothesis of the assignment of these peaks and suggests that in this reaction catalysis did not occur since there was no formation of the expected oxidative addition product $Pd(P^tBu_3)_2(Ph)(Cl)$.

The NMR data does not show many major trends, especially between the two catalytic reactions. It does show that for the catalysed reactions there is a 2:1 ratio of coordinated phosphine:palladium, but not necessarily coordinated in the same species. Analysis of the PhCl and PhBr reactions could show that these phosphines ligands are labile.

The palladium^{1+} species $[Pd(\mu\text{-}X)(PBu^t_3)]_2$ (X = Br, I) was not present in either of the previous reaction mixtures, since their ^{31}P NMR shifts are 87.0 and 102.9 ppm respectively.[13]

5.5.2 X-ray crystallography analysis of crystals obtained from the bromobenzene reaction

Crystals of $Pd(P^tBu_3)_2$ were isolated from the $Pd(OAc)_2$ / P^tBu_3 reaction and the crystal structure (hydrogens omitted) is shown in figure 5.10. The main bond lengths of interest are P1–Pd1 at 2.282(4) Å and P2–Pd1 at 2.284(4) Å, with the nearest P—C interaction at 3.49 Å. The P2–Pd1–P1 bond angle is 179.3(2)° and the average Pd-P-C angle is ~111°. The crystal structure was first reported in 1992[14] and the quoted interatomic distances and angles are very similar, but the space group is $P2_1/a$.

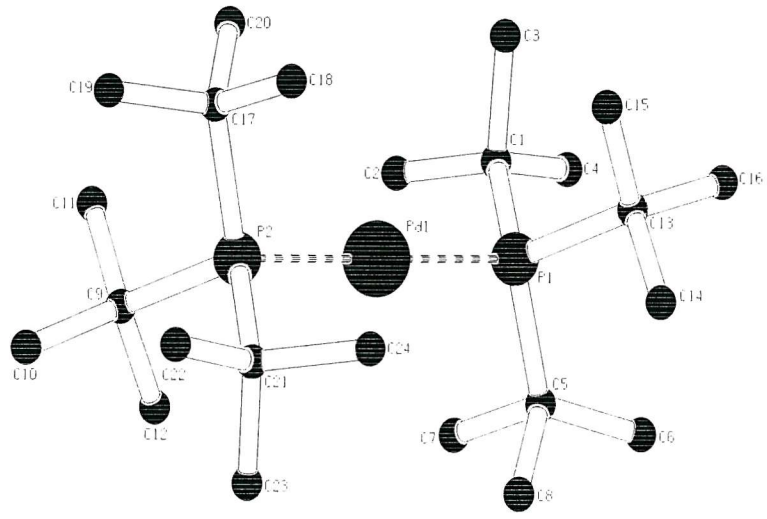

Figure 5.10 Crystal structure refinement for $Pd(P(^tBu_3))_2$ (obtained from the PhBr experiment).

5.5.3 QEXAFS analysis of the PhI reaction

QEXAFS analysis was undertaken at the start of the PhI reaction after dissolving the catalyst mixture into solution at RTP, the results are shown in figure 5.11. The data refines well to a model of 1 carbon, 1 phosphorus and 0.7 iodine atoms. Trying to establish the best model for the fit is very difficult, since there is a real possibility from the NMR data that there could be carbon, phosphorus, oxygen and iodine coordinated to the palladium. Fitting an iodine shell is relatively easy since it is discrete from the other shells. From the compounds analysed in chapter 4, Debye-Waller terms between 0.011 and 0.014 $Å^2$ seem to be very reasonable values to calculate the average iodine coordination number. This information was used in refining the previous data set and the value of 0.7 is probably very accurate. Fitting the carbon, oxygen and phosphorus shells is unfortunately less facile. As stated before it is very difficult to distinguish between the carbon and oxygen shells. But, the phosphorus shell is not discrete from these shells, which makes accurate quantitative and qualitative analysis for these shells extremely difficult. For example the previous fit makes the average palladium atom 2.7 coordinate, which is unsaturated compared with the normal four coordinated species. ^{31}P NMR showed that $Pd(P^tBu_3)_2$ is present, so this and similar species will reduce the average number of atoms around the palladium atoms. But,

from the NMR analysis only 2 % of the palladium species is present as $Pd(P^tBu_3)_2$ and 50 % is present as the palladium phosphine iodide species (presumably $Pd(P^tBu_3)_2PhI$). Therefore it is highly unlikely that the average of 2.7 atoms bonded to palladium is correct. But trying to improve the model is very difficult.

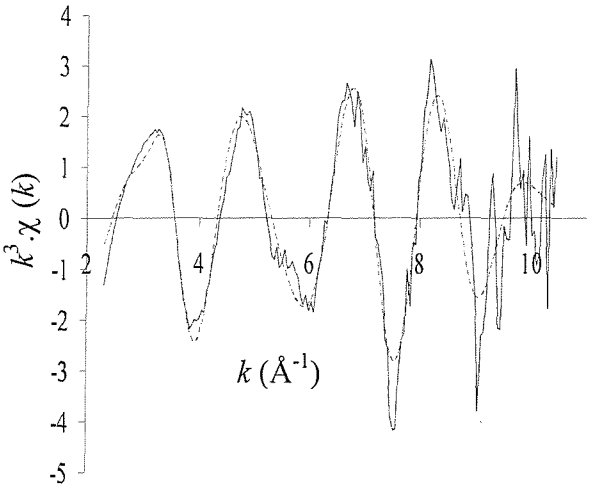

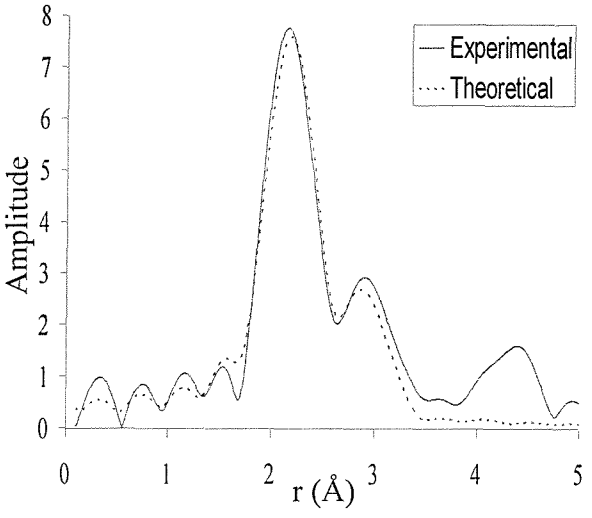

Atom	C.N.	r / Å	$2\sigma^2$ / Å^2
C	1.0(4)	2.08(3)	0.001(7)
P	1.0(3)	2.28(2)	0.011(5)
I	0.7(1)	2.64(2)	0.012(3)

E_f = -8.1 (19) eV

R = 34.5 %

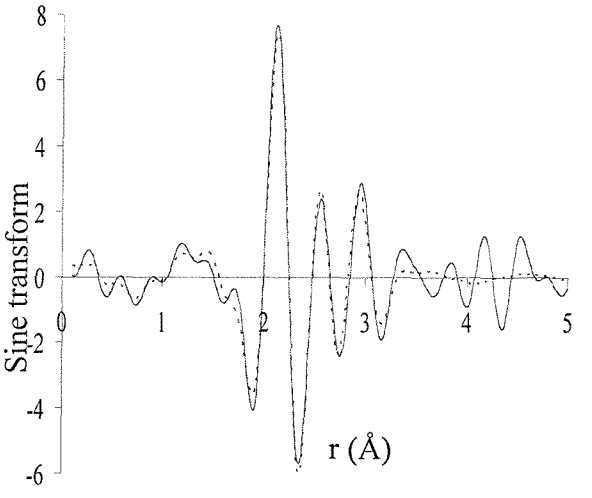

Figure 5.11 The palladium K-edge k^3-weighted QEXAFS data (5 x 6 minutes averaged), sine and Fourier transform for the $Pd(OAc)_2$ / P^tBu_3 / PhI reaction (RTP), solution was homogeneous at room temperature.

The carbon Debye-Waller value is very low, indicating that the coordination number should be increased. But by increasing the coordination number to 1.5, the interatomic distance increases to 2.12 Å, which is too long. The new Debye-Waller term is only 0.005 Å^2, which is still low, but by increasing the coordination number again the Pd-C bond length continues to increase. The phosphine shell is only slightly affected with the bond length reducing to 2.27 Å, which is acceptable.

By increasing the phosphorus rather than the carbon coordination number, the phosphorus Debye-Waller value rises as expected (0.022(7) $Å^2$), but again the Pd-C distance increases (2.10(2) Å), also the Debye-Waller refines to negative values.

By substituting the carbon shell for an oxygen shell the R factor increases slightly to 36.0 % and the Pd-O bond length refines to 2.06 Å(3), with a Debye-Waller value of 0.015(10) $Å^2$. There are no main variations in the other refinable parameters.

Taking into account the problems encountered with the analysis, the model given is deemed to be the most appropriate, even though when considering the carbon shell it must be remembered that it is very difficult to determine whether it is carbon or oxygen and could also be a mixture. For this report it is a major problem, since it makes it very difficult to distinguish between oxygens in the starting species (palladium acetate) and carbons in the species formed during the reaction (due to oxidative addition products of the Ph I etc.). The model shows that a small amount of iodine is already coordinated to the palladium at room temperature. This agrees with the NMR assignment that the peak at -6.1 ppm contains iodine and palladium and could be $Pd(P^tBu_3)_2(Ph)(I)$. This species is present as 33 % of the total phosphorus content, which would contain 50 % of the palladium content. Therefore each palladium on average would see 0.5 iodines. Since not all of the ^{31}P NMR species are accounted for, this iodine contribution could increase slightly, which agrees with the model of 0.7 iodines. Phosphorus was integral to the fit and the coordination number for phosphorus refined to 1, which is not unfeasible. Since, 43 % of the free ligand is present in the NMR so the maximum phosphine coordination to palladium is 1.7. Assuming that the $Pd(P^tBu_3)_2(Ph)(I)$ assignment is correct then the minimum (including the $Pd(P^tBu_3)_2$) phosphine coordination is 1. Therefore a value of 1 or greater is a realistic amount. Finally, calculations show that due to the oxidative addition product of the PhI the coordination number of carbon is at least 0.5. But, due to any contributions from oxygen due to residual $Pd(OAc)_2$ and any other carbon and oxygen contributions from other species, this number would increase. As stated before a refined value of 1 is small, but due to the limitations of the technique no further information can be gained.

The reaction was heated in a vessel for 1.5 hours and the solution was transferred to the XAFS cell and QEXAFS analysis was undertaken (figure 5.12). The k^3 EXAFS spectrum and the Fourier Transform looks very similar to the spectrum obtained of species **3a**, which

suggested a model of 1 carbon, 1 phosphorus and two iodine atoms. The model fitted very well to the noisy data giving a high R factor (34.3 %). The errors are low and the refined interatomic distances and coordination numbers are close to the expected values. The Debye-Waller values for the smaller atoms are low, but again a very reasonable value for the iodine shell.

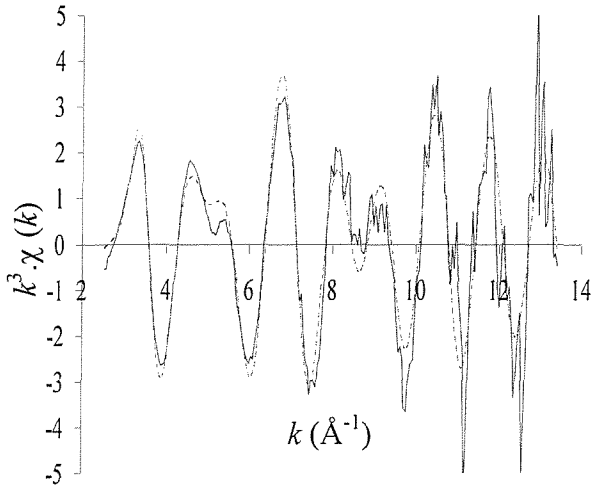

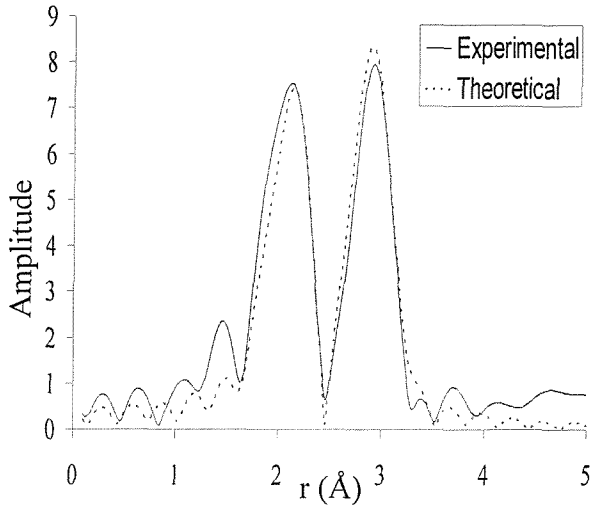

Atom	C.N.	r / Å	$2\sigma^2$ / Å^2
C	1.1(2)	2.04(2)	0.003(3)
P	0.9(1)	2.28(1)	0.006(2)
I	1.9(2)	2.71(1)	0.014(1)

E_f = -8.8 (11) eV

R = 34.3 %

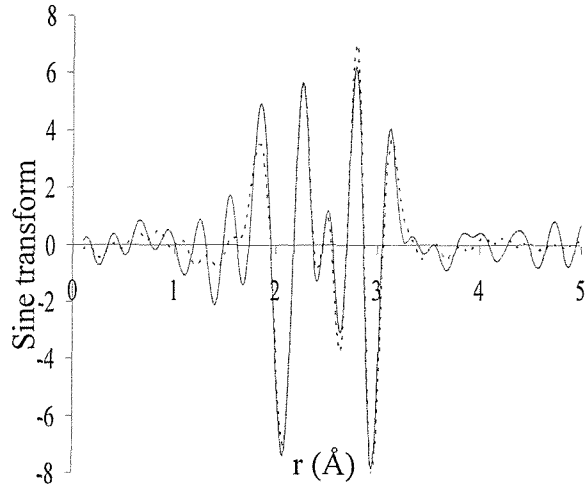

Figure 5.12 The palladium K-edge k^3-weighted QEXAFS data (10 x 6 minutes averaged), sine and Fourier transform for the $Pd(OAc)_2$ / P^tBu_3 / PhI reaction (RTP), after heating for 1.5 hours at 115 °C.

These results only show us the average structure and it is known from the NMR results that there is a mixture of palladium species. So the results shown us that there is on average only one phosphorus per palladium, the NMR results showed a third of the phosphorus was uncoordinated, so therefore a third of the phosphorus is present as oxidised species. The average number of iodines coordinated to palladium is two. Therefore the suggested peak

assignment of $Pd(P^tBu_3)_2(Ph)(I)$ is more likely, because it would contain 30 % of the phosphorus species and count for the Pd-P shell of 1 phosphorus. This would give a Pd-I shell of 0.5 iodines and the only other species to increase the iodine coordination number without affecting the phosphine total is $[Pd(I)(Ph)(\mu\text{-}I)]_2$. Since 50 % of the palladium is contained in the palladium iodide complex (and contributes 0.5 iodines and 0.5 carbons to the model), 50 % of the remaining palladium species would be $[Pd(I)(Ph)(\mu\text{-}I)]_2$. This would contribute another 1.5 iodines and 0.5 carbons. This is highly unlikely, since the results so far in this thesis have shown a mixture of palladium phosphorus halogen species present during the reactions and there were many phosphorus peaks unassigned in the NMR spectrum and some had appreciable contributions which were in the same NMR region as the previously assigned $Pd(P^tBu_3)_2(Ph)(I)$ region. Therefore a more realistic assignment is $[Pd(P^tBu_3)(Ph)(\mu\text{-}I)]_2$ which would account for ~90 % of the palladium. The remainder of the model could be made up from the other phosphorus peaks in the same area of the NMR spectrum which could be similar structures.

5.5.4 QEXAFS on the iodobenzene Heck reaction (excluding methallyl alcohol)

The XAFS experiment was repeated on a similar sample to the last experiment, but the alcohol was excluded from the reaction mixture. The results are shown in figure 5.13.

The final structure looks very similar to the final species for the full Heck reaction with the alcohol. It shows there is considerable coordination of iodine to palladium. By inspection of the Fourier transform the iodine peak is less intense than the carbon / phosphorus peak which suggests that the iodine coordination is fewer than 2. This is confirmed because the Debye-Waller term is slightly higher than expected for the refined value of 1.9. This shows that without the olefin the final species $[Pd(P^tBu_3)(Ph)(\mu\text{-}I)]_2$ is not reached in the same concentration.

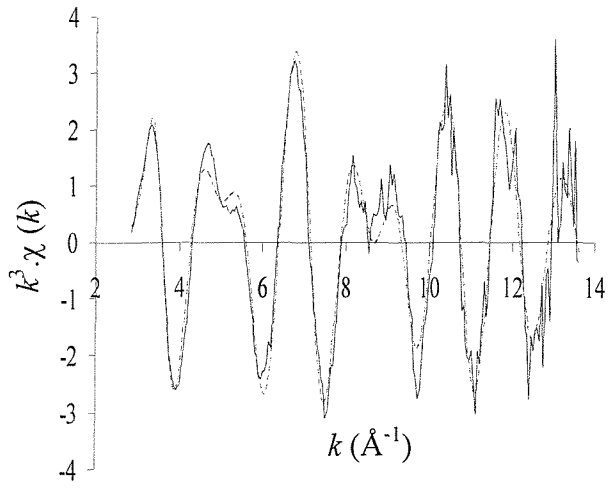

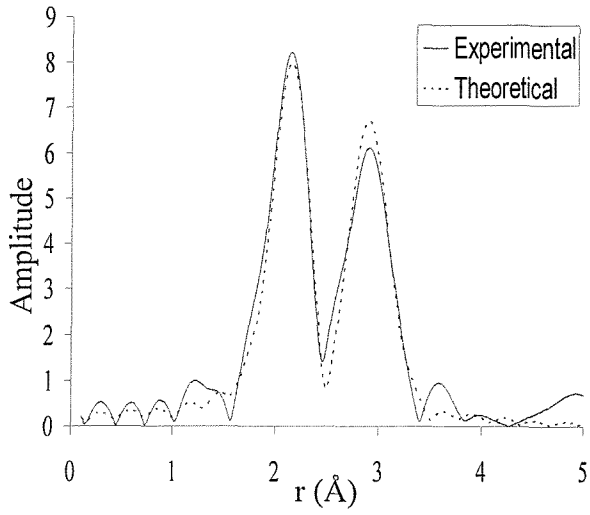

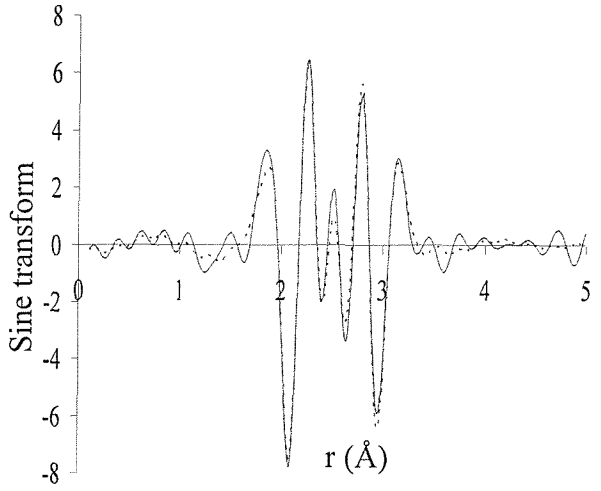

Atom	C.N.	r / Å	$2\sigma^2$ / Å^2
C	1.1(3)	2.08(2)	0.007(4)
P	0.9(1)	2.26(1)	0.008(2)
I	1.9(1)	2.72(1)	0.017(1)

E_f = -7.6 (11) eV

R = 29.4 %

Figure 5.13 The palladium K-edge k^3-weighted QEXAFS data (10 x 6 minutes averaged), sine and Fourier transform for the $Pd(OAc)_2$ / P^tBu_3 / PhI reaction, without alcohol (RTP), after heating for 1.5 hours at 115 °C.

5.5.5 QEXAFS analysis of the bromobenzene reaction

The starting solution for the PhBr reaction catalysed by P^tBu_3 and $Pd(OAc)_2$ was prepared as normal, stirred at RTP and transferred to the XAFS cell for QEXAFS analysis, with the results shown in figure 5.14.

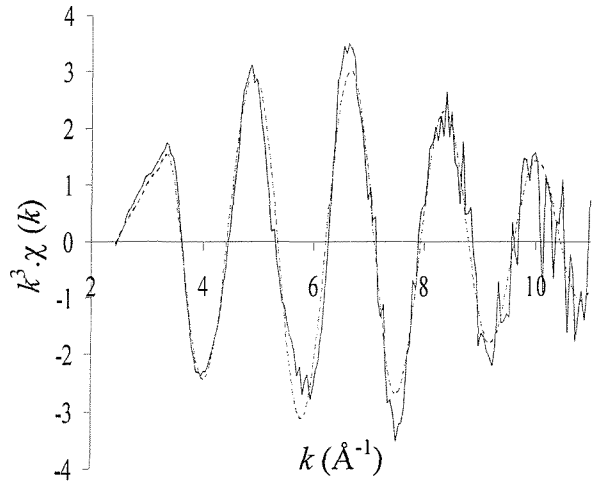

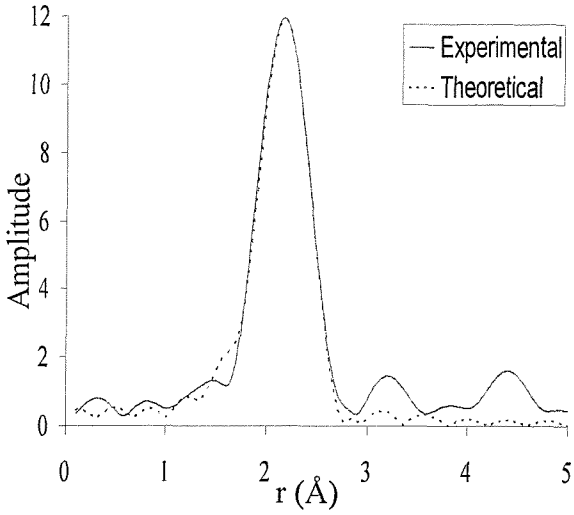

Atom	C.N.	r / Å	$2\sigma^2$ / Å^2
O	1.7(4)	2.09(2)	0.022(4)
P	1.0(1)	2.31(1)	0.005(2)

E_f = -14.8 (16) eV

R = 25.7 %

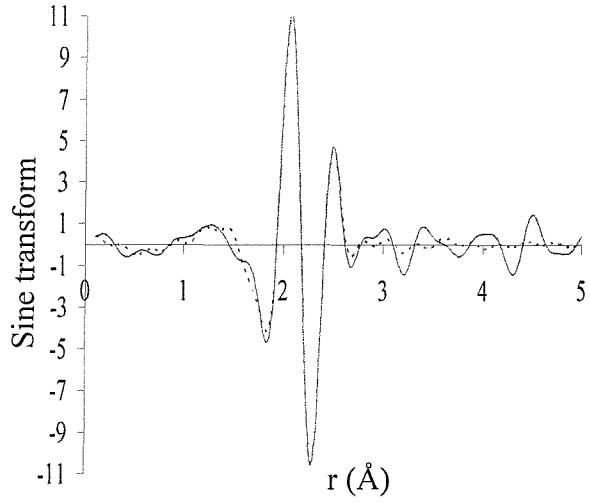

Figure 5.14 The palladium K-edge k^3-weighted QEXAFS data (5 x 6 minutes averaged), sine and Fourier transform for the start of the $Pd(OAc)_2$ / P^tBu_3 / PhBr reaction (RTP), which was homogeneous at room temperature.

Unlike the PhI experiment there was no initial observation of halogen coordinated to palladium. This agrees with the NMR which shows only 6 % of the phosphine coordinated as $[Pd(P^tBu_3)(Ph)(\mu\text{-}Br)]_2$, which would give a Pd-Br shell with a coordination number of 0.3. This is difficult to model, especially if this amount is reduced slightly, due to shorter reaction times for the XAFS analysis compared with the NMR analysis. This difference in time scales has not appeared to affect the results where the reaction has been quenched, but since the initial mixing was undertaken at RTP, this could lead to greater discrepancies between the two techniques.

The model shown is for a 50:50 mixture of $Pd(OAc)_2$ and $Pd(P^tBu_3)_2$ (i.e. 1 phosphorus and

2 oxygen). The model refines fairly well to the experimental spectrum, but the Pd-O bond length is longer than expected (2.00 Å in $Pd(OAc)_2$, suggesting that the coordination number is too large (also the Debye-Waller is large). By varying the coordination numbers in the model it was not possible to reduce the Pd-O bond length. A model (0.8 phosphorus and 2.4 oxygens) was calculated from the ^{31}P NMR results (40 % of initial palladium species was $Pd(P^tBu_3)_2$ and the rest was assumed to be $Pd(OAc)_2$). On refinement the R factor was worse and the phosphorus coordination number wanted to increase considerably and the oxygen shells coordination number was too high.

The reaction solution was heated at 115 °C in a reaction vessel (1.5 hours) and transferred to the XAFS cell where QEXAFS analysis was undertaken with the reaction solution held at 40 °C (results are shown in figure 5.15).

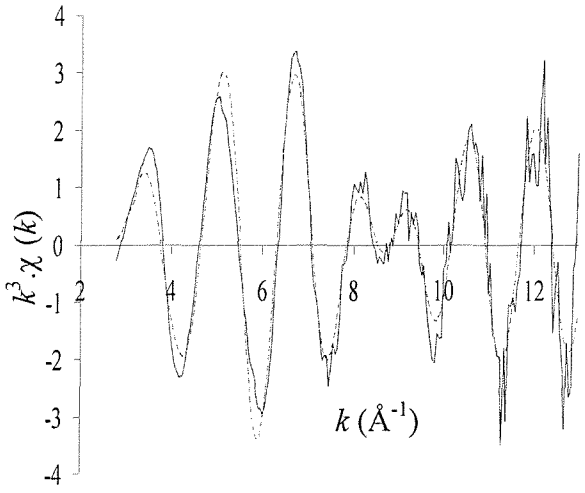

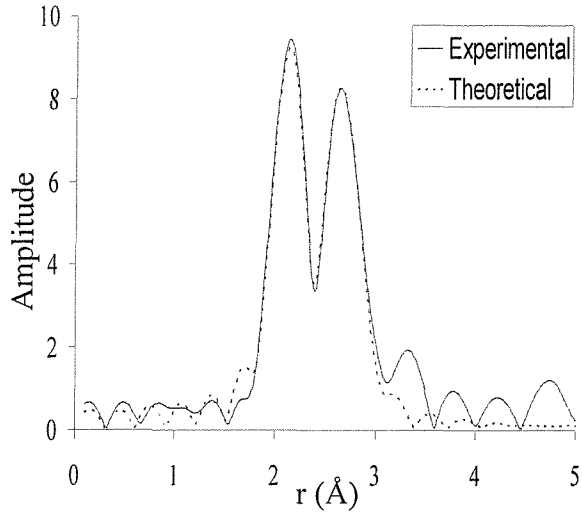

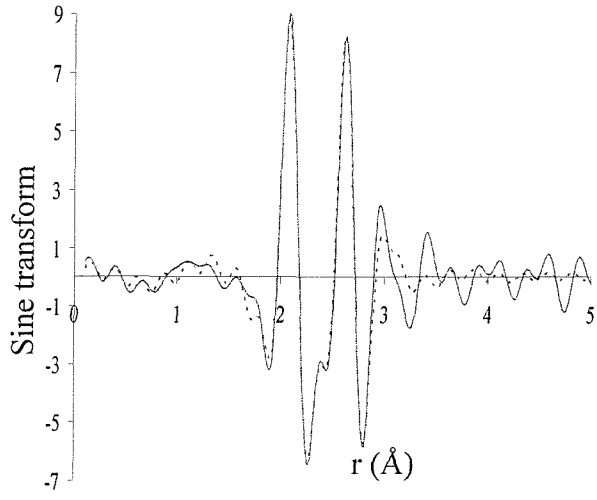

Atom	C.N.	r / Å	$2\sigma^2$ / Å^2
C	0.6(4)	2.03(6)	0.013(8)
P	1.1(2)	2.24(1)	0.005(2)
Br	1.9(1)	2.54(1)	0.018(1)

E_f = -5.2 (24) eV

R = 30.3 %

Figure 5.15 The palladium K-edge k^3-weighted QEXAFS data (10 x 6 minutes averaged), sine and Fourier transform for the $Pd(OAc)_2$ / P^tBu_3 / PhBr reaction (40°C), after heating for 1.5 hours at 115 °C.

Similar to the end of the PhI reaction with the same catalyst, the final spectrum visually resembles the halogen bridged palladacycle (**3b**). The Pd-Br peak in the Fourier transform is less intense then expected and the bromine shell Debye-Waller terms are higher than for **3b**, which again suggests that the actual coordination number is lower then the refined value of 1.9. This agrees with the NMR data that shows that only a third of the palladium is present in the form of $[Pd(P^tBu_3)(Ph)(\mu\text{-}Br)]_2$ (assigned since it is -7.2 ppm which is just upfield of the iodine analogue at -5.7 ppm). The ^{31}P NMR also shows two peaks at -12.5 and -15.7 ppm which also probably are bromine containing species (all other peaks are greater than 52 ppm). These two peaks each contribute 6 % to the total phosphorus species present, which could contribute a sixth or a third each to the palladium contribution depending whether the P:Pd ratio is 1:1 or 2:1. In the model the phosphorus coordination number wants to refine higher than 1, whist the carbon has reasonable Debye-Waller values at 0.6. This could be due to a higher level of $Pd(P^tBu_3)_2$ being present than shown in the NMR data.

5.5.6 QEXAFS analysis of the chlorobenzene reaction

As stated previously, when the phosphine was neat it aided the $Pd(OAc)_2$ to catalyse the PhCl reaction. But, for the ^{31}P NMR and this QEXAFS analysis the reaction was not catalysed since the phosphine was diluted in hexane. The results from the start of this reaction (i.e. reaction mixture was stirred at RTP) are shown in figure 5.16.

NMR data (figure 5.9) showed that at room temperature ~90 % of the total palladium present was in the form of $Pd(P^tBu_3)_2$. A phosphorus shell of 2 atoms was refined and gave a Pd-P distance of 2.29 Å (crystal structure was 2.28 Å). By adding an oxygen shell the R factor improved by 15 % so was included in the fit, but the inclusion increased the bond length to 2.31 Å.

So the XAFS data and the NMR results show that the main species present at the start of the PhCl reaction is $Pd(P^tBu_3)_2$ with a very small amount of residual $Pd(OAc)_2$ present.

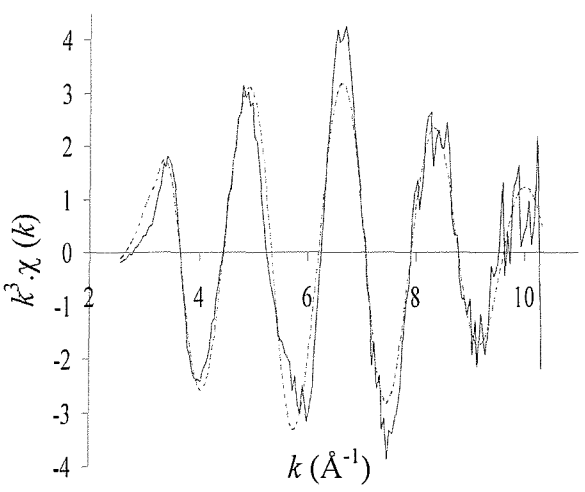

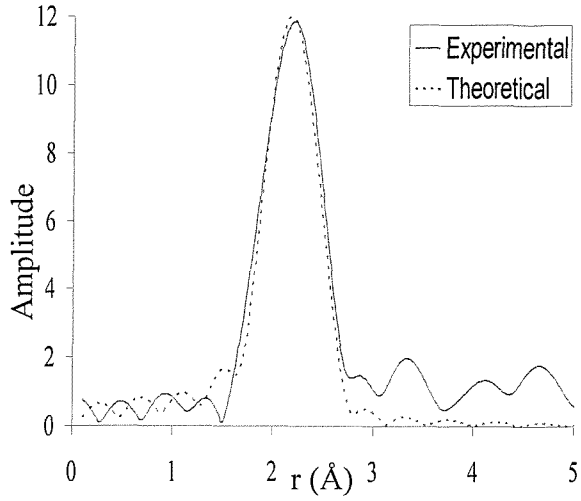

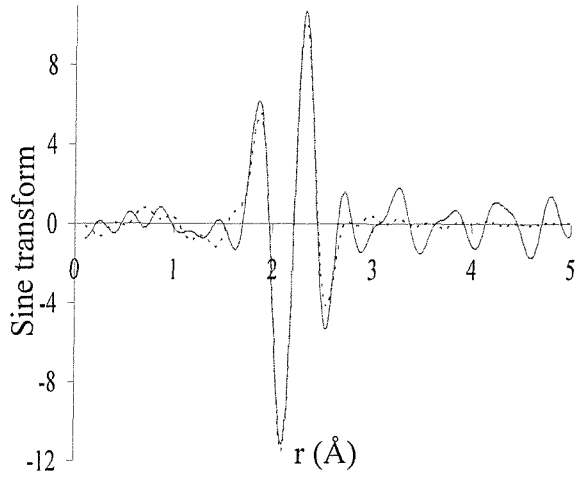

Atom	C.N.	r / Å	$2\sigma^2$ / Å^2
O	0.6(3)	2.03(2)	0.002(6)
P	1.9(3)	2.31(1)	0.012(2)

E_f = -12.8 (30) eV

R = 28.3 %

Figure 5.16 The palladium K-edge k^3-weighted QEXAFS data (5 x 6 minutes averaged), sine and Fourier transform for the $Pd(OAc)_2$ / P^tBu_3 / PhCl reaction (RTP), which was homogeneous at room temperature.

5.5.7 Conclusions

These results show that the concentrations of main phosphine species present during the two experiments which the catalytic system catalyses is different. Phosphorus NMR of the PhI reaction shows a low concentration of the diphosphine and a high concentration of $[Pd(P^tBu_3)(Ph)(\mu\text{-}X)]_2$ (X = Br or I), but the PhBr shows the opposite trend. QEXAFS also showed that there was more coordination of iodine to palladium at the end of the reaction, compared with the bromobenzene reaction. Undertaking the PhI reaction but excluding the alcohol showed that the overall iodine coordination number around the palladium did not reach the same level as for the normal catalytic run.

$[Pd(P^tBu_3)(Ph)(\mu\text{-}X)]_2$ was present throughout both reactions, but the chlorine analogue did not form in the PhCl reaction. The main area in the ^{31}P NMR spectra attributed to halogen coordination, did not show any Pd-Cl bond formation. The main species present at the start of the reaction was $Pd(P^tBu_3)_2$, which decreased over time. It is therefore likely that in all three reactions $Pd(P^tBu_3)_2$ forms at the start of the reaction. For the iodobenzene reaction this quickly has PhI coordinated and then catalysis occurs. This process is slower for the PhBr reaction, hence the lower concentration of $[Pd(P^tBu_3)(Ph)(\mu\text{-}Br)]_2$ and does not occur in the PhCl reaction, hence there is no catalysis.

5.6 An attempt to catalyse the Heck reaction with palladium acetate and tricyclohexylphosphine

The Heck reaction (with PhI, PhBr and PhCl) was studied with tricyclohexylphosphine (PCy_3) and palladium acetate as catalyst.

5.6.1 NMR analysis of the Heck reactions

The reaction between $Pd(OAc)_2$ and PCy_3 forms a mixture of free ligand, $Pd(PCy_3)_2$ and $O{=}PCy_3$ (chapter 3). Addition of chlorobenzene, bromobenzene or iodobenzene to this solution does not produce any new ^{31}P NMR peaks, which shows there is no facile coordination of any halobenzene to the above species.

Using carbon NMR to study the Heck reaction with the phosphine included, in all the reactions there was no production of new carbon NMR peaks which shows there was no product (or biphenyl) production, in all the reactions. This shows that the incorporation of PCy_3 in the system impedes the reaction (the only phosphine ligand investigated in this thesis which prevents catalysis occurring in the iodobenzene experiment). In an attempt to understand why there is no reaction, the normal Heck reaction procedure was undertaken and followed with ^{31}P NMR. The samples were taken after the solution was completely homogeneous at 90 °C and after 30 minutes at 115 °C as the palladium started to precipitate out.

Table 5.5 shows that for all samples roughly half of the phosphorus species is still present as the unreacted ligand, a third is present as $Pd(PCy_3)_2$ and there is a small amount of $O{=}PCy_3$ present. During the heating process there is formation of small peaks between 24.8-27.3 ppm dependent on the reaction. These peaks are presumably the halogenated phosphorus palladium species, since there is a slight shift upfield, as the halogen is changed from iodine to bromine to chlorine. This is a very similar trend shown in chapter 4, with halogen atoms replacing acetate ligands in species **1**. The iodine and bromine examples appear to form two species, whilst the chlorine only forms one. One of the species formed could be the logical oxidative addition product of $Pd(PCy_3)_2(Ph)X$, or another possibility is the double halogenated complex $Pd(PCy_3)_2X_2$. Assuming that there is one halogen atom in

the unassigned peaks, then at the end of the iodine reaction 52 % of the palladium is still present as palladium acetate or has precipitated out, with 54 % in the PhBr reaction and only 46 % of the palladium unaccounted for in the PhCl reaction (these numbers would slightly decrease if the unassigned species contained two halogen atoms). Investigation of the starting NMR spectra shows that these values are a mix of palladium acetate and reduction of palladium content through precipitation, because at the start of the reaction (before commencement of precipitation), there was only 43 % (PhI reaction), 31 % (PhBr reaction) and 48 % (PhCl reaction), which suggests that the rest is present in the form of $Pd(OAc)_2$. Since it is highly unlikely that $Pd(OAc)_2$ will be formed during the reaction, the decrease in the amount of palladium coordinated to phosphine indicates a reduction in coordinated palladium (i.e. precipitation). There is no formation of the protonated phosphine since this appears at 62.2 ppm.

PhX	Temp. °C	^{31}P NMR shift / ppm							
		50.0 O= PCy_3	27.3	26.8	25.9	25.1	24.8	22.7 $Pd(PCy_3)_2$*	10.8 PCy_3
I	90	4	11	-	-	-	-	33 (50)	52
	115	4	11	6	-	-	-	25 (38)	51
Br	90	4	-	-	2	3	-	42 (63)	38
	115	4	-	-	8	12	-	23 (35)	48
Cl	90	3	-	-	-	-	6	31 (47)	58
	115	10	-	-	-	-	8	27 (41)	55

*Percentage of total palladium present in solution in brackets

Table 5.5 Selected ^{31}P NMR integration values for the Heck reactions with $Pd(OAc)_2$ and PCy_3.

Overall, the table shows that the main phosphorus palladium species formed during the reactions is $Pd(PCy_3)_2$, there is also a small amount of halogen coordinated to palladium at the start of each reaction and this amount increases slightly over the course of the reaction. This is presumably the oxidative addition product of the previous species, since there is a reduction in the concentration of $Pd(PCy_3)_2$. There is only minimal formation of this species and could explain why catalysis does not occur.

5.6.2 QEXAFS analysis of the iodobenzene reaction

The QEXAFS PhI reaction solution was made as normal and stirred at 40 °C (note cooler than for the first NMR sample). The reaction solution was held at 40 °C and 5 x 6 minute QEXAFS scans were recorded and averaged as usual (figure 5.17).

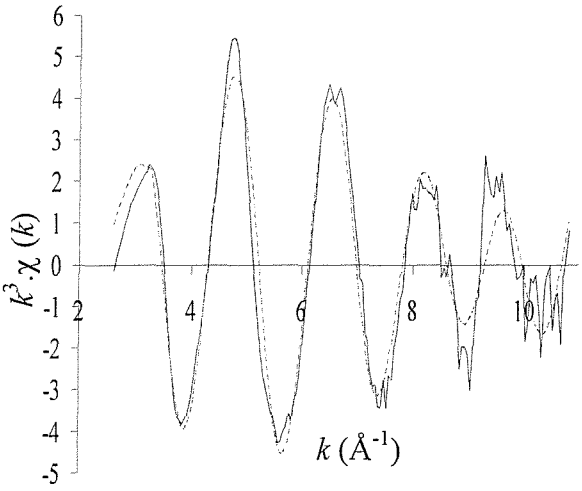

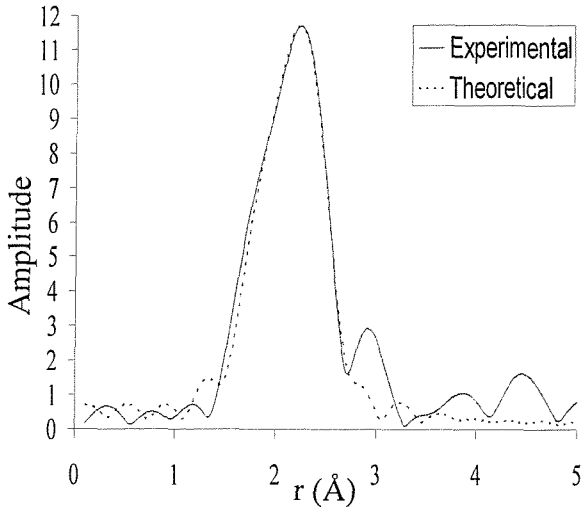

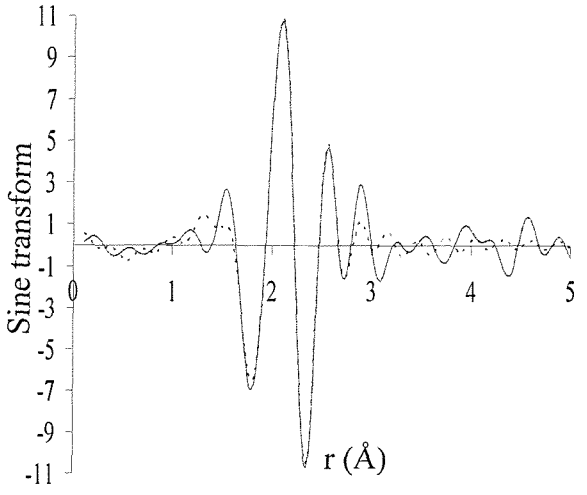

Atom	C.N.	r / Å	$2\sigma^2$ / Å^2
O	2.1(2)	2.02(1)	0.009(2)
P	1.2(1)	2.36(1)	0.001(2)

E_f = -0.45 (115) eV

R = 26.9 %

Figure 5.17 The palladium K-edge k^3-weighted QEXAFS data (5 x 6 minutes averaged), sine and Fourier transform for the $Pd(OAc)_2$ / PCy_3 / PhI reaction (40 °C), after heating to 40 °C.

The QEXAFS spectrum refined well to the model devised (2 oxygens and 1 phosphorus), which was a 50:50 mix of $Pd(OAc)_2$ and $Pd(PCy_3)_2$. This agrees well with the NMR data that approximately half of the palladium is incorporated as palladium acetate. The fit is good with low errors, but the Debye-Waller values are low and the Pd-P bond length is fairly high.

After heating the reaction solution to 115 °C for 20 minutes the final sample was taken and measured by QEXAFS (figure 5.18).

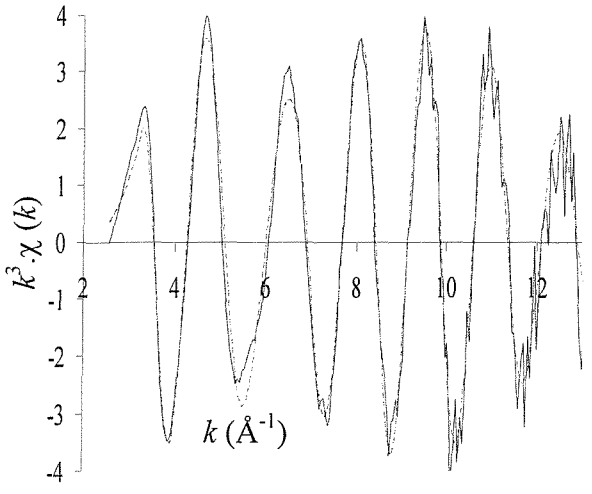

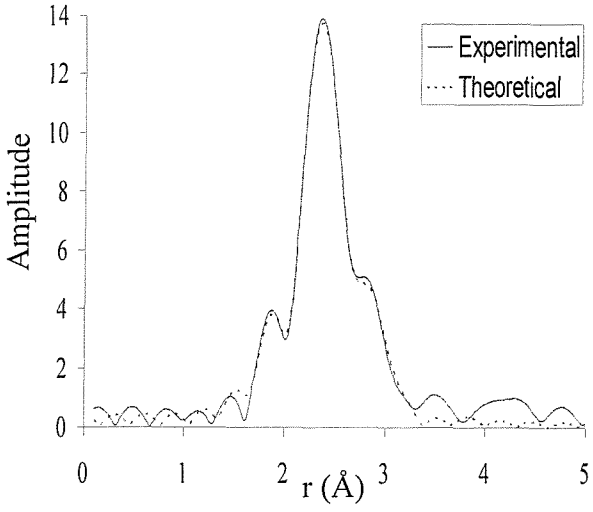

Atom	C.N.	r / Å	$2\sigma^2$ / Å^2
O	1.0(1)	2.03(1)	0.016(3)
P	1.5(1)	2.38(0)	0.003(1)
I	1.0(1)	2.65(1)	0.014(1)

E_f = -0.5 (11) eV

R = 26.9 %

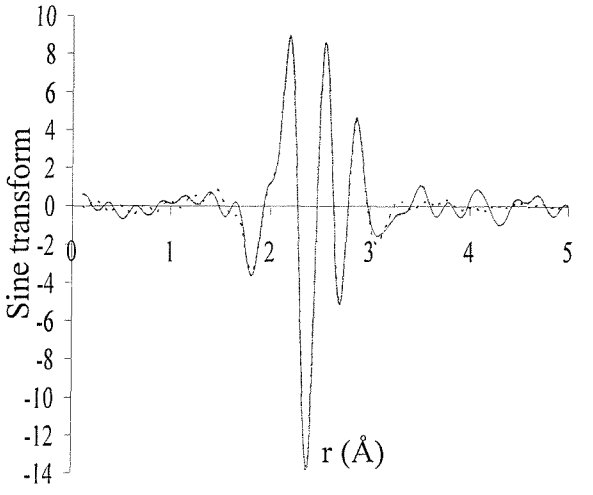

Figure 5.18 The palladium K-edge k^3-weighted QEXAFS data (10 x 6 minutes averaged), sine and Fourier transform for the $Pd(OAc)_2$ / PCy_3 / PhI reaction (40 °C), 115 °C for 20 minutes.

The change in the EXAFS (relative to the start solution) and the increase in the intensity of the peaks at high k indicates coordination of a heavier atom (iodine). The iodine atom fits very well to a shell of 1, with reasonable Debye-Waller values, but the peak in the Fourier transform only appears as a shoulder, not a distinct peak as previous results. So this could possibly imply that the average coordination number is less than 1. The NMR shows a reduction in $Pd(PCy_3)_2$ and at the same time a new peak of very similar intensity appears at 26.8 ppm, the other phosphorus integrations do not change, which suggests this species has 2 phosphorus atoms per palladium and could be $Pd(PCy_3)_2PhI$. The species present at 27.3 ppm could be $[Pd(PCy_3)(Ph)(\mu\text{-}I)]_2$. Assuming these assignments are correct this means 38

% of the palladium content is $Pd(PCy_3)_2$, 33 % is $[Pd(PCy_3)(Ph)(\mu\text{-}I)]_2$ and 9 % is $Pd(PCy_3)_2(Ph)(I)$, this means 20 % could be unreacted $Pd(OAc)_2$. This makes the model around the palladium atom 0.4 carbons, 0.6 oxygens, 1.4 phosphorus and 0.8 iodines, which agrees exceptionally well with the refined model (note that the carbon and oxygen has been refined as one shell). If $[Pd(PCy_3)(Ph)(\mu\text{-}I)]_2$ was assigned incorrectly and the species had a phosphorus to metal ratio of 1:1, the iodine coordination number in the EXAFS model would decrease by 0.3 and the oxygen/carbon number would increase by 0.3.

5.6.3 QEXAFS analysis for the bromobenzene and chlorobenzene reactions

The initial reaction mixtures for both reactions were analysed by QEXAFS as for the PhI reaction. Both results were very similar so the results are not shown but the two model tables are shown in table 5.6.

A

Atom	C.N.	R/Å	$2\sigma^2$ / Å^2
O	1.2(1)	2.04(1)	0.007(2)
P	2.3(2)	2.36(1)	0.001(1)

E_f = -1.2 (11) eV

R = 24.2 %

B

Atom	C.N.	R/Å	$2\sigma^2$ / Å^2
O	1.7(1)	2.01(1)	0.001(2)
P	1.5(1)	2.36(1)	0.002(3)

E_f = -0.5 (12) eV

R = 23.8 %

Table 5.6 The model tables for the palladium K-edge k^3-weighted QEXAFS data (5 x 6 minutes averaged) for the PhBr (A) and PhCl (B) reactions (40 °C), after heating to 40 °C.

These results show that in both experiments there is no initial coordination of halogen. Both solutions are a mixture of $Pd(OAc)_2$ and $Pd(PCy_3)_2$, with the PhBr experiment showing a greater coordination of phosphorus to the palladium, which is in agreement with the NMR experiments.

QEXAFS analysis was carried out on the reaction solution after heating the reaction for 20 minutes at 115 °C. The results are shown in figure 5.19.

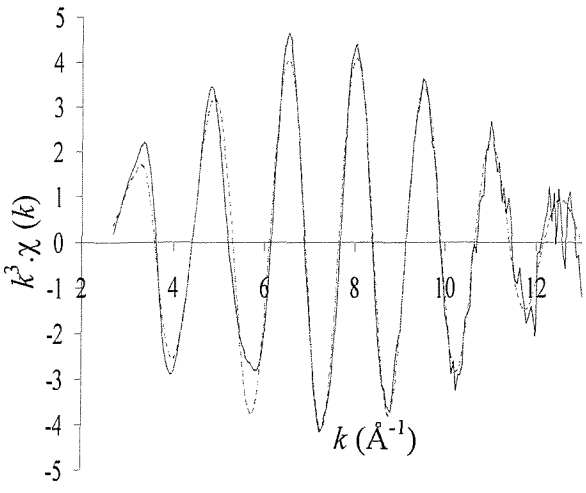

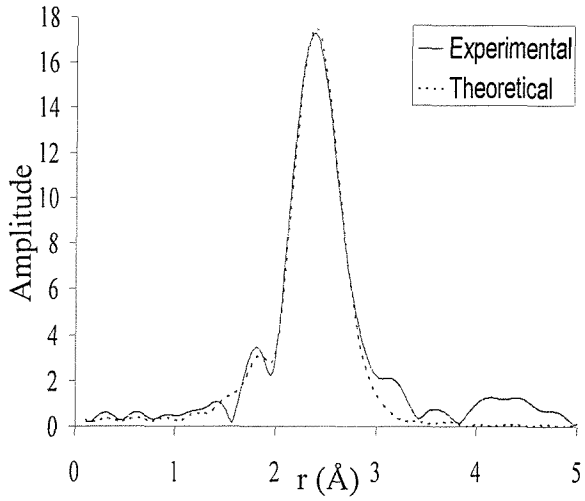

Atom	C.N.	r / Å	$2\sigma^2$ / Å^2
O	0.9(2)	1.98(3)	0.025(7)
P	1.6(1)	2.34(1)	0.005(1)
Br	0.9(1)	2.52(1)	0.009(1)

E_f = -8.1 (12) eV

R = 18.1 %

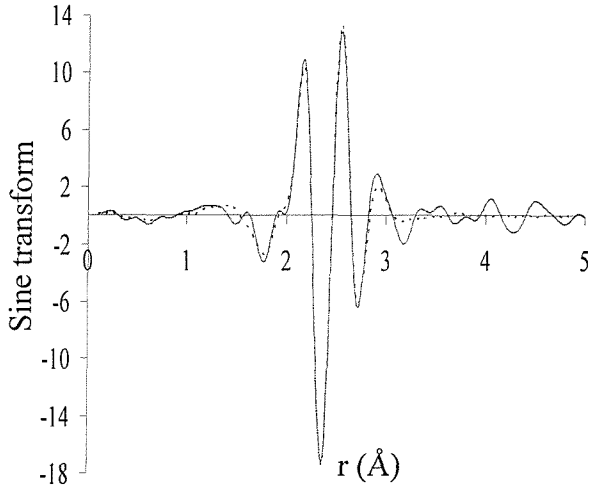

Figure 5.19 The palladium K-edge k^3-weighted QEXAFS data (10 x 6 minutes averaged), sine and Fourier transform for the $Pd(OAc)_2$ / PCy_3 / PhBr reaction (40 °C), after heating to 115 °C for 20 minutes.

Again initial observation of the EXAFS indicates coordination of heavier atoms to the starting solution. This is harder to observe in the Fourier transform, but the peak apex moves to higher R values.

The ^{31}P NMR integration values are very similar to the PhI experiment, so there is a very similar concentration of species present (e.g. $[Pd(PCy_3)(Ph)(\mu\text{-}Br)]_2$. So the same model was applied as for the PhI experiment and again gives a very good for the mixture of species present. The main difference observable is that the Debye-Waller value for the bromine shell is lower than the iodine shell, indicating that there is on average more bromine coordinated to palladium than for the PhI experiment.

To complete the XAFS analysis on the catalyst system, QEXAFS was used to analyse the PhCl system after heating the reaction for 20 minutes at 115 °C (figure 5.20).

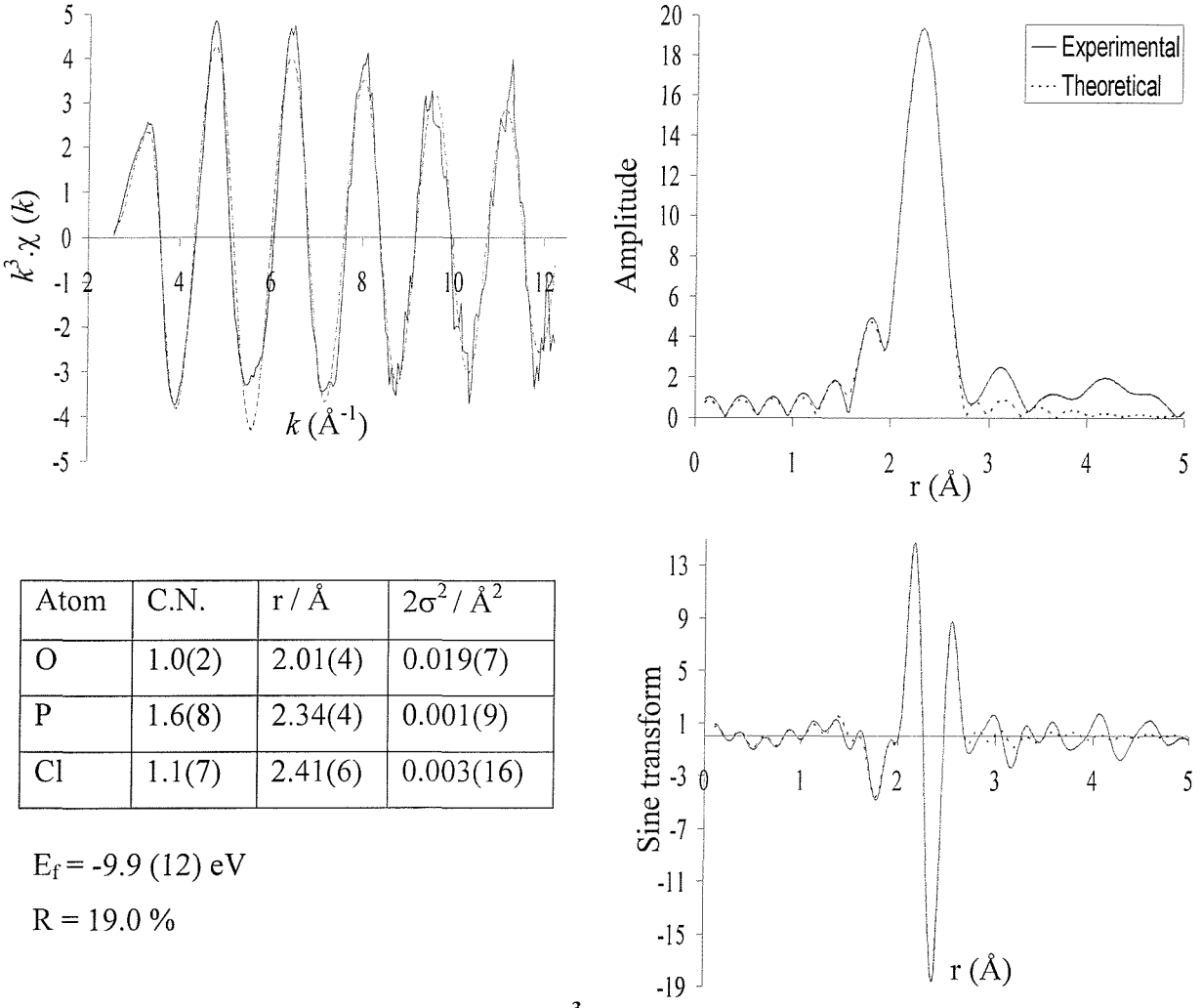

Atom	C.N.	r / Å	$2\sigma^2$ / Å^2
O	1.0(2)	2.01(4)	0.019(7)
P	1.6(8)	2.34(4)	0.001(9)
Cl	1.1(7)	2.41(6)	0.003(16)

E_f = -9.9 (12) eV

R = 19.0 %

Figure 5.20 The palladium K-edge k^3-weighted QEXAFS data (10 x 6 minutes averaged), sine and Fourier transform for the $Pd(OAc)_2$ / PCy_3 / PhCl reaction (40 °C), after heating to 115 °C for 20 minutes.

The model refines well to the experimental data, but the coordination number is considerably higher than expected from the ^{31}P NMR data. The errors are very large for the majority of the refined parameters. This suggests that problems have arisen in the refinement process due to the phosphorus and chlorine shells being very similar, so they are not discrete. From the ^{31}P NMR spectra (and assuming the peak at 24.8 ppm is $[Pd(PCy_3)(Ph)(\mu\text{-}Cl)]_2$) the model should be 1.2 carbons, 1.3 phosphorus and 0.5 chlorines.

5.6.4 Conclusions

Tricyclohexylphosphine prevented the palladium acetate from catalysing any of the reactions. In all reactions the diphosphine species formed, but there was no formation of the oxidised ligand. In all three reactions there was formation of halogenated products (probably $[Pd(PCy_3)(Ph)(\mu\text{-}X)]_2$ and $Pd(PCy_3)_2(Ph)(X)$), but only in very small quantities. Therefore due to the stability of the palladium diphosphine species, this prevented substantial coordination of the halogen species and stopped the reactive species from forming.

5.7 Investigation of the Heck reaction with palladium acetate and tri(1-naphthyl)phosphine as catalyst

The investigation was further extended to include the Heck reaction with PhI and using $Pd(OAc)_2$ and tri(1-naphthyl)phosphine (PNp_3) as catalyst. Due to poor solubility of the ligand, the ratio of Pd:P was 1:2.

5.7.1 Phosphorus NMR analysis of the iodobenzene Heck reaction

^{31}P NMR analysis was undertaken in the usual way and the results from the reaction are shown in figure 5.21.

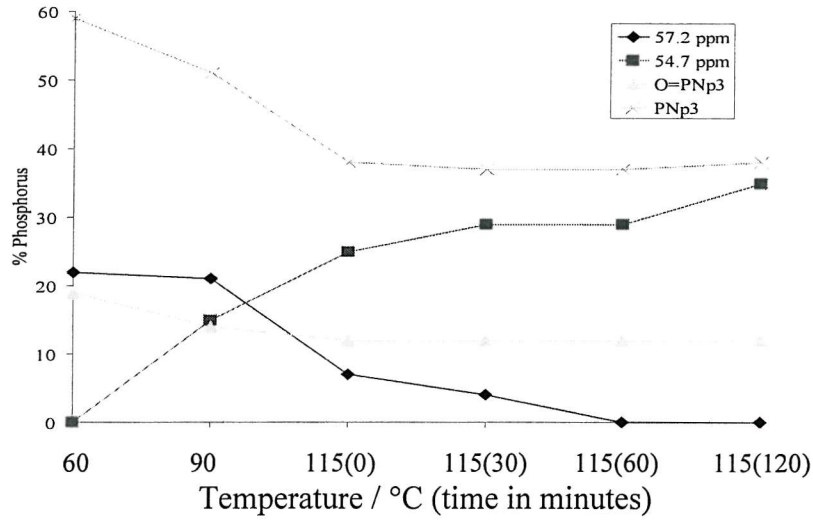

Figure 5.21 The selected ^{31}P NMR integration values for the iodobenzene Heck reaction.

The results show that there is an appreciable amount of oxidised phosphine present which decreases slightly over the course of the reaction. At the start of the reaction 59 % of the ligand is still uncoordinated, this reduces to 38 % over the course of the reaction. Considering that 12 % of the phosphorus species is present as $O=PNp_3$, this means on average the maximum ratio of phosphorus coordinated to palladium is 1:1, which could suggest formation of a palladacycle.

Shaw synthesised the palladacycle (figure 5.22) formed by reacting PNp_3 with $Pd(OAc)_2$.[15]

This was repeated in house and the palladacycle was found to have a ^{31}P NMR shift at 50.3 ppm.

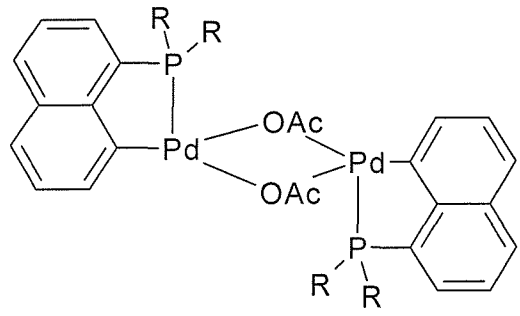

R = Np

Figure 5.22 Palladacycle formed by reacting $Pd(OAc)_2$ and PNp_3.[15]

This peak is not present during the Heck reaction, but comparison with the Heck reaction with **1** as catalyst (chapter 4), gave shifts downfield when the acetate ligands were replaced with iodine atoms (~4 and 9 ppm with the exchange of each ligand). Therefore the two peaks (57.2 ppm and 54.7 ppm) formed could be species containing iodine. The results show the same trend but in this experiment the peak most downfield appears before the second peak. This could suggest that the NMR shifts do not follow the same trend (as for **1**), the iodated species form in a different order, or one of the species may not be iodated.

5.7.2 Matrix Assisted Laser Desorption Ionisation (MALDI) mass spectroscopy

The MALDI reactions were carried out using acetonitrile instead of NMP, since the solvent had to be more volatile than NMP. Analysis was taken of the reaction mixture after heating it for thirty minutes at 115 °C. There were three main peaks attributed to species containing palladium (calculated from isotopic pattern) and are shown in figure 5.23.

These results agree with the previous NMR results. They show that there is coordination of the phosphine to palladium. It also shows that there is formation of the doubly bridged iodine dimer (**C**) (the missing naphthyl group is probably due to fragmentation caused by the laser, very common with the MALDI technique, shown by the fragmentation of **B** to form **A**). The formation of **A** shows that the diphosphine palladium species does form and would be the logical assignment for the NMR peak at 57.2 ppm, since it forms early in the reaction and then gradually disappears. This means the assignment at 54.7 ppm is **C**, which again makes chemical sense as the amount of free iodine for the PhI increases during the

reaction.

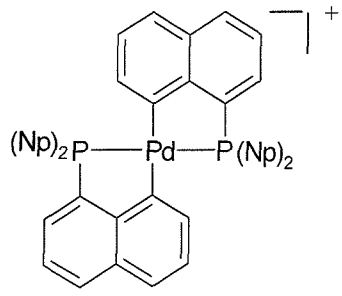

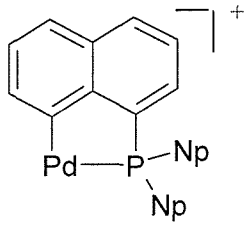

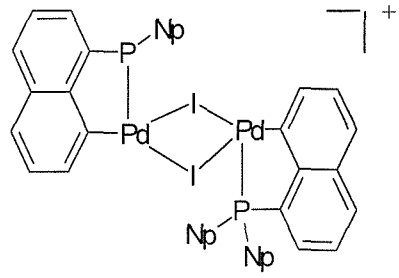

A – Mass = 929 (927) **B** – Mass = 517 (517) **C** – Mass 1163 (1162)

*N.B. The assignments are all cyclopalladated, but the actual species could be uncyclised (since the mass would only be 1 or 2 amu different).

Figure 5.23 Possible assignments of the MALDI peaks (major isotope mass (amu) shown underneath with relative molecular mass in brackets)*.

The MALDI works very well with the NMR data to assign unknown NMR peaks. From these assignments the amount of palladium coordinated to phosphine can be calculated. At the start only 22 % is coordinated to phosphine, which increases to 51, 57, 62, 58, 70 % as the reaction progresses (as species **A** and **C**). The later values could be higher, since there are small unassigned phosphine peaks, which could be Pd-P species. As stated earlier 50 % of the phosphine is known not to be bonded to palladium, therefore the average Pd-P coordination could be 1. Assuming that the maximum amount of phosphine to bond to palladium is in a 1:1 ratio, then this value is achieved when the reaction reaches 115 °C. If the free phosphine is not labile in this reaction then the new phosphine species formed after this time, are formed from the reduction in $Pd(PNp_3)_2$.

5.7.3 QEXAFS analysis of the iodobenzene reaction

QEXAFS analysis was taken after heating the solution to 40 °C and transferring the solution to the XAFS cell which was also held at 40 °C. The results are shown in figure 5.24.

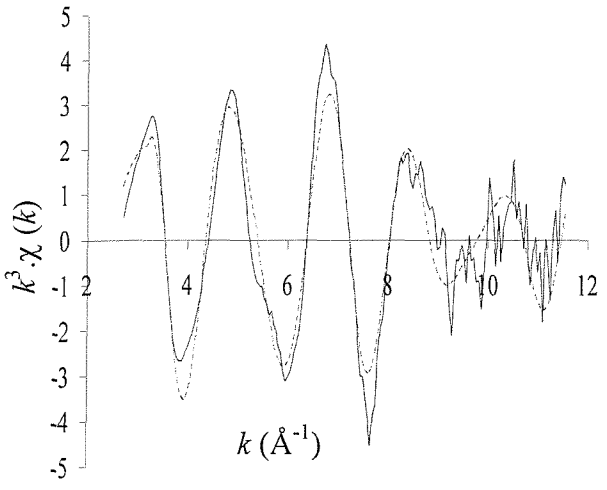

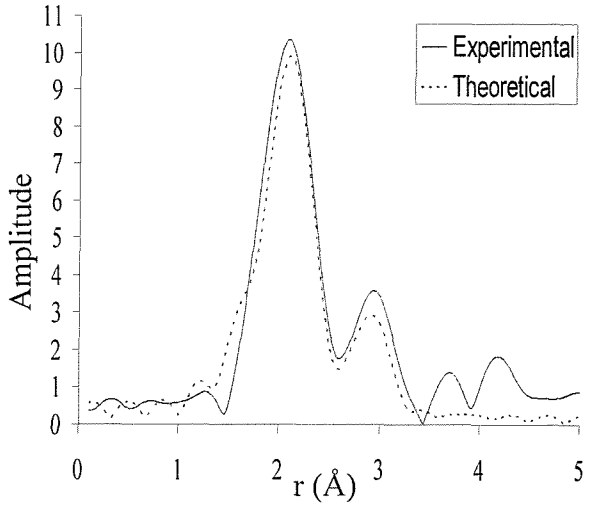

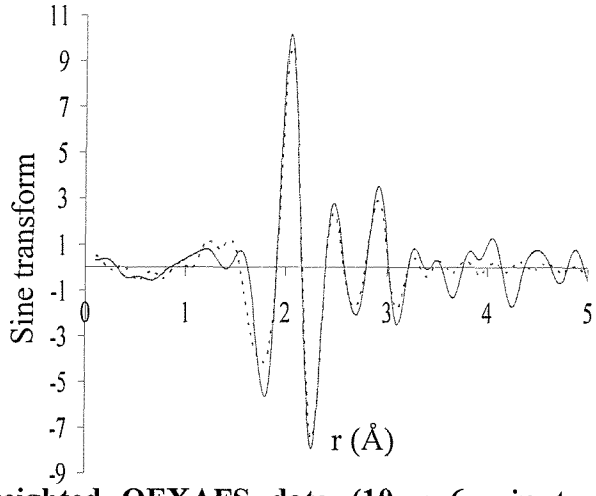

Atom	C.N.	r / Å	$2\sigma^2$ / Å^2
O	2.5(3)	2.02(3)	0.018(3)
P	0.7(1)	2.26(1)	0.002(2)
I	0.3(1)	2.66(2)	0.009(4)

E_f = -6.6 (14) eV

R = 33.6 %

Figure 5.24 The palladium K-edge k^3-weighted QEXAFS data (10 x 6 minutes averaged), sine and Fourier transform for the $Pd(OAc)_2$ / PNp_3 / PhI reaction (40 °C), after heating to 40 °C.

Investigation of the ^{31}P NMR shows that 78 % of the phosphorus species is not coordinated to palladium. The QEXAFS shows that there is a small amount of iodine coordinated, therefore the peak at 57.2 ppm must contain iodine, phosphorus and palladium. Two possible species are the iodine bridged dimer $[Pd(PNp_3)(Ph)(\mu\text{-}I)]_2$ or $Pd(PNp_3)_2(Ph)(I)$. Assuming the species is present as 22 % (NMR data) of the total phosphorus species and the only other palladium species is the starting material then the first model is 3.4 oxygens, 0.2 phosphorus and 0.4 iodine and the second model is 3.4 oxygens, 0.4 phosphorus, 0.2 iodines. When the first model was refined the oxygen shell refined to a coordination number of 2.2 and the phosphorus refined up to 0.6 but the Debye-Waller was negative, which meant the phosphorus coordination number would have to be increased, which meant the phosphorus coordination number was too high. The second model was refined and the

results are shown in figure 5.19. Again the oxygen coordination number refines too low, but the phosphorus and iodine stay at their target values and this means that the phosphorus coordination number stays at twice the iodines. This shows that the ^{31}P NMR species at 57.2 ppm could be $Pd(PNp_3)_2(Ph)(I)$.

The reaction was then heated to 115 °C for 1.5 hours and (10 x 6 minute) QEXAFS scans were taken and averaged (figure 5.25).

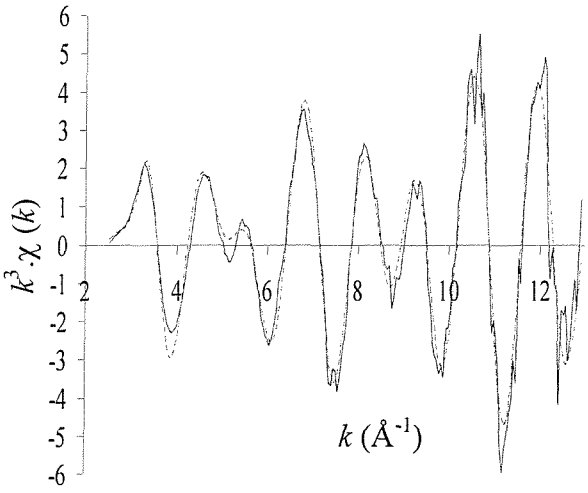

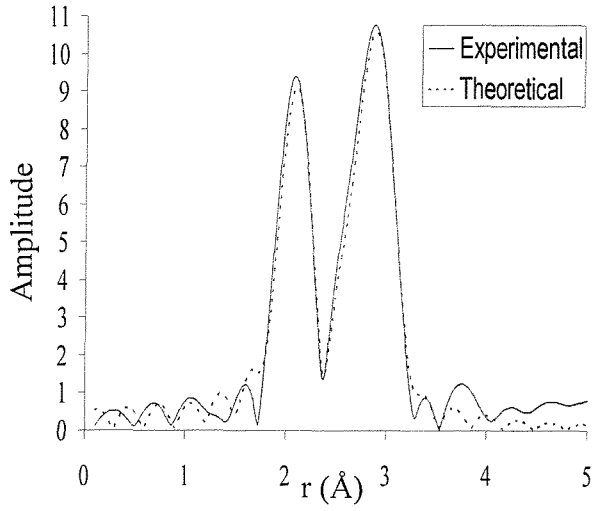

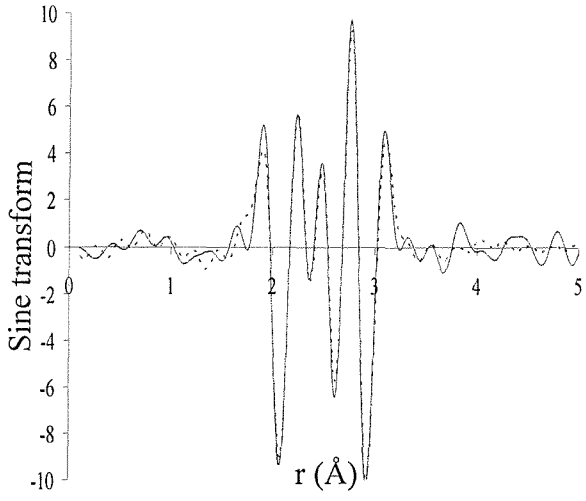

Atom	C.N.	r / Å	$2\sigma^2$ / Å^2
C	1.3(2)	2.08(1)	0.001(3)
P	0.8(2)	2.26(1)	0.010(3)
I	1.9(1)	2.69(0)	0.011(1)

E_f = -7.9 (8) eV

R = 22.6 %

Figure 5.25 The palladium K-edge k^3-weighted QEXAFS data (10 x 6 minutes averaged) and Fourier transform for the $Pd(OAc)_2$ / PNp_3 / PhI reaction (RTP), after heating at 115 °C for 1.5 hours.

Again the QEXAFS data resembled species **3a** and fitted fairly well to the model of 1 carbon, 1 phosphorus and 2 iodine atoms. The model is not quite the quality expected, which could suggest that the species is not 100 % abundant and there might be some residual $Pd(OAc)_2$ present. Which would explain the slightly lower than expected

phosphorus and slightly higher carbon (and oxygen) coordination numbers. The ^{31}P NMR values showed that this species at 54.7 ppm was present as 70 % of the palladium species. The concentration looks higher in the QEXAFS data since the interference in the k^3 data is negligible. It is possible for the NMR experiment the species degraded in the NMR tube. A logical suggestion for this species is $[Pd(PNp_3)Ph(\mu\text{-}I)]_2$.

5.7.4 Conclusions

The results show that for the PhI reaction is catalysed by PNp_3 and $Pd(OAc)_2$. ^{31}P NMR shows that throughout the reaction there is never more than one phosphine atom per palladium (average).

At the start of the reaction there is already substantial coordination of iodine to the palladium metal. The species is likely to be of the form $Pd(PNp_3)_2(Ph)(I)$ (the oxidative addition product of PhI to the Pd^0 species $Pd(PNp_3)_2$). This agrees with NMR, XAFS and MALDI spectra (fragment A, figure 5.23 is this species with the loss of the PhI coordination).

As the reaction proceeds ^{31}P NMR shows a reduction in concentration of the first species and the increase in concentration of a new species ($[Pd(PNp_3)(Ph)(\mu\text{-}I)]_2$), which was characterised by MALDI and QEXAFS analysis.

There was no formation of Shaw's acetate bridged palladacycle (figure 5.22) at any stage during the reaction. This result is identical to the P(*o*-tolyl)$_3$ reaction, which did not form Hermann's catalyst **1**.

5.8 Investigation of the Heck reaction with palladium acetate and tri(*o*-methoxyphenyl)phosphine as catalyst

The Heck reaction between PhI and $Pd(OAc)_2$ catalysed by tri(*o*-methoxyphenyl)phosphine ($P(C_6H_4(OMe))_3$) was investigated. Again due to poor solubility of the ligand, the ratio of ligand to metal was 2:1

5.8.1 Phosphorus NMR analysis

Temp / °C (time / min)	^{31}P NMR shift/ppm							
	47.7	42.2	27.1	20.2	17.9[a]	12.8[a]	-3.0	PR_3
60					7	54	18	17
90					15	70		10
115			9	63	11			
115(30)	8	3	11	74				
115(60)	9	3	8	77				
115(120)	5	2	7	86				

[a] Formed during the reaction between $Pd(OAc)_2$ and PR_3

Table 5.7 Selected phosphorus NMR shifts for the Heck reaction with PhI.

The NMR results table 5.7 shows that at the start of the reaction there is only a small amount of free ligand (-36.0 ppm[16], the remainder is probably bonded to Pd (the ^{31}P NMR shift for $H^+(P(C_6H_4(OMe))_3$ is -17.0 ppm and $O=(P(C_6H_4(OMe))_3$ is 20.6 ppm), but does not include iodine in the species, since the same species were formed when $Pd(OAc)_2$ was reacted with the free ligand, without the alcohol or PhI being present. After reaching 115 °C, there is a very small initial amount of product formed, the majority of the initial precursors have disappeared, leaving two main peaks at 20.2 ppm and 27.1 ppm. During the remainder of the reaction, the peak at 20.2 ppm remains the major phosphorus species and increases in concentration. After being at the reaction temperature for 30 minutes there is only a trace of PhI left and it has disappeared after an hour at this temperature. Towards the end of the reaction some small peaks appear downfield, but in total only contribute to 20 % of the phosphine species present (and appear after catalysis starts). Therefore the main peak of interest and the only peak to be present in any large concentration during catalysis is the peak at 20.2 ppm. It is worth noting that the only two peaks present during the whole stage

of catalysis are at 27.1 ppm and 20.2 ppm. These results also show that for the majority of the reaction (assuming the three peaks most downfield are palladium phosphine species), on average the palladium has two phosphine ligands coordinated. (i.e. probably not cyclopalladated).

5.8.2 MALDI analysis of the iodobenzene reaction

MALDI analysis was undertaken on the reaction solution after heating to 90°C. The main palladium containing species peak that was assigned is shown in figure 5.26.

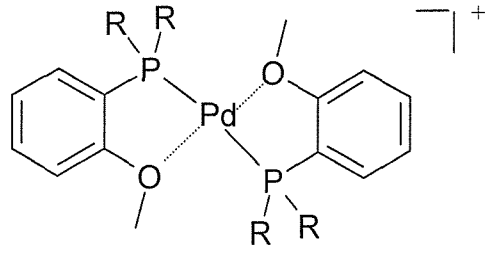

R = (C_6H_4(OMe)) **A- Mass – 810.2 (810)**

Figure 5.26 Possible assignments of the MALDI peak (major isotope mass (amu) shown underneath with relative molecular mass in brackets)*.

The results show an ion **A**. Using MALDI it is not possible to determine if **A** is cyclopalladated since the linear model would have identical mass. There is a real possibility that the oxygen uses its lone pair to bond to the palladium, which would put the palladium in a square planar geometry, which could increase stability of the molecule. The MALDI data did not show any peaks which included palladium and iodine in the same molecule.

The NMR results for a similar reaction solution showed two peaks at 12.8 and 17.9 ppm. It is likely that that one of these peaks is compound **A**. The peak at 17.9 ppm might be the more likely candidate since it was broad and this might be caused by fluxionality in the system, due to rapid cleavage and formation of the Pd-O bond.

5.8.3 QEXAFS analysis of the iodobenzene reaction

As before the reaction solution was heated to 40 °C and QEXAFS analysis was undertaken at 40 °C (figure 5.27).

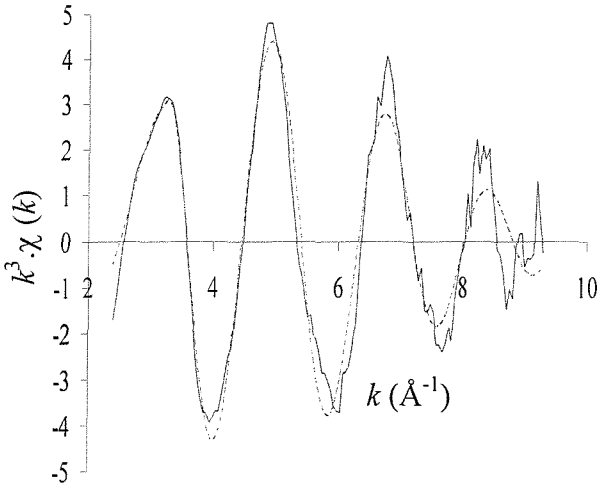

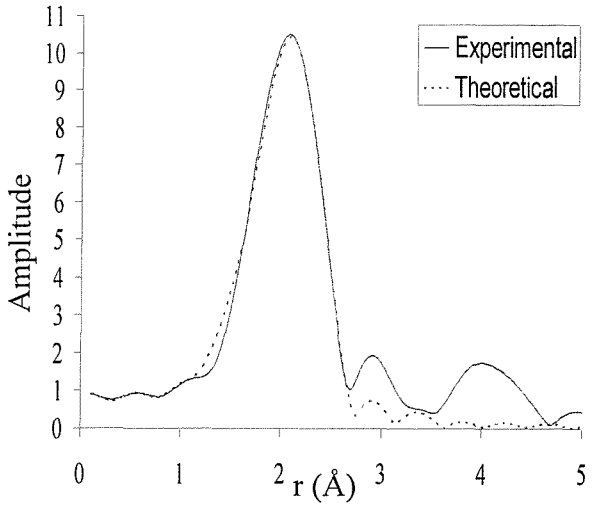

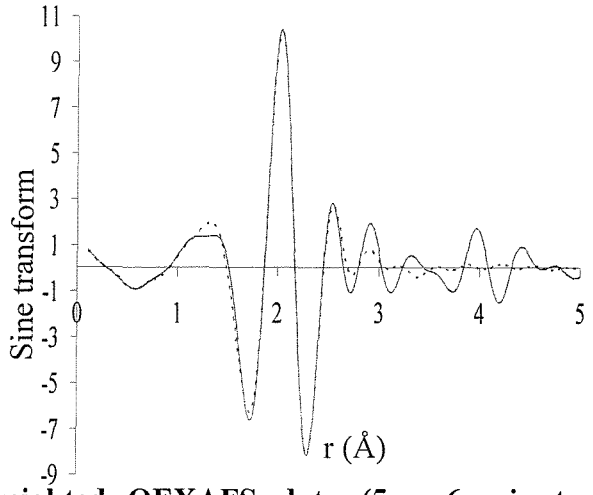

Atom	C.N.	r / Å	$2\sigma^2$ / Å^2
O	2.6(3)	1.98(2)	0.022(3)
P	1.3(2)	2.31(1)	0.010(3)

E_f = -4.8 (15) eV

R = 22.4 %

Figure 5.27 The palladium K-edge k^3-weighted QEXAFS data (5 x 6 minutes averaged), sine and Fourier transform for the $Pd(OAc)_2$ / $P(C_6H_4(OMe))_3$ / PhI reaction (40 °C), after heating to 40 °C.

Unlike the PNp_3 example there was no initial coordination of iodine and this agrees with the ^{31}P NMR results. The best model obtained was assuming that there was a 40 % concentration of $Pd(OAc)_2$ and 60 % $Pd(P(C_6H_4(OMe))_3)_2$. The palladium phosphine was modelled as a four coordinated species (i.e. coordinated to the palladium through the phosphorus and the oxygen atoms in the ligand). The values are very close to the expected values with low errors.

The model was altered so the $Pd(P(C_6H_4(OMe))_3)_2$ ligand was only coordinated by the phosphine ligands. The data fitted fairly well to the model (1.6 oxygens and 1.2 phosphorus) with low errors, but the R factor increased to 23.2 % and the Pd-P bond length was slightly long (2.32 Å) whilst the Pd-O was too short (1.94 Å) also the Debye-Waller values were low (~0.003 Å). Therefore since the first model gives a better fit, QEXAFS shows that the phosphine ligand is stabilised by oxygen coordination to the palladium.

The reaction was then heated for 1.5 hrs at 115 °C and QEXAFS measurements were taken and averaged (figure 5.28).

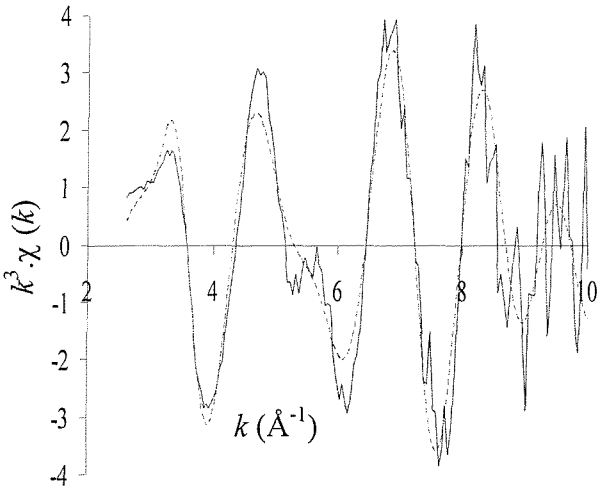

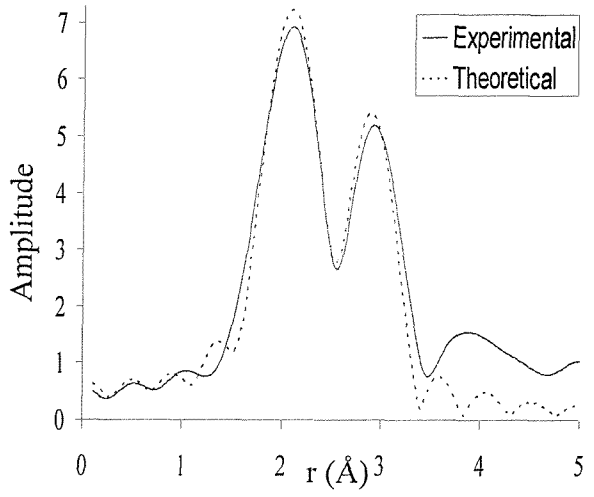

Atom	C.N.	r / Å	$2\sigma^2$ / Å^2
C	1.8(4)	2.09(4)	0.007(8)
P	0.9(2)	2.25(3)	0.012(7)
I	1.6(2)	2.65(1)	0.013(2)

E_f = -7.2 (17) eV

R = 33.3 %

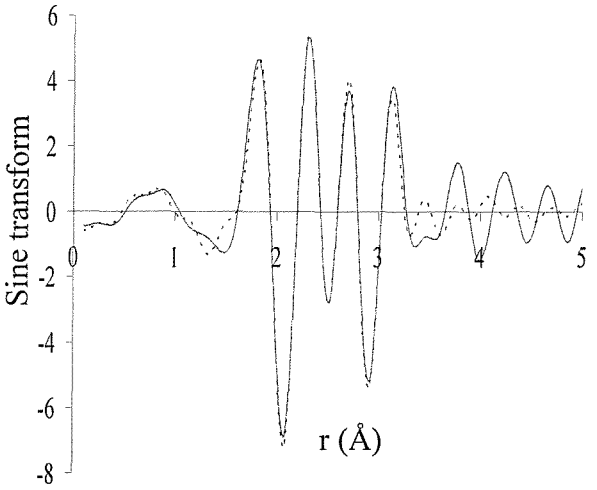

Figure 5.28 The palladium K-edge k^3-weighted QEXAFS data (10 x 6 minutes averaged), sine and Fourier transform for the $Pd(OAc)_2$ / $P(C_6H_4(OMe))_3$ / PhI reaction (RTP), after heating for 1.5 hours at 115 °C.

The data quality is poor and this could be due to a mixture of palladium species being present, which was indicated by the mixture of phosphine species present in the NMR data.

The model fitted has good values and fits well to the experimental data. It shows that the average coordination number of iodine to palladium is approximately 1.6. Since the species at 20.2 ppm is roughly 80 % abundant (w.r.t. phosphorus) this means that there must be two phosphorus atoms per palladium. Also it must have iodine coordinated to ensure the coordination number for iodine is 1.6. Therefore a likely assignment is the oxidative addition product to the initial diphosphine of $Pd(P(C_6H_4(OMe))_3)_2(Ph)(I)$.

5.8.3 Conclusions

Again the PhI reaction is catalysed by $(P(C_6H_4(OMe))_3$ and $Pd(OAc)_2$, but in this reaction there is no initial coordination of iodine (unlike the PNp_3 reaction). There is also only a small concentration of free phosphine present, which quickly disappears, which is again very different to the PNp_3 study. The phosphorus ligand quickly coordinates to the palladium metal and it is likely to form the cyclopalladated species in figure 5.26 (MALDI and QEXAFS analysis).

As the reaction proceeds there is one dominant phosphorus NMR species which increases in intensity with time. The NMR integration shows that this species has two phosphine ligands per palladium and the QEXAFS shows that the species has one iodine per palladium (and only one iodine atom coordinated to the palladium atom) which conclusively points to the species $Pd(P(C_6H_4(OMe))_3)_2(Ph)(I)$ being present. There are also a few unassigned phosphorus peaks at 42.2 ppm and 47.7 ppm, which could be due to the presence of cyclopalladated halogenated species e.g. the iodine bridged dimer of the species shown in figure 5.26.

5.9 Conclusions

This chapter has shown that palladium acetate catalyses the Heck reaction between methallyl alcohol and iodobenzene, but not the bromobenzene or chlorobenzene reactions. The addition of phosphine ligands to the catalytic system either promoted catalysis or deactivated the catalyst:

- PPh_3 and P(*o*-tolyl)$_3$ stabilised and promoted catalysis in the bromobenzene reaction
- P^tBu_3 was the only phosphine to promote catalysis in the chlorobenzene reaction
- PCy_3 was the only ligand which prevented the palladium acetate from catalysing the iodobenzene reaction
- $P(C_6H_4(OMe))_3$ and $P(Np)_3$ were both used to catalyse the iodobenzene reaction and both showed the formation of cyclopalladated complexes

These results show a huge variety in the catalytic property of the systems and the results also show that there was a large difference in the palladium and phosphorus species formed before, during and after catalysis.

The main trend shown in all the reactions which were catalysed proceeded, the amount of halogen coordinated to the palladium increased (in some reactions iodine was coordinated to the metal at the start (e.g. PNp_3), whilst in other reactions heat was needed to promote iodine coordination (e.g. $P(C_6H_4(OMe))_3$). Conversely, in reactions not catalysed (e.g. PCy_3) there was negligible halogen coordination. XAFS showed that in the reaction solutions at the end of the reaction, the average halogen coordination to palladium was two. But, depending on the reaction this varied to a higher value for PPh_3 and a lower value for $P(C_6H_4(OMe))_3$.

The palladium phosphine and halogen species which were formed, were of the form $Pd(PR_3)_2(Ph)(X)$, $[Pd(Ph)(PR_3)(\mu\text{-}X)]_2$ and $[Pd(X)(PR_3)(\mu\text{-}X)]_2$. Generally the former appeared first in the reaction, which is formed by the oxidative addition of PhX to $Pd(PR_3)_2$. This was then followed by the formation of the bridged species. There were also signs of formation of halogen bridged cyclopalladated complexes formed by P(*o*-tolyl)$_3$, PNp_3 and $P(C_6H_4(OMe))_3$.

There were also many differences in the species formed. Some reactions had a large presence of oxidised phosphine (formed due to reduction of palladium acetate), others didn't. Some reactions had a lot of free ligand, whilst others had none. Some reactions proceed after formation of $Pd(PR_3)_2$ or $Pd(PR_3)_3$, others didn't show formation of these species. In the reactions which were catalysed, phosphine coordination decreased with time and halogen increased.

Others main points of interest was that the *in situ* and *ex situ* phosphorus NMR results were very similar for the triphenylphosphine reaction. This shows that in this reaction that the intermediate species formed are stable at temperatures below the reaction temperature. This suggests that the same is applicable for the other *ex situ* experiments (i.e. the reaction is 'quenched' when transferred to the NMR tube and the phosphine species do not change), but is not necessarily the situation.

It was not possible to model coordination of olefin to the metal centre. The Pd-O (or carbon) bond length did increase to lengths observed for the Pd-C bond length for olefins coordinated to palladium. But, due to limitations in the XAFS technique it is not possible to calculate if the increase Pd-O interatomic distance quoted was due to olefin coordination, or due to a bad model fit caused by correlation between the carbon, oxygen and phosphorus shells.

5.10 References

1 V.L.Kambhampati, PhD Thesis, University of Southampton, **1998**

2 J. Evans, L. O'Neill, L. Kambhampati, G. Rayner, S. Turin, A. Genge, A.J. Dent, T. Neisus, *J. Chem. Soc., Dalton Trans.*, **2002**, 2207

3 S. Chen, S-M. Lee, Z. Lin, W-T. Wong, *J. Organomet. Chem.*, **1996**, *510*, 219

4 N.W. Alcock, W.L. Wilson, J.H. Nelson, *Inorg. Chem.*, **1993**, *32*, 3193

5 M.I.M-Vida, E.C-Rodriguez, M.N.M-Carretero, J.M.S-Peregrin, M. Simard, A.L. Beauchamp, *Inorg. Chim. Acta.*, **1989**, *157*, 201

6 J.Evans, L. O'Neill, G.Rayner, T. Nesius *to be submitted*

7 B.E. Mann, J.A. Musco, *J. Chem. Soc., Dalton Trans.*, **1975**, 1673

8 E. Negishi, S. Baba, T. Takahashi, D.E. Van Horn, N. Okukado *J. Am. Chem. Soc.*, **1987**, *109*, 2393

9 V.V. Grushin, *Organometallics,* **2000**, *19*, 1888.

10 A.L. Rheingold, W.C. Fultz, *Organometallics*, **1984**, *3*, 1414

11 W.A.Herrman, V.P.W.Bohm, C Reisinger, *J. Organomet. Chem.*, **1999**, *576*, 23-41

12 C. Dai, G.C. Fu, *J. Am Chem. Soc.*, **2001,** *123*, 2719

13 V.D-Vila, D.M.P. Mingos, R. Vilar, A.J.P. White, D.J. Williams, *J. Organomet. Chem,*. **2000**, *600*, 198

14 M. Tanaka, *Acta Cryst C,* **1992,** *48*, 739.

15 B.L. Shaw, S.D. Perera, E.A. Staley, *Chem. Commun.*, **1998**, *13*, 1361

16 F.P. Pruchnik, R. Starosta, M.W. Kowalska, E. Galdecka, Z. Galdecki, A. Kowalski, *J. Organomet. Chem.*, **2000**, *597*, 20

Chapter 6

Conclusions

Palladium K-edge XAFS (EXAFS, QEXAFS and EDE) techniques were used in conjunction with phosphorus NMR to characterise the palladium species present in a variety of reactions.

The work started with EDE analysis of the formation of the palladacycle **1** and XAFS techniques were used to elucidate the structure of **1** in solution. It was shown that multiple scattering effects were negligible and the most suitable model constructed was 1 carbon, 2 oxygen and 1 phosphorus atom bonded to the palladium atom. It was not possible to fit a palladium or carbon shell to determine if the species was a monomer or dimer in solution. Heating the preformed palladacycle in solution showed a slight shift of the Fourier transform peak to lower average interatomic distances around the palladium atom. This indicates that the broad phosphorus NMR peak (of **1**) is due to a monomer / dimer equilibrium which shifts towards the production of more monomer with temperature (i.e. an increase in contribution to the EXAFS from the increase in coordination number of the Pd-C shell. Analysis of the solid state form of **1** (known to be a dimer), showed very similar XAFS results and therefore showed that it is not possible to include the palladium-palladium interaction in the model.

In the formation of **1** from palladium acetate and tri-*o*-tolyphosphine an intermediate was observed in the white line plot and the ^{31}P NMR data which is attributed to coordination of palladium before the palladated ring closes $[Pd(P(o\text{-tolyl})_3)(CH_3COO)(\mu\text{-}CH_3COO)]_2$.

In the reaction of PCy_3 with palladium acetate, the palladium was reduced to $Pd^0(PCy_3)_2$. It was shown by ^{31}P NMR that this was achieved by the free ligand, which was oxidised to $O{=}PPh_3$. Very similar results were obtained from the EDE results of the other reactions studied, but the results are not as definitive due to the lack of NMR data. White line plots were extremely useful in pinpointing changes in the palladium environment.

The Heck reactions were catalysed by a variety of systems. The general trend was the increase of halogen coordination to the palladium as the reaction proceeded. Reactions that were not catalysed showed negligible or no coordination of halogen to the metal, which suggests that this is an important early step in the catalytic cycle. Enforced, since heating the catalytic species with PhI led to a stable mixture of species, whilst heating with alcohol led to decomposition of the metal precatalytic complex and liberation of free phosphine.

Reactions catalysed by the palladacycles showed similar trends and the palladacycle ring stayed intact. Reactions catalysed by **1**, showed early addition of halide (**2a** and **2b**), followed by the halogen bridged dimers (**3a** and **3b**), with the species **4a** and **4b** being the dominant species at the end. As stated the species present where the same, when **3b** was the catalyst, except at the start of the iodobenzene reaction when there was a mixture of bromide and iodide complexes present. The catalytic species are likely to be of similar structure to **2a**, **2b**, **4a** and **4b**, which allows easy coordination of the olefin. The catalytic structure is likely to have halogen coordinated (which disagrees with Hermann's hypothesis of a reactive two coordinate palladacycle) since catalysis occurs in the PhBr reaction before the PhI reaction, indicating that **3b** is closer in structure to the catalyst for the PhBr reaction compared with the corresponding PhI reaction.

The Heck reaction catalysed by palladium acetate and a mixture of monodentate phosphine showed a mixture of catalytic activity; PPh_3 and P(*o*-tolyl)$_3$ stabilised and promoted catalysis in the bromobenzene reaction, P(*t*-Bu)$_3$ was the only phosphine to promote catalysis in the chlorobenzene reaction, PCy_3 was the only ligand which prevented the palladium acetate from catalysing the iodobenzene reaction, $P(C_6H_4(OMe))_3$ and P(Np)$_3$ were both used to catalyse the iodobenzene reaction and both showed the formation of cyclopalladated complexes. A variety of trends were shown by the different systems; amount of free ligand in solution, amount of oxidised ligand in solution, rate of initial iodine addition and amount of iodine coordinated to palladium at the end of the reaction. Generally, similar species were present in the reaction mixture and were of the form $Pd(PR_3)_2(Ph)X$, $[Pd(Ph)(PR_3)(\mu\text{-}X)]_2$ and $[PdX(PR_3)(\mu\text{-}X)]_2$.

Appendix

A.1. X-ray crystallography data for $Pd(P^tBu_3)_2$ (section 5.5.2)

Empirical formula	$C_{24}H_{54}P_2Pd$	
Formula weight	511.01	
Temperature	120(2) K	
Wavelength	0.71073 Å	
Crystal system	Triclinic	
Space group	*P*1	
Unit cell dimensions	$a = 8.4487(5)$ Å	$\alpha = 96.326(5)°$
	$b = 8.4621(6)$ Å	$\beta = 105.280(5)°$
	$c = 11.8211(10)$ Å	$\gamma = 118.177(4)°$
Volume	690.75(9) $Å^3$	
Z	1	
Density (calculated)	1.228 Mg / m^3	
Absorption coefficient	0.795 mm^{-1}	
F(000)	274	
Crystal	Plate; colourless	
Crystal size	0.14 × 0.06 × 0.005 mm^3	
θ range for data collection	2.93 – 27.49°	
Index ranges	$-10 \le h \le 10, -10 \le k \le 10, -15 \le l \le 14$	
Reflections collected	8794	
Independent reflections	5520 [$R_{int} = 0.0523$]	
Completeness to $\theta = 27.49°$	94.7 %	
Absorption correction	Semi–empirical from equivalents	
Max. and min. transmission	0.9613 and 0.8969	
Refinement method	Full-matrix least-squares on F^2	
Data / restraints / parameters	5520 / 27 / 264	
Goodness-of-fit on F^2	1.010	
Final *R* indices [$F^2 > 2\sigma(F^2)$]	*R1* = 0.0509, *wR2* = 0.0989	
R indices (all data)	*R1* = 0.0869, *wR2* = 0.1122	
Absolute structure parameter	0.31(8)	
Extinction coefficient	0.008(2)	
Largest diff. peak and hole	0.470 and –0.484 e $Å^{-3}$	